Fluorescent Dissolved Organic Matter in Yellowstone National Park Hot Springs

by

Joshua Nye

A Dissertation Presented in Partial Fulfillment
of the Requirements for the Degree
Doctor of Philosophy

Approved February 2020 by the
Graduate Supervisory Committee:

Hilairy Hartnett, Chair
Everett Shock
Anne Jones

ARIZONA STATE UNIVERSITY

May 2020

ABSTRACT

I present for the first time a broad-scale assessment of dissolved organic matter in the continental hot springs of Yellowstone National Park. The concentration of dissolved organic carbon in hot springs is highly variable, but demonstrates distinct trends with the geochemical composition of springs. The dissolved organic carbon concentrations are lowest in the hottest, most deeply sourced hot springs. Mixing of hydrothermal fluids with surface waters or reaction with buried sedimentary organic matter is typically indicated by increased dissolved organic carbon concentrations. I assessed the bulk composition of organic matter through fluorescence analysis that demonstrated different fluorescent components associated with terrestrial organic matter, microbial organic matter, and several novel fluorescent signatures unique to hot springs. One novel fluorescence signature is observed exclusively in acidic hot springs, and it is likely an end product of thermally-altered sedimentary organic matter. This acid-spring component precipitates out of solution under neutral or alkaline conditions and characterization of the precipitate revealed evidence for a highly condensed aromatic structure. This acid-spring component serves as a reliable tracer of acidic, hot water that has cycled through the subsurface. Overall, dissolved organic carbon concentrations and fluorescent features correlate with the inorganic indicators traditionally used to infer spring fluid mixing in the subsurface. Further, the fluorescence information reveals subtle differences in mixing between fluid phases that are not distinguishable through classic inorganic indicator species. My work assessing dissolved organic carbon in the Yellowstone National Park hot springs reveals that the organic matter in hydrothermal systems is different from that found in surface waters, and that the concentration and composition of hot spring dissolved organic matter reflects the subsurface geochemical and hydrological environment.

ACKNOWLEDGMENTS

There are many people that have supported me throughout my graduate career. First and foremost I thank my advisor Hilairy Hartnett for the immense support she has given me over the course of my PhD. Without the opportunities and experiences she provided me, I would not have become the scientist I am today. I also acknowledge my other committee members Anne Jones and Everett Shock, and other professors including Ian Gould, Ariel Anbar, Eric Boyd, and Scott Sayres who have made an impact on my career through classes taught or advice given.

I acknowledge my colleagues in the CaNDy lab: Donny Glaser, Nick Elms, Monica Palta, Zach Smith, Maggie Bowman, and our many fantastic undergraduate student researchers for helpful discussion and laboratory work. I thank members of the GEOPIG lab including Kris Fecteau and Randall "Vince" Debes for their instrumental role in planning and conducting the extensive field expeditions in Yellowstone National Park, as well as Kirt Robinson, Alta Howells, and Grant Loescher for helpful discussion and instrumental analysis. Members of the HOG group were instrumental to the start of my career at ASU and I thank Lynda Williams, Christa Bockisch, Kristin Johnson, Ziming Yang, and Charlene Estrada for helpful discussion and assistance in experimental design.

Other colleagues and friends that I want to thank include Marely Tejeda, Brian Woodrum, Stephen Romaniello, Aleisha Johnson, Alyssa Sherry, Amanda Young-Gonzalez, Claire Crowther, Chris Rock, Alex Buchberger, and Jake Garcia for their contributions to both my academic and social life. I graciously acknowledge Brian Hedlund and the PIRE group as well as Steven Desch and the NExSS group for providing funding throughout my career. Additionally, I thank the team members and

animal inhabitants of OdySea Aquarium as they have provided me with many learning opportunities over the past several years in regards to animal husbandry, conservation, and environmental protection. I specifically thank Eric Anderson, Courtney Church, and Courtney Holden as team members who taught me how water quality impacts animal health.

Last, but certainly not least, I thank my family: my parents Jim and Julie, my sisters Britta, Maria, and Greta, and my grandparents, aunts, uncles, and cousins who are too numerous to name here. I never would have made it this far without the immeasurable support they have given me during my entire academic career. I also acknowledge my animal companions: Dionysus, Ariadne, Persephone, Demeter, Hermes, Ares, Selene, Diana, Artemis, and Athena that have been, and continue to be, an important part of my life.

TABLE OF CONTENTS

CHAPTER Page

CHAPTER Page

CHAPTER Page

LIST OF TABLES

LIST OF FIGURES

Figure Page

Figure Page

Figure Page

Chapter 1

INTRODUCTION

1.1 What Is Dissolved Organic Matter?

The overarching theme of the research presented in this dissertation is to evaluate dissolved organic carbon concentrations and compositions in the hot springs of Yellowstone National Park. Dissolved organic matter (DOM) is a complex mixture of small and large organic compounds, primarily derived from plant, animal, and microbial biomass and consisting of large biopolymers and their degradation products and is an essential component of the carbon cycle on Earth. These large biopolymers (lignin, cellulose, other plant and animal material) are broken down by chemical reactions (Pettersen, 1984; Alberts and Takács, 2004; Ohno et al., 2007; Beggs and Summers, 2011; LaRowe and Van Cappellen, 2011), photo-reactions (Laurion et al., 2000; Hansell et al., 2009; Stubbins et al., 2010; De Laurentiis et al., 2012; Bianco et al., 2014), and microbial activity (Kalbitz et al., 2000; Hansell et al., 2009; Meng et al., 2012; Kellerman et al., 2018; Shah Walter et al., 2018) and can be incorporated into new biomass (Hardison et al., 2010; Singh et al., 2010), buried in sediments and sequestered (Berner, 1982; Hedges et al., 1997; Meyers, 2007; Jiao et al., 2010; Müller et al., 2010; Kellerman et al., 2018), or released back into the atmosphere as CO_2 or CH_4 (Reeburgh, 2007; Kirschke et al., 2013; Catalán et al., 2016). Changes in DOM composition result in changing bioavailability of carbon and other essential elements (Lovley et al., 1996; Mayer et al., 1998; Müller et al., 2010; Meng et al., 2014; Wichard, 2016), mobility in aquatic environments (Meybeck, 1993; Kandasamy and Nagender Nath, 2016), ability to bind metals (Bailey et al., 1999; Rose and

Waite, 2003; Ohno et al., 2008; Yamashita and Jaffé, 2008; Taha et al., 2009; Gledhill, 2012; Riedel et al., 2012; Adegboyega et al., 2013; Chiasson-Gould et al., 2014; He and Chen, 2014), and capacity for ultra-violet (UV) light absorption (Laurion et al., 2000; Weishaar et al., 2003; Stubbins et al., 2010; Bianco et al., 2014). A primary challenge in characterizing DOM is that it is enormously complex material that is impractical to describe by the molecular formulas of its many individual components. Bulk properties such as molecular mass, particle size, elemental makeup, functional group character, or optical properties are often determined (Briucaud et al., 1981; Chin et al., 1994; Parlanti et al., 2002; Alberts and Takács, 2004; Del Vecchio and Blough, 2004; Cory and McKnight, 2005; Coble, 2007; Hudson et al., 2007; Stedmon and Bro, 2008; Murphy et al., 2010; Stubbins et al., 2014; Kellerman et al., 2018). DOM serves as a connector in understanding the relationship between hydrology and biogeochemistry as they relate to the total environment.

The role DOM plays in the global carbon cycle through surface water environments has been increasingly investigated over the past several decades, but there is still a significant knowledge gap when it comes to DOM circulation in hydrothermal environments. Although hydrothermal fluids make up a relatively small fraction of liquid water on Earth, they may play a profound role in carbon cycling due to enhanced rates of reactivity (Hawkes et al., 2015, 2016; Kompanichenko et al., 2016; Rossel et al., 2017). The alteration of DOM in lakes, rivers, estuaries, and oceans can be investigated by direct sampling at regular intervals as water moves laterally across the land and mixes in coastal environments (Meybeck, 1993; Mayer et al., 1998; Raymond and Bauer, 2001; Boehm et al., 2011; Chen et al., 2013; Maie et al., 2014), or also cycles between deep and shallow reservoirs (Berner, 1982; Carlson et al., 1994; Hedges et al., 1997; Kandasamy and Nagender Nath, 2016). Point sources of new carbon can also be identified (Parlanti et al., 2000; Wilson and Xenopoulos, 2009;

Cawley et al., 2012). Hydrothermal systems pose a challenge for hydrological study because the majority of the system is inaccessible, being underground, and the only direct analysis that can be done is on the surface discharges of thermal fluid, such as hot springs. The geochemical range of surface waters is limited relative to hydrothermal systems; freshwaters typically range in pH from 6.0 to 8.5 and seawater ranges from 7.5 to 8.5 (Fondriest Environmental, Inc., 2013, 2014), but some "black water" rivers in the Amazon can have pH values below 4.5 (Duarte et al., 2016) and rare soda lakes or serpentinized fluids can reach a pH as high as 12 (Miller et al., 2016). Temperatures in these surface water systems rarely exceed 35℃. The geochemical and physical conditions in hot springs encompass a broader range (Figure 1.1). Additionally, hydrothermal fluids in the subsurface can reach temperatures as high as 400℃ as well as increased pressures, exceeding 1000 bar (Arnórsson et al., 2007; Liebscher, 2007; Hawkes et al., 2016). There is very limited information on how DOM circulation and alteration in the extreme physical and geochemical environments of hydrothermal systems. Experimental work reveals greatly increased reactivity and available alteration mechanisms of target organic compounds in high temperature, high pressure laboratory reactions.

1.2 Hydrothermal Transformation of Organic Compounds

The reactivity of organic compounds at high temperatures and pressures has been studied experimentally in laboratory conditions (McCollom et al., 1999a,b; Yang et al., 2012; McCollom, 2013; Shipp et al., 2013; Shock et al., 2013; Bockisch et al., 2018; Mißbach et al., 2018; Robinson et al., 2019; Shock et al., 2019). Under hydrothermal conditions, the dielectric constant of water decreases making it more nonpolar and a better solvent for organic compounds (Bradley and Pitzer, 1979; Shock and Helgeson, 1990; Fernández et al., 1995; Liebscher, 2010). Additionally, the pKa

of water drops so that the pH of a neutral solution hits a minimum of 5.6 at 230℃ (Bandura and Lvov, 2006; Liebscher, 2010), increasing the potential for acid and base catalysis. Organic compounds in high temperature environments are traditionally assumed to degrade to smaller molecules and eventually, to CO_2 or CH_4. While large, complex organic matter does break down into smaller products (Hawkes et al., 2016), these small organic compounds can be highly resistant to complete degradation, but readily subject to compositional alteration. In closed systems many organic reactions are in fact reversible and the equilibrium of such reactions can reflect the redox conditions of the environment (Simoneit, 1993; Bockisch et al., 2018; Robinson et al., 2020). Most experimental work currently involves mechanistic study of simple compound mixtures in the presence of single mineral catalysts so application of these results to explain environmental reactions of complex, natural organic matter is not yet possible. Field work and direct analysis of environmental organic matter in hydrothermal systems will serve as a top-down approach to complement the bottom-up experimental work to tackle the question of what happens to organic matter in hydrothermal conditions.

1.3 Yellowstone National Park

The largest continental hot spring system in the world is located in Yellowstone National Park, Wyoming, USA and is a prime field site to study DOM circulation and alteration in hydrothermal conditions as it contains over 10,000 thermal features encompassing a broad range in geochemical and physical character. I took part in five field expeditions over the course of my dissertation, sampled hundreds of springs, and in every trip, I observed completely new and unique hot springs, some of which have only ever been seen by a select few researchers. The earliest scientific descriptions of the Yellowstone National Park thermal features date from the late 1800's

(Gooch and Whitfield, 1888) and the first major publication of spring chemistry was presented in Allen and Day (1935). Since then, thousands of papers and reports have been published assessing the relationship between the geophysics, geochemistry, hydrology, and microbiology as they relate to the thermal fluids in Yellowstone. The thermal features in Yellowstone are fed by a single, 370℃ parent fluid 3.4 km beneath Yellowstone (Fournier, 1977, 1989; Rye and Truesdell, 2007; Hurwitz and Lowenstern, 2014). The geochemical composition of this deep fluid is driven by mantle-derived gases (HCl, CO_2, and SO_2) and deep water-rock reactions. As the hydrothermal fluid rises, chemical and physical processes alter this composition, similar to how the chemical makeup of a river changes as it flows across the land. Alteration processes include water-rock reactions, high temperature and pressure reactions, boiling processes, phase separations, discharge of volatile gases, mixing with surface fluids, and microbial activity near the surface (Brock and Mosser, 1975; White et al., 1971; Fournier, 1989; Werner et al., 2000; Kharaka et al., 2002; Nordstrom et al., 2009; Holloway et al., 2011; Gardner et al., 2011). Many inorganic chemical indicators are used to generate geochemical models that explain the diverse chemical compositions of hot springs that rely on inorganic indicators such as pH, temperature, silica, chloride, bicarbonate, sulfate, sodium, potassium, calcium, magnesium, helium isotopes, water isotopes, and gas discharges. Despite the extensive chemical analysis of springs that has been occurring for nearly a century, there has been very little work done analyzing the bulk organic matter issuing from hot springs. Most work involving organic carbon is specific to certain compounds in local environments and not to the bulk DOM across the entire park.

Research on bulk organic carbon in hydrothermal systems is limited, and the majority of work that exists is very recent and dominantly for marine seafloor vent environments (Simoneit, 1993; Hawkes et al., 2015; Gomez-Saez et al., 2016; Rossel

et al., 2017). The amount of organic carbon in end-member hydrothermal fluids is low relative to surface environments and their organic composition is unique (Hawkes et al., 2015; Gomez-Saez et al., 2016; Kompanichenko et al., 2016; Gonsior et al., 2018). In one recent publication (Gonsior et al., 2018) the bulk DOM was analyzed in 10 hot springs in Yellowstone National Park. Novel molecular formula and compositions were observed, especially in relation to organic sulfur and nitrogen species, but 10 samples are unlikely to be representative of the entire system and there is need for a broad scale assessment. In Yellowstone, most research involving organic carbon is focused on hydrocarbon gas discharge (Des Marais et al., 1981; Lorenson and Kvenvolden, 1993; Giggenbach, 1997; Werner et al., 2000), petroleum discharge (Clifton et al., 1990), microbial heterotrophy of small organics (Windman et al., 2007; Hamilton et al., 2011; Xie et al., 2014), and microbial metabolites (lipids) that serve as biomarkers of geochemical conditions (Boyd et al., 2013; Xie et al., 2014). The total contributions of thermally-altered, surface-derived organic matter and released buried sedimentary organic matter into hydrothermal fluids as they circulate within the subsurface has not been evaluated. The research in this dissertation serves as the first assessment of the geochemical and geographic distribution of DOC concentrations and compositions in Yellowstone National Park hot springs.

1.4 Layout of This Dissertation

In this dissertation I present a novel quantification of DOC and characterization of DOM in a large number of hot spring samples from Yellowstone National Park. The hot springs sampled for my data set encompass a broad range of pH, temperature, and other geochemical variability. What follows is a brief overview of the chapters of my dissertation. In my second chapter I employed fluorescence spectroscopy as an analytical technique to characterize major components of DOM. I identified and

quantified major fluorescence components through the generation of a five-component parallel-factor (PARAFAC) analysis model. I found three components connected with "humic-like", surface-derived organic matter, one novel fluorescence component appearing exclusively in acidic hot springs, and a protein-like component. I assess the distribution of DOC and the major PARAFAC components amongst hot springs as a function of spring pH. These initial findings reveal that the DOM composition in hot springs is widely variably, but also connected to spring geochemistry. I also concluded that fluorescence indices developed from surface water models were insufficient to describe hot spring FDOM.

My third chapter focuses on operational characterization of the novel acid-spring component. I demonstrate through experimentation that the acid-spring component fluorophores are exclusively acid-soluble and precipitate out of solution above a pH of 5. Sampling of hot spring sediments revealed these fluorophores in solid phase of a few higher pH springs, but largely revealed that these fluorophores are exclusive to a specific, acid-sulfate type of hydrothermal fluid. Analysis of the precipitated material revealed graphitic-like character through Raman spectroscopy, indicating a highly condensed aromatic structure consistent with a thermal degradation product. Natural wood samples were digested in simple hydrothermal experiments to evaluate the reactivity of refractory forms of organic matter (lignin) and fluorescence revealed the rapid breakdown of woody organic matter, but no generation of an exclusively acid-soluble fluorophore matching the novel component.

In my fourth chapter I investigate the variability of hot spring DOC concentrations and FDOM composition in the context of spring type classification as determined by chloride and sulfate concentrations (Nordstrom et al., 2009). It was revealed that DOM correlates highly with spring type and hydrothermal fluid sources and mixing processes. Analysis of DOC concentration and major FDOM distribution in

the park also revealed evidence of mixing that were not previously identifiable by inorganic indicators. Previously, acidic springs and vapor-phase dominated systems were assumed to be highly mixed and altered by surface water and ground, but my DOC and fluorescence data revealed the presence of some "pristine" acidic and vapor-phase dominated features. Additionally, it was made evident that not all dilution of hydrothermal fluid by dilute, MO-type water involves input of surface-derived organic matter.

The final chapter of this dissertation summarizes my research findings on dissolved organic matter in Yellowstone hot springs. I present major conclusions and new information provided by my work. I also suggest future directions on the study of organic matter in Yellowstone.

REFERENCES

Adegboyega, N. F., Sharma, V. K., Siskova, K., Zbořil, R., Sohn, M., Schultz, B. J., and Banerjee, S. (**2013**); Interactions of aqueous Ag with fulvic acids: Mechanisms of silver nanoparticle formation and investigation of stability. *Environmental Science & Technology* 47(2), pp. 757–764, doi:10.1021/es302305f.

Alberts, J. J. and Takács, M. (**2004**); Comparison of the natural fluorescence distribution among size fractions of terrestrial fulvic and humic acids and aquatic natural organic matter. *Organic Geochemistry* 35(10), pp. 1141–1149, doi:10.1016/j.orggeochem.2004.06.010.

Allen, E. T. and Day, A. L. (**1935**); Hot springs of the Yellowstone National Park. Carnegie Institution of Washington Publication 466, Carnegie Institute, Washington D. C., USA.

Arnórsson, S., Stefánsson, A., and Bjarnason, J. O. (**2007**); Fluid-fluid interactions in geothermal systems. *Reviews in Mineralogy and Geochemistry* 65(1), pp. 259–312, doi:10.2138/rmg.2007.65.9.

Bailey, S. E., Olin, T. J., Bricka, R., and Adrian, D. (**1999**); A review of potentially low-cost sorbents for heavy metals. *Water Research* 33(11), pp. 2469–2479, doi:10.1016/S0043-1354(98)00475-8.

Bandura, A. V. and Lvov, S. N. (**2006**); The ionization constant of water over wide ranges of temperature and density. *Journal of Physical and Chemical Reference Data* 35(1), pp. 15–30, doi:10.1063/1.1928231.

Beggs, K. M. and Summers, R. S. (**2011**); Character and chlorine reactivity of dissolved organic matter from a mountain pine beetle impacted watershed. *Environmental Science & Technology* 45(13), pp. 5717–5724, doi:10.1021/es1042436.

Berner, R. A. (**1982**); Burial of organic carbon and pyrite sulfur in the modern ocean; its geochemical and environmental significance. *American Journal of Science* 282(4), pp. 451–473, doi:10.2475/ajs.282.4.451.

Bianco, A., Minella, M., De Laurentiis, E., Maurino, V., Minero, C., and Vione, D. (**2014**); Photochemical generation of photoactive compounds with fulvic-like and humic-like fluorescence in aqueous solution. *Chemosphere* 111, pp. 529–536, doi:10.1016/j.chemosphere.2014.04.035.

Bockisch, C., Lorance, E. D., Hartnett, H. E., Shock, E. L., and Gould, I. R. (**2018**); Kinetics and mechanisms of dehydration of secondary alcohols under hydrothermal conditions. *ACS Earth and Space Chemistry* 2(8), pp. 821–832, doi:10.1021/acsearthspacechem.8b00030.

Boehm, A. B., Yamahara, K. M., Walters, S. P., Layton, B. A., Keymer, D. P., Thompson, R. S., Knee, K. L., and Rosener, M. (**2011**); Dissolved inorganic nitrogen, soluble reactive phosphorous, and microbial pollutant loading from tropical

rural watersheds in Hawai'i to the coastal ocean during non-storm conditions. *Estuaries and Coasts* 34(5), pp. 925–936, doi:10.1007/s12237-010-9352-8.

Boyd, E. S., Hamilton, T. L., Wang, J., He, L., and Zhang, C. L. (**2013**); The role of tetraether lipid composition in the adaptation of thermophilic archaea to acidity. *Frontiers in Microbiology* 4(62), doi:10.3389/fmicb.2013.00062.

Bradley, D. J. and Pitzer, K. S. (**1979**); Thermodynamics of electrolytes. 12. Dielectric properties of water and Debye-Hückel parameters to 350℃ and 1 kbar. *The Journal of Physical Chemistry* 83(12), pp. 1599–1603, doi:10.1021/j100475a009.

Briucaud, A., Morel, A., and Prieur, L. (**1981**); Absorption by dissolved organic matter of the sea (yellow substance) in the UV and visible domains. *Limnology and Oceanography* 26(1), pp. 43–53, doi:10.4319/lo.1981.26.1.0043.

Brock, T. and Mosser, J. (**1975**); Rate of sulfuric acid production in Yellowstone National Park. *Geological Society of America Bulletin* 86(2), pp. 194–198, doi:10.1130/0016-7606(1975)86⟨194:ROSPIY⟩2.0.CO;2.

Carlson, C. A., Ducklow, H. W., and Michaels, A. F. (**1994**); Annual flux of dissolved organic carbon from the euphotic zone in the northwestern Sargasso Sea. *Nature* 371(6496), pp. 405–408, doi:10.1038/371405a0.

Catalán, N., Marcé, R., Kothawala, D. N., and Tranvik, L. J. (**2016**); Organic carbon decomposition rates controlled by water retention time across inland waters. *Nature Geoscience* 9(7), pp. 501–504, doi:10.1038/ngeo2720.

Cawley, K. M., Butler, K. D., Aiken, G. R., Larsen, L. G., Huntington, T. G., and McKnight, D. M. (**2012**); Identifying fluorescent pulp mill effluent in the Gulf of Maine and its watershed. *Marine Pollution Bulletin* 64(8), pp. 1678–1687, doi:10.1016/j.marpolbul.2012.05.040.

Chen, M., Maie, N., Parish, K., and Jaffé, R. (**2013**); Spatial and temporal variability of dissolved organic matter quantity and composition in an oligotrophic subtropical coastal wetland. *Biogeochemistry* 115(1-3), pp. 167–183, doi:10.1007/s10533-013-9826-4.

Chiasson-Gould, S. A., Blais, J. M., and Poulain, A. J. (**2014**); Dissolved organic matter kinetically controls mercury bioavailability to bacteria. *Environmental Science & Technology* 48(6), pp. 3153–3161, doi:10.1021/es4038484.

Chin, Y.-P., Aiken, G. R., and O'Loughlin, E. (**1994**); Molecular weight, polydispersity, and spectroscopic properties of aquatic humic substances. *Environmental Science & Technology* 28(11), pp. 1853–1858, doi:10.1021/es00060a015.

Clifton, C., Walters, C., and Simoneit, B. (**1990**); Hydrothermal petroleums from Yellowstone National Park, Wyoming, U.S.A. *Applied Geochemistry* 5(1-2), pp. 169–191, doi:10.1016/0883-2927(90)90047-9.

Coble, P. G. (**2007**); Marine optical biogeochemistry: The chemistry of ocean color. *Chemical Reviews* 107(2), pp. 402–418, doi:10.1021/cr050350+.

Cory, R. M. and McKnight, D. M. (**2005**); Fluorescence spectroscopy reveals ubiquitous presence of oxidized and reduced quinones in dissolved organic matter. *Environmental Science & Technology* 39(21), pp. 8142–8149, doi:10.1021/es0506962.

De Laurentiis, E., Minella, M., Maurino, V., Minero, C., Brigante, M., Mailhot, G., and Vione, D. (**2012**); Photochemical production of organic matter triplet states in water samples from mountain lakes, located below or above the tree line. *Chemosphere* 88(10), pp. 1208–1213, doi:10.1016/j.chemosphere.2012.03.071.

Del Vecchio, R. and Blough, N. V. (**2004**); Spatial and seasonal distribution of chromophoric dissolved organic matter and dissolved organic carbon in the Middle Atlantic Bight. *Marine Chemistry* 89(1-4), pp. 169–187, doi:10.1016/j.marchem.20 04.02.027.

Des Marais, D. J., Donchin, J. H., Nehring, N. L., and Truesdell, A. H. (**1981**); Molecular carbon isotopic evidence for the origin of geothermal hydrocarbons. *Nature* 292(5826), pp. 826–828, doi:10.1038/292826a0.

Duarte, R. M., Smith, D. S., Val, A. L., and Wood, C. M. (**2016**); Dissolved organic carbon from the upper Rio Negro protects zebrafish (*Danio rerio*) against ionoregulatory disturbances caused by low pH exposure. *Scientific Reports* 6(1), p. 20377, doi:10.1038/srep20377.

Fernández, D. P., Mulev, Y., Goodwin, A. R. H., and Sengers, J. M. H. L. (**1995**); A database for the static dielectric constant of water and steam. *Journal of Physical and Chemical Reference Data* 24(1), pp. 33–70, doi:10.1063/1.555977.

Fondriest Environmental, Inc. (**2013**); pH of Water. Fundamentals of Environmental Measurements. 19 Nov 2013. https://www.fondriest.com/environmental-measur ements/parameters/water-quality/ph/.

Fondriest Environmental, Inc. (**2014**); Water Temperature. Fundamentals of Environmental Measurements. 7 Feb 2014. https://www.fondriest.com/environmental-measurements/parameters/water-quality/water-temperature/.

Fournier, R. (**1977**); Chemical geothermometers and mixing models for geothermal systems. *Geothermics* 5(1-4), pp. 41–50, doi:10.1016/0375-6505(77)90007-4.

Fournier, R. O. (**1989**); Geochemistry and dynamics of the Yellowstone National Park hydrothermal system. *Annual Review of Earth and Planetary Sciences* 17(1), pp. 13–53, doi:10.1146/annurev.ea.17.050189.000305.

Gardner, W. P., Susong, D. D., Solomon, D. K., and Heasler, H. P. (**2011**); A multitracer approach for characterizing interactions between shallow groundwater and the hydrothermal system in the Norris Geyser Basin area, Yellowstone National Park. *Geochemistry, Geophysics, Geosystems* 12(8), doi:10.1029/2010GC003353.

Giggenbach, W. F. (**1997**); Relative importance of thermodynamic and kinetic processes in governing the chemical and isotopic composition of carbon gases in high heatflow sedimentary basins. *Geochimica et Cosmochimica Acta* 61(17), pp. 3763–3785, doi:10.1016/S0016-7037(97)00171-3.

Gledhill, M. (**2012**); The organic complexation of iron in the marine environment: A review. *Frontiers in Microbiology* 3(69), doi:10.3389/fmicb.2012.00069.

Gomez-Saez, G. V., Niggemann, J., Dittmar, T., Pohlabeln, A. M., Lang, S. Q., Noowong, A., Pichler, T., Wörmer, L., and Bühring, S. I. (**2016**); Molecular evidence for abiotic sulfurization of dissolved organic matter in marine shallow hydrothermal systems. *Geochimica et Cosmochimica Acta* 190, pp. 35–52, doi: 10.1016/j.gca.2016.06.027.

Gonsior, M., Hertkorn, N., Hinman, N., Dvorski, S. E.-M., Harir, M., Cooper, W. J., and Schmitt-Kopplin, P. (**2018**); Yellowstone hot springs are organic chemodiversity hot spots. *Scientific Reports* 8(1), p. 14155, doi:10.1038/s41598-018-32593-x.

Gooch, F. A. and Whitfield, J. E. (**1888**); *Analyses of Waters of the Yellowstone National Park*. Bulletin of the United States Geological Survey no. 47, United States Geoglical Survey, doi:10.3133/b47.

Hamilton, T. L., Boyd, E. S., and Peters, J. W. (**2011**); Environmental constraints underpin the distribution and phylogenetic diversity of nifH in the Yellowstone geothermal complex. *Microbial Ecology* 61(4), pp. 860–870, doi:10.1007/s00248-011-9824-9.

Hansell, D., Carlson, C., Repeta, D., and Schlitzer, R. (**2009**); Dissolved organic matter in the ocean: A controversy stimulates new insights. *Oceanography* 22(4), pp. 202–211, doi:10.5670/oceanog.2009.109.

Hardison, A., Canuel, E., Anderson, I., and Veuger, B. (**2010**); Fate of macroalgae in benthic systems: carbon and nitrogen cycling within the microbial community. *Marine Ecology Progress Series* 414, pp. 41–55, doi:10.3354/meps08720.

Hawkes, J. A., Rossel, P. E., Stubbins, A., Butterfield, D., Connelly, D. P., Achterberg, E. P., Koschinsky, A., Chavagnac, V., Hansen, C. T., Bach, W., and Dittmar, T. (**2015**); Efficient removal of recalcitrant deep-ocean dissolved organic matter during hydrothermal circulation. *Nature Geoscience* 8, pp. 856–860, doi: 10.1038/ngeo2543.

Hawkes, J. A., Hansen, C. T., Goldhammer, T., Bach, W., and Dittmar, T. (**2016**); Molecular alteration of marine dissolved organic matter under experimental hydrothermal conditions. *Geochimica et Cosmochimica Acta* 175, pp. 68–85, doi: 10.1016/j.gca.2015.11.025.

He, J. and Chen, J. P. (**2014**); A comprehensive review on biosorption of heavy metals by algal biomass: Materials, performances, chemistry, and modeling simulation tools. *Bioresource Technology* 160, pp. 67–78, doi:10.1016/j.biortech.2014.01.068.

Hedges, J., Keil, R., and Benner, R. (**1997**); What happens to terrestrial organic matter in the ocean? *Organic Geochemistry* 27(5-6), pp. 195–212, doi:10.1016/S0146-6380(97)00066-1.

Holloway, J. M., Nordstrom, D. K., Böhlke, J., McCleskey, R. B., and Ball, J. W. (**2011**); Ammonium in thermal waters of Yellowstone National Park: Processes affecting speciation and isotope fractionation. *Geochimica et Cosmochimica Acta* 75(16), pp. 4611–4636, doi:10.1016/j.gca.2011.05.036.

Hudson, N., Baker, A., and Reynolds, D. (**2007**); Fluorescence analysis of dissolved organic matter in natural, waste and polluted waters: A review. *River Research and Applications* 23(6), pp. 631–649, doi:10.1002/rra.1005.

Hurwitz, S. and Lowenstern, J. B. (**2014**); Dynamics of the Yellowstone hydrothermal system. *Reviews of Geophysics* 52(3), pp. 375–411, doi:10.1002/2014RG000452.

Jiao, N., Herndl, G. J., Hansell, D. A., Benner, R., Kattner, G., Wilhelm, S. W., Kirchman, D. L., Weinbauer, M. G., Luo, T., Chen, F., and Azam, F. (**2010**); Microbial production of recalcitrant dissolved organic matter: Long-term carbon storage in the global ocean. *Nature Reviews Microbiology* 8(8), pp. 593–599, doi:10.1038/nrmicro2386.

Kalbitz, K., Solinger, S., Park, J.-H., Michalzik, B., and Matzner, E. (**2000**); Controls on the dynamics of dissolved organic matter in soils. *Soil Science* 165(4), pp. 277–304, doi:10.1097/00010694-200004000-00001.

Kandasamy, S. and Nagender Nath, B. (**2016**); Perspectives on the terrestrial organic matter transport and burial along the land-deep sea continuum: Caveats in our understanding of biogeochemical processes and future needs. *Frontiers in Marine Science* 3, doi:10.3389/fmars.2016.00259.

Kellerman, A. M., Guillemette, F., Podgorski, D. C., Aiken, G. R., Butler, K. D., and Spencer, R. G. M. (**2018**); Unifying concepts linking dissolved organic matter composition to persistence in aquatic ecosystems. *Environmental Science & Technology* 52(5), pp. 2538–2548, doi:10.1021/acs.est.7b05513.

Kharaka, Y., Thordsen, J., and White, L. (**2002**); Isotope and chemical compositions of meteoric and thermal waters and snow from the greater Yellowstone National Park region. Open File Report 02-194, United States Geological Survey, doi:10.3133/ofr02194.

Kirschke, S., Bousquet, P., Ciais, P., Saunois, M., Canadell, J. G., Dlugokencky, E. J., Bergamaschi, P., Bergmann, D., Blake, D. R., Bruhwiler, L., Cameron-Smith, P., Castaldi, S., Chevallier, F., Feng, L., Fraser, A., Heimann, M., Hodson, E. L., Houweling, S., Josse, B., Fraser, P. J., Krummel, P. B., Lamarque, J.-F., Langenfelds, R. L., Le Quéré, C., Naik, V., O'Doherty, S., Palmer, P. I., Pison, I., Plummer, D., Poulter, B., Prinn, R. G., Rigby, M., Ringeval, B., Santini, M., Schmidt, M., Shindell, D. T., Simpson, I. J., Spahni, R., Steele, L. P., Strode, S. A., Sudo, K., Szopa, S., van der Werf, G. R., Voulgarakis, A., van Weele, M., Weiss, R. F., Williams, J. E., and Zeng, G. (**2013**); Three decades of global methane sources and sinks. *Nature Geoscience* 6(10), pp. 813–823, doi:10.1038/ngeo1955.

Kompanichenko, V. N., Poturay, V. A., and Karpov, G. A. (**2016**); Organic compounds in thermal water: The Mutnovskii area and the Uzon caldera. *Journal of Volcanology and Seismology* 10(5), pp. 305–319, doi:10.1134/S0742046316050031.

LaRowe, D. E. and Van Cappellen, P. (**2011**); Degradation of natural organic matter: A thermodynamic analysis. *Geochimica et Cosmochimica Acta* 75(8), pp. 2030–2042, doi:10.1016/j.gca.2011.01.020.

Laurion, I., Ventura, M., Catalan, J., Psenner, R., and Sommaruga, R. (**2000**); Attenuation of ultraviolet radiation in mountain lakes: Factors controlling the among- and within-lake variability. *Limnology and Oceanography* 45(6), pp. 1274–1288, doi:10.4319/lo.2000.45.6.1274.

Liebscher, A. (**2007**); Experimental studies in model fluid systems. *Reviews in Mineralogy and Geochemistry* 65(1), pp. 15–47, doi:10.2138/rmg.2007.65.2.

Liebscher, A. (**2010**); Aqueous fluids at elevated pressure and temperature: Aqueous fluids at elevated pressure and temperature. *Geofluids* 10(1-2), pp. 3–19, doi:10.1111/j.1468-8123.2010.00293.x.

Lorenson, T. D. and Kvenvolden, K. A. (**1993**); A comparison of hydrocarbon gases from natural sources in the Northwestern United States. In: Howell, D. G., Wiese, K., Fanelli, M., Zink, L., and Cole, F. (eds.), *The Future of Energy Gases*, pp. 453–469, Professional Paper 1570, United States Geological Survey, doi:10.3133/pp1570.

Lovley, D. R., Coates, J. D., Blunt-Harris, E. L., Phillips, E. J. P., and Woodward, J. C. (**1996**); Humic substances as electron acceptors for microbial respiration. *Nature* 382(6590), pp. 445–448, doi:10.1038/382445a0.

Maie, N., Sekiguchi, S., Watanabe, A., Tsutsuki, K., Yamashita, Y., Melling, L., Cawley, K. M., Shima, E., and Jaffé, R. (**2014**); Dissolved organic matter dynamics in the oligo/meso-haline zone of wetland-influenced coastal rivers. *Journal of Sea Research* 91, pp. 58–69, doi:10.1016/j.seares.2014.02.016.

Mayer, L. M., Keil, R. G., Macko, S. A., Joye, S. B., Ruttenberg, K. C., and Aller, R. C. (**1998**); Importance of suspended participates in riverine delivery of bioavailable nitrogen to coastal zones. *Global Biogeochemical Cycles* 12(4), pp. 573–579, doi:10.1029/98GB02267.

McCollom, T. M. (**2013**); Miller-Urey and beyond: What have we learned about prebiotic organic synthesis reactions in the past 60 years? *Annual Review of Earth and Planetary Sciences* 41(1), pp. 207–229, doi:10.1146/annurev-earth-040610-133457.

McCollom, T. M., Ritter, G., and Simoneit, B. R. T. (**1999**a); Lipid synthesis under hydrothermal conditions by Fischer-Tropsch-type reactions. *Origins of Life and Evolution of the Biosphere* 29(2), pp. 153–166, doi:10.1023/A:1006592502746.

McCollom, T. M., Simoneit, B. R. T., and Shock, E. L. (**1999**b); Hydrous pyrolysis of polycyclic aromatic hydrocarbons and implications for the origin of PAH in hydrothermal petroleum. *Energy & Fuels* 13(2), pp. 401–410, doi:10.1021/ef980089i.

Meng, F., Huang, G., Li, Z., and Li, S. (**2012**); Microbial transformation of structural and functional makeup of human-impacted riverine dissolved organic matter. *Industrial & Engineering Chemistry Research* 51(17), pp. 6212–6218, doi:10.1021/ie300504d.

Meng, J., Yao, P., Yu, Z., Bianchi, T. S., Zhao, B., Pan, H., and Li, D. (**2014**); Speciation, bioavailability and preservation of phosphorus in surface sediments of the Changjiang Estuary and adjacent East China Sea inner shelf. *Estuarine, Coastal and Shelf Science* 144, pp. 27–38, doi:10.1016/j.ecss.2014.04.015.

Meybeck, M. (**1993**); Riverine transport of atmospheric carbon: Sources, global typology and budget. *Water, Air, & Soil Pollution* 70(1-4), pp. 443–463, doi:10.1007/BF01105015.

Meyers, S. R. (**2007**); Production and preservation of organic matter: The significance of iron. *Paleoceanography* 22(4), doi:10.1029/2006PA001332.

Mißbach, H., Schmidt, B. C., Duda, J.-P., Lünsdorf, N. K., Goetz, W., and Thiel, V. (**2018**); Assessing the diversity of lipids formed via Fischer-Tropsch-type reactions. *Organic Geochemistry* 119, pp. 110–121, doi:10.1016/j.orggeochem.2018.02.012.

Miller, H. M., Matter, J. M., Kelemen, P., Ellison, E. T., Conrad, M. E., Fierer, N., Ruchala, T., Tominaga, M., and Templeton, A. S. (**2016**); Modern water/rock reactions in Oman hyperalkaline peridotite aquifers and implications for microbial habitability. *Geochimica et Cosmochimica Acta* 179, pp. 217–241, doi:10.1016/j.gca.2016.01.033.

Müller, M., Handley, K. M., Lloyd, J., Pancost, R. D., and Mills, R. A. (**2010**); Biogeochemical controls on microbial diversity in seafloor sulphidic sediments. *Geobiology* 8(4), pp. 309–326, doi:10.1111/j.1472-4669.2010.00242.x.

Murphy, K. R., Butler, K. D., Spencer, R. G. M., Stedmon, C. A., Boehme, J. R., and Aiken, G. R. (**2010**); Measurement of dissolved organic matter fluorescence in aquatic environments: An interlaboratory comparison. *Environmental Science & Technology* 44(24), pp. 9405–9412, doi:10.1021/es102362t.

Nordstrom, K. D., McCleskey, B. R., and Ball, J. W. (**2009**); Sulfur geochemistry of hydrothermal waters in Yellowstone National Park: IV Acid-sulfate waters. *Applied Geochemistry* 24(2), pp. 191–207, doi:10.1016/j.apgeochem.2008.11.019.

Ohno, T., Fernandez, I. J., Hiradate, S., and Sherman, J. F. (**2007**); Effects of soil acidification and forest type on water soluble soil organic matter properties. *Geoderma* 140(1-2), pp. 176–187, doi:10.1016/j.geoderma.2007.04.004.

Ohno, T., Amirbahman, A., and Bro, R. (**2008**); Parallel factor analysis of excitation-emission matrix fluorescence spectra of water soluble soil organic matter as basis for the determination of conditional metal binding parameters. *Environmental Science & Technology* 42(1), pp. 186–192, doi:10.1021/es071855f.

Parlanti, E., Wörz, K., Geoffroy, L., and Lamotte, M. (**2000**); Dissolved organic matter fluorescence spectroscopy as a tool to estimate biological activity in a coastal zone submitted to anthropogenic inputs. *Organic Geochemistry* 31(12), pp. 1765–1781, doi:10.1016/S0146-6380(00)00124-8.

Parlanti, E., Morin, B., and Vacher, L. (**2002**); Combined 3D-spectrofluorometry, high performance liquid chromatography and capillary electrophoresis for the characterization of dissolved organic matter in natural waters. *Organic Geochemistry* 33(3), pp. 221–236, doi:10.1016/S0146-6380(01)00154-1.

Pettersen, R. C. (**1984**); The chemical composition of wood. In: Rowell, R. (ed.), *The Chemistry of Solid Wood*, *Advances in Chemistry*, volume 207, pp. 57–126, American Chemical Society, Washington, D. C., USA, doi:10.1021/ba-1984-0207.ch002.

Raymond, P. A. and Bauer, J. E. (**2001**); Riverine export of aged terrestrial organic matter to the North Atlantic Ocean. *Nature* 409(6819), pp. 497–500, doi:10.1038/35054034.

Reeburgh, W. S. (**2007**); Oceanic methane biogeochemistry. *Chemical Reviews* 107(2), pp. 486–513, doi:10.1021/cr050362v.

Riedel, T., Biester, H., and Dittmar, T. (**2012**); Molecular fractionation of dissolved organic matter with metal salts. *Environmental Science & Technology* 46(8), pp. 4419–4426, doi:10.1021/es203901u.

Robinson, K. J., Gould, I. R., Fecteau, K. M., Hartnett, H. E., Williams, L. B., and Shock, E. L. (**2019**); Deamination reaction mechanisms of protonated amines under hydrothermal conditions. *Geochimica et Cosmochimica Acta* 244, pp. 113–128, doi:10.1016/j.gca.2018.09.020.

Robinson, K. J., Fecteau, K. M., Gould, I. R., Hartnett, H. E., Williams, L. B., and Shock, E. L. (**2020**); Metastable equilibrium of substitution reactions among oxygen- and nitrogen-bearing organic compounds at hydrothermal conditions. *Geochimica et Cosmochimica Acta* 272, pp. 93–104, doi:10.1016/j.gca.2019.12.030.

Rose, A. L. and Waite, T. (**2003**); Kinetics of iron complexation by dissolved natural organic matter in coastal waters. *Marine Chemistry* 84(1-2), pp. 85–103, doi:10.1016/S0304-4203(03)00113-0.

Rossel, P. E., Stubbins, A., Rebling, T., Koschinsky, A., Hawkes, J. A., and Dittmar, T. (**2017**); Thermally altered marine dissolved organic matter in hydrothermal fluids. *Organic Geochemistry* 110, pp. 73–86, doi:10.1016/j.orggeochem.2017.05.003.

Rye, R. O. and Truesdell, A. H. (**2007**); The question of recharge to the deep thermal reservoir underlying the geysers and hot springs of Yellowstone National Park. Professional Paper 1717-H, United States Geological Survey, doi:10.3133/pp1717H.

Shah Walter, S. R., Jaekel, U., Osterholz, H., Fisher, A. T., Huber, J. A., Pearson, A., Dittmar, T., and Girguis, P. R. (**2018**); Microbial decomposition of marine dissolved organic matter in cool oceanic crust. *Nature Geoscience* 11(5), pp. 334–339, doi:10.1038/s41561-018-0109-5.

Shipp, J., Gould, I. R., Herckes, P., Shock, E. L., Williams, L. B., and Hartnett, H. E. (**2013**); Organic functional group transformations in water at elevated temperature and pressure: Reversibility, reactivity, and mechanisms. *Geochimica et Cosmochimica Acta* 104, pp. 194–209, doi:10.1016/j.gca.2012.11.014.

Shock, E., Bockisch, C., Estrada, C., Fecteau, K., Gould, I. R., Hartnett, H., Johnson, K., Robinson, K., Shipp, J., and Williams, L. (**2019**); Earth as organic chemist. In: Orcutt, B. N., Daniel, I., and Dasgupta, R. (eds.), *Deep Carbon: Past and Present*, pp. 415–446, Cambridge University Press, Cambridge, UK, doi:10.1017/97811086 77950.014.

Shock, E. L. and Helgeson, H. C. (**1990**); Calculation of the thermodynamic and transport properties of aqueous species at high pressures and temperatures: Standard partial molal properties of organic species. *Geochimica et Cosmochimica Acta* 54(4), pp. 915–945, doi:10.1016/0016-7037(90)90429-O.

Shock, E. L., Canovas, P., Yang, Z., Boyer, G., Johnson, K., Robinson, K., Fecteau, K., Windman, T., and Cox, A. (**2013**); Thermodynamics of organic transformations in hydrothermal fluids. *Reviews in Mineralogy and Geochemistry* 76(1), pp. 311–350, doi:10.2138/rmg.2013.76.9.

Simoneit, B. R. (**1993**); Aqueous high-temperature and high-pressure organic geochemistry of hydrothermal vent systems. *Geochimica et Cosmochimica Acta* 57, pp. 3231–3243.

Singh, B. K., Bardgett, R. D., Smith, P., and Reay, D. S. (**2010**); Microorganisms and climate change: terrestrial feedbacks and mitigation options. *Nature Reviews Microbiology* 8(11), pp. 779–790, doi:10.1038/nrmicro2439.

Stedmon, C. A. and Bro, R. (**2008**); Characterizing dissolved organic matter fluorescence with parallel factor analysis, a tutorial: Fluorescence-PARAFAC analysis of DOM. *Limnology and Oceanography: Methods* 6(11), pp. 572–579, doi: 10.4319/lom.2008.6.572.

Stubbins, A., Spencer, R. G. M., Chen, H., Hatcher, P. G., Mopper, K., Hernes, P. J., Mwamba, V. L., Mangangu, A. M., Wabakanghanzi, J. N., and Six, J. (**2010**); Illuminated darkness: Molecular signatures of Congo River dissolved organic matter and its photochemical alteration as revealed by ultrahigh precision mass spectrometry. *Limnology and Oceanography* 55(4), pp. 1467–1477, doi: 10.4319/lo.2010.55.4.1467.

Stubbins, A., Lapierre, J.-F., Berggren, M., Prairie, Y. T., Dittmar, T., and del Giorgio, P. A. (**2014**); What's in an EEM? Molecular signatures associated with dissolved organic fluorescence in boreal Canada. *Environmental Science & Technology* 48(18), pp. 10598–10606, doi:10.1021/es502086e.

Taha, H. M., Said, H. A., Abbas, N. H., and Khaleafa, A. F. M. (**2009**); Biosorption and biodegradation of the antifouling compound tributyltin (TBT) by microalgae. *American-Eurasian Journal of Scientific Research* 4(1), pp. 1–6.

Weishaar, J. L., Aiken, G. R., Bergamaschi, B. A., Fram, M. S., Fujii, R., and Mopper, K. (**2003**); Evaluation of specific ultraviolet absorbance as an indicator of the chemical composition and reactivity of dissolved organic carbon. *Environmental Science & Technology* 37(20), pp. 4702–4708, doi:10.1021/es030360x.

Werner, C., Brantley, S. L., and Boomer, K. (**2000**); CO2 emissions related to the Yellowstone volcanic system. *Journal of Geophysical Research: Solid Earth* 105(B5), pp. 10831–10846, doi:10.1029/1999JB900331.

White, D. E., Muffler, L. J. P., and Truesdell, A. H. (**1971**); Vapor-dominated hydrothermal systems compared with hot-water systems. *Economic Geology* 66(1), pp. 75–97, doi:10.2113/gsecongeo.66.1.75.

Wichard, T. (**2016**); Identification of metallophores and organic ligands in the chemosphere of the marine macroalga ulva (chlorophyta) and at land-sea interfaces. *Frontiers in Marine Science* 3, doi:10.3389/fmars.2016.00131.

Wilson, H. F. and Xenopoulos, M. A. (**2009**); Effects of agricultural land use on the composition of fluvial dissolved organic matter. *Nature Geoscience* 2(1), pp. 37–41, doi:10.1038/ngeo391.

Windman, T., Zolotova, N., Schwandner, F., and Shock, E. L. (**2007**); Formate as an energy source for microbial metabolism in chemosynthetic zones of hydrothermal ecosystems. *Astrobiology* 7(6), pp. 873–890, doi:10.1089/ast.2007.0127.

Xie, W., Zhang, C. L., Wang, J., Chen, Y., Zhu, Y., de la Torre, J. R., Dong, H., Hartnett, H. E., Hedlund, B. P., and Klotz, M. G. (**2014**); Distribution of ether lipids and composition of the archaeal community in terrestrial geothermal springs: Impact of environmental variables: Archaeal lipids from terrestrial hot springs. *Environmental Microbiology* 17(5), pp. 1600–1614, doi:10.1111/1462-2920.12595.

Yamashita, Y. and Jaffé, R. (**2008**); Characterizing the interactions between trace metals and dissolved organic matter using excitation emission matrix and parallel factor analysis. *Environmental Science & Technology* 42(19), pp. 7374–7379, doi:10.1021/es801357h.

Yang, Z., Gould, I. R., Williams, L. B., Hartnett, H. E., and Shock, E. L. (**2012**); The central role of ketones in reversible and irreversible hydrothermal organic functional group transformations. *Geochimica et Cosmochimica Acta* 98, pp. 48–65, doi:10.1016/j.gca.2012.08.031.

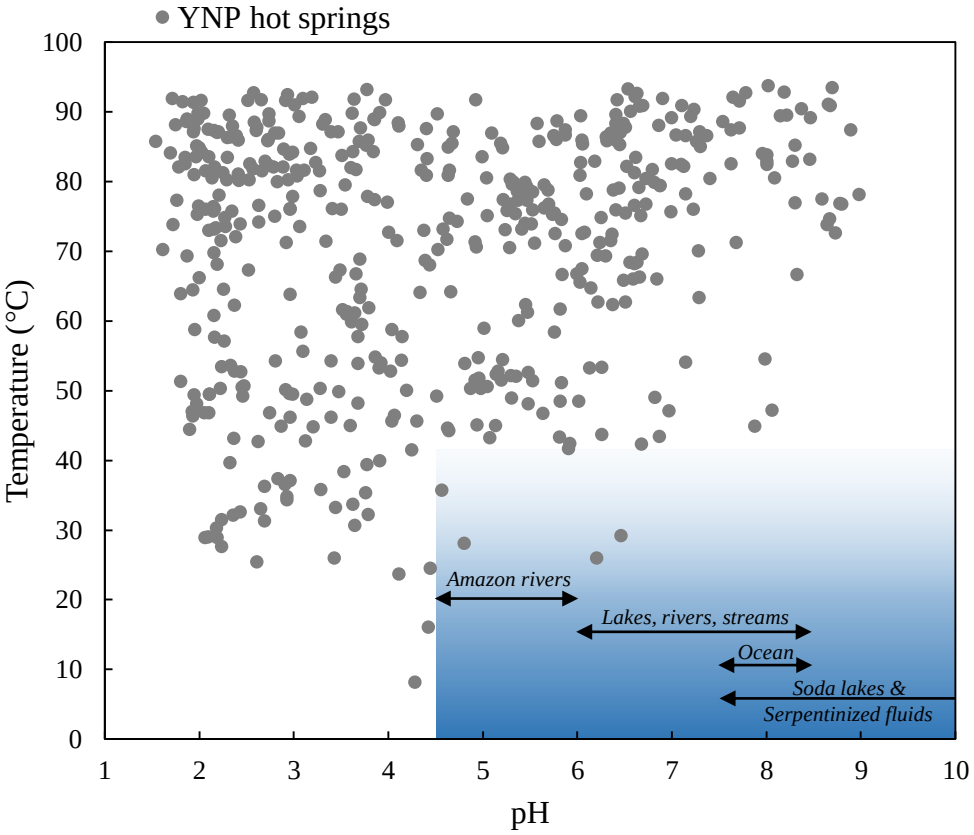

Figure 1.1: Global water pH and temperature. Thermal features sampled in YNP between 2012 and 2018 are shown as gray circles. The range of pH and temperatures in non-thermal, natural waters is shown in the blue box (Fondriest Environmental, Inc., 2013, 2014). Serpentinized fluids can reach pH values as high as 12 (Miller et al., 2016).

Chapter 2

A NOVEL PARAFAC MODEL FOR CONTINENTAL HOT SPRINGS REVEALS UNIQUE ORGANIC CARBON COMPOSITIONS

2.1 Abstract

Dissolved organic carbon in hot springs reflects a range of sources and biogeochemical processes. We evaluated ∼200 continental hot spring samples, with a range in pH and temperature, collected from the Tengchong hydrothermal region, Yunnan Province, China and Yellowstone National Park, Wyoming, USA. Dissolved organic carbon concentrations ranged from 16.7 μM to 2.97 mM. Acidic springs displayed the highest values and widest range in carbon concentration. Alkaline springs had a narrower range and lower average concentrations. Carbon composition was evaluated using ultraviolet absorption and 3D-fluorescence spectroscopy. Total fluorescence was correlated ($p < 0.05$) with dissolved organic carbon (DOC) concentration. Fluorescence excitation-emission matrices were deconvolved using parallel factor analysis. We validated a five-component model that represented >97% of the total fluorescence. Our model includes three humic-like components, one protein-like component, and one novel component exclusively observed in highly acidic springs. The closest spectral match to the novel component is an acid-soluble lignin produced during high-temperature, acid digestion of wood pulp. Humic-like components were dominant in mid-pH springs ($4 < pH < 7$) indicating these springs had greater terrestrial carbon input. Acidic springs also exhibited evidence for terrestrial carbon input. Alkaline springs, in contrast, consistently had low dissolved organic carbon content and low fluorescence intensity suggesting that these springs had little terrestrial input. This

absence of terrestrial carbon implies a predominantly hydrothermal fluid source. A comparison of the traditional fluorescence indices with our five model components suggest that these indices may have limited utility in continental hot springs with multiple organic matter sources and alteration processes.

2.2 Introduction

The composition and distribution of organic compounds in aquatic systems depends on both the source of the organic matter and its alteration by physical and/or biological processes. In the case of hydrothermal systems, our knowledge of these sources and processes is more limited because water is cycled through the Earth's subsurface, rather than above ground, where we can easily sample it. Investigations of deep, subsurface hydrothermal systems typically involve sampling the rare surface expressions of thermal fluid; namely hot springs, in the case of continental hydrothermal systems, such as Yellowstone National Park, Wyoming, USA. Dissolved organic matter (DOM) is a complex mixture of small organic compounds with multiple sources and a range of chemical reactivity. Briefly, in surface waters the major sources of DOM include allochthonous organic matter from terrestrial plants and soils, and autochthonous, microbially derived organic matter (Stedmon et al., 2003; Cory and McKnight, 2005; Yamashita et al., 2008; Hernes et al., 2009; Kowalczuk et al., 2009; Fellman et al., 2010; Murphy et al., 2010; Ishii and Boyer, 2012; Hansell and Carlson, 2014). Processes that alter DOM concentration and composition include photo-degradation, chemical transformation, metal complexation, microbial degradation, and human activity (Murphy et al., 2006; Stedmon et al., 2007; Ohno et al., 2008; Yamashita and Jaffé, 2008; Yamashita et al., 2008; Klevenz et al., 2010; Cawley et al., 2012; Ishii and Boyer, 2012; Carstea et al., 2014; Hansell and Carlson, 2014; He et al., 2016; Shah Walter et al., 2018; Kellerman et al., 2018). Our understanding

of DOM cycling in hydrothermal systems is more limited, but at a minimum we must also consider thermal alteration of DOM and the contribution of subsurface organic matter to hydrothermal fluids as major factors that affect hydrothermal DOM concentration and composition. The majority of the research to date on hydrothermal DOM has focused on seafloor vent systems; much less information is available for continental hot springs.

Bulk DOM in surface waters is frequently assessed using excitation-emission matrix (EEM) fluorescence spectroscopy (Cory and McKnight, 2005; Coble, 2007; Fellman et al., 2010; Murphy et al., 2010). The optical properties of FDOM have been widely correlated with autochthonous and allochthonous sources, changes in organic input across environments or time, mixing in estuaries and coastal environments, general water quality, anthropogenic input, bioreactivity, photo-degradability, 'humification' of soil organic matter, microbial degradation, and the total extent of DOM degradation (Murphy et al., 2006; Fellman et al., 2010; Ishii and Boyer, 2012; Cawley et al., 2012; Maie et al., 2014; Kellerman et al., 2018). EEM spectroscopy characterizes the fluorescent fraction of DOM (FDOM) according to the wavelengths of light that organic compounds absorb and emit. Typically, fluorescence results from the π to π^* excitation of the conjugated π-system in aromatic structures, so only organic compounds with aromatic character (e.g., aromatic rings) will fluoresce (Cory and McKnight, 2005). Given that aromatic DOM is susceptible to thermal alteration, but notably resistant to complete degradation (McCollom et al., 1999b, 2001), we expect FDOM to be prevalent in hydrothermal fluids. Although fluorescence spectroscopy is selective for an optically active fraction of bulk DOM, it has the advantage that it can be applied to a minimally processed sample that is only filtered and not chemically fractionated. Fluorescence measurement is also a relatively fast technique, it requires minimal sample preparation and low sample volumes, and it is a non-destructive anal-

ysis. All this makes it a useful technique that can be applied to a large number of samples collected in remote field locations.

An important source of organic matter unique to the Yellowstone ecosystem, in contrast to typical riverine or estuarine environments, is thermally altered, sedimentary organic matter (Des Marais et al., 1981; Clifton et al., 1990; Lorenson and Kvenvolden, 1993; Bergfeld et al., 2014). Degradation of buried biomass can cause multiple changes to carbon composition. Major products of the hydrothermal decomposition of buried sedimentary organic matter are gaseous hydrocarbons and refractory polycyclic aromatic hydrocarbons (PAHs; e.g., Clifton et al., 1990; Simoneit, 1993; Kawka and Simoneit, 1994; Simoneit and Fetzer, 1996; McCollom et al., 1999a,b; Simoneit et al., 1998; Seewald, 2003; Ventura et al., 2012; Urschel et al., 2015; Kompanichenko et al., 2016; Mißbach et al., 2018). The light hydrocarbons are often volatilized and released in gaseous discharges, contributing to a decreasing dissolved organic carbon (DOC) concentration in deep hydrothermal fluids. The refractory PAHs may have reactive functional groups or heteroatoms present, but the six-member carbon ring is highly resistant to thermal alteration (McCollom et al., 1999b, 2001). Thermal alteration of surface-derived organic matter generally decreases DOC concentrations and produces notable differences in DOM composition. The lowest concentrations of DOC in continental hot springs are found in fluids with the greatest hydrothermal influence, as compared to the surrounding low-temperature surface waters (Hawkes et al., 2016; Kompanichenko et al., 2016; Gonsior et al., 2018). A similar pattern is found for marine high-temperature hydrothermal fluids compared with ocean bottom waters (Lang et al., 2006; Lin et al., 2012; McCollom et al., 2015; Gomez-Saez et al., 2016; Rossel et al., 2017; Zheng et al., 2017; Longnecker et al., 2018). A recent study of low-temperature marine sub-surface fluids also identified very low DOM concentrations and attributed them to long-term microbial decomposition rather than

to thermal degradation (Shah Walter et al., 2018). DOC concentrations in deep, subsurface hydrothermal systems are expected to be low because at sufficiently high temperatures and pressures organic carbon can be converted to fully oxidized or fully reduced gaseous end products such as carbon dioxide, methane, or other light hydrocarbons (Clifton et al., 1990; McCollom et al., 1999a, 2001; Seewald, 2003; Hawkes et al., 2015) and thus lost from the dissolved phase.

In recent years, ultra-high resolution molecular characterization (FT-ICR-MS) of solid-phase extractable DOM (SPE-DOM) has been applied to hydrothermal fluids from continental hot springs (Hawkes et al., 2016; Kompanichenko et al., 2016; Gonsior et al., 2018), high-temperature seafloor vent fluids (McCollom et al., 2015; Gomez-Saez et al., 2016; LaRowe et al., 2017; Rossel et al., 2017; Zheng et al., 2017; Longnecker et al., 2018), and low-temperature deep-subsurface fluids (Shah Walter et al., 2018). This literature reveals exquisite detail on the wide range of molecular masses present in environmental samples. In the high-temperature environments, there are a significant number of molecular formulas exclusive to the hydrothermal fluids as well as elemental signatures that appear to be distinct for hydrothermal DOM. The molecular formulas exclusive to hydrothermal fluids generally have lower O/C ratios (Gomez-Saez et al., 2016; Rossel et al., 2017), higher S content (Gomez-Saez et al., 2016; LaRowe et al., 2017; Gonsior et al., 2018), and lower molecular weights (Hawkes et al., 2016; LaRowe et al., 2017; Rossel et al., 2017; Longnecker et al., 2018). The elevated sulfur content in hydrothermal organic matter is attributed to reaction of DOM with H_2S and other inorganic sulfur species at high temperatures and pressures.

The detailed information on molecular formulae in DOM obtained from FT-ICR data is unparalleled. However, these analyses require large volumes of sample to be processed, and like all DOM isolation techniques, the extraction method is selective

for a specific fraction of the DOM. FT-ICR-MS analysis of a small number (10) of hot springs in Yellowstone National Park found differences in the composition of organic matter in each sample (Gonsior et al., 2018). There are many thousands of hydrothermal features in Yellowstone National Park with correspondingly wide ranges in pH, temperature, conductivity, and chemical composition (White et al., 1971; Fournier, 1989; Arnórsson et al., 2007; Cox et al., 2011). The Gonsior et al. (2018) results strongly suggest there is an underlying pattern in organic matter composition that reflects inorganic hot spring geochemistry; that study, however, included a limited number of springs. A better of understanding of the relationships among DOM concentration, composition, and the wide array of inorganic and physical characteristics present in continental hot springs could be obtained through studies employing a much larger number of samples. While EEM fluorescence cannot provide the level of molecular detail available with FT-ICR-MS, it has the advantage that it is fast, inexpensive and sensitive for specific fractions of the DOM pool.

Here we present data for DOC concentration and fluorescent DOM (FDOM) composition from 222 continental hot springs and assess the relationships among DOC concentration, FDOM composition, and basic geochemical parameters, such as hot spring pH. We apply EEM spectroscopy and PARAFAC analysis to determine FDOM composition. PARAFAC models are a type of linear combination model that separates a complex signal into a discrete number of statistically separable components (Bro, 1997; Stedmon and Bro, 2008). We applied the robust PARFAC model developed for surface waters (Cory and McKnight, 2005) to the hot spring data set, but determined there were significant residuals due to unmodelled fluorescence (Appendix A Figure A1). This result strongly implies that there are fluorophores in continental hot springs that are not present in typical surface waters. Therefore, we developed a new validated PARAFAC model using a large data set with large spectral variability from

222 continental hot springs in Yellowstone National Park, USA and the Tengchong hydrothermal region in Yunnan Province China. Our model identifies five fluorescence components including: three typical humic-like components, one protein-like component (tyrosine), and a novel component exclusive to acidic hot springs. We use residual analysis from the new model to identify other potentially novel fluorophores in continental hot springs. We have also evaluated the utility of standard fluorescence indices commonly used in surface water analysis (i.e., the fluorescence index, humification index, and β/α) and find that they are inadequate to describe hydrothermal FDOM due to the presence of the novel fluorophores.

2.3 Methods and Materials

2.3.1 Field Sampling

Water samples were collected from Yellowstone National Park in Wyoming, USA during July/August 2012, 2013 and 2014, and from the Tengchong hydrothermal region in Yunnan Province, China during January 2011, June 2011 and July 2013. Field measurements of water temperature, conductivity, and pH (WTW, Germany; YSI, OH, USA; LaMotte, MD, USA respectively) were made using hand-held meters (Shock et al., 2010; Xie et al., 2014) that were calibrated daily. Surface water samples from hot spring source pools were collected using a polypropylene scoop or sampled directly using a 140 mL syringe (BD Inc., New Jersey, USA) when the springs were too shallow to use the scoop. Approximately 250 mL of hot spring water was collected into a high-density polyethylene (HDPE) Nalgene$^{\text{tm}}$ bottle and then filtered on-site through a series of 1.2 μm, 0.8 μm, and 0.2 μm Supor$^{\text{tm}}$ membrane filters (Pall Corp., New York, USA) into 125 mL acid-washed, fluorinated-polyethylene (FLPE) bottles. The FLPE bottles have less effect on the samples during storage because they

leach/adsorb less carbon than regular HDPE bottles. The filters were rinsed with 100 mL of sample water prior to sample collection to reduce organic contamination from the filters. The collection bottles were pre-acidified with HCl to ensure the samples were maintained below pH 2. A minimum of 20 mL of filtered water was required for analysis of DOC concentration, ultraviolet–visible absorption, and fluorescence. This low volume requirement allowed us to sample a large number of springs, including very small springs and springs that have little to no flow. Upon returning to the laboratory, samples were stored in the dark at 4°C until analysis. All samples were analyzed for DOC concentration, absorption, and fluorescence within four to six weeks of collection.

2.3.2 Total Dissolved Organic Carbon

DOC concentrations were measured on 20 mL subsamples of our filtered, acidified water using a Shimadzu TOC-V^{tm} analyzer according to standard methods (Hedges et al., 1993; Sharp et al., 1993; Sharp, 1997; Sharp et al., 2004). Our limit of detection for this method is 1.4×10^{-5} mol C L^{-1}. Carbon calibration curves using potassium hydrogen phthalate (Nacali Tesque Inc., Kyoto, Japan) and check standards made from sucrose (Spectrum Chemical Mfg. Corp., CA, USA) and caffeine (MP Biomedicals LLC, OH, USA) were run each day for quantification and quality assurance, respectively.

2.3.3 Optical Properties

Optical properties were determined on 3 mL samples using ultraviolet–visible (UV-Vis) absorbance spectroscopy and 3D-fluorescence spectroscopy. Absorbance spectra from 190 to 1100 nm were obtained using a Shimadzu UVmini-1240. We performed inner-filter corrections on all fluorescence data to account for light absorbance by the

sample. Samples that were strongly absorbing at 254 nm (i.e., absorbance > 0.3) were diluted with deionized water (18.2 MΩ·cm; Barnstead^{tm} Nanopure) that was acidified to pH = 2.5 with HCl so that these inner-filter corrections could be made using data from the absorbance spectrum (Yang and Zhang, 1995; Ohno, 2002).

Fluorescence excitation-emission matrices (EEMs) were produced on a Jobin Yvon Horiba Fluoromax-4 spectrofluorometer over a range of excitation wavelengths (λ_{EX}) from 240 nm to 450 nm (in 10 nm increments) and a range of emission wavelengths (λ_{EM}) from 300 nm to 550 nm (in 2 nm increments). Each day, the EEMs were corrected for instrumental bias, blank subtracted using acidified (pH = 2.5 with HCl) deionized water, and normalized to the area under the Raman peak of deionized water at λ_{EX} = 350 nm (Cox et al., 2000; Stedmon et al., 2003). First- and second-order Rayleigh scattering ($\lambda_{EM} = \lambda_{EX} \pm 10$ nm and $\lambda_{EM} = 2 \times \lambda_{EX} \pm 10$ nm, respectively) were removed from the EEMs according to the method of Zepp et al. (2004). All post-processing of EEMs was conducted in MATLAB® (MATLAB, 2010).

2.3.4 Fluorescence Indices

Standard fluorescence indices were calculated from the EEMs for each sample. Total fluorescence was calculated as the sum of all emission signals in the corrected EEM. The fluorescence index (FI) is traditionally interpreted as a measure of terrestrial vs microbial contribution to the DOM, and is calculated as the emission intensity at 470 nm divided by the emission intensity at 520 nm obtained at an excitation wavelength of 370 nm (McKnight et al., 2001; Cory and McKnight, 2005). The humification index (HIX) is interpreted as the degree of humic-like character, with higher values indicating higher carbon to hydrogen (C:H) ratios, larger molecular weight, and more structural complexity. It is calculated as the integrated area between emission wavelengths 435 nm and 480 nm divided by the integrated area

between emission wavelengths 300 nm and 345 nm obtained at an excitation wavelength of 254 nm (Zsolnay et al., 1999). The 'β/α' index is generally interpreted to indicate the presence of more recently produced, autochthonous DOM. The 'β' peak corresponds to autochthonous, microbially derived humic-like fluorescence and the 'α' peak corresponds to allochthonous, terrestrially derived humic-like fluorescence (Parlanti et al., 2000; Fellman et al., 2010). It is calculated as the emission intensity at 380 nm divided by the emission maximum intensity between 420 and 436 nm obtained at excitation 310 nm (Wilson and Xenopoulos, 2009).

2.3.5 PARAFAC Modelling

The blank-corrected, Raman-normalized EEMs for 222 samples from Yellowstone National Park, Wyoming, USA and from the Tengchong hydrothermal region in Yunnan Province, China were used to generate and split-half validate a five-component model using parallel factor (PARAFAC) analysis (Bro, 1997) according to the methods presented in Stedmon and Bro (2008). Samples from hot spring outflow channels were not included in the model. Prior to model generation, data in the first-order scattering range (i.e., $\pm$10 nm along the $\lambda_{EM} = \lambda_{EX}$ line) were removed and replaced with 'not a number', e.g., NaN, values and data in the area below the first-order scattering range (i.e., $\lambda_{EM} < \lambda_{EX}$) were replaced with zeros so that residual scattering signal would not be interpreted during modelling. Any data at an excitation wavelength of 240 nm were also removed due to low signal-to-noise. Leverages were calculated for each sample to prevent uneven weighting of the model by outlier samples that were not representative of the whole dataset. Leverage values ranged from 0 to 1 with 0 indicating no deviation from the average data set fluorescence and 1 indicating samples that had outlier fluorescence signal not present in other samples. Samples with high leverages (> 0.15) were removed from the model data. The model

was split-half validated by first generating two separate five-component models from 111 discrete samples and then using a Tucker Congruence Coefficients test to confirm identical components between the two models, assuming a convergence coefficient of 0.95 (Stedmon and Bro, 2008). We were not able to validate models with more than five components by this method.

2.3.6 Statistical Analysis

Pearson's linear regression testing was performed in SigmaPlot (SigmaPlot, 2008) to test two-parameter, linear correlations. Significant correlation was assumed for a p-value < 0.05. Pearson's correlation coefficients (PCC) ranged from –1 to +1 with –1 indicating a perfect, negative linear correlation and +1 indicating a perfect, positive linear correlation. Linear regression models using a mixed model method were applied to assess the relationship between total fluorescence, DOC, temperature, conductivity, and pH. Total fluorescence, DOC concentration, temperature, and conductivity were treated as continuous variables; pH was treated as a categorical variable with three categories: strongly acidic (pH < 4), weakly acidic ($4 <$ pH < 7), and alkaline (pH > 7). The choice of pH categories is based on the ranges buffered by relevant acids. In highly acidic systems (pH < 4), sulfuric acid (pKa ~ 2) is the dominant buffer. In weakly acidic systems, carbonic acid/bicarbonate (pKa ~ 6) is the predominant buffer. In highly alkaline systems, silicic acid (pKa ~ 9.7) predominates. These pH categories also correspond to shifts in DOC concentration and total fluorescence. We note that pH was measured as a continuous variable, but is used as a categorical variable for this statistical modelling and for some data visualizations. Temperature and conductivity were not found to be predictors of total fluorescence (data not shown). The mixed models were implemented using R (R Core Team, 2018).

2.4 Results and Discussion

2.4.1 Water Chemistry of Yellowstone and Tengchong Hot Springs

The hot springs sampled at Yellowstone and Tengchong had temperatures ranging from 16.1°C to 94.0°C, and pH values ranging from 1.7 to 9.4 (Figure 2.1; Appendix A Table A1). This is a much wider pH range than is found in typical, non-hydrothermal waters (e.g., pH 5-7, and perhaps as high as 8.5 in marine systems). There were fewer springs overall in the Tengchong sample suite; many with pH > 7 (n = 32), but several with pH < 7 (n = 8). The springs included from Yellowstone were mostly pH < 7 (n = 175), but a few had pH > 7 (n = 6). Across all springs, cooler temperatures ($<$ 40°C) were most commonly observed for weakly acidic or circum-neutral springs ($4 <$ pH < 7). Springs with pH > 7 consistently have temperatures above 70°C. Springs with pH < 4 are generally hot ($>$ 70°C), but do exhibit a wider range of temperatures. We note that there are, of course, many alkaline springs in Yellowstone; these springs generally have very consistent geochemistry from spring to spring and year to year (e.g., Fournier (1989) and our own field observations). Because they are so consistent the alkaline springs are well represented by a fairly small number of samples. Most of the alkaline spring have very low DOC and low FDOM (Figure 2.4, Appendix A Table A1). The FDOM in the alkaline springs is predominantly due to tyrosine fluorescence (see Section 2.3.5).

Hot spring conductivity values ranged from 0.063 mS cm^{-1} to 8.1 mS cm^{-1} and low pH springs generally had a wider range in conductivity values than high pH springs (Figure 2.1; Appendix A Table A1). Hot spring DOC concentrations ranged from 16 μM to 3 mM (Figure 2.2). The highest DOC concentrations were found in low pH springs. Springs with pH > 8 consistently had low DOC concentrations. The low DOC concentrations in alkaline springs can be explained by input of carbon-

depleted hydrothermal fluid (as described in the Introduction) that has not mixed with groundwater or surface water. Precipitated silica sinter is commonly observed around these springs as a result of the cooling of silica-saturated waters (White et al., 1971; Fournier, 1977; Arnórsson, 1985; Arnórsson et al., 2007). Some springs precipitate enough sinter to create mounds at the surface that raise the springs up to 3 m above the plane of the surrounding environment, preventing surface water runoff into the springs after rain events. White et al. (1971) describe systems that are 'self-sealing' through the precipitation of silica and other minerals. If this cooling-driven silica precipitation occurs along the underground flow path as hydrothermal fluid is rising, but does not fully seal the system, it could potentially block, or reduce, mixing with subsurface ground water. We note that the total fluorescence (see Section 2.3.2; Figure 2.2) is also very low in these alkaline springs, which further implies a lack of surface organic matter.

2.4.2 Visual Peak Identification and Fluorescence Indices

Several spectral features can be identified visually in the hot spring EEM data set, as demonstrated by the representative EEMs from six hot springs shown in Figure 2.3. Many springs exhibit the typical humic-like fluorescence (max. $\lambda_{EX} < 250$ nm, max. $\lambda_{EM} = 410$–480 nm) that is associated with terrestrial organic matter (e.g., Figure 2.3, peak '1'). Some springs also contain a secondary humic peak (max. $\lambda_{EX} = 350$ nm, max. $\lambda_{EM} = 430$ nm). We note the overly broad nature of humic-like fluorescence as this fluorescence signature is not unique to the operationally defined humic acids but can indicate a wide range of complex organic compounds that make up terrestrially derived organic matter. We use the term humic-like to describe the fluorescence signal of this type because it is a widely recognized terminology, but we interpret it to indicate surface-derived terrestrial organic matter as a whole in order

to distinguish this signal from the novel hydrothermal fluorescence signals. The short wavelength, traditionally defined protein-like region in EEM space ($\lambda_{EX} < \sim$300 nm, $\lambda_{EM} < \sim$350 nm) correlated to microbial activity is similarly contentious and is known to also contain fluorescence from non-microbial, small aromatic indoles and phenols (Maie et al., 2007; Hernes et al., 2009). We only refer to fluorescence signals in this region as protein-like when they exhibit explicit spectral matches to the free amino acid signatures of tyrosine (max. $\lambda_{EX} = 270$ nm, max. $\lambda_{EM} = 305$ nm; Figure 2.3, peak '2') and tryptophan (max. $\lambda_{EX} = 275$ nm, max. $\lambda_{EM} = 340$ nm; Figure 2.3, peak '3'; e.g., (Coble et al., 1990; Yamashita and Tanoue, 2003)). Tyrosine-like fluorescence is more common than tryptophan-like fluorescence in these springs. A prominent fluorescent peak (Figure 2.3, peak '4') is also observed (max. $\lambda_{EX} = 250$ nm, max. $\lambda_{EM} = 350$ nm) exclusively in highly acidic (pH < 4) hot springs. The closest spectral match we found in the literature is to acid-soluble lignins that are produced during high-temperature, acidic processing of woody material, i.e., lignin (Albinsson et al., 1999). Polycyclic aromatic hydrocarbon (PAH) fluorescence (Murphy et al., 2006) is also observed (Figure 2.3, peak '5') in the Calcite Springs region in Yellowstone. In this region, PAHs have been previously identified and characterized (Clifton et al., 1990) by mass spectrometry.

Total fluorescence values (Figure 2.2, Appendix A Table A1) were overall lower in alkaline (pH > 7) springs than in either weakly acidic ($4 <$ pH < 7) or strongly acidic (pH < 4) springs. The mean total fluorescence values (10.32, 61.97, and 38.94, respectively) for each of the three pH categories are significantly different from one another ($p < 0.05$). Linear regression modelling reveals that DOC is a significantly correlated ($p < 0.001$) with total fluorescence (Figure 2.4) in the total data set. We tested separate linear regression models for each pH category and found that DOC is a significant predictor of total fluorescence for the strongly acidic springs ($p < 0.001$,

$R^2 = 0.519$) and for the weakly acidic springs ($p < 0.001$, $R^2 = 0.872$). This analysis suggests DOC concentration and total fluorescence in the acidic and weakly acidic springs are controlled by similar factors. We found that DOC was not a significant predictor of total fluorescence ($p > 0.05$, $R^2 = 0.018$) in the alkaline springs.

In a mixed model, DOC concentration (a continuous variable) and the pH category (i.e., strongly acidic, weakly acidic, or alkaline) are both significant predictors of total fluorescence ($p < 0.001$). When an interference term (DOC $\times$ pH category) was included with this model all three predictors (DOC, pH category, and DOC $\times$ pH category) are statistically significant ($p < 0.001$). The significance of the interference term indicates that the effect DOC has on predicting total fluorescence depends on the pH category. Within the three pH categories, the interference term was significant for the weakly acidic springs relative to the strongly acidic springs, implying that these two pH categories have different slopes for total fluorescence as a function of DOC. The interference term for alkaline springs is not significant (as compared to either strongly acidic or weakly acidic springs), presumably because there is not a significant relationship between total fluorescence and DOC in the alkaline springs in the first place.

The fluorescence index (FI) values range from 1.25 to 2.63. Traditionally, higher FI values are interpreted to suggest microbially sourced DOM and lower values terrestrially sourced DOM. The commonly observed range of FI values in surface waters is 1.2 to 1.8 (McKnight et al., 2001; Cory and McKnight, 2005). Although we observed a wide range in FI values, the median value in all pH bins (Figure 2.5) is relatively constant (FI $\sim$1.5). In several springs with pH 5-6 we observed FI values as high as 2.6, which are higher than any value observed in the 379-sample data set used in Cory and McKnight (2005). The EEMs from these high FI samples reveal the presence of prominent fluorescent peaks (λ_{EX} = 240, 290, and 350 nm; λ_{EM} = 450 nm; Figure

2.10D) that do not correspond to any traditional humic-like components (Cory and McKnight, 2005; Coble, 2007; Fellman et al., 2010; Ishii and Boyer, 2012) despite being in the "humic region" of the EEM (see Section 2.3.6 for further discussion of this unknown peak). The unknown peak at λ_{EX} = 350 nm overlaps the EEM region that the FI calculation attributes to microbially derived DOM. The novel peaks in hydrothermal FDOM are not accounted for by the indices developed for surface water FDOM. Additionally, the traditional interpretation of FI only accommodates 'terrestrial' or 'microbial' sources of FDOM. Novel sources of FDOM in hydrothermal systems are, as yet, unaccounted for. Thus, it may be inappropriate to interpret FI as an indicator of the source of hydrothermal FDOM.

The humification index (HIX) values range from 0.042 to 9.5, with larger values suggesting a higher C:H ratio (more aromatic, high molecular weight DOM) and smaller values suggesting a lower C:H (more aliphatic, lower molecular weight DOM). We observe the highest HIX values in the circum-neutral pH range and consistently low HIX values (HIX < 3) in both the most acidic and the most alkaline springs. Humification index values as high as 16-22 have been reported for water-soluble extracts of soil DOM (Zsolnay et al., 1999; Huguet et al., 2009). The traditional interpretation of high HIX is that higher degrees of humification are associated with more aromatic, condensed structures, a quality we expected to observe in hydrothermally altered DOM. However, high HIX values are also associated with higher molecular weight, more structurally complex molecules; compounds with these qualities are notably lacking in hydrothermal DOM relative to surface seawater DOM (Hawkes et al., 2015; Rossel et al., 2017; Longnecker et al., 2018). Thus, HIX should be interpreted with care in continental hydrothermal systems.

The β/α values range from 0.271 to 1.38. Higher β/α values are traditionally interpreted to indicate an autochthonous origin for the organic matter. The β peak

corresponds to a type of humic fluorescence that indicates autochthonous, microbially derived humic material, as opposed to the terrestrially sourced αpeak (Stedmon and Markager, 2005; Coble, 2007; Murphy et al., 2008; Wilson and Xenopoulos, 2009). The β peak is also described as representing more recently produced, less degraded organic matter, whereas the α peak represents highly degraded DOM (Parlanti et al., 2000; Wilson and Xenopoulos, 2009). Median β/α values are constant ($\sim$0.75) across most springs. The most alkaline springs (pH $>$ 8) with the highest β/α values would traditionally be interpreted has having FDOM of predominantly microbial origin. However, low FDOM and the presence of non-humic fluorescence in the region of the α peak complicates this interpretation. Low values of β/α are observed in several samples in the pH range 5-6. All samples with low β/α values are from the same springs that had high FI values; once again, suggesting the presence of unknown fluorophores in the hydrothermal environment may complicate or even invalidate the application of traditional fluorescence indices developed for riverine and estuarine systems.

2.4.3 The Five-Component PARAFAC Model

We used 222 sample EEMs to generate a five-component PARAFAC model. The component EEMs from the model and the excitation and emission loadings are presented in Figure 2.6. Four of the components in our model are present in most surface water models and one component appears to be unique to hot springs. In order of predominance, our model has three humic-like components, one component found exclusively in acidic springs, and one protein-like component.

Components 1, 2, and 3 in our model are humic-like components. Humic-like component 1 is the largest contributor to total component fluorescence in the model data set. It has an excitation peak at 260 nm and an emission peak at 480 nm. Our

humic-like component 1 is identical to traditional humic-like components presented by many researchers (Stedmon et al., 2003; Stedmon and Markager, 2005; Kowalczuk et al., 2009; Williams et al., 2010; Baghoth et al., 2011; Yamashita et al., 2011, 2013; Carstea et al., 2014; Maie et al., 2014). Some of these other PARAFAC models describe this component with a secondary excitation peak at 380 nm. Our component has a shoulder that extends past 400 nm but does not form a second peak. A primary terrestrial source has been attributed to this component (Carstea et al., 2014). Our humic-like component 2 has an excitation peak at 270 nm and an emission peak at 416 nm and our humic-like component 3 has a major excitation peak at <250 nm, a minor excitation peak at 330 nm, and an emission peak at 416 nm. Humic-like components 2 and 3 also appear in the literature both as separate components (Stedmon et al., 2003; Stedmon and Markager, 2005) and as a combined component (Ohno et al., 2007; Yamashita et al., 2011, 2013).

The fourth component in our model appears exclusively in strongly acidic (pH < 4) springs. This component has an excitation peak at 250 nm and an emission peak at 348 nm. Similar spectral properties (λ_{EX} = 240–320 nm, λ_{EM} = 360 nm) have been described for acid-soluble lignins (Albinsson et al., 1999). The conditions in our springs (high temperature, acidic) are similar to the industrial conditions described in Albinsson et al. (1999). The presence of thermally altered, wood-sourced organic matter would not be surprising given that 86% of Yellowstone is forest covered, with roughly three-quarters of that forest being lodgepole pine Notaro et al. (2019). Until confirmation of a lignin (or other woody organic matter) source can be made, we refer to this component as the acid-spring component due to its exclusive presence in acidic springs. We note, based on fluorescence, that this component may be similar to a fluorophore described in one hot spring by Gonsior et al. (2018). Additional potential

sources for this novel fluorescence signature include acid-leachate from rocks and sediments, or microbial activity unique to acidic thermal systems.

Our fifth model component is a protein-like component. It has an excitation peak at 270 nm and emission peak at <300 nm. An identical component is reported commonly in the literature where it is attributed to microbial activity (Coble et al., 1990; Coble, 2007; Fellman et al., 2010) and presented as a 'tyrosine-like'protein component, due to its spectral match to the free amino acid tyrosine. This component is traditionally associated with microbial productivity (Cory and McKnight, 2005; Fellman et al., 2010). A protein-like component in our model is not surprising given the active microbial communities found in these hot springs (Hou et al., 2013; Xie et al., 2014; Urschel et al., 2015). The protein-like fluorescence is often the dominant feature in highly alkaline springs that have low FDOM. The fluorescence that we visually observed in some EEMs (Figure 2.3, peak '3') identical to the free amino acid tryptophan was not resolved as a component in this model. Again, we use the term protein-like only to refer to peaks in this region that explicitly match the signals of the free amino-acid tyrosine and tryptophan. Previously described non-microbially derived indoles and phenols that fluoresce in this general region (Maie et al., 2007; Hernes et al., 2009) have distinctly different excitation and emission wavelengths from what we observe.

2.4.4 Trends of PARAFAC Components with pH and Fluorescence Indices

The humic-like component loadings were summed (Σ-humic) and evaluated as a fraction of the total component loadings. The Σ-humic components with the highest fluorescence intensity appeared in weakly acidic and circum-neutral springs with pH 5-7. In these springs, the Σ-humic components were also the most dominant components relative to the total component loadings. These components appeared with lower

intensity in springs with pH < 5 and appeared only sparsely in springs with pH > 7 (Figure 2.7). Significant mixing of ground water in end member acidic and alkaline hot springs results in cooler, circum-neutral pH springs (White et al., 1971; Fournier, 1989; Arnórsson et al., 2007). The enhanced humic-like fluorescence in such springs is consistent with a groundwater mixing contribution of material from the surrounding forests and meadows. The fluorescence indices discussed here were mainly developed for riverine and estuarine systems and rely heavily on the fluorescence intensity in the traditional "humic" region of an EEM. Humic-like fluorescence is prevalent throughout riverine and estuarine waters, but in our hot springs there are many end member hydrothermal springs (pH > 8 or pH < 4) that demonstrate little to no humic-like fluorescence at all and we suggest these indices should not be applied to hot spring FDOM.

The correlation of the Σ-humic fraction with each of the three fluorescence indices (i.e., FI, β/α, and HIX) was tested by Pearson's correlation coefficients (PCC). The PCC values can range from –1 to +1, with a value of –1 indicating a perfect, negative linear correlation between two variables and a value of +1 indicating a perfect positive linear correlation. The Σ-humic fraction is significantly correlated to HIX (PCC = 0.887, $p < 0.001$, $R^2 = 0.786$; Figure 2.8) and β/α (PCC = –0.444, $p < 0.001$, $R^2 = 0.197$; Figure 2.8). We note the relationship between the humic-like components and HIX is better described with an exponential fit. This positive correlation of HIX with the fraction of Σ-humic components suggests HIX may be an indicator of springs with a high contribution of terrestrial organic matter, as opposed to the microbially derived protein-like component or the novel acid-spring component. This is not surprising given that our three humic-like components are good matches to humic-like components from other studies. The negative correlation of the Σ-humic fraction to β/α could suggest humic-like fluorescence in hot springs is more similar to

terrestrially derived organic matter than to microbially derived organic matter, but it is difficult to say this definitively. We found no statistically significant correlation between the Σ-humic fraction and FI (PCC = –0.0268, $p > 0.05$, $R^2 < 0.001$).

Visually, the acid-spring component appears exclusively in EEMs from springs with pH < 4. However, the PARAFAC modelling suggests a significant contribution from the acid-spring component in several springs with pH values between 5 and 7 (Figure 2.7, top-center plot). The acid-spring component was not visually apparent in those EEMs. Instead, what we observe is humic-like fluorescence with very high intensity, at least an order of magnitude higher than most other samples in the data set (we think this is a result of the PARAFAC model attempting to fit the very high intensities for these springs; see further discussion in Sections 2.3.5 and 2.3.6). We note the acid-spring component was not observed in the few acidic (pH < 7) spring samples from the Tengchong hydrothermal region. This could be due to the extremely limited number of Tengchong samples with pH < 4 (n = 1) or to some fundamental difference in the organic composition of the Tengchong springs.

The acid-spring component fraction of total component loadings is significantly correlated to both HIX (PCC = –0.480, $p < 0.001$, $R^2 = 0.230$; Figure 2.8) and β/α (PCC = 0.397, $p < 0.001$, $R^2 = 0.158$; Figure 2.8). The negative correlation of the acid-spring component to HIX is likely driven by the positive correlation between HIX and Σ-humic since the five components are expressed fractionally. At best, we can interpret this to mean HIX can distinguish humic-like fluorescence from non-humic-like fluorescence, rather than using HIX to say something about the acid-spring component or the protein-like component. The positive correlation of the acid-spring component to β/α also likely reflects a similar parallel relation between HIX and Σ-humic. These results are consistent with the dependence of these traditional indices on the presence of humic-like fluorescence and are further evidence that indices are

impractical to apply to the end-member hydrothermal springs where there is minimal to no humic-like fluorescence. We found no statistical correlation between the acid-spring component fraction and FI (PCC = –0.0228, $p > 0.05$, $R^2 < 0.001$).

Protein-like fluorescence appeared at nearly all sites and did not appear to correlate with pH (Figure 2.7), temperature, or conductivity (data not shown). The protein-like component loadings were not statistically different for alkaline and acidic springs. In alkaline springs the protein-like component was commonly the dominant fluorescent component (Figure 2.7); however, this is due to a distinct lack of humic-like and acid-spring component fluorescence rather than to a higher amount of protein-like component fluorescence. An absence of the humic-like components suggests the DOM in alkaline springs is dominated by microbial or deep thermal sources, rather than terrestrial sources. This is consistent with our observation that many of the alkaline springs are associated with sinter mounds that elevate the spring and inhibit run-off into the springs from the surrounding landscape. The 'isolation' of the springs by the sinter mounds supports the lack of wood-derived organic matter (e.g., lignin phenols) and lower DOC concentrations. Taken together, this supports the idea that our protein-like component really does reflect a microbially (or thermally) derived source and not remnant lignin phenols.

The protein-like component fraction of total component loadings is significantly negatively correlated with the HIX (PCC = –0.450, $p < 0.001$, $R^2 = 0.202$; Figure 2.8). This negative correlation indicates that in springs where the protein component is the dominant fluorophore, the DOM is less 'humic'. We found no significant correlation between the protein component fraction and FI (PCC = 0.0505, $p > 0.05$, $R^2 = 0.003$) or β/α (PCC = 0.0700, $p > 0.05$, $R^2 = 0.005$). This is likely because the FI and β/α are calculated based on different types of 'humic' fluorescence (i.e., at longer

wavelengths), rather than from protein-like fluorescence. Additionally, the protein component loadings are relatively low and roughly constant across all springs.

The traditional indices (FI, HIX, and β/α) are calculated from an EEM space that requires the presence of some amount of humic-like fluorescence. In riverine and estuarine aquatic systems this is a reasonable expectation, but it is not in the hot springs described here. The significant correlation between the fraction of Σ-humic components and HIX suggests that the humic-like fluorescence in continental hot springs may be an indicator of surface-derived, terrestrial organic matter (rather than microbially derived organic matter) and thus HIX may have utility as an indicator in circum-neutral, moderate temperature springs for mixing between hydrothermal fluids and cooler groundwater. FI and β/α, in contrast, are much more difficult to interpret due to the presence of the non-humic, non-protein acid spring component. The indices are premised on simple endmembers (autochthonous/allochthonous, terrestrial/microbial) and in continental hot springs the additional subsurface and thermally derived carbon sources cannot be accounted for. The indices are also generally interpreted along simple alteration vectors (e.g., microbial degradation or ageing). In continental hot springs, microbial processes, aging, and thermal degradation all contribute to changes in DOM composition. In summary, the traditional fluorescence indices are likely difficult to apply to continental hydrothermal systems.

2.4.5 The Acid-Spring Component

A pH-dependent solubility explains why the acid-spring component is only observed in springs with a pH < 4. To demonstrate this, we raised the pH of samples containing the acid-spring component from pH = 2 to pH = 7. The fluorescence of the acid-spring component disappeared completely after this pH change. This shift in pH also resulted in the formation of a yellow, solid precipitate. Re-acidification

of the sample dissolved the precipitate and resulted in the reappearance of the acid-spring component fluorescence. In a follow-on experiment, we filtered the sample after raising the pH to 7. The filtrate was re-acidified, and the acid-spring fluorescence did not reappear (Figure 2.9). In this filtrate we observed distinct humic and protein fluorescence (Appendix A Figure A2) that was not observable in the unaltered sample due to an order-of-magnitude difference in the fluorescence intensity between these components and the acid-spring component. The precipitate on the filter was subsequently dissolved with acidified, deionized water and the acid-spring fluorescence reappeared. This indicates that the fluorophores were removed on the filter with the precipitate. Furthermore, it indicates that the disappearance of the acid-spring component fluorescence at pH 7 is not simply the result of a pH-dependent fluorescence.

We replicated this experiment with a sample from a spring with a pH = 5.57 that had high values for the acid-spring component ($\sim$0.3; see Figure 2.7) to confirm whether the acid-spring component was present in a sample from a spring with a pH $>$ 4. The humic fluorescence intensity decreased after the sample was raised to pH = 7, filtered, and re-acidified (Figure 2.10). We ran acidified, deionized water through the filter to dissolve any precipitated material. There was no observable acid-spring fluorescence in this filtrate; however, there was some low-intensity (relative to the original sample) humic fluorescence. In the initial sample, as well as the neutral filtrate, we note there is a hint of tryptophan fluorescence (λ_{EX} = 270 nm, λ_{EM} = 350 nm). The spectral overlap of tryptophan fluorescence and our acid-spring component leads to a false-positive assignment of the acid-spring component when those fluorophores are not actually present. This interference is discussed further in Section 2.3.6. This experiment demonstrates the importance of critical interpretation of data from PARAFAC analysis.

Acid-soluble lignins are spectrally characterized in the literature (Albinsson et al., 1999; Hernes et al., 2009). They are a potential candidate for our acid-spring component because they are characterized with similar spectral properties (see Section 2.3.4) and because the industrial conditions (high temperature, low pH) that produce these compounds are comparable to the subsurface conditions in hydrothermal systems. Previous lignin characterization by EEM fluorescence and PARAFAC modelling reported by Hernes et al. (2009) relies on proxies within the total EEM and not discrete, identifiable peaks. Further, the characterization by Hernes et al. (2009) considers lignins present in ambient, surface waters and likely does not reflect the unique compounds produced by thermal degradation of terrestrial organic matter. We observed the fluorescence of the acid-spring component in a few acidic springs (n = 25) with temperatures below 50°C. This suggests that the water in these springs is hydrothermally sourced, but it either cooled down before reaching the surface or it mixed significantly with surface water. Thus, the presence of the acid-spring component fluorescence may serve as an indicator of hydrothermally sourced water and potentially for thermally altered organic matter.

2.4.6 Model Residual Analysis

PARAFAC analysis characterizes the prominent fluorescent features in a data set; however, an assessment of what is not explained by the model is also useful. Residual analysis reveals distinct residual fluorescence signatures from PAHs, free tryptophan, protein-bound tryptophan, and an uncharacterized sulfur-associated fluorescence (Figure 2.11).

The fluorescence of PAHs in the environment has been characterized previously in a PARAFAC model Murphy et al. (2006) as an environmental contaminant from fuel oils (Rudnick and Chen, 1998). Further, PAHs have been identified and characterized

in the Calcite Springs region in Yellowstone National Park using mass spectrometry (Clifton et al., 1990). Clifton et al. (1990) explained the PAH presence as the alteration of shallow sedimentary rocks by rising hydrothermal fluid. Our samples from the Calcite Springs region demonstrate fluorescence (Figure 2.3, peak '5') that matches the Murphy et al. (2006) PARAFAC component. The PAH fluorescence overlaps the acid-spring component identified in our model; yet it leaves a distinct negative residual peak (λ_{EX} = 250-270 nm (maximum intensity at 250 nm), λ_{EM} = 314-352 nm (maximum intensity at 332 nm); Figure 2.11). This residual signature was observed in every hot spring sample from the Calcite Springs region. The fluorescence intensities for all samples from this region were ∼1-2 orders of magnitude higher than the rest of the data so these samples were removed during model generation to prevent uneven weighting of the model by high-leverage samples.

The tryptophan-like fluorescence identified through visual peak picking was not resolved into a component in our model, but it is distinguishable by several residual signals. Different residual signals indicate free amino-acid tryptophan and protein-bound tryptophan fluorescence. Free tryptophan appears with a positive residual peak (λ_{EX} = 290 nm, λ_{EM} = 326 nm) and two negative residual peaks (λ_{EX} = 260 nm, λ_{EM} = 344 nm; λ_{EX} = 270 nm, λ_{EM} = 300 nm). The positive residual peak indicates a signal that cannot be accounted for by any of the five model components; the negative residual peaks indicate that the model attempts to use the acid-spring component and the tyrosine-like component to account for some of the fluorescence in this region. Protein-bound tryptophan-like fluorescence produces a positive residual (λ_{EX} = 290 nm, λ_{EM} = 338 nm) and a negative residual (λ_{EX} = 260 nm, λ_{EM} = 348 nm). The difference between free and protein-bound tryptophan is that the fluorescence of the latter does not overlap our tyrosine-like component, so only a

single negative residual peak is observed because of the assignment to the acid-spring component.

The unidentified fluorescent signature in several samples that is responsible for the anomalously high FI values and low β/α values leaves a distinct residual. There are two prominent positive residual peaks (λ_{EX} = 300 nm and 370 nm, both at λ_{EM} = 446 nm) indicating a signal that cannot be accounted for by our humic-like components, despite being in the conventional 'humic region' of the EEM. The springs that demonstrate this fluorescence (n = 5) all have notable amounts of native sulfur (personal communication, Eric Boyd, July 2017) and in some cases, yellow sulfur crystals can be found around the springs. It is possible that this novel fluorescence signature is the result of organo-sulfur fluorophores; sulfur-containing organic matter is common in hydrothermal systems due to the reaction of organic matter with reactive sulfur species (Reeves et al., 2014; Gomez-Saez et al., 2016). Previous work has found that organic sulfur is present in up to 80% of all DOM formulas identified by FT-ICR-MS associated with hydrothermal fluids (Gomez-Saez et al., 2016; Gonsior et al., 2018).

2.5 Conclusions

We have expanded the application of fluorescent DOM to include a large number of continental hot springs. The fluorescent DOM in hot springs was not described well by a PARAFAC model tuned for surface water, indicating there are fundamental compositional differences between the DOM of surface water systems and hydrothermal systems. The most interesting difference is the presence of fluorophores exclusive to strongly acidic springs that we propose indicate the presence of thermally altered organic matter. The observation of humic components in hot springs can also serve as an indicator of terrestrial input through surface runoff or mixing with groundwater. We found that common fluorescence indices (FI, HIX, and β/α) may be inadequate

in describing hydrothermal DOM due to the presence of previously unknown fluorophores. The indices track terrestrially derived material when it is present, but it is not surprising that they are insensitive to the hydrothermally derived organic material. Our PARAFAC model allows quantification of fluorescent components from multiple sources and provides a robust tool for assessing mixing of hydrothermal fluids and surface water as well as alteration of DOM in Yellowstone continental hot springs.

2.6 Data Availability

Datasets related to this article can be found at https://data.mendeley.com/datasets/47rp3drbfs/draft?a=28b34e5b-bd72-44a2-a1e8-c4283eb47f70, an open-source online data repository hosted at Mendeley Data (Nye, Shock, and Hartnett, 2019).

2.7 Acknowledgements

We thank the members of the GEOPIG research group and the YNP field teams for help sampling the YNP hot springs and for critical discussion of these results. We thank Eric Boyd for helpful discussions, Jesse Coe and Brian St. Clair for their help sampling the Tengchong hot springs, and Monica Palta for help with the statistical analysis. We appreciate the helpful comments from three anonymous reviewers that allowed us to improve the manuscript. Yellowstone samples were collected as part of study YELL-5434 (E.L.S.). We gratefully acknowledge funding from NSF CAREER (0846188), NSF OISE/PIRE (0968421), and NASA NExSS (NNX15AD53G) awards to H.E.H., and NASA Exobiology grant (NNX16AJ61G) to E.L.S.

REFERENCES

Albinsson, B., Li, S., Lundquist, K., and Stomberg, R. (**1999**); The origin of lignin fluorescence. *Journal of Molecular Structure* 508(1-3), pp. 19–27, doi:10.1016/S0022-2860(98)00913-2.

Arnórsson, S. (**1985**); The use of mixing models and chemical geothermometers for estimating underground temperatures in geothermal systems. *Journal of Volcanology and Geothermal Research* 23(3-4), pp. 299–335, doi:10.1016/0377-0273(85)90039-3.

Arnórsson, S., Stefánsson, A., and Bjarnason, J. O. (**2007**); Fluid-fluid interactions in geothermal systems. *Reviews in Mineralogy and Geochemistry* 65(1), pp. 259–312, doi:10.2138/rmg.2007.65.9.

Baghoth, S., Sharma, S., and Amy, G. (**2011**); Tracking natural organic matter (NOM) in a drinking water treatment plant using fluorescence excitation emission matrices and PARAFAC. *Water Research* 45(2), pp. 797–809, doi:10.1016/j.watres.2010.09.005.

Bergfeld, D., Lowenstern, J. B., Hunt, A. G., Shanks, W. C. P., and Evans, W. C. (**2014**); Gas and isotope chemistry of thermal features in Yellowstone National Park, Wyoming. Scientific Investigations Report 2011-5012, United States Geological Survey, doi:10.3133/sir20115012.

Bro, R. (**1997**); PARAFAC. Tutorial and applications. *Chemometrics and Intelligent Laboratory Systems* 38(2), pp. 149–171, doi:10.1016/S0169-7439(97)00032-4.

Carstea, E. M., Baker, A., Bieroza, M., Reynolds, D. M., and Bridgeman, J. (**2014**); Characterisation of dissolved organic matter fluorescence properties by PARAFAC analysis and thermal quenching. *Water Research* 61, pp. 152–161, doi:10.1016/j.watres.2014.05.013.

Cawley, K. M., Butler, K. D., Aiken, G. R., Larsen, L. G., Huntington, T. G., and McKnight, D. M. (**2012**); Identifying fluorescent pulp mill effluent in the Gulf of Maine and its watershed. *Marine Pollution Bulletin* 64(8), pp. 1678–1687, doi:10.1016/j.marpolbul.2012.05.040.

Clifton, C., Walters, C., and Simoneit, B. (**1990**); Hydrothermal petroleums from Yellowstone National Park, Wyoming, U.S.A. *Applied Geochemistry* 5(1-2), pp. 169–191, doi:10.1016/0883-2927(90)90047-9.

Coble, P. G. (**2007**); Marine optical biogeochemistry: The chemistry of ocean color. *Chemical Reviews* 107(2), pp. 402–418, doi:10.1021/cr050350+.

Coble, P. G., Green, S. A., Blough, N. V., and Gagosian, R. B. (**1990**); Characterization of dissolved organic matter in the Black Sea by fluorescence spectroscopy. *Nature* 348(6300), pp. 432–435, doi:10.1038/348432a0.

Cory, R. M. and McKnight, D. M. (**2005**); Fluorescence spectroscopy reveals ubiquitous presence of oxidized and reduced quinones in dissolved organic matter. *Environmental Science & Technology* 39(21), pp. 8142–8149, doi:10.1021/es0506962.

Cox, A., Shock, E. L., and Havig, J. R. (**2011**); The transition to microbial photosynthesis in hot spring ecosystems. *Chemical Geology* 280(3-4), pp. 344–351, doi:10.1016/j.chemgeo.2010.11.022.

Cox, L., Celis, R., Hermosín, M. C., Cornejo, J., Zsolnay, A., and Zeller, K. (**2000**); Effect of organic amendments on herbicide sorption as related to the nature of the dissolved organic matter. *Environmental Science & Technology* 34(21), pp. 4600–4605, doi:10.1021/es0000293.

Des Marais, D. J., Donchin, J. H., Nehring, N. L., and Truesdell, A. H. (**1981**); Molecular carbon isotopic evidence for the origin of geothermal hydrocarbons. *Nature* 292(5826), pp. 826–828, doi:10.1038/292826a0.

Fellman, J. B., Hood, E., and Spencer, R. G. M. (**2010**); Fluorescence spectroscopy opens new windows into dissolved organic matter dynamics in freshwater ecosystems: A review. *Limnology and Oceanography* 55(6), pp. 2452–2462, doi:10.4319/lo.2010.55.6.2452.

Fournier, R. (**1977**); Chemical geothermometers and mixing models for geothermal systems. *Geothermics* 5(1-4), pp. 41–50, doi:10.1016/0375-6505(77)90007-4.

Fournier, R. O. (**1989**); Geochemistry and dynamics of the Yellowstone National Park hydrothermal system. *Annual Review of Earth and Planetary Sciences* 17(1), pp. 13–53, doi:10.1146/annurev.ea.17.050189.000305.

Gomez-Saez, G. V., Niggemann, J., Dittmar, T., Pohlabeln, A. M., Lang, S. Q., Noowong, A., Pichler, T., Wörmer, L., and Bühring, S. I. (**2016**); Molecular evidence for abiotic sulfurization of dissolved organic matter in marine shallow hydrothermal systems. *Geochimica et Cosmochimica Acta* 190, pp. 35–52, doi:10.1016/j.gca.2016.06.027.

Gonsior, M., Hertkorn, N., Hinman, N., Dvorski, S. E.-M., Harir, M., Cooper, W. J., and Schmitt-Kopplin, P. (**2018**); Yellowstone hot springs are organic chemodiversity hot spots. *Scientific Reports* 8(1), p. 14155, doi:10.1038/s41598-018-32593-x.

Hansell, D. A. and Carlson, C. A. (eds.) (**2014**); *Biogeochemistry of Marine Dissolved Organic Matter*. Second edition, Academic Press, doi:10.1016/C2012-0-02714-7.

Hawkes, J. A., Rossel, P. E., Stubbins, A., Butterfield, D., Connelly, D. P., Achterberg, E. P., Koschinsky, A., Chavagnac, V., Hansen, C. T., Bach, W., and Dittmar, T. (**2015**); Efficient removal of recalcitrant deep-ocean dissolved organic matter during hydrothermal circulation. *Nature Geoscience* 8, pp. 856–860, doi:10.1038/ngeo2543.

Hawkes, J. A., Hansen, C. T., Goldhammer, T., Bach, W., and Dittmar, T. (**2016**); Molecular alteration of marine dissolved organic matter under experimental hydrothermal conditions. *Geochimica et Cosmochimica Acta* 175, pp. 68–85, doi: 10.1016/j.gca.2015.11.025.

He, W., Lee, J.-H., and Hur, J. (**2016**); Anthropogenic signature of sediment organic matter probed by UV-Visible and fluorescence spectroscopy and the association with heavy metal enrichment. *Chemosphere* 150, pp. 184–193, doi:10.1016/j.chemosphere.2016.01.116.

Hedges, J. I., Bergamaschi, B. A., and Benner, R. (**1993**); Comparative analyses of DOC and DON in natural waters. *Marine Chemistry* 41(1-3), pp. 121–134, doi: 10.1016/0304-4203(93)90110-A.

Hernes, P. J., Bergamaschi, B. A., Eckard, R. S., and Spencer, R. G. M. (**2009**); Fluorescence-based proxies for lignin in freshwater dissolved organic matter. *Journal of Geophysical Research* 114, p. G00F03, doi:10.1029/2009JG000938.

Hou, W., Wang, S., Dong, H., Jiang, H., Briggs, B. R., Peacock, J. P., Huang, Q., Huang, L., Wu, G., Zhi, X., Li, W., Dodsworth, J. A., Hedlund, B. P., Zhang, C., Hartnett, H. E., Dijkstra, P., and Hungate, B. A. (**2013**); A comprehensive census of microbial diversity in hot springs of Tengchong, Yunnan Province China using 16S rRNA gene pyrosequencing. *PLoS ONE* 8(1), p. e53350, doi:10.1371/journal.pone.0053350.

Huguet, A., Vacher, L., Relexans, S., Saubusse, S., Froidefond, J., and Parlanti, E. (**2009**); Properties of fluorescent dissolved organic matter in the Gironde Estuary. *Organic Geochemistry* 40(6), pp. 706–719, doi:10.1016/j.orggeochem.2009.03.002.

Ishii, S. K. L. and Boyer, T. H. (**2012**); Behavior of reoccurring PARAFAC components in fluorescent dissolved organic matter in natural and engineered systems: A critical review. *Environmental Science & Technology* 46(4), pp. 2006–2017, doi: 10.1021/es2043504.

Kawka, O. E. and Simoneit, B. R. (**1994**); Hydrothermal pyrolysis of organic matter in Guaymas Basin: I. Comparison of hydrocarbon distributions in subsurface sediments and seabed petroleums. *Organic Geochemistry* 22(6), pp. 947–978, doi: 10.1016/0146-6380(94)90031-0.

Kellerman, A. M., Guillemette, F., Podgorski, D. C., Aiken, G. R., Butler, K. D., and Spencer, R. G. M. (**2018**); Unifying concepts linking dissolved organic matter composition to persistence in aquatic ecosystems. *Environmental Science & Technology* 52(5), pp. 2538–2548, doi:10.1021/acs.est.7b05513.

Klevenz, V., Sumoondur, A., Ostertag-Henning, C., and Koschinsky, A. (**2010**); Concentrations and distributions of dissolved amino acids in fluids from Mid-Atlantic Ridge hydrothermal vents. *Geochemical Journal* 44(5), pp. 387–397, doi: 10.2343/geochemj.1.0081.

Kompanichenko, V. N., Poturay, V. A., and Karpov, G. A. (**2016**); Organic compounds in thermal water: The Mutnovskii area and the Uzon caldera. *Journal of Volcanology and Seismology* 10(5), pp. 305–319, doi:10.1134/S0742046316050031.

Kowalczuk, P., Durako, M. J., Young, H., Kahn, A. E., Cooper, W. J., and Gonsior, M. (**2009**); Characterization of dissolved organic matter fluorescence in the South Atlantic Bight with use of PARAFAC model: Interannual variability. *Marine Chemistry* 113(3-4), pp. 182–196, doi:10.1016/j.marchem.2009.01.015.

Lang, S. Q., Butterfield, D. A., Lilley, M. D., Paul Johnson, H., and Hedges, J. I. (**2006**); Dissolved organic carbon in ridge-axis and ridge-flank hydrothermal systems. *Geochimica et Cosmochimica Acta* 70(15), pp. 3830–3842, doi:10.1016/j.gca.2006.04.031.

LaRowe, D. E., Koch, B. P., Robador, A., Witt, M., Ksionzek, K., and Amend, J. P. (**2017**); Identification of organic compounds in ocean basement fluids. *Organic Geochemistry* 113, pp. 124–127, doi:10.1016/j.orggeochem.2017.07.017.

Lin, H.-T., Cowen, J. P., Olson, E. J., Amend, J. P., and Lilley, M. D. (**2012**); Inorganic chemistry, gas compositions and dissolved organic carbon in fluids from sedimented young basaltic crust on the Juan de Fuca Ridge flanks. *Geochimica et Cosmochimica Acta* 85, pp. 213–227, doi:10.1016/j.gca.2012.02.017.

Longnecker, K., Sievert, S. M., Sylva, S. P., Seewald, J. S., and Kujawinski, E. B. (**2018**); Dissolved organic carbon compounds in deep-sea hydrothermal vent fluids from the East Pacific Rise. *Organic Geochemistry* 125, pp. 41–49, doi:10.1016/j.orggeochem.2018.08.004.

Lorenson, T. D. and Kvenvolden, K. A. (**1993**); A comparison of hydrocarbon gases from natural sources in the Northwestern United States. In: Howell, D. G., Wiese, K., Fanelli, M., Zink, L., and Cole, F. (eds.), *The Future of Energy Gases*, pp. 453–469, Professional Paper 1570, United States Geological Survey, doi:10.3133/pp1570.

Maie, N., Scully, N. M., Pisani, O., and Jaffé, R. (**2007**); Composition of a protein-like fluorophore of dissolved organic matter in coastal wetland and estuarine ecosystems. *Water Research* 41(3), pp. 563–570, doi:10.1016/j.watres.2006.11.006.

Maie, N., Sekiguchi, S., Watanabe, A., Tsutsuki, K., Yamashita, Y., Melling, L., Cawley, K. M., Shima, E., and Jaffé, R. (**2014**); Dissolved organic matter dynamics in the oligo/meso-haline zone of wetland-influenced coastal rivers. *Journal of Sea Research* 91, pp. 58–69, doi:10.1016/j.seares.2014.02.016.

MATLAB (**2010**); version 7.10.0 R2010a MatLab: The language of technical computing. The Mathworks Inc., Natick, Massachusetts, USA.

McCollom, T., Seewald, J., and Simoneit, B. (**2001**); Reactivity of monocyclic aromatic compounds under hydrothermal conditions. *Geochimica et Cosmochimica Acta* 65(3), pp. 455–468, doi:10.1016/S0016-7037(00)00533-0.

McCollom, T. M., Ritter, G., and Simoneit, B. R. T. (**1999**a); Lipid synthesis under hydrothermal conditions by Fischer-Tropsch-type reactions. *Origins of Life and Evolution of the Biosphere* 29(2), pp. 153–166, doi:10.1023/A:1006592502746.

McCollom, T. M., Simoneit, B. R. T., and Shock, E. L. (**1999**b); Hydrous pyrolysis of polycyclic aromatic hydrocarbons and implications for the origin of PAH in hydrothermal petroleum. *Energy & Fuels* 13(2), pp. 401–410, doi:10.1021/ef980089i.

McCollom, T. M., Seewald, J. S., and German, C. R. (**2015**); Investigation of extractable organic compounds in deep-sea hydrothermal vent fluids along the Mid-Atlantic Ridge. *Geochimica et Cosmochimica Acta* 156, pp. 122–144, doi:10.1016/j.gca.2015.02.022.

McKnight, D. M., Boyer, E. W., Westerhoff, P. K., Doran, P. T., Kulbe, T., and Andersen, D. T. (**2001**); Spectrofluorometric characterization of dissolved organic matter for indication of precursor organic material and aromaticity. *Limnology and Oceanography* 46(1), pp. 38–48, doi:10.4319/lo.2001.46.1.0038.

Mißbach, H., Schmidt, B. C., Duda, J.-P., Lünsdorf, N. K., Goetz, W., and Thiel, V. (**2018**); Assessing the diversity of lipids formed via Fischer-Tropsch-type reactions. *Organic Geochemistry* 119, pp. 110–121, doi:10.1016/j.orggeochem.2018.02.012.

Murphy, K. R., Ruiz, G. M., Dunsmuir, W. T. M., and Waite, T. D. (**2006**); Optimized parameters for fluorescence-based verification of ballast water exchange by ships. *Environmental Science & Technology* 40(7), pp. 2357–2362, doi:10.1021/es0519381.

Murphy, K. R., Stedmon, C. A., Waite, T. D., and Ruiz, G. M. (**2008**); Distinguishing between terrestrial and autochthonous organic matter sources in marine environments using fluorescence spectroscopy. *Marine Chemistry* 108(1-2), pp. 40–58, doi:10.1016/j.marchem.2007.10.003.

Murphy, K. R., Butler, K. D., Spencer, R. G. M., Stedmon, C. A., Boehme, J. R., and Aiken, G. R. (**2010**); Measurement of dissolved organic matter fluorescence in aquatic environments: An interlaboratory comparison. *Environmental Science & Technology* 44(24), pp. 9405–9412, doi:10.1021/es102362t.

Notaro, M., Emmett, K., and O'Leary, D. (**2019**); Spatio-temporal variability in remotely sensed vegetation greenness across Yellowstone National Park. *Remote Sensing* 11(7), p. 798, doi:10.3390/rs11070798.

Ohno, T. (**2002**); Fluorescence inner-filtering correction for determining the humification index of dissolved organic matter. *Environmental Science & Technology* 36(4), pp. 742–746, doi:10.1021/es0155276.

Ohno, T., Fernandez, I. J., Hiradate, S., and Sherman, J. F. (**2007**); Effects of soil acidification and forest type on water soluble soil organic matter properties. *Geoderma* 140(1-2), pp. 176–187, doi:10.1016/j.geoderma.2007.04.004.

Ohno, T., Amirbahman, A., and Bro, R. (**2008**); Parallel factor analysis of excitation-emission matrix fluorescence spectra of water soluble soil organic matter as basis for the determination of conditional metal binding parameters. *Environmental Science & Technology* 42(1), pp. 186–192, doi:10.1021/es071855f.

Parlanti, E., Wörz, K., Geoffroy, L., and Lamotte, M. (**2000**); Dissolved organic matter fluorescence spectroscopy as a tool to estimate biological activity in a coastal zone submitted to anthropogenic inputs. *Organic Geochemistry* 31(12), pp. 1765–1781, doi:10.1016/S0146-6380(00)00124-8.

R Core Team (**2018**); version 1.1.453 r-Studio version 3.5.0 R: A language and environment for statistical computing. R Studio for Statistical Computing, Vienna, Austria, https://www.R-project.org/.

Reeves, E. P., McDermott, J. M., and Seewald, J. S. (**2014**); The origin of methanethiol in midocean ridge hydrothermal fluids. *Proceedings of the National Academy of Sciences* 111(15), pp. 5474–5479, doi:10.1073/pnas.1400643111.

Rossel, P. E., Stubbins, A., Rebling, T., Koschinsky, A., Hawkes, J. A., and Dittmar, T. (**2017**); Thermally altered marine dissolved organic matter in hydrothermal fluids. *Organic Geochemistry* 110, pp. 73–86, doi:10.1016/j.orggeochem.2017.05.003.

Rudnick, S. M. and Chen, R. F. (**1998**); Laser-induced fluorescence of pyrene and other polycyclic aromatic hydrocarbons (PAH) in seawater. *Talanta* 47(4), pp. 907–919, doi:10.1016/S0039-9140(98)00160-X.

Seewald, J. S. (**2003**); Organic-inorganic interactions in petroleum-producing sedimentary basins. *Nature* 426(6964), pp. 327–333, doi:10.1038/nature02132.

Shah Walter, S. R., Jaekel, U., Osterholz, H., Fisher, A. T., Huber, J. A., Pearson, A., Dittmar, T., and Girguis, P. R. (**2018**); Microbial decomposition of marine dissolved organic matter in cool oceanic crust. *Nature Geoscience* 11(5), pp. 334–339, doi:10.1038/s41561-018-0109-5.

Sharp, J., Beauregard, A., Burdige, D., Cauwet, G., Curless, S., Lauck, R., Nagel, K., Ogawa, H., Parker, A., Primm, O., Pujo-Pay, M., Savidge, W., Seitzinger, S., Spyres, G., and Styles, R. (**2004**); A direct instrument comparison for measurement of total dissolved nitrogen in seawater. *Marine Chemistry* 84(3-4), pp. 181–193, doi:10.1016/j.marchem.2003.07.003.

Sharp, J. H. (**1997**); Marine dissolved organic carbon: Are the older values correct? *Marine Chemistry* 56(3-4), pp. 265–277, doi:10.1016/S0304-4203(96)00075-8.

Sharp, J. H., Benner, R., Bennett, L., Carlson, C. A., Dow, R., and Fitzwater, S. E. (**1993**); Re-evaluation of high temperature combustion and chemical oxidation measurements of dissolved organic carbon in seawater. *Limnology and Oceanography* 38(8), pp. 1774–1782, doi:10.4319/lo.1993.38.8.1774.

Shock, E. L., Holland, M., Meyer-Dombard, D., Amend, J. P., Osburn, G., and Fischer, T. P. (**2010**); Quantifying inorganic sources of geochemical energy in hydrothermal ecosystems, Yellowstone National Park, USA. *Geochimica et Cosmochimica Acta* 74(14), pp. 4005–4043, doi:10.1016/j.gca.2009.08.036.

SigmaPlot (**2008**); version 11.0, SigmaPlot: Exact graphs and data analysis. Systat Software, San Jose, California, USA, www.systatsoftware.com.

Simoneit, B. R. (**1993**); Aqueous high-temperature and high-pressure organic geochemistry of hydrothermal vent systems. *Geochimica et Cosmochimica Acta* 57, pp. 3231–3243.

Simoneit, B. R. and Fetzer, J. C. (**1996**); High molecular weight polycyclic aromatic hydrocarbons in hydrothermal petroleums from the Gulf of California and Northeast Pacific Ocean. *Organic Geochemistry* 24(10-11), pp. 1065–1077, doi: 10.1016/S0146-6380(96)00081-2.

Simoneit, B. R. T., Summons, R. E., and Jahnke, L. L. (**1998**); Biomarkers as tracers for life on early Earth and Mars. *Origins of Life and Evolution of the Biosphere* 28(4/6), pp. 475–483, doi:10.1023/A:1006508012904.

Stedmon, C. A. and Bro, R. (**2008**); Characterizing dissolved organic matter fluorescence with parallel factor analysis, a tutorial: Fluorescence-PARAFAC analysis of DOM. *Limnology and Oceanography: Methods* 6(11), pp. 572–579, doi: 10.4319/lom.2008.6.572.

Stedmon, C. A. and Markager, S. (**2005**); Resolving the variability in dissolved organic matter fluorescence in a temperate estuary and its catchment using PARAFAC analysis. *Limnology and Oceanography* 50(2), pp. 686–697, doi:10.4 319/lo.2005.50.2.0686.

Stedmon, C. A., Markager, S., and Bro, R. (**2003**); Tracing dissolved organic matter in aquatic environments using a new approach to fluorescence spectroscopy. *Marine Chemistry* 82(3-4), pp. 239–254, doi:10.1016/S0304-4203(03)00072-0.

Stedmon, C. A., Thomas, D. N., Granskog, M., Kaartokallio, H., Papadimitriou, S., and Kuosa, H. (**2007**); Characteristics of dissolved organic matter in Baltic coastal sea ice: Allochthonous or autochthonous origins? *Environmental Science & Technology* 41(21), pp. 7273–7279, doi:10.1021/es071210f.

Urschel, M. R., Kubo, M. D., Hoehler, T. M., Peters, J. W., and Boyd, E. S. (**2015**); Carbon source preference in chemosynthetic hot spring communities. *Applied and Environmental Microbiology* 81(11), pp. 3834–3847, doi:10.1128/AEM.00511-15.

Ventura, G. T., Simoneit, B. R., Nelson, R. K., and Reddy, C. M. (**2012**); The composition, origin and fate of complex mixtures in the maltene fractions of hydrothermal petroleum assessed by comprehensive two-dimensional gas chromatography. *Organic Geochemistry* 45, pp. 48–65, doi:10.1016/j.orggeochem.2012.01.002.

White, D. E., Muffler, L. J. P., and Truesdell, A. H. (**1971**); Vapor-dominated hydrothermal systems compared with hot-water systems. *Economic Geology* 66(1), pp. 75–97, doi:10.2113/gsecongeo.66.1.75.

Williams, C. J., Yamashita, Y., Wilson, H. F., Jaffé, R., and Xenopoulos, M. A. (**2010**); Unraveling the role of land use and microbial activity in shaping dissolved organic matter characteristics in stream ecosystems. *Limnology and Oceanography* 55(3), pp. 1159–1171, doi:10.4319/lo.2010.55.3.1159.

Wilson, H. F. and Xenopoulos, M. A. (**2009**); Effects of agricultural land use on the composition of fluvial dissolved organic matter. *Nature Geoscience* 2(1), pp. 37–41, doi:10.1038/ngeo391.

Xie, W., Zhang, C. L., Wang, J., Chen, Y., Zhu, Y., de la Torre, J. R., Dong, H., Hartnett, H. E., Hedlund, B. P., and Klotz, M. G. (**2014**); Distribution of ether lipids and composition of the archaeal community in terrestrial geothermal springs: Impact of environmental variables: Archaeal lipids from terrestrial hot springs. *Environmental Microbiology* 17(5), pp. 1600–1614, doi:10.1111/1462-2920.12595.

Yamashita, Y. and Jaffé, R. (**2008**); Characterizing the interactions between trace metals and dissolved organic matter using excitation emission matrix and parallel factor analysis. *Environmental Science & Technology* 42(19), pp. 7374–7379, doi:10.1021/es801357h.

Yamashita, Y. and Tanoue, E. (**2003**); Chemical characterization of protein-like fluorophores in DOM in relation to aromatic amino acids. *Marine Chemistry* 82(3-4), pp. 255–271, doi:10.1016/S0304-4203(03)00073-2.

Yamashita, Y., Jaffé, R., Maie, N., and Tanoue, E. (**2008**); Assessing the dynamics of dissolved organic matter (DOM) in coastal environments by excitation emission matrix fluorescence and parallel factor analysis (EEM-PARAFAC). *Limnology and Oceanography* 53(5), pp. 1900–1908, doi:10.4319/lo.2008.53.5.1900.

Yamashita, Y., Panton, A., Mahaffey, C., and Jaffé, R. (**2011**); Assessing the spatial and temporal variability of dissolved organic matter in Liverpool Bay using excitation-emission matrix fluorescence and parallel factor analysis. *Ocean Dynamics* 61(5), pp. 569–579, doi:10.1007/s10236-010-0365-4.

Yamashita, Y., Boyer, J. N., and Jaffé, R. (**2013**); Evaluating the distribution of terrestrial dissolved organic matter in a complex coastal ecosystem using fluorescence spectroscopy. *Continental Shelf Research* 66, pp. 136–144, doi:10.1016/j.csr.2013.06.010.

Yang, Y. and Zhang, D. (**1995**); Concentration effect on the fluorescence spectra of humic substances. *Communications in Soil Science and Plant Analysis* 26(15-16), pp. 2333–2349, doi:10.1080/00103629509369451.

Zepp, R. G., Sheldon, W. M., and Moran, M. A. (**2004**); Dissolved organic fluorophores in southeastern US coastal waters: Correction method for eliminating Rayleigh and Raman scattering peaks in excitation-emission matrices. *Marine Chemistry* 89(1-4), pp. 15–36, doi:10.1016/j.marchem.2004.02.006.

Zheng, H., Xu, C., Yang, L., Chen, J., Chen, C.-T. A., and Wang, B.-J. (**2017**); Diurnal variations of dissolved organic matter in the hydrothermal system of Green Island, Taiwan. *Marine Chemistry* 195, pp. 61–69, doi:10.1016/j.marchem.2017.05.003.

Zsolnay, A., Baigar, E., Jimenez, M., Steinweg, B., and Saccomandi, F. (**1999**); Differentiating with fluorescence spectroscopy the sources of dissolved organic matter in soils subjected to drying. *Chemosphere* 38(1), pp. 45–50, doi:10.1016/S0045-6535(98)00166-0.

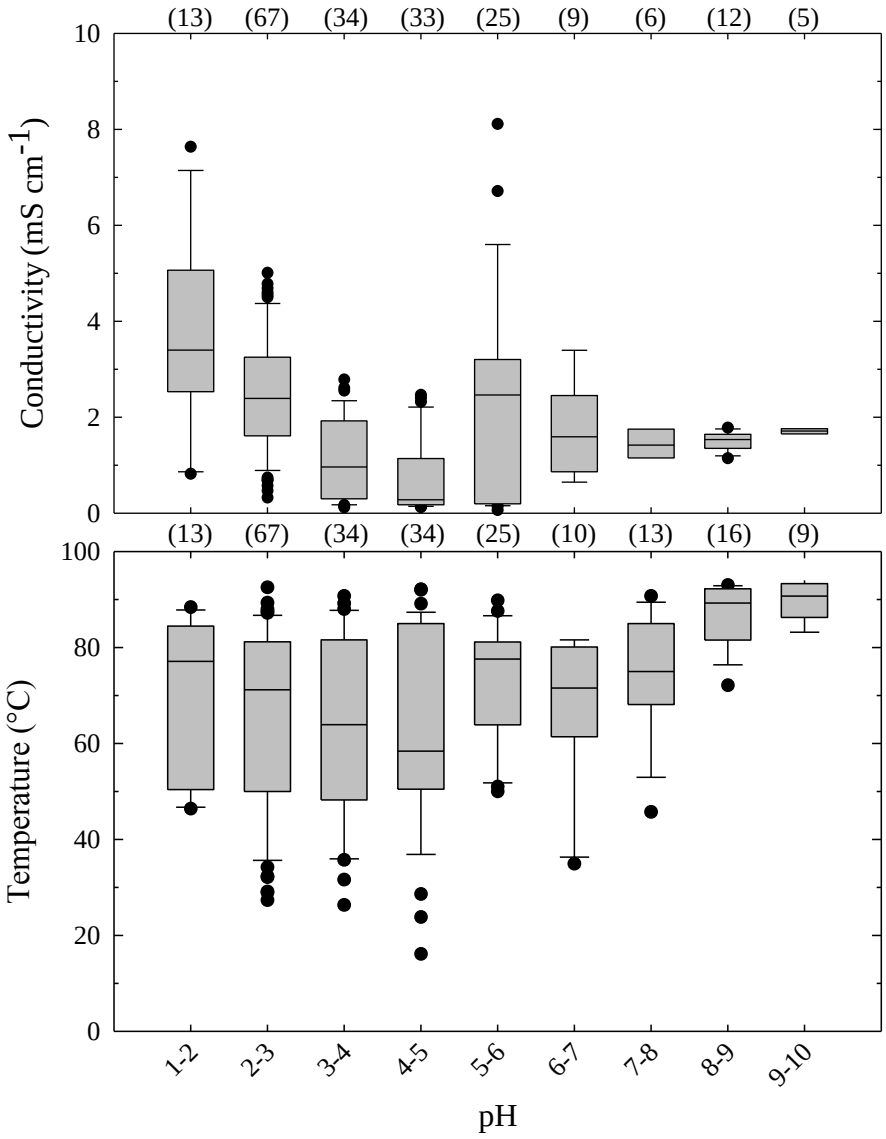

Figure 2.1: Box plots for conductivity and temperature grouped according to pH for hot springs from Yellowstone National Park and the Tengchong hydrothermal region. Each box displays the range in values from all springs in a specific pH range. The numbers in parentheses above each plot indicate the number of samples represented in each box and whisker plot. The line in the middle of each box is the median value. The box boundaries are the 25th and 75th percentiles of the data, the whiskers are the 10th and 90th percentiles, and the circle symbols are outliers. Boxes without whiskers are constructed from 8 or fewer data points.

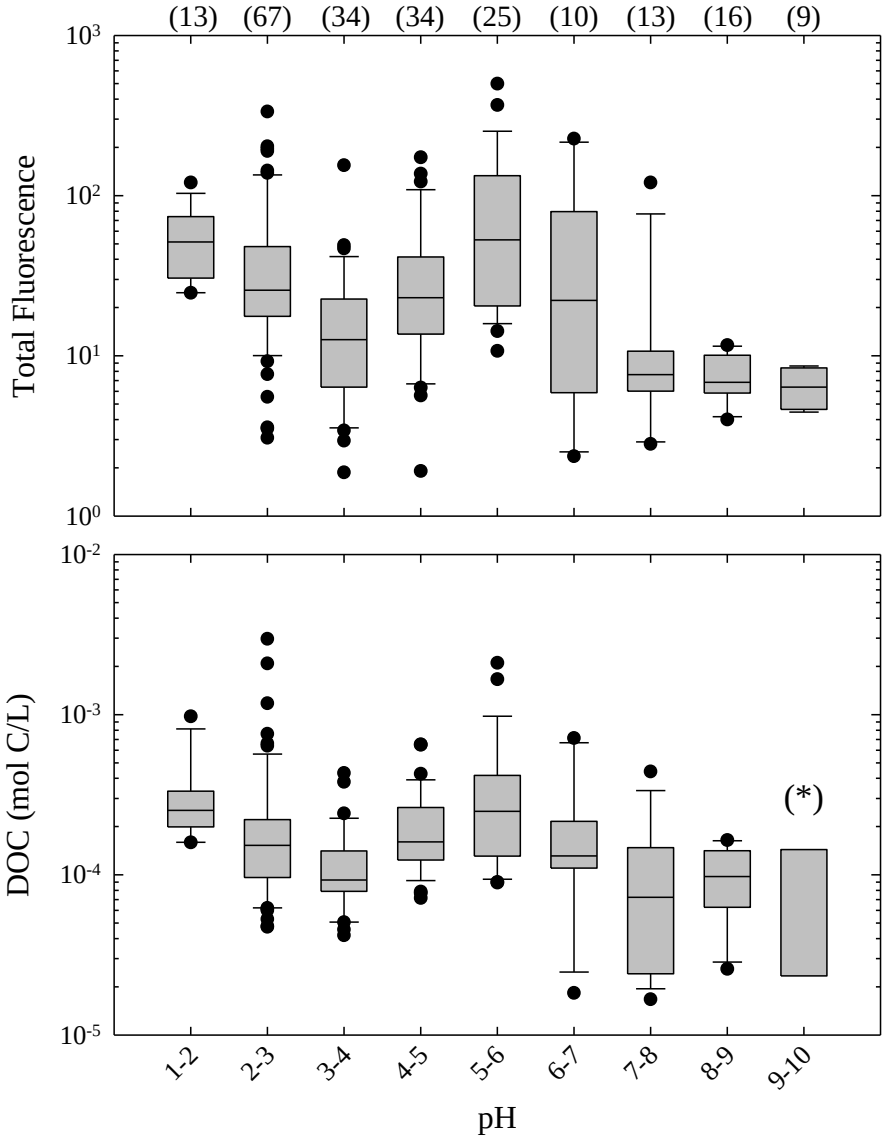

Figure 2.2: Box plots for total fluorescence in Raman-normalized intensity units and for DOC concentrations in hot springs grouped according to pH. The numbers in parentheses at the top indicate the number of samples represented in each pH bin for this plot. The asterisk notes there were only 8 DOC samples available for the pH 9-10 springs. Boxes and whiskers are as described in Figure 2.1.

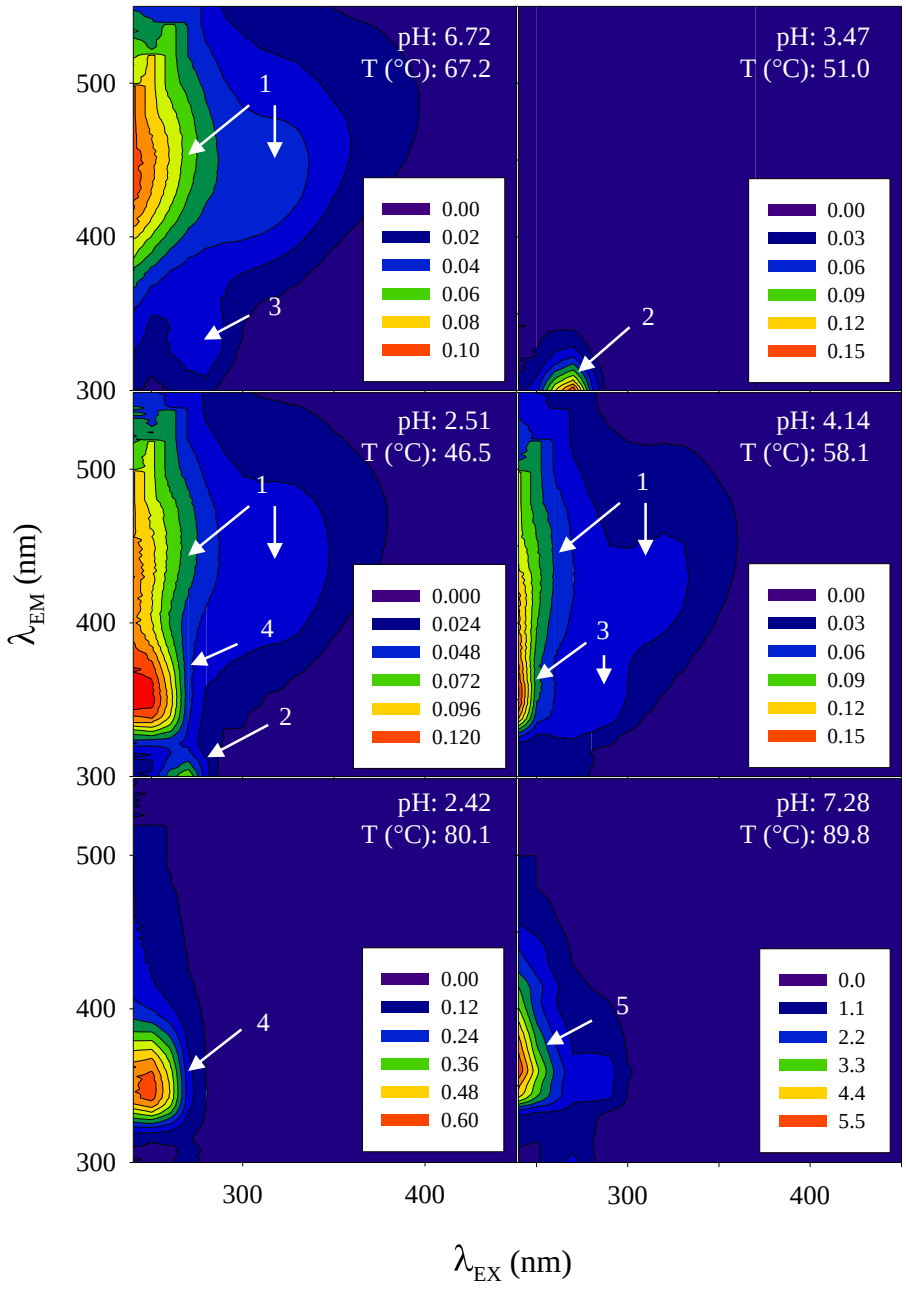

Figure 2.3: Six representative hot spring excitation emission matrices (EEMs). Many of the prominent visual peaks correspond to known fluorophores: 1 – humic substances, 2 – protein-like (tyrosine), 3 – protein-like (tryptophan), 4 – novel, acid-spring fluorophores, and 5 – PAHs. The fluorescence intensity (color scale) is presented in Raman-normalized intensity units; note the scales are different for each of the six panels.

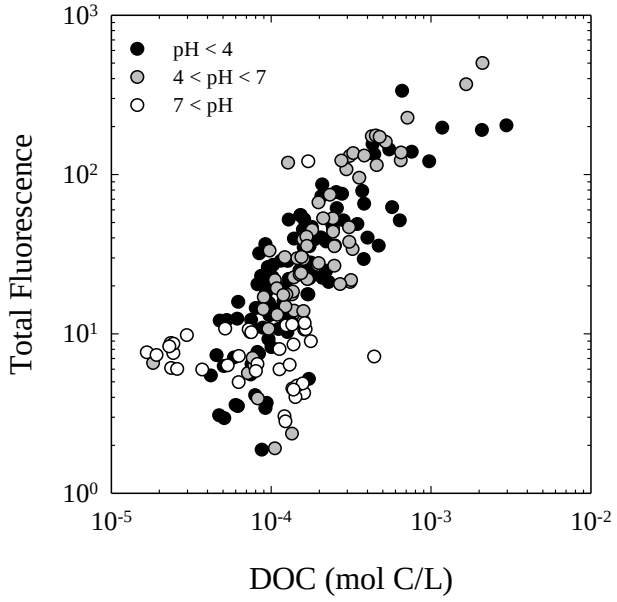

Figure 2.4: Total fluorescence as a function of DOC concentration. Linear regression reveals a statistically significant correlation ($R^2 = 0.6$; $p < 0.05$).

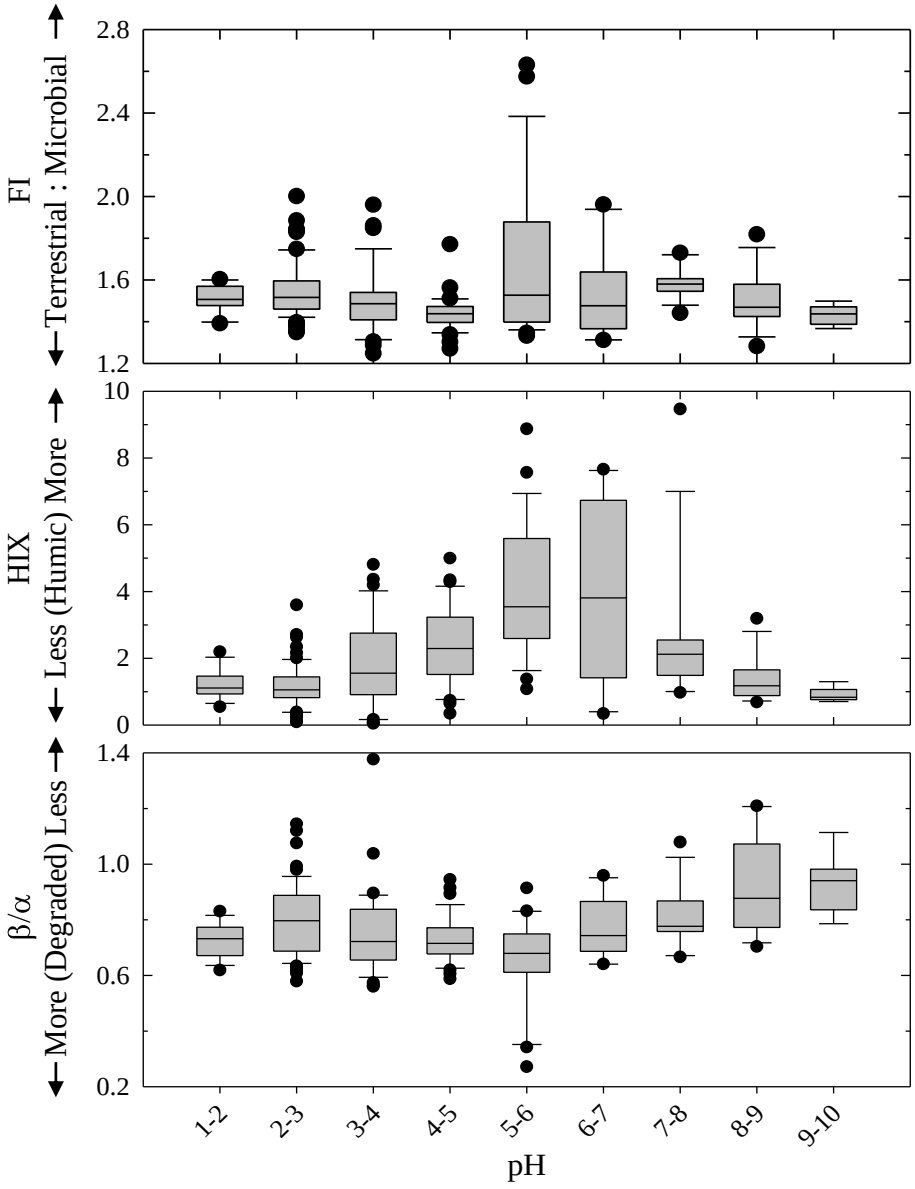

Figure 2.5: Box plots for fluorescence indices (FI, HIX, β/α) in hot springs grouped by pH. The number of samples represented in each box is the same as in Figure 2.3. Traditional interpretations of each index are indicated to the left of each plot. Boxes and whiskers are as described in Figure 2.1.

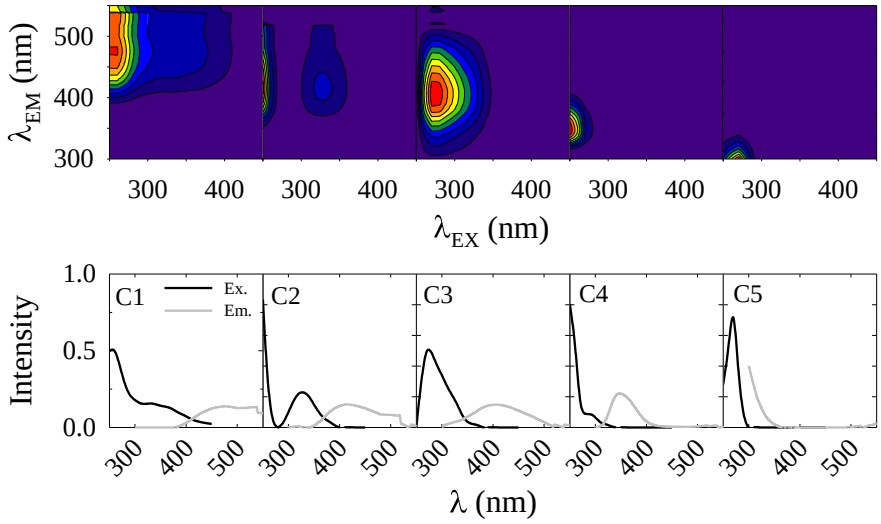

Figure 2.6: (Top) Modelled excitation emission spectra of the five components in our split-half validated hot spring model. (Bottom) Excitation (Ex.) and emission (Em.) loadings for the five model components. Component intensities are relative to each other and scaled from 0 to 1.

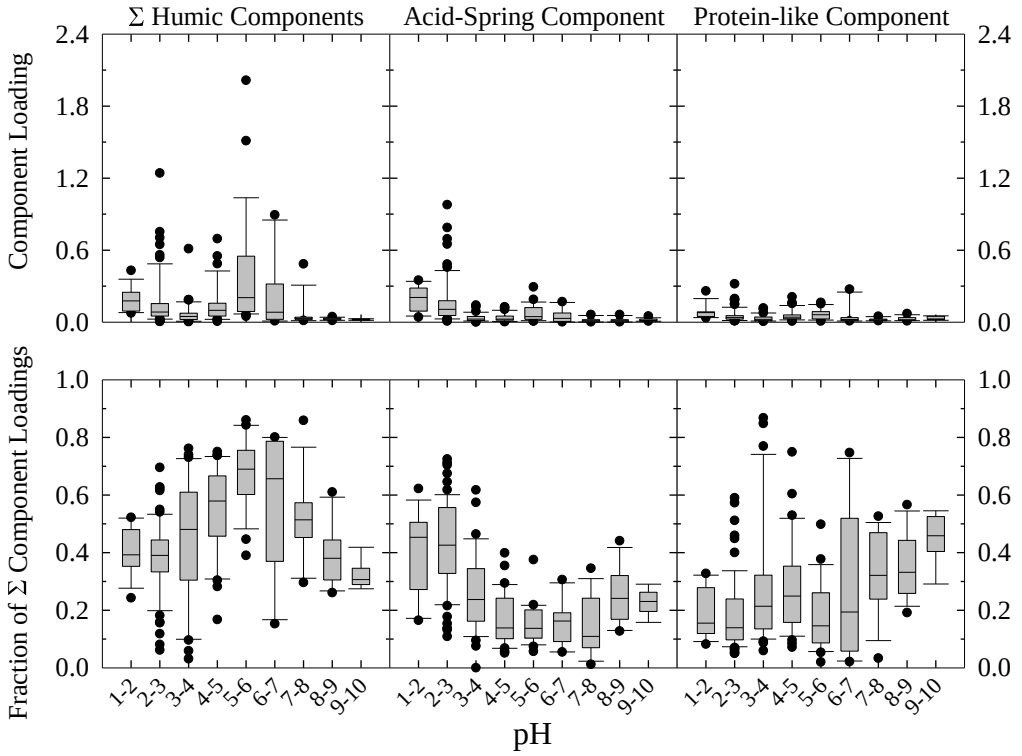

Figure 2.7: Box plots of model component loadings: (Left) Σ humic components, (Center) acid-spring component, and (Right) protein-like component grouped by pH. The three humic components (C1, C2, and C3) are presented as a single summed humic group. (Top) Distribution of the absolute component loadings. (Bottom) Distribution of the component loadings relative to total component loading. Boxes and whiskers are as described in Figure 2.1.

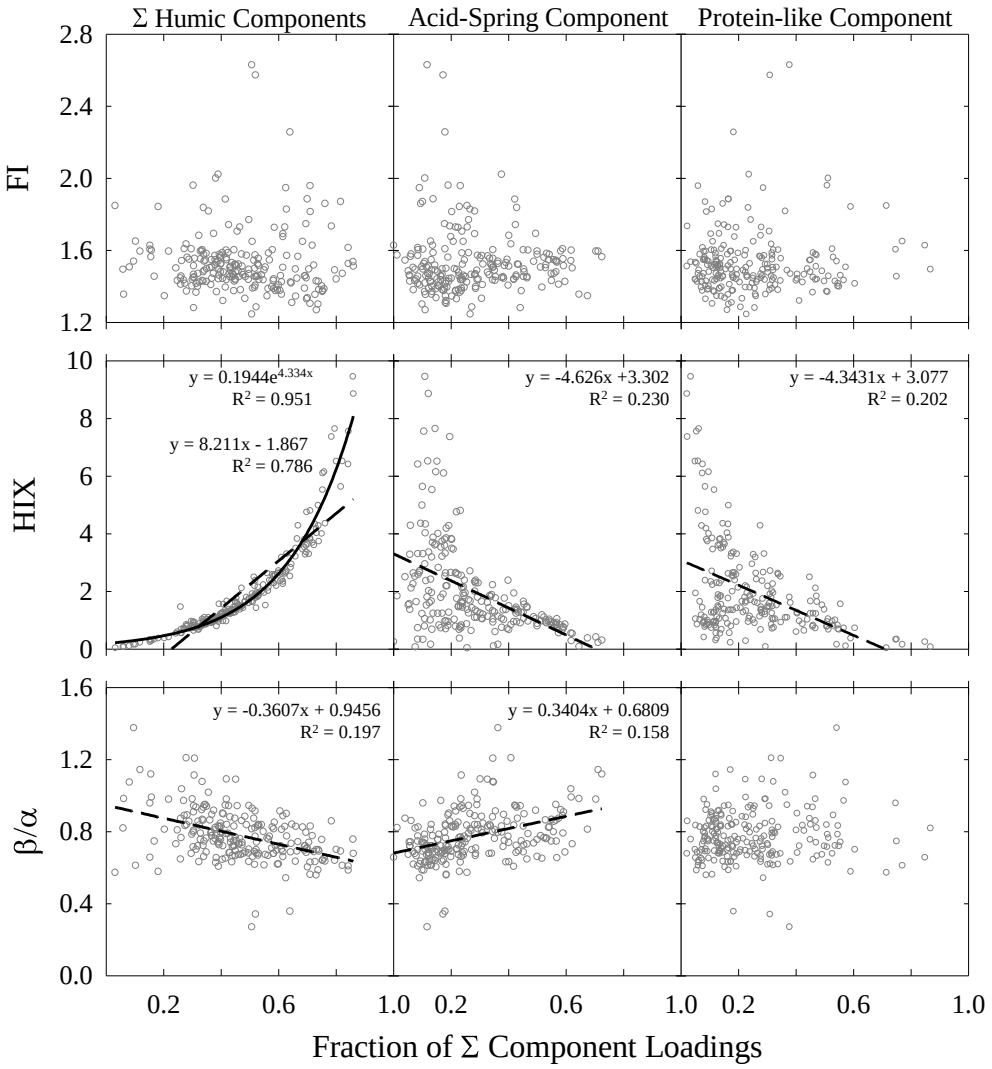

Figure 2.8: Fluorescence indices (Top) FI, (Center) HIX, and (Bottom) β/α as function of the fraction of total component loadings for (Left) Σ humic components, (Center) acid-spring component, and (Right) protein-like component. Plots with a significant ($p < 0.05$) linear correlation are shown with a best fit line (dashed line). An exponential curve (solid line) with a significant correlation was also fit to the Humic vs. HIX plot.

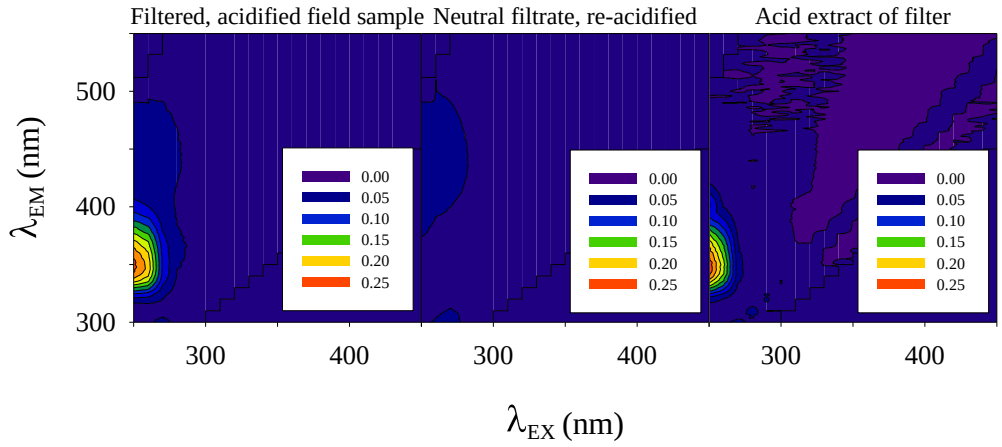

Figure 2.9: EEMs demonstrating the precipitation/removal and subsequent recovery of acid-spring component fluorophores from a strongly acidic spring (pH = 1.93; T = 56.7℃). (Left) The original filtered, acidified field sample. (Center) The neutral filtrate after the sample was raised to pH 7; re-acidified after filtration. (Right) The acid extract of the filter. All EEMs are presented on the same color intensity scale to demonstrate the near total removal (precipitation) of acid-spring component fluorophores after pH adjustment.

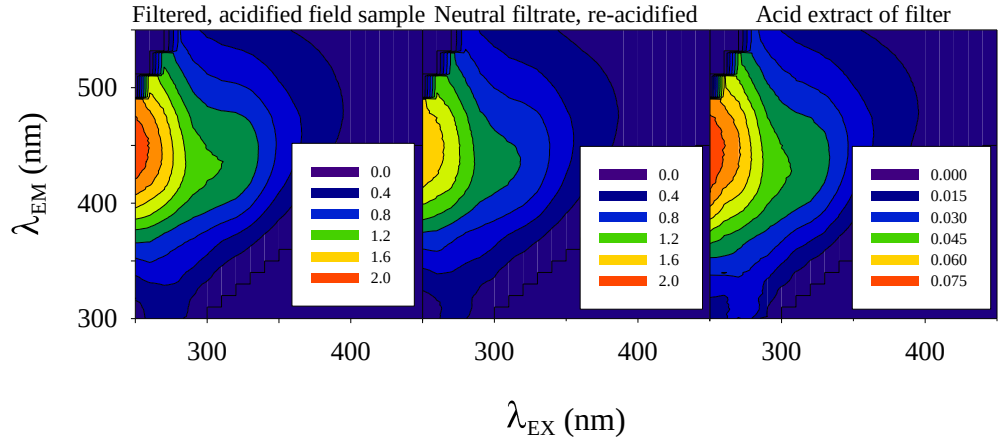

Figure 2.10: EEMs demonstrating the mis-assignment by the PARAFAC model of significant levels of the acid-spring component fluorophores in a weakly acidic spring (pH 5.7). (Left) The filtered, acidified field sample. (Center) The neutral filtrate after the sample was raised to pH 7; re-acidified after filtration. (Right) The acid extract of the filter. The left and center EEMs are normalized to the same intensity scale and do not appear to be significantly different in the region of the acid-spring component (λ_{EX} = 250 nm, λ_{EM} = 350 nm). The right-most EEM is presented with a narrower intensity range and demonstrates that there are no observable acid-spring component fluorophores precipitated and recovered through pH alteration.

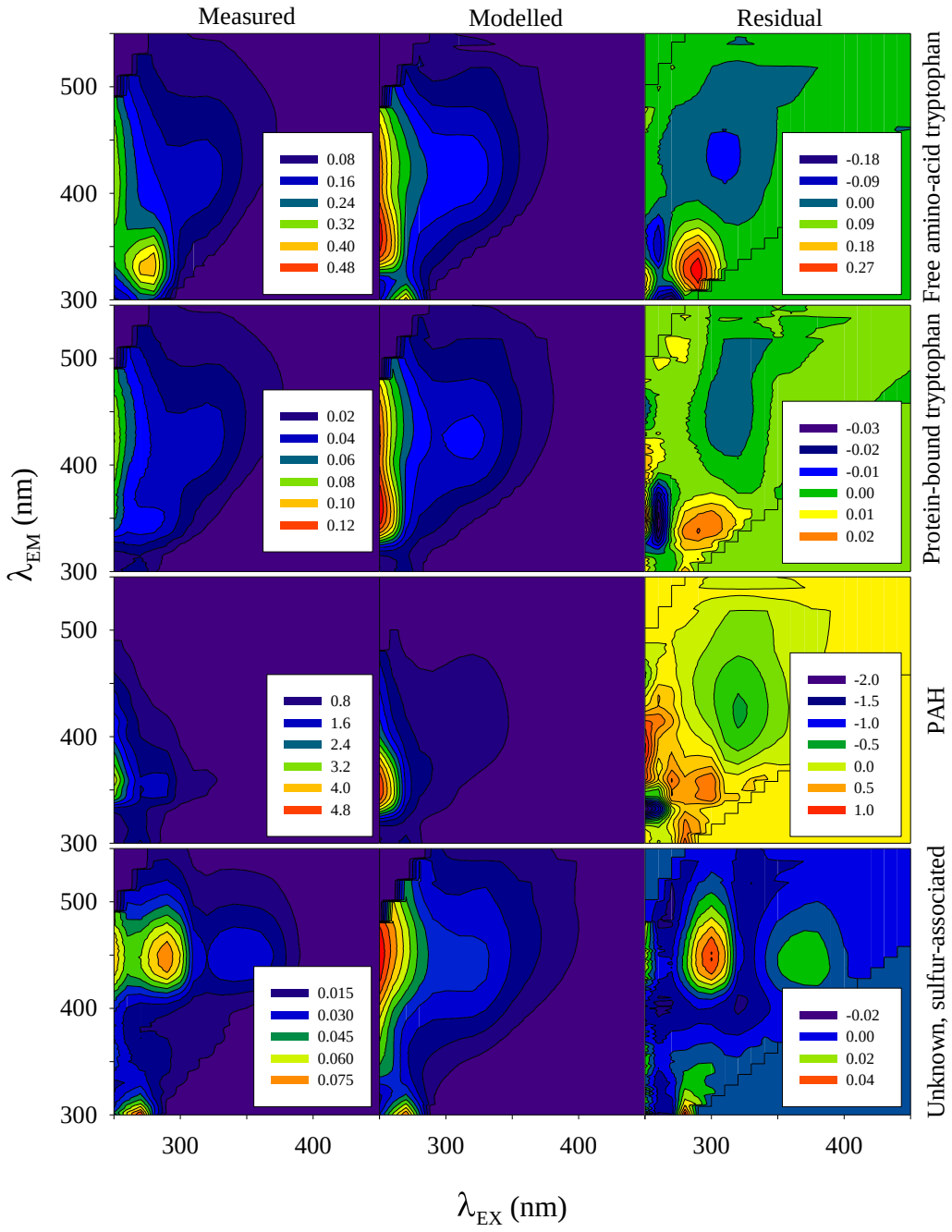

Figure 2.11: Residual analysis of representative sample EEMs. Each row is a single sample chosen because our model was a poor fit to its fluorescence. (Left) Measured EEM of the filtered, acidified, field sample. (Center) PARAFAC modelled EEM, with the same intensity scale as the corresponding measured EEM. (Right) The residual (difference) between the measured and modelled EEMs. Labels on the right-hand side indicate potential fluorophores suggested by the residual analysis; hot (red) spots and cold (blue) spots in the residual plots indicate regions where the model over-fits or under-fits the EEM, respectively.

Chapter 3

OPERATIONALLY CHARACTERIZING THE NOVEL FLUORESCENCE SIGNAL EXCLUSIVE TO ACIDIC HOT SPRINGS

3.1 Introduction

Operational definitions are common in environmental chemistry, especially in relation to natural organic matter (NOM). Major components of terrestrial NOM include wood (Pettersen, 1984; Boerjan et al., 2003) and soil organic matter, which are made up of complex polymeric material that cannot be defined by discrete structural formulas. Instead, NOM composition is described by operationally defined components that are chemically separable or distinguishable by laboratory techniques. Characterization of woody and soil organic matter commonly involves hydrolysis reactions or solvent extractions to break the complex polymeric substances into monomeric units that can be further characterized by molecular weight, elemental abundance, or functional group character. Woody organic matter is made up of two polymeric components: lignin (amorphous polyphenols) and carbohydrates (linear polysaccharides) (Pettersen, 1984; Bajpai, 2018). Monomer phenols in lignin are determined by harsh digestion that destroys all linkages (Bajpai, 2018). Other classifications of lignin are derived from solubility in different organic and aqueous solvents (Fu and Li, 2019). Acid hydrolysis separates acid-insoluble lignin (also referred to as Klason lignin) from acid-soluble lignins and carbohydrates (Kirk and Obst, 1988). The carbohydrate fraction of wood is further sub-divided into cellulose and hemicellulose. Cellulose and hemicellulose are differentiated by their monomeric sugar content following hydrolysis (Pettersen, 1984). The content of each of these fractions is char-

acteristic of different types of wood and has different applications in the biofuel and paper mill industries.

Three main operational components of soil organic matter are humin, humic acids, and fulvic acids (Aiken, 1985). They are distinguished by their solubility in aqueous media. Humin is the fraction that is completely insoluble in water. Humic acids are the fraction that is soluble in alkaline (pH $>$ 13) solution, but insoluble in acidic (pH $<$ 1) solution. Fulvic acids are completely soluble in both acidic and alkaline solutions. Humic substances have a lot of aromatic and carboxyl functionality; however, in truth you could find any functional group described in an undergraduate organic chemistry textbook present in humic substances. Humic and fulvic acids have important roles in surface water environments because they are a refractory sink for organic matter, they bind and transport essential elements and toxic metals, they alter bioavailability of said nutrients and metals, and they absorb ultra-violet (UV) light (Chin et al., 1994; Coble, 2007; Hudson et al., 2007; Gledhill, 2012; Kandasamy and Nagender Nath, 2016).

In aquatic environments, NOM is commonly differentiated as particulate organic matter or dissolved organic matter (DOM; Leenheer, 2009). Conceptually, a dissolved solute is a single molecule surrounded by solvent molecules; however, in a complex environmental sample it is impossible to distinguish such solutes from small aggregates. Instead, DOM is operationally defined as any organic material that passes through a 0.45 µm filter (Leenheer, 1981; Coble, 2007). This operational determination of "dissolved" solutes also includes colloidal aggregates of different organic compounds, organic compounds adsorbed to a colloidal mineral surfaces, and even microbes such as viruses and small bacteria. DOM in aquatic environments is low in concentration and has historically required high volume filtration and solid-phase extraction to obtain sufficient organic material for analysis and characterization (Bader

et al., 1960; Menzel and Vaccaro, 1964; Willams, 1969). Highly sensitive optical techniques, absorbance and fluorescence spectroscopy, are relatively new techniques that characterize the optically active, or colored DOM (CDOM) of a total water sample; these techniques require low sample volume and minimal preparation. One of the earliest descriptions of CDOM (Kalle, 1937) identified yellow-material, or gelbstoff, as a terrestrial component of DOM that significantly contributed to the yellow-brown color of water (Ehrhardt, 1984). Further work identified "yellow" and "blue" CDOM (Briucaud et al., 1981; Coble et al., 1990) in reference to the wavelengths of light that these fractions of organic matter typically absorb. Yellow CDOM, as mentioned previously, became connected with terrestrial-sourced organic matter, also referred to as humic-like CDOM, and blue CDOM was connected with microbially-sourced organic matter, referred to as protein-like CDOM.

A subset of CDOM is the fraction that is also fluorescent (FDOM). The evaluation of FDOM in the environment was comprehensively described three decades prior to this research (Coble et al., 1990). Over time, advancement in analytical techniques has revealed that these two categories (yellow CDOM/humic-like and blue CDOM/protein-like) are over-broad and there are many other fractions of FDOM that can be distinguished. It is now known that a wide range of complex organic matter from terrestrial and microbial sources can produce "humic-like" fluorescence and there are many small aromatic compounds including lignin monomers, indoles, phenols, and tannins that demonstrate "protein-like" optical activity. The terms "humic-like" and "protein-like" are still common in the literature (Fellman et al., 2010; Ishii and Boyer, 2012; Stubbins et al., 2014; Kellerman et al., 2018) albeit, to the sometimes vociferous disapproval of some researchers. Nevertheless, these broad operational classifications can be useful and are sometimes necessary in order to characterize complex materials of unknown origin and composition.

In Chapter 2 I described a parallel factor (PARAFAC) analysis model I generated to describe the major FDOM components in continental hot springs in Yellowstone National Park (Nye et al., 2020). The composition of hydrothermal DOM is known to be different from that of surface water DOM and my fluorescence model revealed as much. There were three "humic-like" components representing complex, surface-derived organic matter, a novel component observed in acidic springs, and a protein-like component resembling tyrosine fluorescence. Each of these component types were found to be dominant in different pH hot springs. In this chapter, I explore the specific spectral and physical characteristics of the novel acid-spring component (ASC) fluorescence identified in the five-component model. This novel fluorescence component is only observed in acidic hot springs (pH < 4.5), but it is observed in nearly every acidic feature sampled in the park. I experimentally determined that these novel fluorophores precipitate out of solution at a pH > 4.5. Further analysis and characterization of the isolated precipitate revealed evidence for a highly condensed, aromatic structure. Such a structure is expected from compounds that have experienced significant thermal alteration. In Yellowstone, thermal alteration of biomass contributes organic carbon to the surface systems and this process is likely the source for this novel fluorescence. Finally, in this research I reacted whole wood samples under hydrothermal conditions in order to reproduce the ASC. Ultimately, I observed the rapid degradation of woody organic matter to produce new fluorescence peaks that were different from the ASC.

3.2 Materials and Methods

3.2.1 Hot Spring Water and Sediment Sampling

Hot spring water samples were collected from Yellowstone National Park between July 2012 and September 2018 as described in Chapter 2. For references to specific sample codes, I refer readers to Appendix E for sample identity and full geochemistry. Briefly, spring water was collected and filtered on site through a series of 1.2 μm and 0.8/0.2 μm Supor^{tm} membrane filters (Pall Corp). All sampling and filtering equipment were triply rinsed with spring water prior to collection. Filtered water for fluorescence samples was collected into fluorinated high-density polyethylene (FLPE) Nalgene^{tm} bottles that were acid-rinsed in 20% HCl and pre-leached with deionized water (18.2 MΩ·cm, Barnstead^{tm} Nanopure) prior to field use. Sample bottles had also been pre-acidified with concentrated HCl to ensure sample acidification to a pH < 2.5. Collected samples were kept in the dark at 4℃ until analysis. Spectrochemical determination of ferrous iron (Fe^{2+}) was performed in the field on filtered water samples using portable Hach spectrophotometers (models 2400 or 2800) and reagent kits (AccuVac®, 1,10 phenanthroline method).

Corresponding sediment samples were also collected from some springs. Sediment was collected into sterile specimen cups and allowed to settle before decanting off as much liquid as possible. After returning from the field, sediment samples were stored in the dark at 4℃ until extraction within one month's time. Sediment samples were centrifuged (Beckman Coulter, Allegra X-22) at 8000 rpm for 1 hour and the supernatant fluid was again discarded. Sediment was then allowed to dry completely at room temperature in a laminar flow hood for 72 hours. Acid-soluble sediment extracts were obtained by mixing ∼0.5 g dry sediment with 10 mL acidified, deionized water (pH = 2.5 with HCl (ACS reagent grade, BDH)). Additional hydrochloric acid

was need to bring some samples to pH < 2.5 due to the presence of carbonates. Samples were then vortexed for five minutes and centrifuged at 8000 rpm for 1 hour. The supernatant fluid was decanted off and then filtered through a pre-rinsed (with 100 mL acidified, deionized water) 0.2 μm Supor^{tm} filter. This yielded the acid-soluble, sediment extract sample used for fluorescence and further chemical analyses.

3.2.2 Isolation of the Acid-Spring Component Fluorophores

The acid-exclusive solubility (see Chapter 2.3.5 and Figure 3.2) of these fluorophores allowed me to collect an isolated sample for direct analysis. The novel fluorophores were precipitated from the acidified, filtered field samples, by neutralization with 1M NaOH, and collected on either 0.2 μm membrane filters (Supor^{tm}) or 0.7 μm glass microfiber filters (GF/F, Whatman®). The precipitated fluorophores were colorless and left a faint waxy residue on the filter. Generally, this isolation was done using 10 mL aliquots to preserve irreplaceable spring samples and never provided more than $\sim$2 mg of precipitated material. The isolated precipitates used for further spectroscopic analysis were either re-dissolved in acidified, deionized water or dried down (at 60℃) to a residue in a pre-combusted glass vial. Fluorescence confirmed that this dried residue re-dissolved easily into acidified water to regenerate the acid-spring fluorescence.

3.2.3 Wood Sample Collection and Digestion Experiments

I collected pine wood samples from the Tonto National Forest near Flagstaff, Arizona to use as a model source of lignin in laboratory experiments. The fluorescence of lignin has been shown to be mostly independent of source wood in terms of excitation and emission maxima (Bublitz and Meng, 1978; Aiken, 2014), although intensities vary among wood types. I chose sticks that were fallen, dry, and finger-sized

or smaller for practical reasons. In the lab they were broken up to be no larger than three inches in length in order to fit into reaction flasks (Figure 3.8), but no further preparation was done prior to digestion experiments.

Experiments for wood sample digestion took place on benchtop hot plates in deionized water using a reflux condenser to supply continuous heat without loss of solvent. The sequence of experimental conditions used is described in Figure 3.8. Acidification was done used either concentrated hydrochloric or concentrated sulfuric acid as listed. Ferrous iron was added in some experiments in the form of dissolved $Fe(NH_4)_2(SO_4)_2$ (ACS reagent grade, Matheson Coleman and Bell). Aqueous products needed to be diluted $\sim$500 fold prior to fluorescence analysis; this dilution was accounted for when correcting the fluorescence data. Additionally, samples were filtered and acidified to pH < 2.5, if they were not already.

The product of experiment 'F' (Figure 3.8) was reacted further under high temperature and pressure conditions in fused silica tubes prepared according to the methods in Bockisch et al. (2018). The product mixture was filtered through a 0.2 μm filter. The filtrate and the leftover loamy sludge were prepared separately in fused silica tubes and reacted in a modified Shimadzu gas chromatograph oven at 150℃ for two weeks. Reaction conditions for these experiments are described in Figure 3.9. Upon reaction completion, the tubes were quenched in water, broken, and the contents collected. The reactions products were all diluted to 10 mL with deionized water that was used to rinse out the tubes for maximum product retrieval. This dilution factor was accounted for in the correction of the fluorescence data. The product solution was filtered (0.2 μm) and prepared for fluorescence analysis as described previously for hot spring water samples.

3.2.4 Absorption and Fluorescence Spectroscopy

Optical properties were determined for aqueous field and experimental samples by ultraviolet-visible (UV-Vis) absorption (Shimadzu UVmini-1240) and 3D-fluorescence (Horiba Jobin Yvon, Fluoromax 4) spectroscopy. Absorbance spectra were obtained using wavelengths from 190 to 1100 nm. Samples that were strongly absorbing at 254 nm (i.e., absorbance > 0.300) were diluted with deionized water so that inner-filter corrections could be made with data from the absorbance spectra (Yang and Zhang, 1995; Ohno, 2002). Fluorescence excitation-emission matrices (EEMs) were collected by scanning through excitation wavelengths from 240 to 450 nm, with a 10 nm stepsize and collecting emission spectra at wavelengths from 300 to 550 nm every 2 nm. Corrections for instrument-specific variability were made using correction files provided by the manufacturer. Sample EEMs were blank-subtracted each day using an EEM of deionized water, and fluorescence intensity was normalized to the area under the Raman scattering signal of water at excitation wavelength 350 nm (Cox et al., 2000; Stedmon et al., 2003). This post-processing of EEMs also corrected for any dilution that occurred during experiments and analysis. Data was removed from the EEMs in the area of first- and second-order Rayleigh scattering ($\lambda_{EM} = \lambda_{EX} \pm 10$ nm and $\lambda_{EM} = 2 \times \lambda_{EX} \pm 10$ nm, respectively) according to the methods in Zepp et al. (2004). All post-processing of EEMs was performed in MATLAB® (MATLAB, 2010). All samples were at pH < 2.5 at the time of fluorescence analysis unless otherwise noted.

3.2.5 Trace Metal Analysis

An especially yellow isolated precipitate from one sample containing the ASC fluorophores was analyzed for trace metal content by inductively coupled plasma

ionization-mass spectrometry (ICP-MS) on a Thermo iCap-Q quadrupole ICP-MS equipped with Ni cones and a quartz spray chamber. Five milligrams of dried, isolated precipitate were digested in 2% nitric acid. The sample was analyzed in kinetic energy discrimination (KED) mode using helium as the collision gas. Internal standards of yttrium were used for quality assurance and quality control. Analytes were quantified by external calibration curves and results are reported in mass percent of the original sample (i.e., prior to nitric acid digestion).

3.2.6 Infrared and Raman Spectroscopy

Several isolated precipitates from samples containing the acid-spring fluorescence as a dominant component were analyzed by Fourier transform infrared (FT-IR) and Raman spectroscopy. For the FT-IR analysis, nearly dried residues (5 mg) were dissolved in several drops of a 50% ethanol-water solution and dropped on a KBR pellet; the solvent was allowed to evaporate before analysis. Spectra were recorded on a Bruker Vertex 70 spectrometer between 800 and 4000 cm^{-1}. Raman spectra were obtained on a micro-Raman spectrometer between 120 and 3800 cm^{-1}. The micro-Raman samples were similarly dissolved in several drops of a 50% ethanol-water solution, dropped on aluminum foil, and allowed to dry. The samples were excited with a 70 mW Ondax® SureLock^{tm} wavelength stabilized diode laser (633 nm). Spectra were collected with an exposure time of 10 seconds and 50 accumulations. The data were recorded with an Action 300i spectrograph and a Princeton Instruments liquid nitrogen cooled, charge-coupled device (CCD) detector.

3.2.7 Additional Analyses

Additional analyses of the ASC were attempted by gas chromatography with flame-ionizing detection (GC-FID) and nuclear magnetic resonance (NMR) spec-

troscopy. There was insufficient signal in these spectra to make any meaningful interpretation. The methods and resulting spectra are found in Appendix C.

3.3 Results and Discussion

3.3.1 Environmental Occurrence of the Acid-Spring Component Fluorophores

In filtered water samples, the acid-spring component (ASC) fluorescence is observed in most springs with a pH < 4, and only in 1 spring with a pH > 4. In the hottest, most acidic, and low volume springs the ASC is usually the dominant fluorophore (Nye et al., 2020). Highly acidic and highly alkaline springs are commonly considered to be minimally mixed with cool surface waters (White et al., 1971; Nordstrom et al., 2009). Mixing of hydrothermal fluids with surface water typically introduces terrestrial organic matter and humic-like fluorescence, so acidic springs with a high relative fraction of the ASC may be considered to have a predominantly hydrothermal source and less mixing. Inferences about mixing between different fluid phases is discussed in detail in Chapter 4. I described the acid-exclusive solubility of these fluorophores in Chapter 2.

To investigate the total presence of the ASC in the environment, I collected sediment samples from hot springs with a wide range in geochemistries. The ASC was present in the sediments (but not the water) of several springs between pH 4 and 5, but only one spring's sediment at a pH > 5 (Figure 3.3). The ASC fluorescence did not appear in the majority of higher pH springs and sediments. The insolubility of these fluorophores in circumneutral pH solutions indicates that the few higher pH (pH > 4) spring sediments with the ASC likely receive input from acid-sulfate water, and are subsequently neutralized by carbonate minerals, or diluted sufficiently by meteoric water. Either way, the pH increases and the ASC fluorophores precipitate

out of solution. The observation of the precipitation of these fluorophores in the environment and the laboratory is an exciting result; often it is difficult to replicate observed natural phenomena in laboratory experiments. In some samples, a yellow or orange precipitate was observed (Figure 3.2) due to co-precipitating iron and aluminum oxides/hydroxides. When this orange precipitate was allowed to air-dry the orange color disappeared and turned into black flecks.

Organic compounds in general have a low solubility in water at ambient temperatures and pressures. Solubility is further decreased by non-polar functional groups such as aromatic rings. The distinctive, pH-dependent solubility of the ASC suggests the compounds have ionizable functional groups that deprotonate at a pH higher than ∼4.5 to produce an uncharged, insoluble species. Among the common organic functional groups, heterocyclic nitrogen and some amines undergo a change in ionization around pH 4-5. For example, pyridine has a pKa of 5.23, quinoline has a pKa of 4.90, and acridine has a pKa of 5.58 at 25℃ (Engineering Toolbox, 2017). These compounds are plausible candidates for the identity of the ASC; thermally altered organic matter generally is highly aromatic and it is known that sulfur and nitrogen heterocyclic inclusion increases with thermal reaction (Hawkes et al., 2016).

However, the hydrothermal subsurface is not at room temperature so changes in solubility with increased temperatures must be considered. Thermodynamic data for the temperature dependence of the pKa values of pyridine and other organics show a general drop in pKa over a circum-ambient range of temperatures between 5℃ and 50℃ (Gagliardi et al., 2015); an exception to this trend is benzoic acid. If the solubility of the ASC fluorophores is a pKa-driven phenomenon, then this thermodynamic trend would suggest that at elevated temperatures, the pH at which the ASC fluorophores precipitates would drop and therefore require more acidic water to mobilize into the dissolved phase. However, thermodynamic data for organic compounds at

temperatures above 100℃ is extremely limited, and thus, it is difficult to speculate on the equllibrium properties of the ASC fluorophores at high temperature. The properties of water also change significantly at elevated temperatures and pressures (Johnson and Norton, 1991; Wagner and Pruß, 2002). For example, the dielectric constant of water decreases with increasing temperature (Bradley and Pitzer, 1979; Fernández et al., 1995) meaning that water becomes more non-polar and thus, a better solvent for organic compounds. Therefore, an uncharged organic compound may in fact readily dissolve at high temperatures when it would precipitate at room temperature.

3.3.2 General Fluorescent Character

The EEM of a natural water sample dominated by the acid-spring fluorescence along with several similar documented fluorophores is shown in Figure 3.1. The excitation spectrum of the novel acid-spring fluorophores ranges from <250 nm to 320 nm, with a peak at <250nm. The true excitation maximum may occur at a wavelength lower than 250 nm; fluorescence analysis at lower excitation wavelengths is by analytical limitations of the fluorometer. The emission spectrum of this component ranges from 310 nm to 430 nm with a peak at 346 nm. This region in EEM space has been traditionally referred to as "protein-like" fluorescence (Coble et al., 1990; Yamashita and Tanoue, 2003; Coble, 2007) due to prevalence of tyrosine, tryptophan, and protein fluorescence (Bridges and Williams, 1968; Krauss et al., 1994; Mayer et al., 1999; Yamashita and Tanoue, 2003); however, it is now understood that many other small aromatic compounds of non-microbial source fluoresce in this area (see Table 3.1). One point to keep in mind is that the majority of these literature-reported fluorophores are analyzed at ambient environmental pH (6 to 8), and the novel acid-spring fluorophores precipitate out of solution pH higher than 4.5. So, it

isn't surprising that this novel fluorescence hasn't been documented in typical surface waters. Additionally, I heated an isolated residue containing the ASC at 450℃ for 6 hours in an Isotemp^{tm} muffle furnace (Fisher Scientific) and found that the fluorescence of the ASC residue (re-dissolved in acidic DI) had not changed significantly in intensity or peak shape.

The observation of the ASC in nearly every acidic feature throughout the park suggests the source of the organic matter is likely as widespread. The largest sources of organic matter include terrestrial plants (namely woody organic matter from trees as well as grasses) and buried sedimentary organic matter. The ASC fluorescence is, spectrally, most comparable to tryptophan, acid-soluble lignins, and polycyclic aromatic hydrocarbons (PAHs). Although a spectral match of excitation and emission maxima does not prove identity (Aiken, 2014), there are general structural trends associated with long wavelength and short wavelength fluorescence that can be inferred. In brief, higher molecular weight compounds typically fluorescence at longer wavelengths and lower molecular weight compounds fluoresce at shorter wavelengths. Wide excitation and emission peaks (such as in humic-like fluorescence) indicates a variety of structural differences, while narrow excitation and emission peaks are usually indicative of discrete compounds or a class of compounds with minimal structural variation.

Tryptophan has two fluorescence peaks; a peak at λ_{EX} = 280nm and λ_{EM} = 350 nm and another of higher intensity at λ_{EX} = 220nm and λ_{EM} = 350 nm. The peak at λ_{EX} = 220nm and λ_{EM} = 350 nm is not as commonly reported; presumably, because of analytical limitations due to low lamp output at short wavelengths. However, it has also been reported that this short wavelength excitation peak only occurs in peptide- or protein-bound tryptophan, while a pure typtopahn standard only produces the longer wavelength excitation peak (Determann et al., 1998; Mayer et al., 1999;

Yamashita and Tanoue, 2003). The ASC has an emission maximum indentical to that of tryptophan (350 nm), but the excitation maximum (< 250 nm) lies squarely between the two excitation maxima for tryptophan. Some of the model compounds for acid-soluble lignins reported by Albinsson et al. (1999) have identical peak maxima to the ASC. However, the solvent for their analysis was a dioxane-water mixture and solvent effects can alter both fluorescence intensity and peak maxima, so it is difficult to say if the peak is the same. Additionally, acid-soluble lignins are not described as being insoluble in neutral or basic pH solutions, like the ASC.

Fluorescence intensities, and sometimes excitation and emission maxima, are pH dependent for many organic molecules, especially ionizable compounds containing -COOH, -OH, -NH_2 functional groups (Chen, 1967; Bridges and Williams, 1968; Krauss et al., 1994; Buna et al., 1996; Hudson et al., 2007; Lakowicz, 2010; Donaldson, 2013). Most natural aquatic environments exist within a narrow pH range of 6 to 8 and it is not generally necessary to correct for pH effects (Hudson et al., 2007; Osburn et al., 2014). The wide range in pH of hot springs (pH ranges from 1.5 to 10) requires some pH correction to be able to account for differences in fluorescence signal from spring to spring. For my research, all samples were analyzed at pH 2 because acidification was the method of preserving samples in the field (as well as removing inorganic carbon); it was convenient to not alter the samples further prior to fluorescence analysis.

Fluorescence spectroscopy is remarkable in that it is highly sensitive and requires very little sample preparation, allowing the analysis of very low concentration organics (provided they fluoresce in the first place). This high sensitivity means analytes that can be identified by fluorescence may not be able to be detected by other methods. I assume this is the reason why I was unable to retrieve any information from GC and NMR analysis. I did a simple calculation, assuming the novel acid-spring fluorophores

had a molar absorptivity constant, quantum yield, and molecular mass identical to that of tryptophan, in order to estimate the potential mass available in a 100 mL water sample. Based on a two-point standard curve for tryptophan, the spring sample with the highest ASC fluorescence intensity (Figure 3.4, Sample 1) in my data set corresponds to a 7.69 μM concentration of the acid-spring fluorophores (Table 3.2). The volume of a typical field sample varies between 20 mL and 100 mL, so at most there would only be 157 μg of material in an entire 100 mL field sample, in this theoretical example. The sample with the lowest ASC fluorescence intensity (Figure 3.4, Sample 2) corresponds to a 0.0394 μM concentration, and at most 0.804 μg in a 100 mL field sample. These are theoretical calculations of course, and the numbers depend strongly on the assumed values for the molar absorptivity, quantum yield, and molecular mass. Nevertheless, it demonstrates how little mass is likely to be obtained from my standard field sampling.

3.3.3 Co-precipitating Metal Content

In many of the samples from which I isolated material, there was a distinct yellow-orange precipitate. ICP-MS analysis of one such precipitate revealed that it was 23% Fe, 6% Al, and 4% other inorganic species, by mass. This result does not indicate whether these metals were present as metal oxides/hydroxides or if they were part of a metal-organic complex. Iron and aluminum both speciate as insoluble oxide and hydroxides at pH $>$ 5, depending on the oxidation-reduction potential of the solution (Hem and Cropper, 1959; Rubin, 1974; Takeno, 2005). It is also possible that these metals are bound in a complex to the ASC fluorophores, and DOM is known to complex with metals (Rose and Waite, 2003; Toner et al., 2009; Remko et al., 2011; Gledhill, 2012; Shams El-Din et al., 2014). Typically, this complexation quenches fluorescence (Hutnik et al., 1991; Dunning Hotopp et al., 2003; Hudson

et al., 2007; Yamashita and Jaffé, 2008; Wu et al., 2011; He et al., 2016). However, morin, a non-fluorescent organic compound, is shown to fluoresce upon complexation with aluminum at low pH (Saari and Seitz, 1983; Browne et al., 1990).

In all the sampled hot springs with pH < 4.5, there is a significant correlation between Fe^{2+} concentration and the ASC loading (Figure 3.5); this correlation is strongest for springs with the lowest pH values (1.5 to 3.0). The correlation between Fe^{2+} and the ASC loadings was stronger (i.e., Pearson's Correlation Coefficient closer to 1) than the correlation between pH and Fe^{2+} or the correlation between pH and the ASC for the same set of samples. This leaves open the possibility that the novel fluorophores are a metal-organic fluorescence complex.

Not all the samples demonstrated a yellow-orange color upon precipitation. There were some samples with no visible precipitate after neutralizing the solution; and yet, they were significantly difficult to filter, and the ASC fluorescence was absent from the filtrate. When the filters were dried, there was a faint, colorless, waxy residue on the filter. I believe such isolates represent the "purest" isolates, free of co-precipitating material. It is still possible that they could contain complexed metals; but in these samples there is notably less of the co-precipitating metal oxides that could potentially interfere with further analysis.

3.3.4 Condensed Aromatic Characteristics

An isolate containing strong yellow precipitate and a sample containing no colored precipitate were each analyzed by FT-IR and Raman spectroscopy (samples 130720TW and 140727SD; see Figure 3.2). Both of these sample's EEMs were dominated by the ASC and were chosen to avoid any potential "contaminant" signal from surface-derived organic matter. The spectra obtained from both methods were nearly identical for both samples, indicating, in the case of FT-IR (Figure 3.6) and Raman

(Figure 3.7) spectroscopy, that the co-precipitating yellow/orange material in sample 140727SD is not interfering.

Peak assignments from the FT-IR are made somewhat loosely, due to the unknown nature of the target, but they do reveal several interesting features. There is a distinctive lack of carboxyl (C=O) peaks that would be found at 1650 and 1850 cm^{-1}. Carboxylic acid groups are common in natural organic matter, but they also provide a means of base solubility, a property not demonstrated by the ASC. Alkane C-H stretching peaks are present at $\sim$2900 cm^{-1}, C=C stretching peaks between 1540 and 1630 cm^{-1}, and -CH_2 and -CH_3 bending peaks around 1430 cm^{-1}. The peaks between 1000 and 1100 cm^{-1} are possibly from C-O stretching, but remain uncertain. Peaks around 1000 cm^{-1} and lower are in the fingerprint region and difficult to interpret, especially in an unknown mixture of compounds. While these assignments cannot be considered definitive, the lack of evidence for carboxyl groups is a striking result.

The Raman spectroscopies produced similarily distinctive results. The pair of peaks at $\sim$1330 cm^{-1} and $\sim$1610 cm^{-1} are highly similar to graphite, graphene, and other polycyclic aromatic graphitic compounds, such as activated carbon (Castiglioni et al., 2001; Kelemen and Fang, 2001; Castiglioni et al., 2004; Li et al., 2009). In graphite, the peak near 1610 cm^{-1} is referred to as the G band. The peak near 1330 cm^{-1} (the D band) only appears in disordered materials containing structural deformities or heteroatoms (Castiglioni et al., 2001, 2004). These two bands are present to some degree in all polycyclic aromatic hydrocarbons, but the peak height and width along with the presence of other peaks are used to distinguish among different types of condensed, aromatic carbon. I wouldn't expect a pure graphite or graphene without imperfections to be present in an environmental system, so these peaks strongly suggest compounds of a highly condensed aromatic structure. These types of Raman

peaks have also been noted in the evolution of keragen to coal (Kelemen and Fang, 2001); giving further evidence that these fluorophores are the result of thermally altered biomass, potentially from buried sediments. The peaks around 2675 cm^{-1} are also common in graphitic spectra and are referred to as the 2D or G' peaks. The peak at 3410 cm^{-1} is from -OH in water or in minerals/inorganic species that may have co-precipitated (Frost et al., 2003). It is possible these condensed aromatic features are consistent with a thermal source for the ASC; graphitic and soot-like material is often formed through burning and combustion reactions.

3.3.5 Rapid Alteration of Wood in High Temperature, Acidic Experiments

I digested natural wood samples in benchtop experiments as model sources of thermally altered natural organic matter. Some of the spectra most similar to the ASC fluorophores that have been described in the literature come from acid-soluble lignins, or lignin derivatives that are produced from the hot, acidic digestion of wood in the paper mill industry. Briefly, this process typically involves digesting a total wood sample in 72% sulfuric acid followed by dilution to 3% sulfuric acid and boiling to produce acid-soluble lignins and insoluble lignins (Kirk and Obst, 1988; Yasuda et al., 2001; Bajpai, 2018). These two lignin pools are then determined separately, following a filtration. Fluorescence spectra for model acid-soluble lignin compounds are reported by (Albinsson et al., 1999). These model lignins had excitation and emission spectra remarkably similar to the ASC spectra; however, these compounds are not exclusively acid-soluble. In the environment, there is extensive time, much higher temperatures and pressure, and the presence of mineral catalysts that might reasonably be expected to produce different products than the industrial wood-processing method (Shipp et al., 2013; Shock et al., 2019).

I reacted natural wood under a gradient of increasing temperatures and acidic conditions (Figures 3.8 and 3.9) and in some cases, addition of ferrous iron. Initially, room temperature leaching of wood resulted in very typical humic-like fluorescence. The major components of soil organic matter (i.e., humin, humic acids, and fulvic acids) are largely sourced from biomass, so this observation is not surprising. These fractions of soil organic matter are considered relatively non-reactive in ambient surface waters; although, gradual "humification" is observed over time that results in longer wavelength fluorescence. Upon the addition of heat and acid, I observed rapid breakdown of the wood. The water in the experiments became darkly colored as material leached from the wood. In experiment "F" (at reflux, in 1N sulfuric acid, with 1.79 mM Fe^{2+}), the physical structure of the wood completely broke down into a loamy material. Fluorescence EEMs revealed the appearance of distinct fluorescence peaks, at shorter wavelengths. This indicates that the large, complex organic material present in the wood samples is breaking down into smaller moieties, consistent with what happens in the paper milling process and also consistent with what has been shown in thermal alteration of marine organic matter (Hawkes et al., 2016). Some of the new fluorescence peaks appeared spectrally comparable to those reported by Albinsson et al. (1999) and to the novel ASC fluorophores. I performed the pH shifting, filtration, and isolation experiment on all wood experiment products, but did not observe the presence of any exclusively acid-soluble fluorophores (Appendix D).

As a further test, the products of experiment "F" were reacted under high temperature (150℃) in fused silica reaction vessels (Figure 3.9). These experiments demonstrated further changes in the fluorescence signal, but no generation of exclusively acid soluble components similar to the novel fluorophores in acidic hot springs. The results of these experiments demonstrate that "non-reactive" surface organic matter quickly breaks down and is transformed by the addition of heat and acid. The ele-

vated temperatures, pressures, and presence of mineral catalysts in the hydrothermal subsurface extensively alters surface organic matter and likely in ways than can not be replicated in simple benchtop experiments. Petroleum seeps (Love and Good, 1970; Clifton et al., 1990) and PAH fluorescence (Nye et al., 2020) are evidence of this extensive degradation, so thermally altered complex organic matter remains a likely source for the novel ASC fluorophores.

3.4 Conclusions

I have further characterized the novel fluorophores present in the acidic springs of Yellowstone National Park. Through laboratory experiments I demonstrated that the exclusive environmental presence in acidic hot springs is due to a pH-dependent solubility. This novel fluorescence appears in nearly all acidic (pH < 4) springs in Yellowstone, with the exception of some that are steam-heated surface water. Additionally, acidic extractions of sediments from hot springs indicate that the ASC is only present in higher pH springs that have had influence from acid-sulfate water. The acid-exclusive solubility likely indicates an ionizable functional group that is protonated at pH < 5 and deprotonated at pH > 5. The most likely functional groups for this are heterocyclic nitrogen bearing compounds because they typically have pKa values between 4 and 5, and because nitrogen is known to be incorporated into aromatic ring structures at high temperatures. Characterization by other techniques was unsuccessful due to insufficient sample and insolubility in DCM, but Raman and FT-IR spectroscopy revealed a lack of C=O bonds and similar spectral character to graphitic material, indicative of a highly condensed aromatic structure lacking oxygenated functional groups.

Lignin and humic substances, which are in part sourced from woody organic matter, are considered refractory members of natural organic matter and relatively re-

sistant to degradation in surface, terrestrial environments. Yet, simple hydrothermal digestion of natural wood resulted in dramatic changes in fluorescence signal. Novel peaks appeared, but none matched the ASC, and, at minimum, confirmed that lignin and humic substances are readily reactive in hydrothermal fluids. These results promote thermally altered, complex organic matter as the source of these novel fluorophores. Whether this complex organic matter, is of woody, soil, or sediment origin is uncertain. The strongest appearance in the hottest, most acidic springs would seem to indicate that a subsurface source (buried sedimentary organic matter) is more likely than a surface source. Despite being easily detectable by fluorescence spectroscopy, these novel fluorophores were at such low natural abundance that analysis by higher resolution molecular characterization techniques was unsuccessful. This in part proves that fluorescence spectroscopy is a powerful, highly sensitive tool that can be applied to tracking different FDOM in hydrothermal systems. Further attempts to identify and characterize the novel ASC fluorophores will require similarly sensitive techniques, or the collection of much greater volumes of water and sediment samples, in order to extract more material.

Aiken, G. R. (ed.) (**1985**); *Humic Substances in Soil, Sediment, and Water: Geochemistry, Isolation, and Characterization*. Wiley, New York, USA.

Aiken, G. R. (**2014**); Fluorescence and dissolved organic matter: A chemist's perspective. In: Coble, P. G., Lead, J., Baker, A., Reynolds, D. M., and Spencer, R. G. M. (eds.), *Aquatic Organic Matter Fluorescence*, pp. 35–74, Cambridge Environmental Chemistry Series, Cambridge University Press, New York, USA, doi: 10.1017/CBO9781139045452.005.

Albinsson, B., Li, S., Lundquist, K., and Stomberg, R. (**1999**); The origin of lignin fluorescence. *Journal of Molecular Structure* 508(1-3), pp. 19–27, doi:10.1016/S0022-2860(98)00913-2.

Bader, R. G., Hood, D. W., and Smith, J. B. (**1960**); Recovery of dissolved organic matter in sea-water and organic sorption by particulate material. *Geochimica et Cosmochimica Acta* 19(4), pp. 236–243, doi:10.1016/0016-7037(60)90031-4.

Bajpai, P. (**2018**); *Raw material and pulp making*. Third edition, Biermann's Handbook of Pulp and Paper, Elsevier, doi:10.1016/C2017-0-00513-X.

Bockisch, C., Lorance, E. D., Hartnett, H. E., Shock, E. L., and Gould, I. R. (**2018**); Kinetics and mechanisms of dehydration of secondary alcohols under hydrothermal conditions. *ACS Earth and Space Chemistry* 2(8), pp. 821–832, doi:10.1021/acsearthspacechem.8b00030.

Boerjan, W., Ralph, J., and Baucher, M. (**2003**); Lignin biosynthesis. *Annual Review of Plant Biology* 54(1), pp. 519–546, doi:10.1146/annurev.arplant.54.031902.134938.

Bradley, D. J. and Pitzer, K. S. (**1979**); Thermodynamics of electrolytes. 12. Dielectric properties of water and Debye-Hückel parameters to 350℃ and 1 kbar. *The Journal of Physical Chemistry* 83(12), pp. 1599–1603, doi:10.1021/j100475a009.

Bridges, J. W. and Williams, R. T. (**1968**); The fluorescence of indoles and aniline derivatives. *Biochemical Journal* 107(2), pp. 225–237, doi:10.1042/bj1070225.

Briucaud, A., Morel, A., and Prieur, L. (**1981**); Absorption by dissolved organic matter of the sea (yellow substance) in the UV and visible domains. *Limnology and Oceanography* 26(1), pp. 43–53, doi:10.4319/lo.1981.26.1.0043.

Browne, B. A., McColl, J. G., and Driscoll, C. T. (**1990**); Aluminum speciation using morin: I. Morin and its complexes with aluminum. *Journal of Environmental Quality* 19(1), pp. 65–72, doi:10.2134/jeq1990.00472425001900010008x.

Bublitz, W. J. and Meng, T. Y. (**1978**); The fluorometric behavior of pulping waste liquors. *Tappi* 61, pp. 27–30.

Buna, M., Aaron, J. J., Prognon, P., and Mahuzier, G. (**1996**); Effects of pH and solvent on the fluorescence properties of biomedically important benzamides. Application to determination in drugs and in human urine. *The Analyst* 121(11), pp. 1551–1556, doi:10.1039/an9962101551.

Castiglioni, C., Mapelli, C., Negri, F., and Zerbi, G. (**2001**); Origin of the D line in the Raman spectrum of graphite: A study based on Raman frequencies and intensities of polycyclic aromatic hydrocarbon molecules. *The Journal of Chemical Physics* 114(2), p. 963, doi:10.1063/1.1329670.

Castiglioni, C., Tommasini, M., and Zerbi, G. (**2004**); Raman spectroscopy of polyconjugated molecules and materials: confinement effect in one and two dimensions. *Philosophical Transactions of the Royal Society of London. Series A: Mathematical, Physical and Engineering Sciences* 362(1824), pp. 2425–2459, doi:10.1098/rsta.2004.1448.

Cawley, K. M., Butler, K. D., Aiken, G. R., Larsen, L. G., Huntington, T. G., and McKnight, D. M. (**2012**); Identifying fluorescent pulp mill effluent in the Gulf of Maine and its watershed. *Marine Pollution Bulletin* 64(8), pp. 1678–1687, doi:10.1016/j.marpolbul.2012.05.040.

Chen, R. F. (**1967**); Fluorescence quantum yields of tryptophan and tyrosine. *Analytical Letters* 1(1), pp. 35–42, doi:10.1080/00032716708051097.

Chin, Y.-P., Aiken, G. R., and O'Loughlin, E. (**1994**); Molecular weight, polydispersity, and spectroscopic properties of aquatic humic substances. *Environmental Science & Technology* 28(11), pp. 1853–1858, doi:10.1021/es00060a015.

Clifton, C., Walters, C., and Simoneit, B. (**1990**); Hydrothermal petroleums from Yellowstone National Park, Wyoming, U.S.A. *Applied Geochemistry* 5(1-2), pp. 169–191, doi:10.1016/0883-2927(90)90047-9.

Coble, P. G. (**2007**); Marine optical biogeochemistry: The chemistry of ocean color. *Chemical Reviews* 107(2), pp. 402–418, doi:10.1021/cr050350+.

Coble, P. G., Green, S. A., Blough, N. V., and Gagosian, R. B. (**1990**); Characterization of dissolved organic matter in the Black Sea by fluorescence spectroscopy. *Nature* 348(6300), pp. 432–435, doi:10.1038/348432a0.

Coble, P. G., Del Castillo, C. E., and Avril, B. (**1998**); Distribution and optical properties of CDOM in the Arabian Sea during the 1995 Southwest Monsoon. *Deep Sea Research Part II: Topical Studies in Oceanography* 45(10-11), pp. 2195–2223, doi:10.1016/S0967-0645(98)00068-X.

Cory, R. M. and McKnight, D. M. (**2005**); Fluorescence spectroscopy reveals ubiquitous presence of oxidized and reduced quinones in dissolved organic matter. *Environmental Science & Technology* 39(21), pp. 8142–8149, doi:10.1021/es0506962.

Cox, L., Celis, R., Hermosín, M. C., Cornejo, J., Zsolnay, A., and Zeller, K. (**2000**); Effect of organic amendments on herbicide sorption as related to the nature of the dissolved organic matter. *Environmental Science & Technology* 34(21), pp. 4600–4605, doi:10.1021/es0000293.

Determann, S., Lobbes, J. M., Reuter, R., and Rullkötter, J. (**1998**); Ultraviolet fluorescence excitation and emission spectroscopy of marine algae and bacteria. *Marine Chemistry* 62(1-2), pp. 137–156, doi:10.1016/S0304-4203(98)00026-7.

Donaldson, L. (**2013**); Softwood and hardwood lignin fluorescence spectra of wood cell walls in different mounting media. *IAWA Journal* 34(1), pp. 3–19, doi:10.1163/22941932-00000002.

Dunning Hotopp, J. C., Auchtung, T. A., Hogan, D. A., and Hausinger, R. P. (**2003**); Intrinsic tryptophan fluorescence as a probe of metal and alpha-ketoglutarate binding to TfdA, a mononuclear non-heme iron dioxygenase. *Journal of Inorganic Biochemistry* 93(1-2), pp. 66–70.

Ehrhardt, M. (**1984**); Marine gelbstoff. In: Hutzinger, O. (ed.), *The Natural Environment and the Biogeochemical Cycles*, pp. 63–77, The Handbook of Environmental Chemistry, volume 1/1C, Springer, Berlin, Germany, doi:10.1007/978-3-540-38829-6_3.

Engineering Toolbox (**2017**); Amines, diamines and cyclic organic nitrogen compounds - pKa values. https://www.engineeringtoolbox.com/amine-diamine-pyridine-cyclic-quinoline-aminobenzene-structure-pka-carboxylic-dissociation-constant-d_1949.html.

Fellman, J. B., Hood, E., and Spencer, R. G. M. (**2010**); Fluorescence spectroscopy opens new windows into dissolved organic matter dynamics in freshwater ecosystems: A review. *Limnology and Oceanography* 55(6), pp. 2452–2462, doi:10.4319/lo.2010.55.6.2452.

Fernández, D. P., Mulev, Y., Goodwin, A. R. H., and Sengers, J. M. H. L. (**1995**); A database for the static dielectric constant of water and steam. *Journal of Physical and Chemical Reference Data* 24(1), pp. 33–70, doi:10.1063/1.555977.

Frost, R. L., Williams, P. A., and Martens, W. (**2003**); Raman spectroscopy of the minerals boléite, cumengéite, diaboléte and phosgenite - implications for the analysis of cosmetics of antiquity. *Mineralogical Magazine* 67(1), pp. 103–111, doi:10.1180/0026461036710088.

Fu, S. and Li, B. (**2019**); Structure and characteristics of lignin. In: Huang, J., Fu, S., Gan, L., and Zhang, L. (eds.), *Lignin Chemistry and Applications*, pp. 25–50, Natural Polymer Based Novel Materials, Elsevier, doi:10.1016/B978-0-12-813941-7.00002-3.

Gagliardi, L. G., Tascon, M., and Castells, C. B. (**2015**); Effect of temperature on acid-base equilibria in separation techniques. A review. *Analytica Chimica Acta* 889, pp. 35–57, doi:10.1016/j.aca.2015.05.053.

Gledhill, M. (**2012**); The organic complexation of iron in the marine environment: A review. *Frontiers in Microbiology* 3(69), doi:10.3389/fmicb.2012.00069.

Hawkes, J. A., Hansen, C. T., Goldhammer, T., Bach, W., and Dittmar, T. (**2016**); Molecular alteration of marine dissolved organic matter under experimental hydrothermal conditions. *Geochimica et Cosmochimica Acta* 175, pp. 68–85, doi: 10.1016/j.gca.2015.11.025.

He, W., Lee, J.-H., and Hur, J. (**2016**); Anthropogenic signature of sediment organic matter probed by UV-Visible and fluorescence spectroscopy and the association with heavy metal enrichment. *Chemosphere* 150, pp. 184–193, doi:10.1016/j.chemosphere.2016.01.116.

Hem, J. D. and Cropper, W. H. (**1959**); Survey of ferrous-ferric chemical equilibria and redox potentials. Water Supply Paper 1459-A, United States Geological Survey, doi:10.3133/wsp1459A.

Hernes, P. J., Bergamaschi, B. A., Eckard, R. S., and Spencer, R. G. M. (**2009**); Fluorescence-based proxies for lignin in freshwater dissolved organic matter. *Journal of Geophysical Research* 114, p. G00F03, doi:10.1029/2009JG000938.

Hudson, N., Baker, A., and Reynolds, D. (**2007**); Fluorescence analysis of dissolved organic matter in natural, waste and polluted waters: A review. *River Research and Applications* 23(6), pp. 631–649, doi:10.1002/rra.1005.

Hutnik, C. M. L., MacManus, J. P., Banville, D., and Szabo, A. G. (**1991**); Metal induced changes in the fluorescence properties of tyrosine and tryptophan site-specific mutants of oncomodulin. *Biochemistry* 30(30), pp. 7652–7660, doi:10.1021/bi00244a038.

Ishii, S. K. L. and Boyer, T. H. (**2012**); Behavior of reoccurring PARAFAC components in fluorescent dissolved organic matter in natural and engineered systems: A critical review. *Environmental Science & Technology* 46(4), pp. 2006–2017, doi: 10.1021/es2043504.

Johnson, J. W. and Norton, D. (**1991**); Critical phenomena in hydrothermal systems: State, thermodynamic, electrostatic, and transport properties of H_2O in the critical region. *American Journal of Science* 291(6), pp. 541–648, doi:10.2475/ajs.291.6.541.

Kalle, K. (**1937**); Meereskundliche chemische untersuchungen mit hilfe des Zeiss-Pulfrich photometers. *Annales hydrographiques* 65, pp. 276–282.

Kandasamy, S. and Nagender Nath, B. (**2016**); Perspectives on the terrestrial organic matter transport and burial along the land-deep sea continuum: Caveats in our understanding of biogeochemical processes and future needs. *Frontiers in Marine Science* 3, doi:10.3389/fmars.2016.00259.

Kelemen, S. R. and Fang, H. L. (**2001**); Maturity trends in raman spectra from kerogen and coal. *Energy & Fuels* 15(3), pp. 653–658, doi:10.1021/ef0002039.

Kellerman, A. M., Guillemette, F., Podgorski, D. C., Aiken, G. R., Butler, K. D., and Spencer, R. G. M. (**2018**); Unifying concepts linking dissolved organic matter composition to persistence in aquatic ecosystems. *Environmental Science & Technology* 52(5), pp. 2538–2548, doi:10.1021/acs.est.7b05513.

Kirk, T. K. and Obst, J. R. (**1988**); Lignin determination. In: Wood, W. A. and Kellogg, S. T. (eds.), *Biomass Part B: Lignin, Pectin, and Chitin*, *Methods in Enzymology*, volume 161, pp. 87–101, Elsevier, doi:10.1016/0076-6879(88)61014-7.

Krauss, M., Jensen, J. O., and Hameka, H. F. (**1994**); Electronic structure of the excited states and phenol fluorescence. *The Journal of Physical Chemistry* 98(40), pp. 9955–9959, doi:10.1021/j100091a004.

Lakowicz, J. R. (ed.) (**2010**); *Principles of fluorescence spectroscopy*. Third edition, Springer, Boston, Massachusetts, USA, doi:10.1007/978-0-387-46312-4.

Leenheer, J. A. (**1981**); Comprehensive approach to preparative isolation and fractionation of dissolved organic carbon from natural waters and wastewaters. *Environmental Science & Technology* 15(5), pp. 578–587, doi:10.1021/es00087a010.

Leenheer, J. A. (**2009**); Systematic approaches to comprehensive analyses of natural organic matter. *Annals of Environmental Science* 3, pp. 1–130.

Li, X., Cai, W., An, J., Kim, S., Nah, J., Yang, D., Piner, R., Velamakanni, A., Jung, I., Tutuc, E., Banerjee, S. K., Colombo, L., and Ruoff, R. S. (**2009**); Large area synthesis of high quality and uniform graphene films on copper foils. *Science* 324(5932), pp. 1312–1314, doi:10.1126/science.1171245.

Love, J. D. and Good, J. M. (**1970**); Hydrocarbons in themal areas, northwestern Wyoming. Professional Paper 644-B, United States Geological Survey, doi:10.313 3/pp644b.

MATLAB (**2010**); version 7.10.0 R2010a MatLab: The language of technical computing. The Mathworks Inc., Natick, Massachusetts, USA.

Mayer, L. M., Schick, L. L., and Loder, T. C. (**1999**); Dissolved protein fluorescence in two Maine estuaries. *Marine Chemistry* 64(3), pp. 171–179, doi:10.1016/S0304-4203(98)00072-3.

Menzel, D. W. and Vaccaro, R. F. (**1964**); The measurement of dissolved organic and particulate carbon in seawater. *Limnology and Oceanography* 9(1), pp. 128–142, doi:10.4319/lo.1964.9.1.0138.

Murphy, K. R., Ruiz, G. M., Dunsmuir, W. T. M., and Waite, T. D. (**2006**); Optimized parameters for fluorescence-based verification of ballast water exchange by ships. *Environmental Science & Technology* 40(7), pp. 2357–2362, doi:10.1021/es0519381.

Nordstrom, K. D., McCleskey, B. R., and Ball, J. W. (**2009**); Sulfur geochemistry of hydrothermal waters in Yellowstone National Park: IV Acid-sulfate waters. *Applied Geochemistry* 24(2), pp. 191–207, doi:10.1016/j.apgeochem.2008.11.019.

Nye, J., Shock, E., and Hartnett, H. (**2020**); A novel PARAFAC model for continental hot springs reveals unique dissolved organic carbon compositions. *Organic Geochemistry* 141(103964), doi:10.1016/j.orggeochem.2019.103964.

Ohno, T. (**2002**); Fluorescence inner-filtering correction for determining the humification index of dissolved organic matter. *Environmental Science & Technology* 36(4), pp. 742–746, doi:10.1021/es0155276.

Osburn, C. L., Del Vecchio, R., and Boyd, T. J. (**2014**); Physicochemical effects on dissolved organic natter fluorescence in natural waters. In: Coble, P., Lead, J., Baker, A., Reynolds, D. M., and Spencer, R. G. (eds.), *Aquatic Organic Matter Fluorescence*, pp. 233–277, Cambridge Environmental Chemistry Series, Cambridge University Press, New York, USA, doi:10.1017/CBO9781139045452.012.

Pettersen, R. C. (**1984**); The chemical composition of wood. In: Rowell, R. (ed.), *The Chemistry of Solid Wood*, *Advances in Chemistry*, volume 207, pp. 57–126, American Chemical Society, Washington, D. C., USA, doi:10.1021/ba-1984-0207.ch002.

Remko, M., Fitz, D., Broer, R., and Rode, B. M. (**2011**); Effect of metal ions (Ni^{2+}, Cu^{2+} and Zn^{2+}) and water coordination on the structure of L-phenylalanine, L-tyrosine, L-tryptophan and their zwitterionic forms. *Journal of Molecular Modeling* 17(12), pp. 3117–3128, doi:10.1007/s00894-011-1000-0.

Rose, A. L. and Waite, T. (**2003**); Kinetics of iron complexation by dissolved natural organic matter in coastal waters. *Marine Chemistry* 84(1-2), pp. 85–103, doi:10.1016/S0304-4203(03)00113-0.

Rubin, A. J. (ed.) (**1974**); *Aqueous-Environmental Chemistry of Metals*. Ann Arbor Science Publishers, Ann Arbor, Michigan, USA.

Saari, L. A. and Seitz, W. R. (**1983**); Immobilized morin as fluorescence sensor for determination of aluminum(III). *Analytical Chemistry* 55(4), pp. 667–670, doi:10.1021/ac00255a020.

Santos, E. H., Filipe, O. M. S., Duarte, R. M. B. O., Pinto, H., and Duarte, A. C. (**2000**); Fluorescence as a tool for tracing organic contamination from pulp mill effluents in surface waters. *Acta Hydrochimica et Hydrobiologica* 28(7), pp. 364–371.

Shams El-Din, N. G., Mohamedein, L. I., and El-Moselhy, K. M. (**2014**); Seaweeds as bioindicators of heavy metals off a hot spot area on the Egyptian Mediterranean Coast during 2008-2010. *Environmental Monitoring and Assessment* 186(9), pp. 5865–5881, doi:10.1007/s10661-014-3825-3.

Shipp, J., Gould, I. R., Herckes, P., Shock, E. L., Williams, L. B., and Hartnett, H. E. (**2013**); Organic functional group transformations in water at elevated temperature and pressure: Reversibility, reactivity, and mechanisms. *Geochimica et Cosmochimica Acta* 104, pp. 194–209, doi:10.1016/j.gca.2012.11.014.

Shock, E., Bockisch, C., Estrada, C., Fecteau, K., Gould, I. R., Hartnett, H., Johnson, K., Robinson, K., Shipp, J., and Williams, L. (**2019**); Earth as organic chemist. In: Orcutt, B. N., Daniel, I., and Dasgupta, R. (eds.), *Deep Carbon: Past and Present*, pp. 415–446, Cambridge University Press, Cambridge, UK, doi:10.1017/9781108677950.014.

Stedmon, C. A. and Markager, S. (**2005**); Resolving the variability in dissolved organic matter fluorescence in a temperate estuary and its catchment using PARAFAC analysis. *Limnology and Oceanography* 50(2), pp. 686–697, doi:10.4319/lo.2005.50.2.0686.

Stedmon, C. A., Markager, S., and Bro, R. (**2003**); Tracing dissolved organic matter in aquatic environments using a new approach to fluorescence spectroscopy. *Marine Chemistry* 82(3-4), pp. 239–254, doi:10.1016/S0304-4203(03)00072-0.

Stubbins, A., Lapierre, J.-F., Berggren, M., Prairie, Y. T., Dittmar, T., and del Giorgio, P. A. (**2014**); What's in an EEM? Molecular signatures associated with dissolved organic fluorescence in boreal Canada. *Environmental Science & Technology* 48(18), pp. 10598–10606, doi:10.1021/es502086e.

Takeno, N. (**2005**); Atlas of Eh pH diagrams. Open File Report 419, Geological Survey of Japan, AIST.

Toner, B. M., Fakra, S. C., Manganini, S. J., Santelli, C. M., Marcus, M. A., Moffett, J. W., Rouxel, O., German, C. R., and Edwards, K. J. (**2009**); Preservation of iron(II) by carbon-rich matrices in a hydrothermal plume. *Nature Geoscience* 2(3), pp. 197–201, doi:10.1038/ngeo433.

Wagner, W. and Pruß, A. (**2002**); The IAPWS formulation 1995 for the thermodynamic properties of ordinary water substance for general and scientific use. *Journal of Physical and Chemical Reference Data* 37, pp. 387–535, doi:10.1063/1.1461829.

Wang, H.-B., Zhang, Y.-J., Xiao, X., Jin, D., Zhao, N.-J., Yin, G.-F., Guo, L.-Q., and Liu, W.-Q. (**2010**); Excitation-emission fluorescence characterization study of the three phenolic compounds. *Spectroscopy and Spectral Analysis* 30(5), pp. 1271–1274, doi:10.3964/j.issn.1000-0593(2010)05-1271-04.

White, D. E., Muffler, L. J. P., and Truesdell, A. H. (**1971**); Vapor-dominated hydrothermal systems compared with hot-water systems. *Economic Geology* 66(1), pp. 75–97, doi:10.2113/gsecongeo.66.1.75.

Willams, P. M. (**1969**); Determination of dissolved organic carbon in seawater: A comparison of two methods. *Limnology and Oceanography* 14(2), pp. 297–298, doi:10.4319/lo.1969.14.2.0297.

Wu, J., Zhang, H., He, P.-J., and Shao, L.-M. (**2011**); Insight into the heavy metal binding potential of dissolved organic matter in MSW leachate using EEM quenching combined with PARAFAC analysis. *Water Research* 45(4), pp. 1711–1719, doi:10.1016/j.watres.2010.11.022.

Yamashita, Y. and Jaffé, R. (**2008**); Characterizing the interactions between trace metals and dissolved organic matter using excitation emission matrix and parallel factor analysis. *Environmental Science & Technology* 42(19), pp. 7374–7379, doi: 10.1021/es801357h.

Yamashita, Y. and Tanoue, E. (**2003**); Chemical characterization of protein-like fluorophores in DOM in relation to aromatic amino acids. *Marine Chemistry* 82(3-4), pp. 255–271, doi:10.1016/S0304-4203(03)00073-2.

Yang, Y. and Zhang, D. (**1995**); Concentration effect on the fluorescence spectra of humic substances. *Communications in Soil Science and Plant Analysis* 26(15-16), pp. 2333–2349, doi:10.1080/00103629509369451.

Yasuda, S., Fukushima, K., and Kakehi, A. (**2001**); Formation and chemical structures of acid-soluble lignin I: Sulfuric acid treatment time and acid-soluble lignin content of hardwood. *Journal of Wood Science* 47(1), pp. 69–72, doi: 10.1007/BF00776648.

Zepp, R. G., Sheldon, W. M., and Moran, M. A. (**2004**); Dissolved organic fluorophores in southeastern US coastal waters: Correction method for eliminating Rayleigh and Raman scattering peaks in excitation-emission matrices. *Marine Chemistry* 89(1-4), pp. 15–36, doi:10.1016/j.marchem.2004.02.006.

Table 3.1: Literature fluorophores similar to the acid-spring component.

Laboratory standards	λ_{EX} (nm)	λ_{EM} (nm)	Reference
Tryptophan	220 (280)	345	Mayer et al. (1999)
	270*	<350*	Cory and McKnight (2005)
	287	352	Bridges and Williams (1968)
	280	355	Yamashita and Tanoue (2003)
	270	348	This research (Figure 3.2)
Tryptophan (pH = 1)	286	345	Bridges and Williams (1968)
Bovine serum albumin	220 (280)	340	Mayer et al. (1999)
Tyrosine	220 (275)	300	Mayer et al. (1999)
	275*	<350*	Cory and McKnight (2005)
	275	300	Yamashita and Tanoue (2003)
	270	350	Aiken (2014)
	287	355	Bridges and Williams (1968)
Cresol	270	310	Aiken (2014)
m-Cresol	274	300	Wang et al. (2010)
Thymol	276	304	Wang et al. (2010)
Phenol	272	300	Wang et al. (2010)
Aniline	294	344	Bridges and Williams (1968)
Tryptamine	290	360	Bridges and Williams (1968)
Lignosulfonic acid	<250 (280)	392	Cawley et al. (2012)
Acid-soluble lignins**	240-320	350-360	Albinsson et al. (1999)
Environmental fluorophores and PARAFAC components	λ_{EX} (nm)	λ_{EM} (nm)	Reference
Tryptophan-like	<220 (275)*	360*	He et al. (2016)
	280*	380*	Cory and McKnight (2005)
	275	340	Stedmon et al. (2003); Coble (2007)
	270	<350	Cawley et al. (2012)
	280	344	Stedmon and Markager (2005)
Tryptophan-like; phytoplankton produced	280 (<240)	368	Stedmon et al. (2003)
Unknown; marine biological	280	370	Coble et al. (1998)
Tyrosine-like	275	305	Stedmon and Markager (2005); Coble (2007)
Protein-like	275	<300	Murphy et al. (2006)
	280	328	Murphy et al. (2006)
	<240 (300)	338	Murphy et al. (2006)
Pulp mill effluent	275 (330)	436	Cawley et al. (2012)
Pulp mill effluent	280	340	Santos et al. (2000)
PAHs	250 (320)	370	Murphy et al. (2006) Nye et al. (2020)
Lignin phenol indicators***	275-285*	320-330*	Hernes et al. (2009)
Novel acid-spring component	<250	346	This research; Nye et al. (2020)

*Wavelengths visually estimated from spectrum or EEM image
**Model lignin derivates include cinnamyl alcohols, phenylcoumarans, phenylcoumarones, and stilbenes in dioxane-water solvent mixtures
***Not distinct peaks or PARAFAC components, but wavelengths in the EEM space that demonstrated strongest predictive capability

Table 3.2: Theoretical mass of the ASC fluorophores in a 100 mL field sample. A two-point calibration from tryptophan standards was determined. This calculation assumes the acid-spring fluorophores have molar absorptivity, quantum yield, and molecular mass identical to tryptophan. The highest (120717SD) and lowest (160726V) intensity samples containing a dominant ASC signal are used as examples. Emission intensities were recorded at wavelengths associated with maximum fluorescence; $\lambda_{EX} = 270$ nm, $\lambda_{EM} = 348$ nm for tryptophan and $\lambda_{EX} = 250$ nm, $\lambda_{EM} = 348$ nm for the field samples.

Tryptophan (**X**) (μM)	Emission (**Y**)	Sample	Emission	Concentration (μM)	Mass in 100 mL (μg)
10.0	1.69	120717SD	1.30	7.69	**157**
0.100	0.0175	160726V	0.00656	0.0394	**0.804**
$0.0006 + 0.169 \times \mathbf{X}$	$= \mathbf{Y}$				

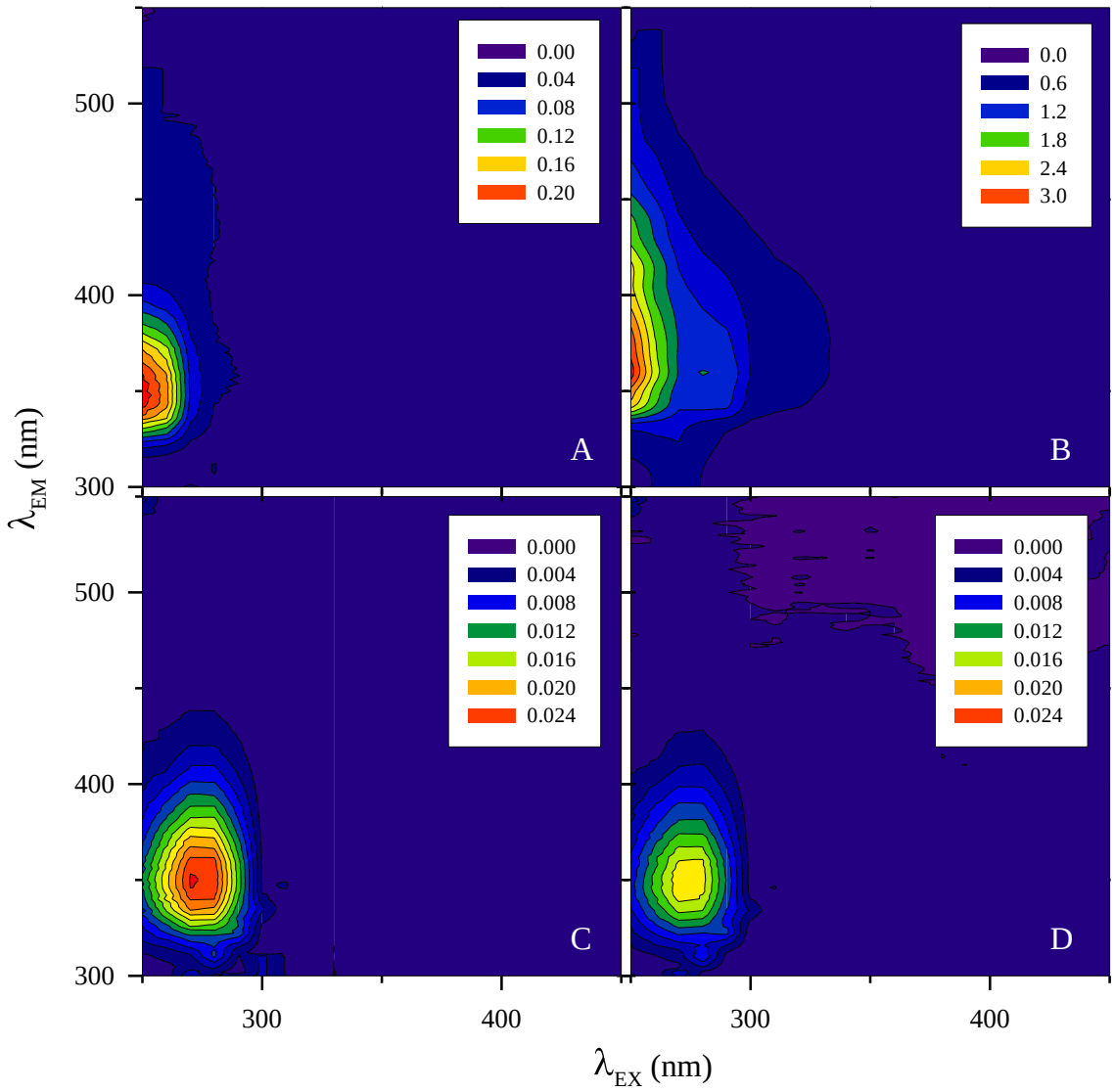

Figure 3.1: Fluorescence spectra for the novel ASC, PAHs, and tryptophan. (A) Acidic spring demonstrating strong ASC fluorescence. (B) PAH fluorescence from a petroleum-influenced hot spring. (C) Tryptophan standard, 100 nM analyzed at pH = 7. (D) Tryptophan standard, 100 nM analyzed at pH = 2.5. The top two samples were analyzed at pH = 2.5.

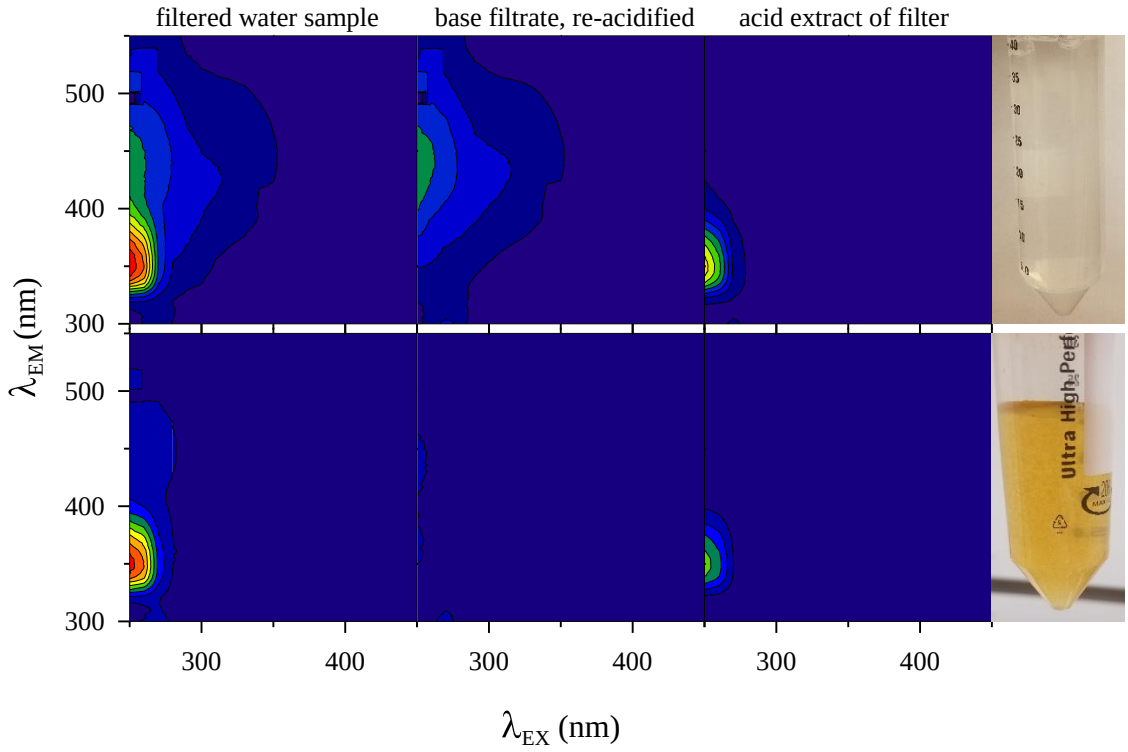

Figure 3.2: Precipitation of the novel acid-spring component fluorophores. (top row) Sample 130720TW. (bottom row) Sample 140727SD. (left) Hot spring field sample EEMs demonstrating strong fluorescence of the ASC. (center-left) EEMs of the same samples after they were adjusted to pH = 7, filtered through a 0.2 μm filter, and re-acidified to pH = 2.5. (center-right) Acidic extraction of isolated precipitate from the filter. (right) Photos of each sample at pH = 7 prior to filtration. The EEMs for each sample are normalized to the same color intensity scale.

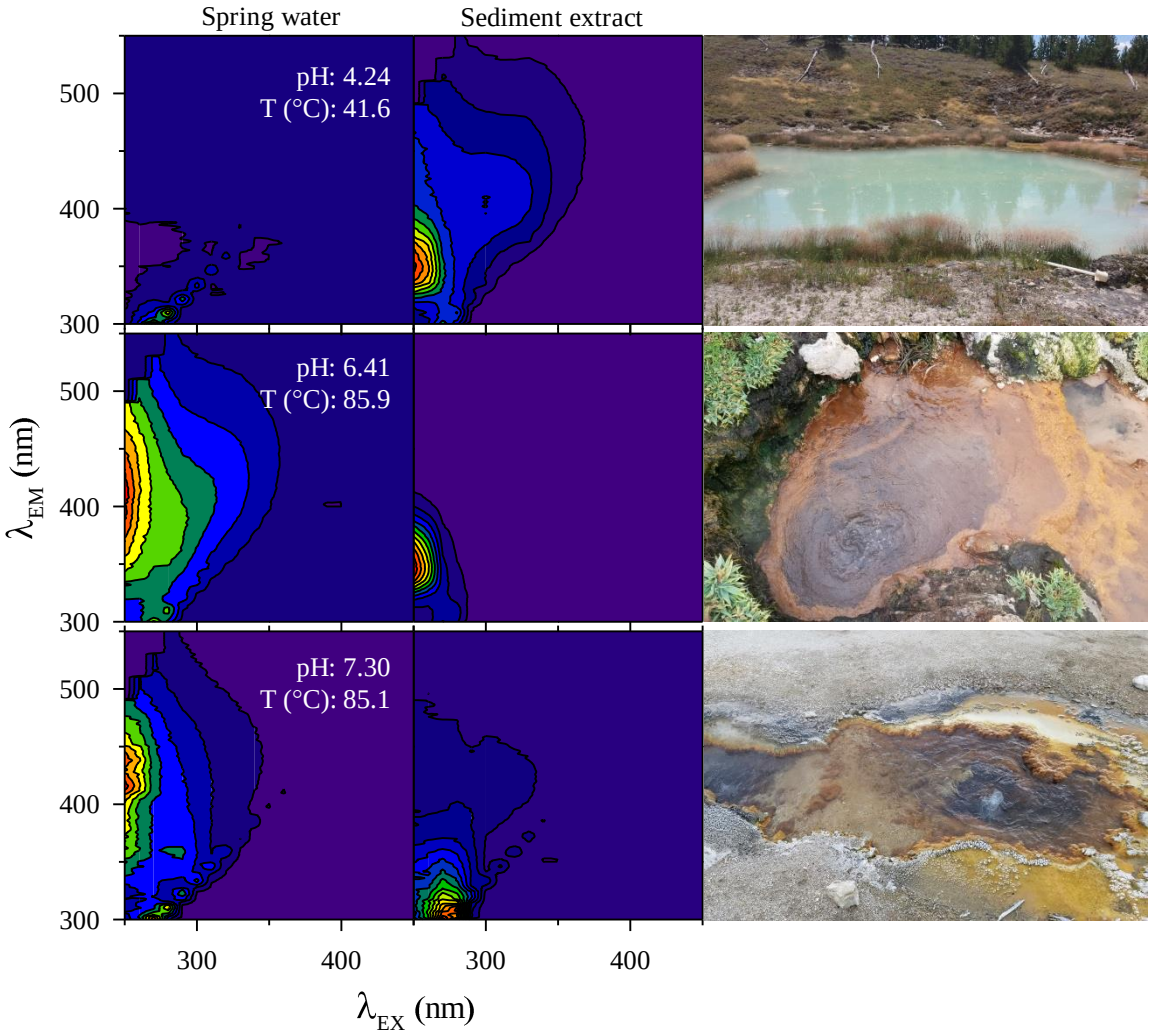

Figure 3.3: Fluorescence in hot spring water and acid-extracted sediments. Each pair of spring and sediment EEMs was taken from the spring shown in photo to the right. The top two springs (samples 160726U and 180923F, respectively) demonstrate environmental precipitation of the novel fluorophores. The bottom spring (sample 170725TN) is an example of a high pH, deep-sourced spring with no evidence of the ASC.

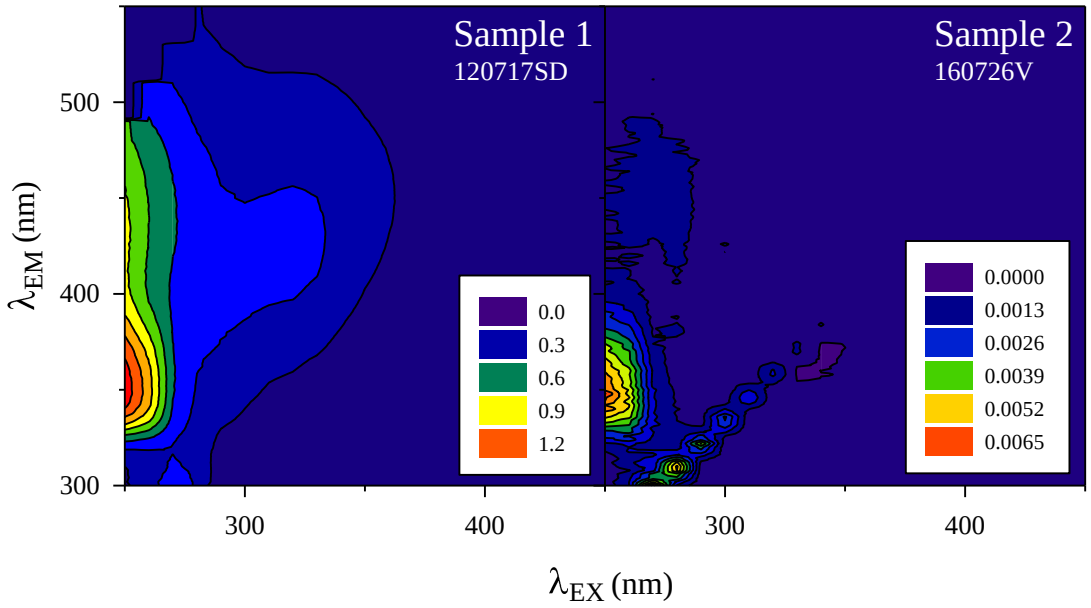

Figure 3.4: EEMs of the samples used for theoretical calculations in Table 3.2

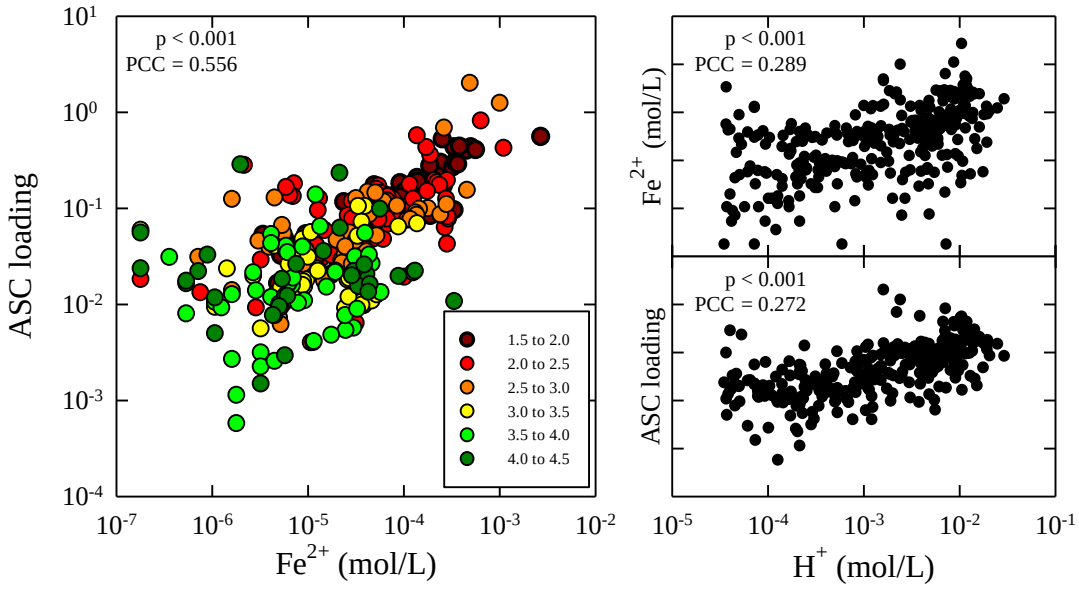

Figure 3.5: Correlation among ferrous iron, the ASC loading, and pH. On these plots, pH is presented as the molar concentration of H^+. The ASC loadings have arbitrary intensity units but they can be applied in the same manner as chemical concentrations. Pearson's correlation test between all three parameters determined statistically significant correlations ($p < 0.001$) for each parameter pair. The Pearson's correlation coefficient (PCC) indicates strength of linear correlation with a value of –1 indicating a perfect, negative linear correlation and value of +1 indicating a perfect, positive correlation.

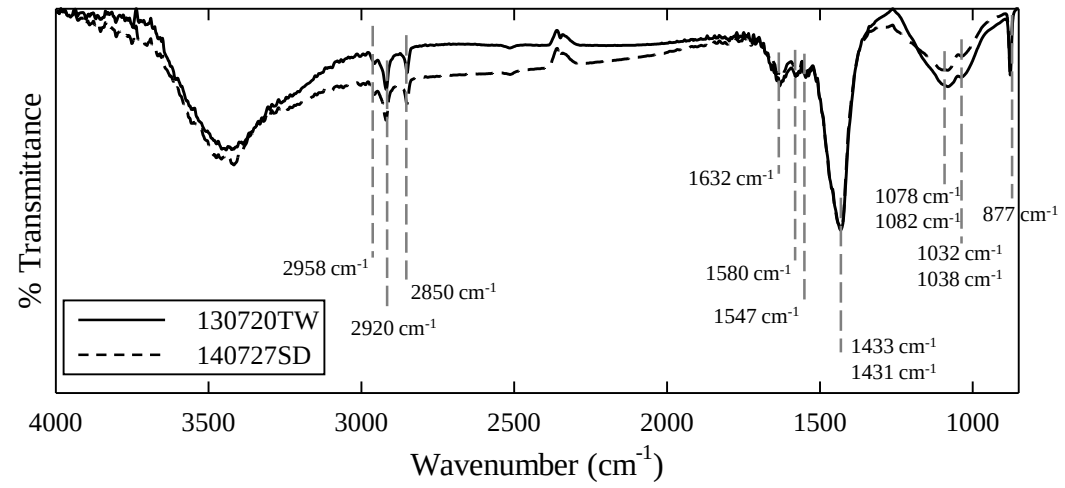

Figure 3.6: FT-IR spectra of the ASC-containing precipitates isolated from samples 130720TW and 140727SD. Peaks identified here by two different wavenumbers were slightly different between samples; in each case the top wavenumber represents the peak in sample 130720TW, and the bottom wavenumber represents the peak in sample 140727SD. Peaks indicated with only one wavenumber had identical positions in both samples.

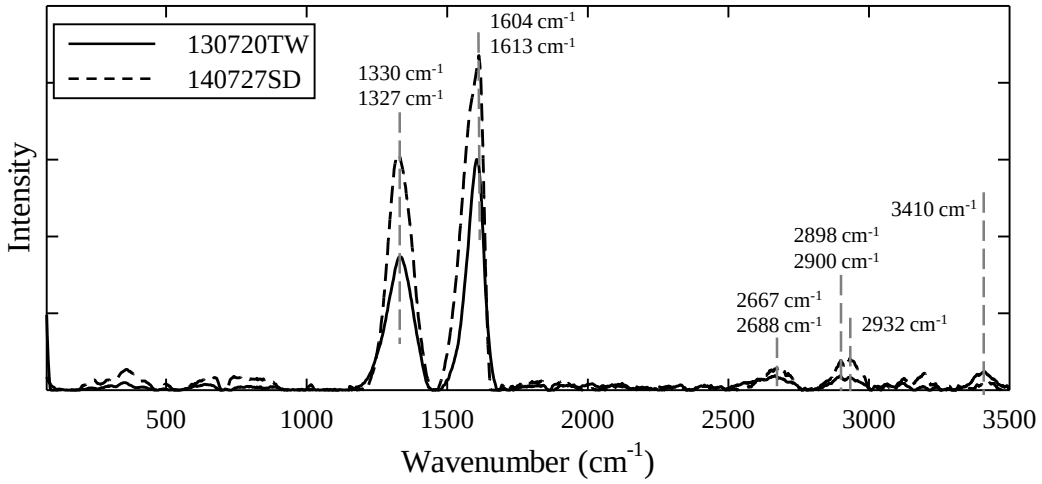

Figure 3.7: Raman spectra of the ASC-containing precipitates isolated from samples 130720TW and 140727SD. Peaks identified here by two different wavenumbers were slightly different between samples; in each case the top wavenumber represents the peak in sample 130720TW, and the bottom wavenumber represents the peak in sample 140727SD. Peaks indicated with only one wavenumber had identical positions in both samples.

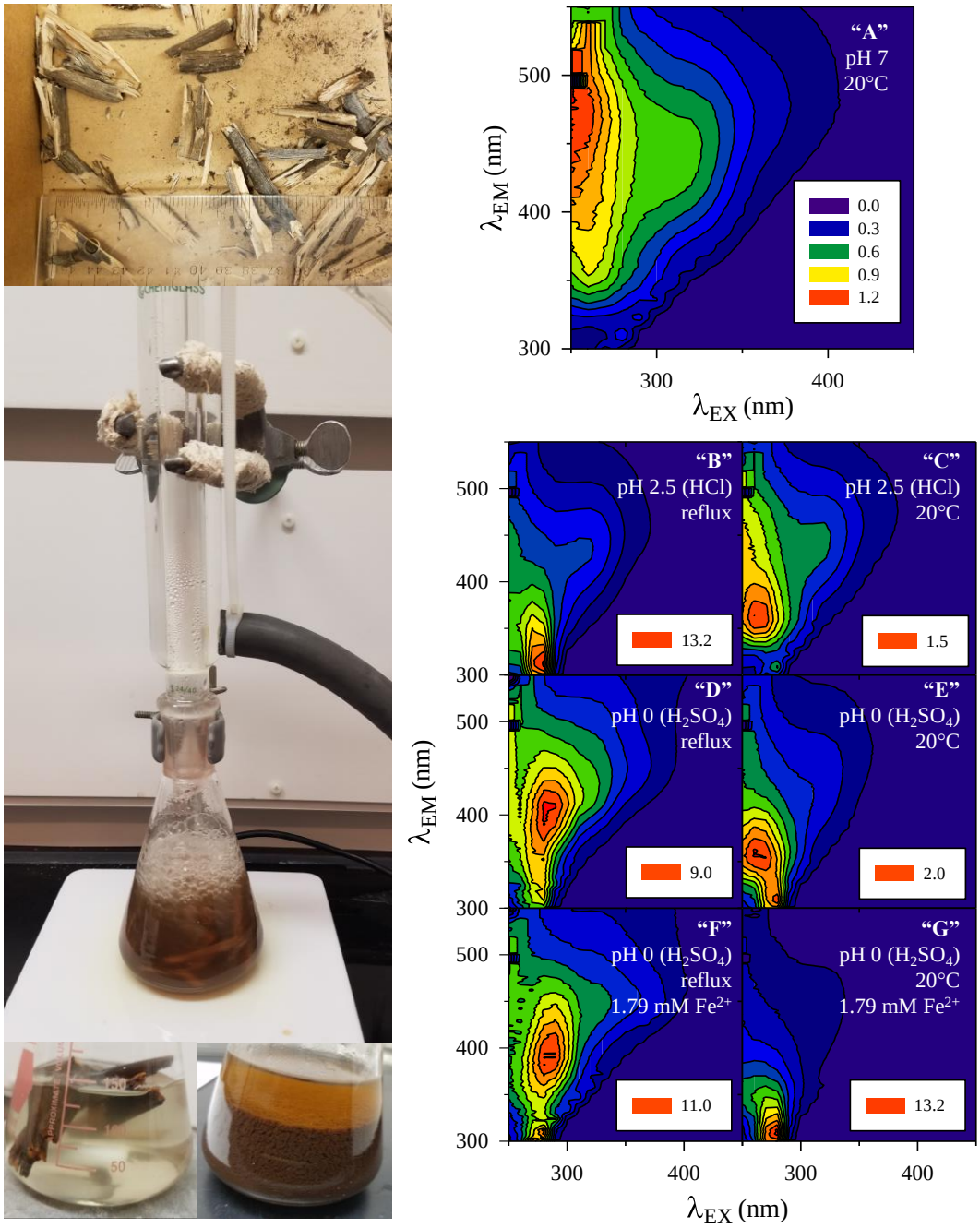

Figure 3.8: Photos of wood digestion experiments and fluorescence results. Photos at left: (top) Examples of wood samples used for all experiments. (middle) Reflux condenser setup with a magnetic stir bar. (bottom-left) Experiment "G" at end of reaction. (bottom-right) Experiment "F" at end of reaction. All wood digestion experiments lasted 72 hours. The EEMs of the filtered products are shown at right for the seven experimental conditions (A-G). Only the maximum contour label is shown for experiments B through G; fluorescence intensities are comparable across experiments.

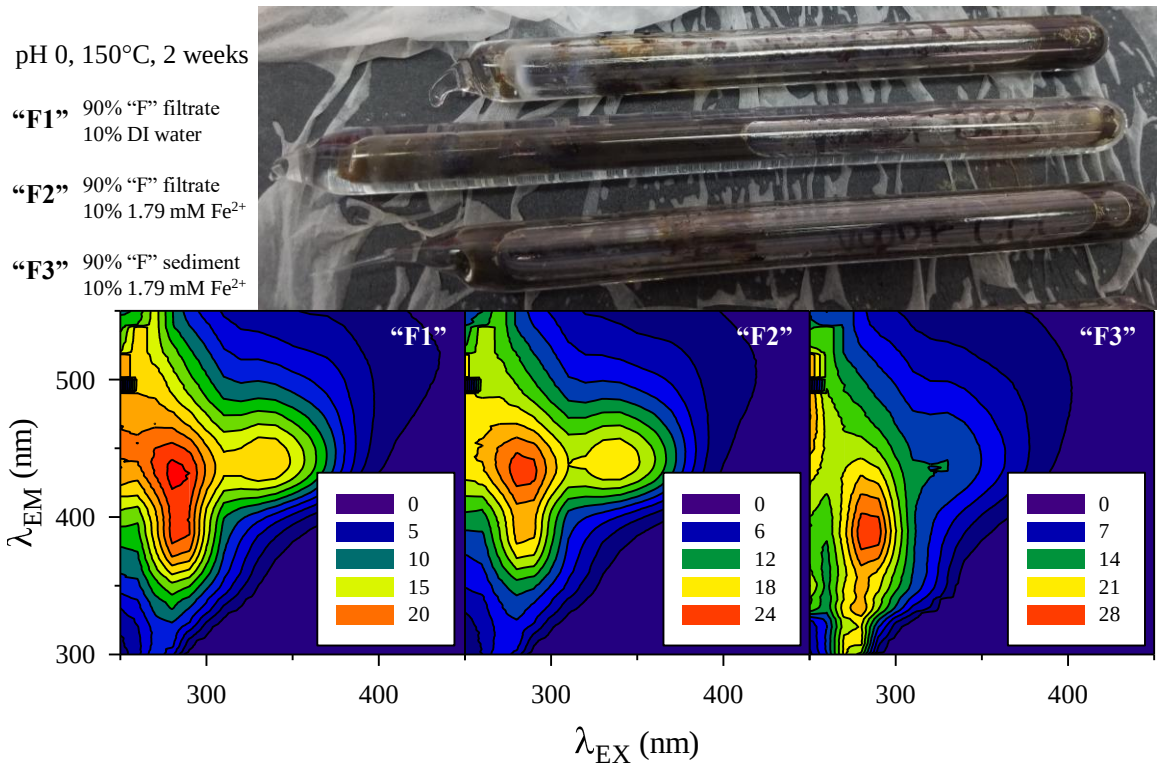

Figure 3.9: Photos and fluorescence data for wood digestion experiments at elevated temperature. (top-left) Reaction conditions for three experiments on the product from experiment "F" described in Figure 3.8. (top-right) Photo of fused silica tubes containing reaction products taken post-experiment. (bottom) EEMs for the three experiments. Fluorescence intensities are comparable to one another and to the EEMs from Figure 3.8.

Chapter 4

CONNECTING MAJOR FLUORESCENT DISSOLVED ORGANIC MATTER FEATURES TO HOT SPRING TYPE AND MIXING COMPOSITIONS

4.1 Introduction

The vast geochemical diversity observed in the Yellowstone National Park hydrothermal system is the result of magmatic influence, water-rock reactions, fluid-fluid interactions, subsurface boiling and phase separation, and microbial activity that alter the deep-sourced parent fluid as it rises and discharges at the surface through hot springs, geysers, and fumaroles. Geochemical models that classify hot springs by geochemical constituents are often invoked to make statements about water source, subsurface fluid alteration, water-rock reactions that occur at depth, or geophysical properties of the deep aquifer. The broadest classification of hot springs uses the terms "acid-sulfate" and "alkaline-chloride", in reference to the bimodal distribution of global, hot spring pH described by Brock (1971). Further classification of Yellowstone hot springs includes vapor-phase or liquid-phase dominated systems in reference to fluids that have experienced subsurface boiling (White et al., 1971; Fournier, 1989; Holloway et al., 2011; Lowenstern et al., 2012). These separated phases can be associated with the Brock (1971) classifications: vapor-phase dominated systems produced acid-sulfate springs rich in volatile gases such as CO_2, H_2S, CH_4, H_2 and N_2 (White et al., 1971; Fournier, 1989; Kharaka et al., 2000; Werner et al., 2000; Kharaka et al., 2002; Lowenstern and Hurwitz, 2008; Holloway et al., 2011) and the remaining liquid phase forms alkaline-chloride springs of higher pH, that are sulfate-poor, but rich in silica, chloride, and other non-volatile solutes. Fluids that are not phase-separated

form springs of acid-chloride or neutral-chloride type, depending on which buffers dominate (sulfuric acid, bicarbonate, or siliceous acid). Each of the fluid types has the potential to be mixex with other fluids or to be diluted by meteoric water, producing springs of intermediate composition. A more recent model (Nordstrom et al., 2009) characterizes hot springs by their chloride and sulfate concentrations and identifies two end-member fluids (Table 4.1, Figure 4.1). The first is a cool, dilute ground water with little to no thermal influence (meteoric-only; MO-type) and the second is a deep hydrothermal source (hydrothermal only; HO-type) characterized by 310 to 400 ppm chloride ($\sim$8500 to 11,000 μmol/kg) and 20 to 200 ppm sulfate ($\sim$200 to 2,000 μmol/kg). Other spring water compositions of are described as intermediate mixed fluids or fluids that have been altered by subsurface boiling (HB- and HBG-type), by evaporative concentration, by gas injection into surface waters (MG- and HBG-type) or by mixing with shallow circulated acid-sulfate waters; illustrations of such processes are shown in Figure 4.3. These intermediate classifications are described in section 4.3.1.

Chloride is considered a conservative tracer of hydrothermal fluid due to its magmatic source, high solubility in water, low reactivity, and lack of partitioning into the vapor phase during boiling events. (White et al., 1971; Fournier, 1989; Giggenbach, 1997; Hurwitz and Lowenstern, 2014). Sulfate's story is more complex; at temperatures below 400℃ it is produced by the disproportionation of magmatic sulfur dioxide into sulfuric acid and H_2S. Unlike chloride, sulfate concentrations are greatly altered through subsurface boiling and by the precipitation of anhydrite at moderately high temperatures. Subsurface boiling and phase separation will volatilize sulfur species as H_2S, forcing a re-equilibration of the dissolved sulfate and sulfide remaining in the liquid phase. In the shallow subsurface, various reduced sulfur species (e.g., sulfide, native sulfur, thiosulfate, and other sulfoxyanions) in both liquid phase and vapor-

phase dominated fluids, will be oxidized by atmospheric oxygen to produce orders of magnitude higher concentrations of sulfate (Xu et al., 1998; Nordstrom et al., 2009) than originally present in the deep source fluid. Microbial processes also contribute to the oxidation of native sulfur at temperatures below 100℃ (Brock, 1971; Brock and Mosser, 1975; Xu et al., 2000), further elevating sulfate concentrations.

The organic carbon content amd composition of hot springs and thermal waters has not been studied as extensively as the inorganic chemistry, but it is known that thermal alteration of buried sediments contributes organic carbon at least in the northeastern part of the park (Love and Good, 1970; Des Marais et al., 1981; Clifton et al., 1990; Bergfeld et al., 2014). Petroleum seeps, containing hydrocarbon gases and polycyclic aromatic hydrocarbons (PAHS), are noted at Calcite Springs and Rainbow Springs (Love and Good, 1970; Clifton et al., 1990; Lorenson and Kvenvolden, 1993), two regions in the far northern part of the park, as further evidence for the thermal alteration of buried biomass. While it has been stated that buried sediments contribute a dominant source of organic carbon to Yellowstone hydrothermal fluids (Hurwitz and Lowenstern, 2014), no extensive assessment of dissolved organic carbon (DOC) concentration and composition has ever been published; certainly not at the same scale that has been done for inorganic constituents. It is unclear how far reaching, or to what extent, the buried sediments in the northeastern part of Yellowstone influence the composition of hydrothermal fluids. Small hydrocarbon (C_1 to C_6) abundance and isotopes indicate thermally altered organic matter contributes (albeit, to a lesser degree) to hydrothermal features throughout the other areas of the park (Allen and Day, 1935; Gunter, 1978; Des Marais et al., 1981; Kvenvolden et al., 1989; Lorenson et al., 1991; Lorenson and Kvenvolden, 1993); this may indicate lateral distibution of pyrolysis products in the subsurface. Other sources of organic carbon in hot springs include terrestrial, soil derived organic matter, dissolved organic matter (DOM) in

surface water introduced through mixing and runoff, and microbially produced or altered organic matter. Natural organic matter is enormously complex (Hem, 1985; Leenheer, 2009; Hawkes et al., 2018; Kellerman et al., 2018), but characterization of different components of DOM in surface water systems has allowed the tracing of hydrologic mixing and alteration by chemical, physical, and microbial processes (Hedges et al., 1997; Del Vecchio and Blough, 2004; Cole et al., 2007; Baghoth et al., 2011; LaRowe and Van Cappellen, 2011; Cawley et al., 2012; Wu et al., 2018).

An assessment and characterization of fluorescent DOM (FDOM) in 222 hot springs was recently published by Nye et al. (2020). The five-component parallel factor (PARAFAC) analysis model revealed contributions from terrestrial, surface-derived organic matter (3 humic-like component); a novel fluorophore unique to acidic hot springs (acid-spring component) and a microbial component (protein-like component). I demonstrated a distinct trend in model component composition as a function of hot spring pH. Here, I apply DOC concentrations and the modelled FDOM signatures to a broader range of hot spring geochemistries. I assess the variability in DOC and FDOM across the geographic distribution of springs throughout the park. Finally, I assess how DOC concentration, total fluorescence intensity, and PARAFAC model component loadings compare to the chloride and sulfate classification of springs (e.g., Nordstrom et al., 2009) to evaluate fluid source and various mixing processes.

4.2 Methods and Analytical Techniques

4.2.1 Field Sampling

Fluid samples from hot springs were collected in Yellowstone National Park during the summer over the period from July 2012 to September 2018. The regions sampled within Yellowstone include: Amphitheater Springs, Bog Creek, Calcite Springs,

Crater Hills, Forest Springs, Geyser Creek, Gibbon Hill, Greater Obsidian Pool Area, Hot Springs Basin, Imperial and Spray Geyser Basins, Lewis Lake, Norris Geyser Basin, Rabbit Creek, Sentinel Meadow, Sylvan Springs, Turbid Lake, Wahb Springs, Washburn, and White Creek (Figure 4.2). The regions known as Geyser Creek and Gibbon Hill are collectively referred to as Gibbon Geyser Basin, due to their proximity and similar geochemistry. Similarly, Sentinel Meadow and White Creek are referred to as the Lower Geyser Basin. Water samples were collected from source pools whenever possible, typically at the hottest accessible location. When a source pool sample was not taken, sampling was collected from outflow channels close to the source pool. Samples from outflow channels were otherwise not included in this research. Non-thermal surface waters (e.g., rivers, streams, lakes) were also sampled to use for comparison as an end-member MO-type water. Basic water chemistry parameters (pH, conductivity, and temperature) were measured in the field using hand-held meters (pH with a WTW model 3300i or 3310 equipped with temperature correcting gel electrodes WTW sentix model 41; conductivity and temperature with a YSI model 30) that were calibrated each day. Conductivity is directly related to the ionic strength of a solution and is used as a simple, field method to approximate total ion content, but it is temperature dependent and must be corrected in order to compare readings between samples of different temperatures. The field conductivity measurements were temperature compensated to 25℃ according to the methods in Hamilton et al. (2011). The geochemical data set for all samples referenced in this dissertation can be found in Appendix E.

Spring water was collected into a 1 L Nalgene^{tm} bottle with a polypropylene scoop, or with a 160 mL syringe for small or shallower springs. All collection materials were rinsed three times with spring water before collection. Water collected for chemical analysis was filtered on-site through a series of 1.2, 0.8, and 0.2 μm Supor^{tm} membrane

filters (polyethersulfone; Pall Corp). Sub-samples (∼30 mL) for ion chromatography were collected into high-density polyethylene (HDPE) Nalgene^{tm} bottles and frozen at the end of each field day until analysis. Sub-samples (∼50 mL) for dissolved organic carbon concentration and fluorescence analysis were collected into acid-washed, fluorinated, high-density polyethylene (FLPE) Nalgene^{tm} bottles that were pre-acidified with HCl to immediately acidify samples to pH 2.5. The FLPE bottles were soaked in acid (20% HCl) for 24 hours and leached with deionized water prior to field use to remove easily extractable carbon. The filtered and acidified samples were kept in the dark at 4℃ until analysis.

4.2.2 Dissolved Organic Carbon

Dissolved organic carbon (DOC) was determined on the filtered, acidified water samples using high temperature combustion oxidation technique over a platinum catalyst (Shimadzu TOC-V) equipped with a non-dispersive infrared detector. Calibration curves of potassium hydrogen phthalate and check standards of sucrose and caffeine were run daily for quantitation and quality analysis, respectively. DOC concentrations are reported here in micromolar (μM) units. The limit of detection with this method was 16 μM, determined as three times the standard deviation of ∼1200 deionized water (18.2 MΩ·cm, Barnstead^{tm} Nanopure) samples analyzed over several years.

4.2.3 Determination of Optical Properties

Fluorescence analysis was performed as described in Nye et al. (2020). Ultraviolet-visible (UV-Vis) absorbance was collected on a Shimadzu UV-Mini 1240 from 190-1100 nm. Fluorescence excitation-emission matrices were collected on a Jobin Yvon Horiba Fluoromax 4. The excitation wavelengths (λ_{EX}) were 240 to 450 nm, collected

every 10 nm (slit width 5 nm). Emission was measured between 300 and 550 nm, collected every 2 nm (slit width 1 nm). Deionized water (18.2 MΩ·cm, Barnstead^{tm} Nanopure) was used as a blank. Fluorescence intensity was normalized to the area under the Raman water peak at an excitation wavelength of 350 nm (Cox et al., 2000; Stedmon et al., 2003). Data from the UV absorbance spectrum were used to perform inner-filter corrections on fluorescence EEMs (Yang and Zhang, 1995; Ohno, 2002). First- and second-order Rayleigh scattering was removed ($\lambda_{EM} = \lambda_{EX} \pm 10$ nm and $\lambda_{EM} = 2 \times \lambda_{EX} \pm 10$ nm, respectively) according to the methods in Zepp et al. (2004). Fluorescence data was removed from the area of non-traditional fluorescence ($\lambda_{EM} < \lambda_{EX}$) and from the area of redundant fluorescence ($\lambda_{EM} < 2 \times \lambda_{EX}$). Total fluorescence was calculated as the sum of all signal in the blank-subtracted, Raman-normalized, scatter-removed EEMs. All post processing of EEMs was done in MATLAB® (MATLAB, 2010). All samples analyzed by UV-Vis and fluorescence analysis were acidified to pH 2.

4.2.4 The Five-Component Hot Spring PARAFAC Model

The five-component PARAFAC developed by Nye et al. (2020) was used to quantify major FDOM peaks. I direct readers to Bro (1997) and Stedmon and Bro (2008) for comprehensive details on the generation and implementation of PARAFAC modelling for EEM data. Briefly, I developed a split-half validated model using 222 hot spring samples that identified five components: 3 humic-like components representing surface or soil organic matter; 1 novel component (that is not reported in the literature) observed exclusively in acidic hot springs; and 1 protein-like component derived from tyrosine-like fluorescence that indicates microbial activity. Several other distinctive fluorescence peaks were noted throughout the dataset but models with more than five components that contained these peaks could not be split-half validated. Compo-

nents are quantified through FMax values determined in the modelling process using the DOMFluor toolbox for Matlab (Stedmon and Bro, 2008). The component loadings can be treated like concentrations. They are semi-quantitative, but they do not represent concentrations of actual chemical species because the quantum yields for the fluorophores are unknown. Since the modelling procedure is purely mathematical residual minimization, some value will almost always be attributed to each component regardless of whether that peak is present or not. Additionally, the model will attempt to fit non-component fluorescence peaks (such as tryptophan, PAHs, and an unknown sulfur-associated peak), which can lead to "false-positive" component loadings. These residual peaks and interferences are discussed in depth in Chapter 2 (i.e., Nye et al., 2020). Because of these limitations it is important to interpret PARAFAC results critically.

4.2.5 Ion Chromatography

Chloride and sulfate concentrations were determined by ion chromatography. Field samples were analyzed on a Dionex DX-600 equipped with Dionex IonPac AS11-HC and AG11-HC columns. Quantification was achieved using external calibration curves of mixed ion standard solutions (Environmental Express). Check standards of a separate ion mixture (Thermo-Scientific) were analyzed daily for quality assurance. Chloride and sulfate concentrations are presented here in micromolal (μmol/kg) units.

4.3 Results and Discussion

4.3.1 Inorganic Geochemical Classification of Springs

The elevation within Yellowstone National Park varies between 5,282 and 11,358 feet (National Park Service, 2019a). The boiling point of water at this elevation varies

between 91℃ and 95℃. At 90℃ the pKa of water is ∼6.2, so a pH between 6 and 7 can be considered circumneutral depending on the temperature of the spring water. Hot spring waters ranged from pH = 1.54 to pH = 8.98 and temperatures ranged from 8.2℃ to 93.6℃. Acidic springs were found across the full temperature range but alkaline hot springs were consistently quite hot (above 60℃). This pattern is the result of significant mixing with cool, dilute surface water in the case of many acidic springs, and the prevention of such mixing in alkaline springs that have precipitated silica sinter or other minerals.

The chloride and sulfate characterization of hot springs by Nordstrom et al. (2009) assumes two end member fluid types, a deep sourced, chloride-rich, hydrothermal-only (HO) fluid and a dilute, cool meteoric-only (MO) fluid. The HO-type springs resemble the deep parent fluid and have chloride concentrations between 8500 and 11,000 μmol/kg (Fournier, 1989; Nordstrom et al., 2009) and sulfate concentrations between 1,000 and 3,000 μmol/kg. Fluids that experience extensive subsurface boiling (hydrothermal-boiling; HB-type) discharge at the surface with elevated chloride (concentrations have been observed as high as 25,000 μmol/kg (Nordstrom et al., 2009)) and decreased sulfate concentrations due to the removal of H_2S in the vapor phase and the subsequent equilibration of the remaining sulfur compounds. Surface evaporation in hot, chloride-rich springs can also contribute to elevated chloride concentrations and decreased sulfate concentrations through the degassing of volatile sulfur species. A few HB-type springs are noted to receive input of thermal gases (hydrothermal-gas-boiling; HGB-type), including H_2S which oxidizes at the surface to form sulfate; these springs have elevated chloride and elevated sulfate concentrations, relative to the HO-type springs. Only two springs of this type have been reported (Nordstrom et al., 2009), of which, only one (Sulfur Spring in Crater Hills) was sampled in this research. Shallow-cycled, acid-sulfate water can also mix with HO-type springs to

dilute chloride and elevate sulfate concentrations; I refer to these systems as acid-sulfate-HO-type springs, as Nordstrom et al. (2009) did not give them a specific label (Table 4.1; Figure 4.1).

The alkaline-chloride springs of the Lower Geyser Basin are characterized by high chloride concentrations (6000 to 9000 μmol/kg), but significantly lower sulfate concentrations ($\sim$200 μmol/kg) compared to the HO-type springs in Norris and Gibbon Geyser Basins. These are some of the liquid-phase dominated springs described by White et al. (1971) that form from the residual liquid phase that follows subsurface boiling and removal of a vapor-phase. It is unclear from Nordstrom et al. (2009) whether these springs would be classified as HO- or HB-type. From their chemistry, it would appear that volatile sulfur species degas without removing much water and thus, there is no corresponding increase in the concentration of chloride. Springs of a similar composition were described in Heart Lake Geyser Basin (not sampled in this research) by Lowenstern et al. (2012) who inferred that the fluid had completely degassed in the subsurface prior to boiling. These liquid-phase dominated alkaline-chloride springs commonly precipitate a silica sinter (Guidry and Chafetz, 2002). The precipitation of silica sinter (Figures 4.3, 4.13, and 4.23) can indicate deep-sourced fluids that experienced temperatures above 225℃ at depth (Fournier, 1977) or concentrated fluids that have experienced significant steam loss through boiling and phase separation (Guidry and Chafetz, 2002). In Norris Geyser Basin, it is well known that springs can change from neutral-chloride type to acid-sulfate type as the seasonal changes in the water table level affect subsurface mixing (Gardner et al., 2011; Hurwitz and Lowenstern, 2014). This seasonal change in composition may be why Norris springs typically contain higher sulfate. If the alkaline-chloride springs in the Lower Geyser Basin do not receive any gas or acid-sulfate water input after the

fluids degas at depth, then their sulfate concentrations could be maintained at low levels.

Vapor-phase dominated (meteoric-gas; MG-type) springs (chloride concentrations below 100 μmol/kg) were dominant in Forest Springs, Hot Springs Basin, Imperial/Spray Geyser Basins, and Washburn. MG-type springs were also present in Bog Creek, Gibbon Geyser Basin, Lewis Lake, Rabbit Creek, and Sylvan Springs alongside some chloride-rich liquid-phase dominated springs. The term "acid-sulfate" is commonly used interchangeably with "vapor-phase dominated" or "MG-type" spring classifications as many of these springs have low pH due to the high sulfuric acid content. High temperatures and high conductivities are common in these springs as they receive continuous heat from discharging gas and the acid produced breaks down minerals and solubilizes ions from rocks and soils (Figure 4.4). Not all MG-type systems are acid-sulfate springs. There are some high sulfate ($>$ 10,000 μmol/kg) springs with weakly acidic to circumneutral pH (i.e., pH between 5 and 7), as well as some hot, moderate sulfate concentration ($\sim$1500 μmol/kg) springs with neutral pH (pH between 6 and 7). Other buffers are in play in these springs to produce high pH, high sulfate springs. Many MG-type springs are also significantly mixed with MO-type waters and are distinguished by low sulfate (below 1000 μmol/kg) and low chloride (below 100 μmol/kg); they generally have cooler temperature, lower conductivity, and higher DOC.

Mixing between any of these fluid types creates springs with intermediate chloride and sulfate composition. Several mixing patterns are shown in Figure 4.1. All spring types, as well as several intermediate, mixed systems, are represented in my data set.

4.3.2 Bulk Dissolved Organic Carbon and Major FDOM Components

Dissolved organic carbon (DOC) concentrations provide evidence for extensive mixing with surface water in acidic springs, and a notable lack of surface water mixing in alkaline springs (Figure 4.5), consistent with initial observations in Nye et al. (2020). DOC concentrations ranged from 39.9 to 4016.6 μM. High chloride, deep-sourced hot springs of alkaline-chloride, HO-, HB-, and HGB-type consistently had the lowest concentrations (below 100 μM) with few exceptions. Acidic hot springs frequently had much higher concentrations and an overall wider concentration range, indicative of more extensive mixing. Non-thermal surface waters had low-to-moderate DOC concentrations (147 to 269 μM; Table 4.3) that were higher than most alkaline-chloride springs and HO-type springs, but typically lower than springs with acid-sulfate water input (mixed acid-sulfate-HO-type and acid-sulfate MG-type). Dilution of HO-type waters by either MO-type or acid-sulfate waters typically resulted in increasing DOC concentrations, notably so for the acid-sulfate mixed springs. The highest DOC concentrations were observed in MG-type springs with either circumneutral or acidic pH (Figure 4.5). All of the liquid-phase dominated, degassed springs (alkaline-chloride and HB-type) had consistently low DOC concentrations and high pH (Figure 4.8).

Fluorescence analysis provides further information about the effects different mixing processes have on the organic composition of the springs. Total fluorescence values largely correlated with DOC concentrations (Figure 4.7); an exception was the Calcite Springs samples which have higher fluorescence due to the presence of PAHs. The distribution of the PARAFAC model components shows obvious differences in the FDOM content among spring types and mixed systems. The PARAFAC components are presented as a fraction of total loadings, that is, the percentage of the total

component loadings assigned to each individual component type (humic-like, acid-spring, protein-like; Figures 4.6, 4.7, and 4.9). This representation can be misleading for samples with low fluorescence where there is almost no discernible signal of any component type. The PARAFAC model uses a residual minimization technique that assigns component values from a purely mathematical point of view. In other words, the model only has five components to account for the potentially hundreds of fluorescent compounds in a solution and the model will always attempt to assign component loadings to measured fluorescence signal, rather than leaving that signal unaccounted for. For example, a component can be assigned to account for signal that only has a partial spectral overlap (e.g., the PAH signal is assigned as acid-spring component loading). Because of this, it is important to critically assess the model results for each sample and consider the absolute and the relative component loadings, the EEM itself, and the geochemical and environmental context of each sample before applying the model results. That being said, in my data set the humic-like, acid-spring, and protein-like components demonstrated trends with hot spring pH and temperature (Figure 4.6) as well as hot spring chloride and sulfate concentrations (Figure 4.9). The humic-like components were most dominant in MG-type springs with circumneutral pH, especially those with high DOC concentrations (Figure 4.7), as well as in springs with significant MO-mixing. The acid-spring component was most dominant in low DOC (Figure 4.7), MG-type springs and in mixed acid-sulfate-HO-type springs. Finally, the protein-like component was most dominant in circumneutral or alkaline, low DOC, low fluorescence intensity springs (Figure 4.7) of the alkaline-chloride, HO-, and HB-types. As described in Nye et al. (2020), the absolute loadings for the protein-like component did not vary across springs as a function of pH, but the lack of the humic-like and acid-spring components in high pH springs led to the protein-like component being relatively more dominant (Figure 4.6).

The term 'humic-like fluorescence' is used in the surface water literature to refer to terrestrial-derived organic matter originally of soil, plant, or animal origin (Aiken, 1985; Senesi et al., 1991; Coble, 2007). Similar fluorescence is also observed in marine systems far from land and is attributed to microbially produced, complex organic matter. In this research, it is evident that thermally altered soil and buried sedimentary organic matter also produce fluorescence that has "humic-like" character. That is, a broad spectral range at long emission wavelengths (400 to 600 nm) and excitation spectra that can range between 250 and 400 nm, but are more prominent at short excitation wavelengths. This type of fluorescence signal could be better described as derived from complex aromatic, natural organic matter of a variety of sources, ultimately biotic in origin. Inspection of the EEMs in my data set reveals that there are notable differences in the "humic-like" signal from different types of hot springs waters (see examples in Figure 4.10).

In surface waters and systems with extensive surface water mixing the humic-like fluorescence may be indicative of surface-derived soil organic matter (e.g., the Amphitheatre Springs and Rabbit Creek regions). In Washburn, Forest Springs, and Hot Springs Basin, areas known for input of sedimentary organic matter, there is also a "humic-like" fluorescence signal that may come from complex organic matter derived from the sediments. This material is, ultimately, of a biotic origin similar to the surface-derived, soil organic matter. Finally there is an unusual, low intensity, double peak in the humic region observed in some of the HO- and HB-type springs. This may be an indicator of refractory, thermally altered sedimentary organic matter given, that it is only present in regions with deep-sourced springs that experience little surface mixing: Geyser Creek, Sentinel Meadow, White Creek, and Norris Geyser Basin all have alkaline springs that exhibit this fluorescence. Curiously, this double peak also appears in a sample from Wahb Springs; a heavily diluted, thermal chloride water

with traces of PAH fluorescence (Figure 4.31). I do not investigate these differences in humic-like fluorescence further in this research, but they may be a promising direction for future work. For the purpose of this paper, I use the term "humic-like" fluorescence to include complex natural organic matter from both soil-derived surface systems and buried sediments. Differentiation between the sources of humic-like fluorescence can be inferred from consideration of spring geochemistry and location.

4.3.3 Regional Trends in Geochemistry

Springs were sampled from regions in all areas of the park in order to assess the geographic and geochemical distribution of dissolved organic carbon and major FDOM features. Over the past several decades, numerous researchers have reported chemical data for thousands of thermal features (Fournier, 1989; Nordstrom et al., 2009; Shock et al., 2010; Cox et al., 2011; Holloway et al., 2011; Hurwitz and Lowenstern, 2014) and there are accepted trends in the geographic distribution of hydrothermal discharge in Yellowstone. Hot water, liquid-phase fluids rich in chloride and silica commonly discharge at lower elevations; while steam and hydrothermal gas discharges are usually found at higher elevations (Gardner et al., 2011; Hurwitz and Lowenstern, 2014). This trend occurs on a park-wide basis, but also in regions with local elevation change (see Gibbon Geyser Basin, Sylvan Springs, Bog Creek, Lewis Lake, Rabbit Creek). This is not an absolute trend, in some areas there are MG-type, low-chloride springs mere meters away from high-chloride, HO-type springs.

The western part of the Yellowstone caldera is known for chloride-rich liquid-phase discharges (see Figure 4.2). Alkaline-chloride springs populate the Lower, Midway, and Upper Geyser Basins in the southwest region of the Yellowstone caldera. Acid-chloride and neutral-chloride springs are found further north in the Norris and Gibbon Geyser Basins on the edge of the caldera. The chloride-rich springs are commonly

found with silica sinter surrounding the springs or built up into mounds (∼3 m in height) in the case of three springs (Steep Cone, Flat Cone, and Mound Spring) in Sentinel Meadow (Figure 4.23). These alkaline-chloride springs are distributed along the western edge of the Mallard Lake resurgent dome (Christiansen, 2001; Hurwitz and Lowenstern, 2014). They are thought to be completely degassed, which provides an explanation for their low sulfate and higher pH.

The eastern side of the caldera, on the other hand, is populated by acid-sulfate, vapor-phase dominated springs. On the edge of the Sour Creek resurgent dome (Christiansen, 2001; Hurwitz and Lowenstern, 2014) are the sulfur-rich, Crater Hills and Mud Volcano regions. This area has the strongest magmatic gas fluxes in the park (Kennedy et al., 1985; Bergfeld et al., 2012, 2014; Hurwitz and Lowenstern, 2014), often evidenced by strong sulfur odors and crystalline sulfur deposits on the ground surrounding springs and fumaroles. The northeast region of the park is known for considerable inputs of ammonia and organic carbon; the source of which is inferred to be buried sediments (Love and Good, 1970; Clifton et al., 1990). Sedimentary components to hydrothermal fluids in the northern and eastern parts of the park are evidenced by petroleum discharge (Allen and Day, 1935; Love and Good, 1970; Clifton et al., 1990), carbon and hydrogen isotopes of methane and/or ethane (Lorenson and Kvenvolden, 1993; Bergfeld et al., 2012), abundance and speciation of larger hydrocarbons (Clifton et al., 1990; Lorenson and Kvenvolden, 1993), and total ammonia concentrations and nitrogen isotopes (Holloway et al., 2011). The specific geochemistry of each regional group of hot springs used in this research is detailed below and regional averages are presented in Table 4.2. Surface water chemistry for several non-thermal samples is shown in Table 4.3. Full geochemical data for all thermal and non-thermal samples can be found in Appendix E.

Amphitheater Springs: The Amphitheater Springs group is found in the Norris-Mammoth corridor, north of Norris Geyser Basin (Figure 4.2). The hottest springs included two acid-sulfate-HO-type springs (∼1700 μmol/kg chloride, ∼5500 μmol/kg sulfate) and three acid-sulfate MG-type springs (<200 μmol/kg chloride, 3800 to 7600 μmol/kg sulfate). All other springs show evidence of extensive mixing between an acid-sulfate-HO-type fluid and MO-type water (Figure 4.11). This dilution is accompanied by increasing pH, cooler temperatures, lower conductivity, increasing DOC, and decreasing total fluorescence. The pH, temperature, and conductivity trends are all expected from dilution of thermal waters with cool, dilute, surface water. The DOC and fluorescence trends indicate that the MO-type water involved in the mixing has higher DOC, but lower total fluorescence than the initial hydrothermal fluid. Looking at the PARAFAC component loadings, this decrease in total fluorescence is largely due to the absence of the acid-spring component as the pH rises from dilution with circumneutral MO-type groundwater.

Bog Creek: The Bog Creek group of springs are in a ravine in the eastern part of park. There were three distinct sampling areas that were topographically separated along an elevation gradient. The terrain was silica-rich, suggesting evidence for historical discharge of alkaline fluids. The lowest elevation group of springs were slightly diluted, HO-type fluids (Figure 4.12) with circumneutral pH (∼3200 μmol/kg chloride, ∼2700 μmol/kg sulfate). The mid-elevation group of springs were of a diluted, MG-type (∼60 μmol/kg chloride, 1700 μmol/kg sulfate) that were all acidic with a pH range from 2 to 5. The highest elevation group of springs were strongly acidic, generally with pH below 2.5. There is no chloride and sulfate data for the highest elevation group of springs, but we may infer them to be acid-sulfate, vapor phase dominated springs based on their physical appearance, very low pH, and very

high conductivity (Table 4.2). The Bog Creek springs are atypical compared to the rest of the park.

Despite the distinctive difference in spring type and inorganic geochemistry between the three elevations, there is very little variation in the DOC and fluorescence data. In fact, the most acidic MG-type springs of upper Bog Creek had lower average DOC concentrations, and a lower range of values than the middle or lower Bog Creek springs (Table 4.2). The upper Bog Creek springs did have higher total fluorescence values; this is due to the presence of the acid-spring component, which is insoluble at the pH of the middle and lower Bog Creek springs. The humic-like fluorescence in the upper Bog Creek springs was similar to, possibly ever lower than, the middle and lower Bog Creek springs.

Alkaline-chloride waters have been reported to discharge through the eastern part of the park in the past (White et al., 1971; Fournier, 1989), depositing carbonates, silica, and other minerals. There was indeed silica sinter present around many Bog Creek springs and there was a hydrothermal outflow stream running through the region on a bed of silica (Figure 4.13). Given that silica exhibits low solubility in acid, it appears that Bog Creek is a system similar to the Lower Geyser Basin where armored silica channels are preventing mixing between groundwater and hydrothermal fluids. This region may be one of the few locations in the park where acidic vapor-phase discharge is protected in this way. The high temperature, low pH, low DOC, and low humic-like fluorescence in the acidic springs of upper Bog Creek indicate that this acidic discharge is relatively "fresh" and is likely condensed hydrothermal steam that has not circulated within the shallow subsurface or interacted extensively with the surface environment.

Calcite Springs: Calcite Springs is an area along banks of the Yellowstone River in the northeastern part of the park, outside of the caldera. Many springs here have an

oily sheen to them; natural oil and petroleum products have been identified here (Love and Good, 1970; Clifton et al., 1990) in seeps and vents. The fluorescence of PAHs has been identified (Nye et al., 2020) in these hot springs. Seasonally the Yellowstone river floods and destroys the springs, which are reformed, (usually in different locations) the following year. However, the high chloride concentrations ($\sim$6000 μmol/kg) indicate that when the river is low, the exposed springs experience little mixing with MO-type surface water (Figure 4.14). Elevated sulfate concentrations ($\sim$6000 μmol/kg) indicate the influence of acid-sulfate water or thermal gas input. Despite the high sulfate, most of the springs have neutral pH, a trend also seen at Washburn and Hot Springs Basin. These springs all experience input from thermally altered, buried organic matter. Extremely high concentrations of total ammonium that are a near perfect charge balance to the sulfate concentrations have been described at Washburn (Holloway et al., 2011). This may be evidence of competition between the ammonium and sulfuric acid buffers.

Crater Hills: Crater Hills is a sulfur-rich area along the Sour Creek resurgent dome in the eastern part of the caldera. Sulfur Spring is the most prominent feature in the region and famous for being a rare acidic geyser. Sulfur Spring is the only spring in this region with notable chloride concentrations; all other features are low chloride, vapor-phase dominated, acid-sulfate, MG type springs (Figure 4.15). Sulfur Spring is described by Nordstrom et al. (2009) as an HGB-type spring; an HO-type spring that has boiled at depth to concentrate chloride and then been charged with hydrothermal vapors to increase sulfate concentrations. In the past decade, Sulfur Spring has changed in appearance from a deep blue to a yellow-green (Figure 5.1). A similar change was noted for Evening Primrose in the mid-1900's (see Sylvan Springs; section 4.4.3) that was connected with high influx of native sulfur (Niermann, 2019). An additional interesting thermal feature in this region is a hydrothermal creek that

is a brilliant emerald color that has high amounts of the acid-spring component and no other prominent fluorescence. Other springs here are chalky yellow in color and sulfur crystals are commonly found around springs and fumaroles. Sulfur Spring and several other springs in this region demonstrated the novel fluorescence that is only connected with the presence of native sulfur (Figure 4.32).

Forest Springs: The Forest Springs group of springs are found in the north-eastern part of the caldera and exhibit similar geochemistry as Washburn and Hot Springs Basin. There are many acid-sulfate, MG-type springs found here with high DOC concentrations and correspondingly high total fluorescence values (Figure 4.16). Only Washburn springs demonstrated higher DOC and fluorescence. Unlike Washburn, Forest Springs were all strongly acidic (pH < 3) and exhibited high, but roughly equal, fluorescence of humic-like and acid-spring components. These springs are likely influenced by the buried sediments in the Absaroka mountain range that are seen in Washburn and Hot Springs Basin.

Gibbon Geyser Basin: Gibbon Geyser Basin includes many groups of springs within a relatively small area south of Norris Geyser Basin. The groups of springs sampled for this research are from Gibbon Hill, Geyser Creek, and Sylvan Spring, the latter of which is discussed separately. The Gibbon Hill and Geyser Creek groups of springs are separated by a short distance ($\sim$1 mile) so the geochemistry of these two regions is comparatively similar. Both groups have a wide range in spring pH and feature HO-type springs, MO-diluted HO-type springs, acid-sulfate-HO-type springs, HB-type springs, and acid-sulfate MG type springs (Figure 4.17). This region is an excellent location to investigate mixing processes. The MO-diluted HO-type springs in Gibbon Hill have higher DOC and total fluorescence relative to the most HO-type springs, evidence that, in this instance, the dilution of HO fluids with groundwater introduces more organic carbon. In the acid-sulfate, diluted HO-type springs in

Geyser Creek, there is not a discernible difference in DOC concentrations or total fluorescence, except for the presence of the acid-spring component, compared to the most typical HO-type springs (Figure 4.17). Only the acid-sulfate, MG-type springs demonstrate notably higher DOC and fluorescence. There are HB-type springs in both Gibbon Hill and Geyser Creek, but the Gibbon Hill springs were more concentrated, indicating more complete boiling and degassing in the subsurface, or more extensive evaporative concentration at the surface. These HB-type springs had the lowest DOC concentrations and total fluorescence in the region and close to the lowest in the park (Figure 4.17). This region also hosted an unusual "humic-like" fluorescence signal in many of the low DOC, low fluorescence springs (Figure 4.10). It is difficult to know whether this type of fluorescence is present in other regions because the "humic-like" fluorescence from surface organic matter or buried sediments often occurs at higher intensities and would potentially mask this signal.

Greater Obsidian Pool Area: The Greater Obsidian Pool Area (GOPA) is a dynamic group of springs found south of the Mud Volcano area, near Crater Hills. It is named for one of the most prominent features, Obsidian Pool, which has been diminishing in size and volume since its description in Meyer-Dombard et al. (2005). Many of the springs in this area change in appearance and chemistry from year to year. Obsidian Pool has an outflow channel that flows into Goose Lake. Along the channel are a series of source pools that are mixed into, and contribute to, the hydrothermal stream. All springs here exhibit chloride concentrations above 500 μmol/kg that suggest a liquid water dominated system, albeit one that has been heavily diluted. Sulfate concentrations were wide ranging but reached as high as 13,000 μmol/kg (Figure 4.18). There are several springs here that provide strong evidence the acid-spring component is associated with acid-sulfate water that circulates in the shallow subsurface. This is discussed further in section 4.4.4.

Hot Springs Basin: Hot Springs Basin is wide ranging region located along the northeastern border of the caldera. There were multiple basins and clearings featuring thermal features spread over several square miles. The ground in many areas was very unstable and spongy, evidence of extensive acid digestion. The springs here are dominantly MG-type springs with some diluted, MG-MO-type springs as well (Figure 4.19). They bear many similarities to Washburn springs; they have high sulfate, high DOC, high total fluorescence, and the unusual circumneutral pH, high-sulfate springs. There are also high sulfate, MG-type springs of circumneutral pH, similar to Washburn (Smedes and Prostka, 1972; Werner et al., 2008; Holloway et al., 2011). Methane and ammonia concentrations were higher in Hot Springs Basin than most regions in Yellowstone, except for Washburn, and some others in the northeast region of the park (Werner et al., 2008). Most likely Hot Springs Basin is influenced by sedimentary carbon, but not to the degree that Washburn is. My DOC and fluorescence data corroborate this conclusion. The circumneutral, MG-type springs in Hot Springs Basin exhibit higher DOC and fluorescence than the acidic MG-type springs. Once again, this may be evidence that these unusually high pH MG-type springs are being partially buffered by ammonia.

Imperial/Spray Geyser Basins: There were several acidic, vapor-phase dominated springs found around Imperial Geyser and Spray Geyser in the Lower Geyser Basin. Acidic, vapor-dominated systems are less common in the Lower Geyser Basin but are known. The acid-spring component was only obvious in the most acidic spring (sample 140804TG). The other springs had relatively low sulfate for acidic, MG-type springs, which reflects mixing with MO-type water (Figure 4.20).

Lewis Lake: Lewis Lake is located in the southern region of the park, close to the caldera boundary and far from the resurgent dome boundaries. The hot springs were found on the western side of the lake in two separate groups. The 'channel'

group of springs were on the edge of the lake south of the channel to Shoshone Lake and the 'hills' group of springs were up a ravine about a mile away. All of the channel group springs had consistent chloride (∼1800 μmol/kg) and sulfate (∼300 μmol/kg) concentrations suggestive of a diluted HO-type (Figure 4.21). The distance of Lewis Lake from the resurgent domes and the unusual chemistry in the Lewis Lake hot springs suggests the thermal fluid discharging here has been mixed with a dilute groundwater that lacked influence from surface organic matter. Lewis Lake itself was classified as a surface water sample (Table 4.3), but it had a DOC concentration higher than any hot spring as well as a much higher total fluorescence; so, it is unlikely that the source of MO-type mixing is Lewis Lake. Similar springs are described in Heart Lake Geyser Basin (Lowenstern et al., 2012).

The Lewis Lake hills group of springs also had circumneutral pH, but were vapor-phase dominated, MG-type springs, as evidenced by their low chloride (<50 μmol/kg) and moderately-high sulfate (∼1500 μmol/kg). With 1500 μM sulfate, these springs might be expected to have lower pHs. This is likely indicative of a bicarbonate-buffered, vapor phase system that is driven by the dissolution of carbonate minerals. One of the largest thermal features was dark red in color (Figure 4.21), indicative of high iron content, and the ground near this spring pulsed from the hydrothermal activity below the surface. This dark red spring had the highest pH with evidence of the acid-spring component in the sediment (see Chapter 3), evidence that the water discharging here had been acidic at one point but was later neutralized. These springs had low DOC concentrations, total fluorescence values, again, an unusual situation for hot, MG-type springs.

Lower Geyser Basin: The Sentinel Meadow group and White Creek group are both found in the Lower Geyser Basin and I refer to them collectively in this research because they have similar geochemistry (Figure 4.22). Sentinel Meadow has famous

alkaline-chloride springs (i.e., Mound Spring, Flat Cone, and Steep Cone) perched atop large mounds of silica sinter (Figure 4.23). They were described by Allen and Day (1935) and remain consistent in appearance today. The springs here had consistently low DOC concentrations and total fluorescence values that provide evidence for the barrier to mixing provided by precipitated silica channels described earlier. Some springs in the area have submerged logs that have become coated in silica, giving visual evidence for both the preservation of organic matter and the prevention of surface organic matter input (Figure 4.23). There were two different compositions of springs present at Sentinel Meadow and White Creek. The springs in Sentinel Meadow (and some in White Creek) had moderately-high chloride ($\sim$6500 μmol/kg) and low sulfate ($\sim$150 μmol/kg) indicating a degassed, liquid-phase dominated, deep-sourced water.

Several springs in White Creek were sampled further up the creek at a slightly higher elevation. These springs had lower pH ($\sim$6 to 7), and lower chloride concentrations ($\sim$1500 μmol/kg), and slightly higher sulfate concentrations ($\sim$270 μmol/kg). This composition puts them in an interesting position. They have identical chloride and sulfate concentrations to the diluted MO-HO-type springs in Gibbon Geyser Basin (Table 4.4). However, their DOC and fluorescence data suggest a different mixing process must be invoked to explain these springs. The springs had even lower DOC concentrations and total fluorescence values than the other low DOC, low fluorescence springs of the Lower Geyser Basin; this would be not be expected to occur if these were heavily diluted MO-HO-type fluids. Possibly mixing explanations are further discussed in section 4.3.4.

Norris Geyser Basin: The Norris Geyser Basin is home to many high-chloride, deep-sourced thermal springs. This area hosts the largest number of thermal regions in Yellowstone as well as some of the oldest described features (White et al.,

1988; Hurwitz and Lowenstern, 2014). All springs sampled from Norris were HO-type or HB-type at the time of sampling (Figure 4.24); but these springs are known to experience seasonal transitions from alkaline- or neutral-chloride to acid-sulfate compositions due to the shifting water table (Gardner et al. 2011). Cinder Pool, one of the most interesting thermal springs in the park is found in Norris Geyser Basin. It is known for the subsurface pool of molten sulfur that creates spherules or beads of sulfur that rise to the surface before breaking up and cycling back down. Perpetual Spouter is another famous spring found in Norris Geyser Basin, next to Tantalus Creek. Perpetual Spouter is an alkaline spring with beautiful geyserite (opaline sinter) precipitation around the edges that is known for being one of the most evaporated features in the park. It has chloride concentrations reaching 20,000 μmol/kg (see the third spring in Figure 3.3).

Rabbit Creek: Rabbit Creek has the most geochemically diverse group of springs in the Lower Geyser Basin. A hydrothermal creek sourced by a large acidic hot spring runs through the region. Rabbit Creek is divided into 'north' and 'south' subregions. Rabbit Creek north has several liquid-phase dominated, alkaline-chloride springs, diluted, HO-type springs, and vapor-phase dominated, MG-type springs. Rabbit Creek south has acidic, MG-type springs found along a fault line at the base of a hill. Many Rabbit Creek south springs appear to be steam-heated rainwater: they have very low conductivities, weakly acidic pH (pH between 3 and 5), and a wide range of DOC concentrations and fluorescence (Table 4.2). Hotter, more acidic springs are found, slightly higher up the hillside, in Rabbit Creek south, including one large, violently discharging spring that first appeared in 2014 (Figure 4.26). The fluorescence signal in this spring (sample 140730TK) was dominated by the acid-spring component. This spring also had remarkably low DOC (60 μM), suggesting

that the acid-spring component does come from a deep source and not the surface environment.

Sylvan Springs: This group of springs is part of the Gibbon Geyser Basin but is located further west than Gibbon Hill and Geyser Creek. Most of the springs here are found on a sinter covered hillside that can be seen from the roadside 1 mile away. This region is a great demonstration of how local elevation changes influence spring type. There are acidic, MG-type springs at higher elevations and neutral, HO-type springs at lower elevations, along with a range of mixed compositions (Figure 4.27). Sylvan Springs is home to the famous Evening Primrose spring, which currently demonstrates considerable fluorescence of the unknown, sulfur-associated peak (Figure 4.32). This spring has an interesting history as it used to be a remarkably clear, blue alkaline spring in the early 1900's, but has since changed to be a muddy, yellow acidic spring (Brock et al., 1972; Niermann, 2019). This change is further discussed in relation to the unknown sulfur-associated fluorescence peak in section 4.3.4.

Turbid Lake: Turbid Lake is located in Pelican Valley in the eastern part of the park. It has a few, small volume springs that might be better described as seeps. The seeps have circumneutral to weakly acidic pH values. The chloride and sulfate concentrations suggest these seeps are slightly diluted HO fluids. One sample also demonstrated the influence of hydrothermal vapor or dilution by shallow acidic water (Figure 4.28). The lake itself was acidic (pH 3) with relatively high sulfate ($\sim$500 μmol/kg), demonstrating significant influence from hydrothermal vapor (Table 4.3). The lake fluorescence suggested the presence of some signal in the acid-spring component region, but the signal is overshadowed by humic-like fluorescence.

Wahb Springs: Wahb Springs is located in Death Gulch, along Cache Creek in the far northeast corner of Yellowstone. There are very few thermal fluid discharges, but there is hot gas discharging in multiple locations. In the middle of Cache Creek

there is an outcrop with several seeps of diluted, HO-type fluid; one of these seeps was covered in an oily sheen (Figure 4.29). This spring demonstrated PAH fluorescence, similar to that of Calcite Springs although much more dilute (Figure 4.31). In addition, on the nearby hillside there was a cold spring (T = 30℃) that hosted the highest pH water (pH = 4.27) in the park that demonstrated acid-spring component fluorescence. This spring had remarkably high conductivity at 14,000 μS/cm; evidence that it was likely formed as an acid-sulfate fluid that travelled underground and cooled before discharging. Despite its high conducitivity, this spring had only ∼20 to 30% of the sulfate found in Crater Hills or Washburn springs (Table 4.2). This is evidence that the major ions in this spring are not sulfate or chloride as is typical of other hot springs. This spring also had a deep red outflow that stained a considerable area of the hill slope.

Washburn: The mudpots of Washburn are frequently described in the literature as unique relative to other Yellowstone hot springs. This region has many of the highest sulfate (> 10,000 μmol/kg) and ammonia concentrations (Holloway et al., 2011; Bergfeld et al., 2014) in the park. This is typically attributed to the influence of sedimentary organic matter (Allen and Day, 1935; Love and Good, 1970; Fournier, 1989; Hurwitz and Lowenstern, 2014). The Washburn mudpots also have the highest average DOC concentrations in the park, and second highest total fluorescence signal (Table 4.2). Only the highly fluorescent PAHs from the petroleum seep springs in Calcite Springs (Figure 4.30) were higher. All of the Washburn springs are predominantly MG-type, vapor phase springs with little chloride and high sulfate. Interestingly, many of the springs here have weakly acidic to neutral pH, in supposed conflict with their high sulfate concentration. The extremely high ammonia concentrations are described being in almost perfect charge balance with sulfate and may be acting as a buffer on the system (Holloway et al., 2011). These springs are de-

scribed as inkpots or mudpots because they have the appearance of bubbling mud. The fluorescence signal they show is classically "humic-like"; but it is probably better described as complex organic matter that has been thermally altered, but not to the extent of the PAHs from Calcite Springs.

4.3.4 Novel Fluorescence in Hydrothermal Fluids

The deepest-sourced and least-mixed hot springs in the park have low DOC and little fluorescent DOM. This pattern is clearest in the alkaline-chloride springs in the Lower Geyser Basin and Rabbit Creek, the HB-type springs in the Norris and Gibbon Geyser Basins, and the MG-type springs in Bog Creek, Lewis Lake, and Rabbit Creek. The greatest source of organic matter to hydrothermal fluids appears to be its introduction by acid-sulfate waters; either by direct dissolution and extraction from the soil, or from shallow subsurface cycling and discharge. Subsurface degassing through boiling events contributes to fluid preservation in the alkaline-chloride and HB-type springs by volatilizing the acid-forming gases (mainly H_2S and CO_2). Precipitation of minerals as rising hydrothermal fluid cools also aids in creating physical barriers that prevent mixing with shallow waters. The silica sinter observed most commonly in the Lower Geyser Basin generally occurs in alkaline or liquid-phase dominated systems that are hot enough at depth to become super-saturated with silica as the rising fluid cools (either through conduction or boiling).

This silica precipitation also contributes to the low carbon and low fluorescence in the strongly acidic, MG-type springs at Bog Creek and in the acidic HO-type springs in Norris Geyser Basin. In Norris Geyser Basin the seasonal discharge of alkaline-chloride fluid precipitates silica that prevents later mixing when acid-sulfate fluid is discharged. The acidic HO-type springs exhibit the novel acid-spring component and low levels of humic-like fluorescence. This low humic-like fluorescence is consistent

with a lack of mixing with MO-waters or dissolution of soil organic matter. There are novel fluorescence peaks in several other springs that are not known in natural surface waters. These peaks may also serve as indicators of distinct hydrothermal fluids or mixing processes. The acid-spring component was prominent throughout acidic springs (pH < 4) and was resolved as a component in the PARAFAC model described in Nye et al. (2020). Two other unique fluorescence signatures were also noted: the PAH fluorescence in Calcite Springs, and an unknown fluorescence signal associated with the presence of native sulfur.

The acid-spring component is strongly indicative of acid-sulfate water. The fluorophores themselves are most likely thermal degradation products of buried sedimentary organic matter. I believe they are relatively refractory and persist in the acid-sulfate fluids circulating in the subsurface, but they do not exist in the deep-sourced parent fluid. The fluorophores are exclusively acid-soluble, and their fluorescence is present in almost all acidic springs across the park. Acidic springs with low DOC (< 100 μM) consistently had the acid-spring component as the dominant component ($> 60\%$ fraction of total component loadings). Typically, these springs discharge violently, usually indicative of a rising thermal fluid decompressing or boiling, rather than a steam-heated surface water. The highest intensities of the acid-spring component are associated with higher humic-like fluorescence and higher DOC concentrations in the regions influenced by buried sediments (i.e., Washburn, Forest Springs, and Hot Springs Basin). This correlation with high fluorescence intensity suggests both that the buried sediments are the source of the acid-spring fluorophores, and that they persist in acid-sulfate water as it circulates throughout the park. Acidic springs (pH $\sim$4) that did not exhibit any acid-spring component fluorescence in the water or the sediment frequently had the appearance of stagnant pools and had cooler temperatures. These MG-type springs are formed from surface water pools that become steam

heated and acidified through thermal gas inputs (mostly found in Rabbit Creek). From these observations, I believe that the acid-spring component fluorophores are sourced from high temperature organic matter alteration in the subsurface. They are a rather refractory end product of such reactions that persists in acidic water circulating through the subsurface.

Further evidence that the acid-spring component fluorescence is associated with subsurface acid-sulfate water can be observed in several of the GOPA springs. One spring had a change in pH from 2.42 to 5.48 between 2014 and 2017. In 2014, the spring water demonstrated strong acid-spring component fluorescence. In 2016 the spring pH was 4.73 and the acid-spring component fluorescence was absent from the water but it was present in an acid-extract of the sediment (see Chapter 2, Figure 2.9). In 2017, the pH had increased further to 5.48 and the acid-spring component fluorescence remained absent from the water but had also disappeared from the sediment. The chloride and sulfate concentrations also changed and indicated a transition from an acid-sulfate-HO-type spring in 2014 (5235 μmol/kg chloride, 12,187 μmol/kg sulfate) to an HO-type spring in 2017 (7,825 μmol/kg chloride, 2,292 μmol/kg sulfate). The disappearance of the acid-spring component fluorescence is fairly convincing evidence, in this system at least, that acid-sulfate water and not HO-type water is the source of the acid-spring component fluorophores. Another notable spring in the GOPA region is a heavily diluted, acid-sulfate-HO-type spring (pH = 2.17, 533 μmol/kg chloride, 13,999 μmol/kg sulfate) that is the only spring in my entire data set for which the PARAFAC model assigns a 100% acid-spring component contribution to the fluorescence.

The PAH fluorescence in Calcite Springs and Wahb Springs is also an indicator of hydrothermally altered carbon from buried sediments (Figure 4.31). In this case, the high chloride, liquid-phase dominated fluid PAHs with it. PAHs are a com-

mon product of high-temperature pyrolysis of organic matter (Love and Good, 1970; Smedes and Prostka, 1972; Des Marais et al., 1981; Clifton et al., 1990; Lorenson et al., 1991; Werner et al., 2008; Shock et al., 2013). The other springs in this region of the park (i.e., Washburn, Forest Springs, and Hot Springs Basin) are all MG-type, vapor-phase dominated systems with little chloride. The fluorescence in these springs are dominantly "humic-like" and the acidic springs exhibited high acid-spring component fluorescence. The difference in fluorescence between the liquid-phase dominated systems (Calcite Springs, Wahb Springs) and the vapor-phase dominated systems (Washburn, Forest Springs, Hot Springs Basin) is potentially an effect due to elevation and volatility effect. The difference could also indicate that the sediments beneath the vapor-phase dominated systems are less thermally mature or that pyrolysis is less complete. Given that the complex organic matter buried in sediments was originally biomass, it is not surprising that the fluorescence is similar to that of humic acids and terrestrial organic matter, as opposed to that of pyrolysis end-products (PAHs).

The unmodelled fluorescence associated with the presence of native sulfur, briefly described in Nye et al. (2020), is not currently connected with any other geochemical parameter besides the presence of native sulfur. This fluorescence is seen in the HGB- and MG-type springs in Crater Hills, the acid-chloride-HO- and HB-type springs in Norris Geyser Basin, the neutral-chloride-HO- and HB-type springs in Sylvan Springs, and even faintly in an alkaline-chloride spring in White Creek. This sulfur-associated fluorescence had very low intensity in most springs and given that it is in the same region of the EEM as the "humic-like" fluorescence, it is not easily discernible in systems that have significant mixing with ground water or surface organic matter. The strongest example of this fluorescence is observed in Cinder Pool, Norris Geyser Basin. Cinder Pool is a unique pool with floating sulfur spherules that rise from a

molten sulfur reservoir beneath the surface of the spring (White et al., 1988; Xu et al., 2000). This is one of three known features like this in the world, the others are in New Zealand (Lloyd, 1959) and in Japan (Murozumi et al., 1966). Evening Primrose in Sylvan Springs also has high intensity of this sulfur associated fluorescence (Figure 4.32). This spring was famous in the early 20th century as a beautiful alkaline-chloride spring, similar to those in the Lower, Midway, and Upper Geyser Basins (Niermann, 2019). In 1927 it was documented to have developed a striking yellow coloring around the edges, and it was officially named Evening Primrose for this yellow color (Allen and Day, 1935). The 1959 earthquake disturbed this spring and made it look like yellow mud (National Park Service, 2019b). In the 1970's, the sulfur-oxidizing *Sulfolobus* was described here (Brock et al., 1972; Brock, 1978) and the spring was a muddy brown color, at least through 2000 (Montana State University, 2000). Since I was first there in 2014 Evening Primrose has been a murky yellow-green to yellow color. Sulfur Spring in Crater Hills has recently undergone a color change, similar to that of Evening Primrose in the early 1900's; prior to 2014 Sulfur Spring was blue; it has now become more yellow-green and sulfur deposits can be seen around the edges. Sulfur Spring had little fluorescence and only a weak acid-spring component, in 2014; but in recent years this novel, unknown sulfur-associated fluorescence has appeared (see Figure 5.1).

4.3.5 Organic Carbon Indicators of Fluid Mixing

The introduction of organic matter into hydrothermal fluids appears to have two major sources: surface water and buried sediments. However, not all surface water mixing brings surface organic matter with is. This is a conclusion that could not be drawn without my DOC and fluorescence data. It is generally accepted in the literature that there is only one deep, parent fluid feeding the Yellowstone hy-

drothermal system. This fluid has a chloride concentration between 8,500 and 11,000 μmol/kg. Given that there is no obvious surface source for chloride, (aside from discharged thermal chloride) any intermediate chloride concentrations that are higher than surface water chloride ($\sim$100 μmol/kg) can only be explained by a dilution of the deep hydrothermal fluid by a dilute surface water. Nearly all springs with an HO-type composition have DOC concentrations under 100 μM. All the surface water samples I have measured have DOC concentrations between 147 and 269 μM. Gibbon Geyser Basin, in particular, has a number of springs demonstrating a mixing gradient between deep, hydrothermal fluids and cool, surface-derived MO-type fluids. These springs have lower chloride and sulfate concentrations ($\sim$1000 to 5000 μmol/kg chloride, $\sim$200 to 1000 μmol/kg sulfate) coincident with lower temperatures, lower conductivity, increased DOC, increased total fluorescence, and increased humic-like fluorescence relative to typical HO-type springs (Figure 4.33). One spring in GOPA also exhibited this pattern. Two springs in Rabbit Creek 'north' have identical chloride and sulfate concentrations, but they have lower pH, higher temperature, and higher DOC than the other diluted systems, indicating some minor vapor-phase or acid-sulfate input.

There are springs in the Lewis Lake 'channel', Sylvan Springs, and White Creek that demonstrate mixing with a dilute fluid that has no significant surface-derived organic matter. These springs have low conductivity, and chloride and sulfate concentrations, identical to the Gibbon Geyser Basin springs mentioned above, indicating highly diluted MO-HO-type composition (Figure 4.33). However, all of these springs are hot ($>$ 70℃), and have low DOC (most are between 39 and 85 μM) and low total fluorescence values (below 10; Table 4.4). None of these trends would be expected from mixing with a cool MO-type surface water. If it weren't for the elevated temperatures, I would explain this pattern as dilution by rainwater. Rather, the ex-

planation I offer is that there is some condensed hydrothermal vapor phase that lacks H_2S or other acid producing gases that is responsible for this dilution. If rising hydrothermal fluid decompresses without boiling in the subsurface, then there may be a separation of the dissolved hydrothermal gases (H_2S and CO_2) and steam vapor that forms through a later boiling process which lacks H_2S and CO_2. There are regions in the southwest part of the park (i.e., Heart Lake and Shoshone Geyser Basin) where such degassed, deep-sourced fluids have been described (Hearn et al., 1990; Lowenstern et al., 2012). An alternate explanation is that there is a groundwater reservoir that has neither interacted with the surface environment, nor experienced water-rock reactions at depth (or other chemical alterations), but is still receiving heat input.

The vapor-phase MG-type springs in Lewis Lake also demonstrate a similar dilution by some hot, low-chloride, low-sulfate, low-DOC water. These springs have low chloride (< 30 μmol/kg) and low sulfate ($\sim$1500 μmol/kg) and low conductivities ($\sim$500 μS/cm), all indicators of heavily diluted MG-type springs. However, like the diluted springs in Lewis Lake 'channel', they are hot (60 to 92℃) and have low DOC ($\sim$100 μM) and low total fluorescence (below 10). They also have circumneutral pH (pH $\sim$6.5), which is unusual for hot MG-type springs. It is unlikely that the same explanation can be applied here as for the circumneutral springs in Washburn and Hot Springs Basin, given that Lewis Lake 'hills' springs show no evidence for sedimentary organic matter input. Rather, the most likely explanation is that they are bicarbonate buffered, either from CO_2 in the source vapor-phase or from carbonate minerals near the surface. I collected a sediment sample from the largest spring in the Lewis Lake 'hills' (pictured in Figure 3.3, middle photo). This was the spring with the highest pH that also exhibited the acid-spring component in the acid-extracted sediment. Given the acid-exclusive solubility of the acid-spring component, either the vapor-phase dominated fluid discharging in the Lewis Lake 'hills' springs was acidic

in the subsurface, or the acid-spring component can be transported as particulate matter in higher pH fluids. Because no other high-pH springs demonstrated this fluorescence in their sediments, the first option is more likely.

Surface water mixing is characterized by cooler temperatures, dilution of chloride and sulfate, lower conductivities, DOC concentrations closer to those of surface water ($\sim$150 to 250 μM), and the presence of humic-like fluorescence. The humic-like components in my PARAFAC model are indicators of complex organic matter from sediments, soils, or surface water. The humic-like fluorescence in Forest Springs, Washburn, and Hot Springs Basin is representative of a sedimentary organic matter that has been thermally altered to some extent. In other cases, such as the diluted MG springs of Rabbit Creek, Amphitheater Springs, Sylvan Springs, and Gibbon Geyser Basin, the humic-like fluorescence is introduced as the result of groundwater mixing or acidic breakdown of soils. The springs that consistently lack humic-like fluorescence are the alkaline-chloride springs of the Lower Geyser Basin, the neutral HO- and HB-type springs in the Norris and Gibbon Geyser Basins, and several acidic springs in Bog Creek. The Rabbit Creek 'south' springs also periodically switch between having some humic-like fluorescence and no fluorescence of any kind. In accordance with their other chemistry, (e.g., low conductivity, cool temperatures, low sulfate, low chloride) it is likely that these springs are really just steam heated rainwater pools that leach a little carbon from the surrounding environment.

4.4 Summary and Implications

The deepest sourced hot springs (chloride-rich, HO-type) have very little DOC and little fluorescent DOM. Throughout the Yellowstone system, dissolved organic carbon concentrations and FDOM provide additional information on different types of mixing between deep hydrothermal fluids and the surface environment. The presence, as well

as the lack thereof, of surface-derived organic matter is informative of mixing processes that are not obvious from inorganic indicators alone. Several novel fluorescence peaks are identified that are connected to specific types of hydrothermal fluids, including: the acid-spring component present in all springs influenced by acid-sulfate water, an unknown fluorescence associated with the presence of native sulfur, and PAH fluorescence observed in connection with petroleum seeps in Calcite Springs and Wahb Springs.

The novel acid-spring component is only present in acid-sulfate water. The lack of appearance in the water or the sediments from nearly all high pH springs supports this assertion. The only higher pH springs that had this fluorescence in the sediments have other evidence (e.g., high sulfate concentrations) that the fluid is partially mixed by acid-sulfate water. Strongly acidic springs with low DOC concentrations and minimal surface water mixing demonstrated very little fluorescence, but that fluorescence was predominantly due to the acid-spring component. This component is likely a refractory end product of the thermal degradation of buried sedimentary organic matter, because the strongest fluorescence of this component is found in the acidic springs of Forest Springs, Washburn, and Hot Springs Basin. The northeastern part of the park, where these regions are located, are known to have considerable influence of sedimentary organic matter that has been thermally altered.

Humic-like fluorescence is an indicator of the complex, biomass-derived, natural organic matter present in surface soils and in buried sediments. Humic-like fluorescence is introduced into hot springs in three ways: mixing with surface water, extraction from sediments by rising hydrothermal fluid, or via mixing with acid-sulfate water that has circulated in the subsurface. The humic-like fluorescence associated with sedimentary organic matter is spectroscopically different from the humic-like fluorescence commonly seen in non-thermal surface waters or soils. The organic matter

in buried sediments, especially those impacted by hydrothermal fluids, would hardly be expected to be compositionally similar to the operationally defined humic acids present in soils, despite having an original biomass source. An interesting future direction would be to analyze samples with these different types of humic-like fluorescence using higher resolution molecular characterization to correlate specific fluorescence character with different stages of hydrothermal organic matter alteration.

Multiple mixing processes have been described and I show that DOC concentrations and fluorescence components not only correlate with the inorganic indicators (chloride and sulfate), but also provide new information about mixing in the subsurface with a hot, dilute fluid containing little to no carbon. The high sensitivity and minimum sample prep required for fluorescence spectroscopy make it a robust tool that is useful for broad surveys of many hot springs. My broad sampling, and fluorescence analysis, of many hot springs has identified springs and regions that have unique compositions that are targets for future analysis by higher resolution techniques.

REFERENCES

Aiken, G. R. (ed.) (**1985**); *Humic Substances in Soil, Sediment, and Water: Geochemistry, Isolation, and Characterization*. Wiley, New York, USA.

Allen, E. T. and Day, A. L. (**1935**); Hot springs of the Yellowstone National Park. Carnegie Institution of Washington Publication 466, Carnegie Institute, Washington D. C., USA.

Baghoth, S., Sharma, S., and Amy, G. (**2011**); Tracking natural organic matter (NOM) in a drinking water treatment plant using fluorescence excitation emission matrices and PARAFAC. *Water Research* 45(2), pp. 797–809, doi:10.1016/j.watres.2010.09.005.

Bergfeld, D., Evans, W. C., Lowenstern, J. B., and Hurwitz, S. (**2012**); Carbon dioxide and hydrogen sulfide degassing and cryptic thermal input to Brimstone Basin, Yellowstone National Park, Wyoming. *Chemical Geology* 330-331, pp. 233–243, doi:10.1016/j.chemgeo.2012.09.001.

Bergfeld, D., Lowenstern, J. B., Hunt, A. G., Shanks, W. C. P., and Evans, W. C. (**2014**); Gas and isotope chemistry of thermal features in Yellowstone National Park, Wyoming. Scientific Investigations Report 2011-5012, United States Geological Survey, doi:10.3133/sir20115012.

Bro, R. (**1997**); PARAFAC. Tutorial and applications. *Chemometrics and Intelligent Laboratory Systems* 38(2), pp. 149–171, doi:10.1016/S0169-7439(97)00032-4.

Brock, T. and Mosser, J. (**1975**); Rate of sulfuric acid production in Yellowstone National Park. *Geological Society of America Bulletin* 86(2), pp. 194–198, doi:10.1130/0016-7606(1975)86⟨194:ROSPIY⟩2.0.CO;2.

Brock, T. D. (**1971**); Bimodal distribution of pH values of thermal springs of the world. *Geological Society of America Bulletin* 82(5), p. 1393, doi:10.1130/0016-7606(1971)82[1393:BDOPVO]2.0.CO;2.

Brock, T. D. (**1978**); *Thermophilic Microorganisms and Life at High Temperatures*. Springer, New York, USA, doi:10.1007/978-1-4612-6284-8.

Brock, T. D., Brock, K. M., Belly, R. T., and Weiss, R. L. (**1972**); Sulfolobus: A new genus of sulfur-oxidizing bacteria living at low pH and high temperature. *Archiv für Mikrobiologie* 84(1), pp. 54–68, doi:10.1007/BF00408082.

Cawley, K. M., Butler, K. D., Aiken, G. R., Larsen, L. G., Huntington, T. G., and McKnight, D. M. (**2012**); Identifying fluorescent pulp mill effluent in the Gulf of Maine and its watershed. *Marine Pollution Bulletin* 64(8), pp. 1678–1687, doi:10.1016/j.marpolbul.2012.05.040.

Christiansen, R. L. (**2001**); The quarternary and pliocene Yellowstone plateau volcanic field of Wyoming, Idaho, and Montana. Professional Paper 729-G, United States Geological Survey, doi:10.3133/pp729g.

Clifton, C., Walters, C., and Simoneit, B. (**1990**); Hydrothermal petroleums from Yellowstone National Park, Wyoming, U.S.A. *Applied Geochemistry* 5(1-2), pp. 169–191, doi:10.1016/0883-2927(90)90047-9.

Coble, P. G. (**2007**); Marine optical biogeochemistry: The chemistry of ocean color. *Chemical Reviews* 107(2), pp. 402–418, doi:10.1021/cr050350+.

Cole, J. J., Prairie, Y. T., Caraco, N. F., McDowell, W. H., Tranvik, L. J., Striegl, R. G., Duarte, C. M., Kortelainen, P., Downing, J. A., Middelburg, J. J., and Melack, J. (**2007**); Plumbing the global carbon cycle: Integrating inland waters into the terrestrial carbon budget. *Ecosystems* 10(1), pp. 172–185, doi:10.1007/s10021-006-9013-8.

Cox, A., Shock, E. L., and Havig, J. R. (**2011**); The transition to microbial photosynthesis in hot spring ecosystems. *Chemical Geology* 280(3-4), pp. 344–351, doi:10.1016/j.chemgeo.2010.11.022.

Cox, L., Celis, R., Hermosín, M. C., Cornejo, J., Zsolnay, A., and Zeller, K. (**2000**); Effect of organic amendments on herbicide sorption as related to the nature of the dissolved organic matter. *Environmental Science & Technology* 34(21), pp. 4600–4605, doi:10.1021/es0000293.

Del Vecchio, R. and Blough, N. V. (**2004**); Spatial and seasonal distribution of chromophoric dissolved organic matter and dissolved organic carbon in the Middle Atlantic Bight. *Marine Chemistry* 89(1-4), pp. 169–187, doi:10.1016/j.marchem.2004.02.027.

Des Marais, D. J., Donchin, J. H., Nehring, N. L., and Truesdell, A. H. (**1981**); Molecular carbon isotopic evidence for the origin of geothermal hydrocarbons. *Nature* 292(5826), pp. 826–828, doi:10.1038/292826a0.

Fournier, R. (**1977**); Chemical geothermometers and mixing models for geothermal systems. *Geothermics* 5(1-4), pp. 41–50, doi:10.1016/0375-6505(77)90007-4.

Fournier, R. O. (**1989**); Geochemistry and dynamics of the Yellowstone National Park hydrothermal system. *Annual Review of Earth and Planetary Sciences* 17(1), pp. 13–53, doi:10.1146/annurev.ea.17.050189.000305.

Gardner, W. P., Susong, D. D., Solomon, D. K., and Heasler, H. P. (**2011**); A multitracer approach for characterizing interactions between shallow groundwater and the hydrothermal system in the Norris Geyser Basin area, Yellowstone National Park. *Geochemistry, Geophysics, Geosystems* 12(8), doi:10.1029/2010GC003353.

Giggenbach, W. F. (**1997**); Relative importance of thermodynamic and kinetic processes in governing the chemical and isotopic composition of carbon gases in high heatflow sedimentary basins. *Geochimica et Cosmochimica Acta* 61(17), pp. 3763–3785, doi:10.1016/S0016-7037(97)00171-3.

Guidry, S. A. and Chafetz, H. S. (**2002**); Factors governing subaqueous siliceous sinter precipitation in hot springs: examples from Yellowstone National Park, USA. *Sedimentology* 49(6), pp. 1253–1267, doi:10.1046/j.1365-3091.2002.00494.x.

Gunter, B. (**1978**); C1-C4 hydrocarbons in hydrothermal gases. *Geochimica et Cosmochimica Acta* 42(1), pp. 137–139, doi:10.1016/0016-7037(78)90223-5.

Hamilton, T. L., Boyd, E. S., and Peters, J. W. (**2011**); Environmental constraints underpin the distribution and phylogenetic diversity of nifH in the Yellowstone geothermal complex. *Microbial Ecology* 61(4), pp. 860–870, doi:10.1007/s00248-011-9824-9.

Hawkes, J. A., Patriarca, C., Sjöberg, P. J. R., Tranvik, L. J., and Bergquist, J. (**2018**); Extreme isomeric complexity of dissolved organic matter found across aquatic environments: Extreme isomeric complexity of DOM. *Limnology and Oceanography Letters* 3(2), pp. 21–30, doi:10.1002/lol2.10064.

Hearn, E., Kennedy, B., and Truesdell, A. (**1990**); Coupled variations in helium isotopes and fluid chemistry: Shoshone Geyser Basin, Yellowstone National Park. *Geochimica et Cosmochimica Acta* 54(11), pp. 3103–3113, doi:10.1016/0016-7037(90)90126-6.

Hedges, J., Keil, R., and Benner, R. (**1997**); What happens to terrestrial organic matter in the ocean? *Organic Geochemistry* 27(5-6), pp. 195–212, doi:10.1016/S0146-6380(97)00066-1.

Hem, J. D. (**1985**); Study and interpretation of the chemical characteristics of natural water. Water Supply Paper 2254, United States Geological Survey, doi:10.3133/wsp2254.

Holloway, J. M., Nordstrom, D. K., Böhlke, J., McCleskey, R. B., and Ball, J. W. (**2011**); Ammonium in thermal waters of Yellowstone National Park: Processes affecting speciation and isotope fractionation. *Geochimica et Cosmochimica Acta* 75(16), pp. 4611–4636, doi:10.1016/j.gca.2011.05.036.

Hurwitz, S. and Lowenstern, J. B. (**2014**); Dynamics of the Yellowstone hydrothermal system. *Reviews of Geophysics* 52(3), pp. 375–411, doi:10.1002/2014RG000452.

Kellerman, A. M., Guillemette, F., Podgorski, D. C., Aiken, G. R., Butler, K. D., and Spencer, R. G. M. (**2018**); Unifying concepts linking dissolved organic matter composition to persistence in aquatic ecosystems. *Environmental Science & Technology* 52(5), pp. 2538–2548, doi:10.1021/acs.est.7b05513.

Kennedy, B., Lynch, M., Reynolds, J., and Smith, S. (**1985**); Intensive sampling of noble gases in fluids at Yellowstone: I. Early overview of the data; regional patterns. *Geochimica et Cosmochimica Acta* 49(5), pp. 1251–1261, doi:10.1016/0016-7037(85)90014-6.

Kharaka, Y., Sorey, M., and Thordsen, J. (**2000**); Large-scale hydrothermal fluid discharges in the Norris-Mammoth corridor, Yellowstone National Park, USA. *Journal of Geochemical Exploration* 69-70, pp. 201–205, doi:10.1016/S0375-6742(00)00025-X.

Kharaka, Y., Thordsen, J., and White, L. (**2002**); Isotope and chemical compositions of meteoric and thermal waters and snow from the greater Yellowstone National Park region. Open File Report 02-194, United States Geological Survey, doi:10.3133/ofr02194.

Kvenvolden, K. A., Simoneit, B. R. T., and Love, J. D. (**1989**); Chemical and isotopic compositions of natural gas from seeps in Yellowstone and Grand Teton National Parks, Wyoming. In: *Gas Resources of Wyoming, Fourtieth Annual Field Conference Guidebook*, pp. 241–246, Wyoming Geological Association.

LaRowe, D. E. and Van Cappellen, P. (**2011**); Degradation of natural organic matter: A thermodynamic analysis. *Geochimica et Cosmochimica Acta* 75(8), pp. 2030–2042, doi:10.1016/j.gca.2011.01.020.

Leenheer, J. A. (**2009**); Systematic approaches to comprehensive analyses of natural organic matter. *Annals of Environmental Science* 3, pp. 1–130.

Lloyd, E. F. (**1959**); The hot springs and hydrothermal eruptions of Waiotapu. *New Zealand Journal of Geology and Geophysics* 2(1), pp. 141–176, doi:10.1080/00288306.1959.10431319.

Lorenson, T. D. and Kvenvolden, K. A. (**1993**); A comparison of hydrocarbon gases from natural sources in the Northwestern United States. In: Howell, D. G., Wiese, K., Fanelli, M., Zink, L., and Cole, F. (eds.), *The Future of Energy Gases*, pp. 453–469, Professional Paper 1570, United States Geological Survey, doi:10.3133/pp1570.

Lorenson, T. D., Kvenvolden, K. A., Simoneit, B. R. T., and Leif, R. N. (**1991**); Composition of gas seeps in northwestern Wyoming. Open File Report 91-121, United States Geological Survey, doi:10.3133/ofr91121.

Love, J. D. and Good, J. M. (**1970**); Hydrocarbons in themal areas, northwestern Wyoming. Professional Paper 644-B, United States Geological Survey, doi:10.3133/pp644b.

Lowenstern, J. B. and Hurwitz, S. (**2008**); Monitoring a supervolcano in repose: Heat and volatile flux at the Yellowstone caldera. *Elements* 4(1), pp. 35–40, doi:10.2113/gselements.4.1.35.

Lowenstern, J. B., Bergfeld, D., Evans, W. C., and Hurwitz, S. (**2012**); Generation and evolution of hydrothermal fluids at Yellowstone: Insights from the Heart Lake Geyser Basin. *Geochemistry, Geophysics, Geosystems* 13(1), doi:10.1029/2011GC003835.

Luhr, S. (**2020**); GIS Data. Wyoming State Geological Survey, https://www.wsgs.wyo.gov/pubs-maps/gis.

MATLAB (**2010**); version 7.10.0 R2010a MatLab: The language of technical computing. The Mathworks Inc., Natick, Massachusetts, USA.

Meyer-Dombard, D. R., Shock, E. L., and Amend, J. P. (**2005**); Archaeal and bacterial communities in geochemically diverse hot springs of Yellowstone National Park, USA. *Geobiology* 3(3), pp. 211–227, doi:10.1111/j.1472-4669.2005.00052.x.

Montana State University (**2000**); Evening Primrose Spring details. Yellowstone Research Coordination Network, http://rcn.montana.edu/Features/Detail.aspx?id=1898.

Murozumi, M., Abiko, T., and Nakamura, S. (**1966**); Geochemical investigation of the Noboribetsu Oyunuma explosion crater lake. *Second Series Bulletin of the Volcanological Society of Japan* 11(1), pp. 1–16.

National Park Service (**2019**a); Park Facts - Yellowstone National Park. U.S. National Park Service, https://www.nps.gov/yell/planyourvisit/parkfacts.htm.

National Park Service (**2019**b); Yellowstone's Photo Collection. U.S. National Park Service, https://www.nps.gov/features/yell/slidefile/history/1946_1999/thermalfeatures/Page-1.htm.

Niermann, D. (**2019**); Sylvan Springs group. Volcanic-springs.com, http://volcanic-springs.com/index.php?section=USA&usasection=gibbongeyserbasin&usasubsection=sylvanspringsgroup.

Nordstrom, K. D., McCleskey, B. R., and Ball, J. W. (**2009**); Sulfur geochemistry of hydrothermal waters in Yellowstone National Park: IV Acid-sulfate waters. *Applied Geochemistry* 24(2), pp. 191–207, doi:10.1016/j.apgeochem.2008.11.019.

Nye, J., Shock, E., and Hartnett, H. (**2020**); A novel PARAFAC model for continental hot springs reveals unique dissolved organic carbon compositions. *Organic Geochemistry* 141(103964), doi:10.1016/j.orggeochem.2019.103964.

Ohno, T. (**2002**); Fluorescence inner-filtering correction for determining the humification index of dissolved organic matter. *Environmental Science & Technology* 36(4), pp. 742–746, doi:10.1021/es0155276.

Senesi, N., Miano, T. M., Provenzano, M. R., and Brunetti, G. (**1991**); Characterization, differentiation, and classification of humic substances by fluorescence spectroscopy. *Soil Science* 152(4), pp. 259–271, doi:10.1097/00010694-199110000-00004.

Shock, E. L., Holland, M., Meyer-Dombard, D., Amend, J. P., Osburn, G., and Fischer, T. P. (**2010**); Quantifying inorganic sources of geochemical energy in hydrothermal ecosystems, Yellowstone National Park, USA. *Geochimica et Cosmochimica Acta* 74(14), pp. 4005–4043, doi:10.1016/j.gca.2009.08.036.

Shock, E. L., Canovas, P., Yang, Z., Boyer, G., Johnson, K., Robinson, K., Fecteau, K., Windman, T., and Cox, A. (**2013**); Thermodynamics of organic transformations in hydrothermal fluids. *Reviews in Mineralogy and Geochemistry* 76(1), pp. 311–350, doi:10.2138/rmg.2013.76.9.

Smedes, H. W. and Prostka, H. J. (**1972**); Stratigraphic framework of the Absaroka Volcanic Supergroup. Professional Paper 729-C, United States Geological Survey, doi:10.3133/pp729C.

Stedmon, C. A. and Bro, R. (**2008**); Characterizing dissolved organic matter fluorescence with parallel factor analysis, a tutorial: Fluorescence-PARAFAC analysis of DOM. *Limnology and Oceanography: Methods* 6(11), pp. 572–579, doi: 10.4319/lom.2008.6.572.

Stedmon, C. A., Markager, S., and Bro, R. (**2003**); Tracing dissolved organic matter in aquatic environments using a new approach to fluorescence spectroscopy. *Marine Chemistry* 82(3-4), pp. 239–254, doi:10.1016/S0304-4203(03)00072-0.

Werner, C., Brantley, S. L., and Boomer, K. (**2000**); CO2 emissions related to the Yellowstone volcanic system. *Journal of Geophysical Research: Solid Earth* 105(B5), pp. 10831–10846, doi:10.1029/1999JB900331.

Werner, C., Hurwitz, S., Evans, W. C., Lowenstern, J. B., Bergfeld, D., Heasler, H., Jaworowski, C., and Hunt, A. (**2008**); Volatile emissions and gas geochemistry of Hot Spring Basin, Yellowstone National Park, USA. *Journal of Volcanology and Geothermal Research* 178(4), pp. 751–762, doi:10.1016/j.jvolgeores.2008.09.016.

White, D. E., Muffler, L. J. P., and Truesdell, A. H. (**1971**); Vapor-dominated hydrothermal systems compared with hot-water systems. *Economic Geology* 66(1), pp. 75–97, doi:10.2113/gsecongeo.66.1.75.

White, D. E., Hutchinson, R. A., and Keith, T. E. C. (**1988**); The geology and remarkable thermal activity of Norris Geyser Basin, Yellowstone National Park, Wyoming. Professional Paper 1456, United States Geological Survey, doi:10.3133/pp1456.

Wu, X., Wu, L., Liu, Y., Zhang, P., Li, Q., Zhou, J., Hess, N. J., Hazen, T. C., Yang, W., and Chakraborty, R. (**2018**); Microbial interactions with dissolved organic matter drive carbon dynamics and community succession. *Frontiers in Microbiology* 9(1234), doi:10.3389/fmicb.2018.01234.

Xu, Y., Schoonen, M., Nordstrom, D., Cunningham, K., and Ball, J. (**1998**); Sulfur geochemistry of hydrothermal waters in Yellowstone National Park: I. The origin of thiosulfate in hot spring waters. *Geochimica et Cosmochimica Acta* 62(23-24), pp. 3729–3743, doi:10.1016/S0016-7037(98)00269-5.

Xu, Y., Schoonen, M., Nordstrom, D., Cunningham, K., and Ball, J. (**2000**); Sulfur geochemistry of hydrothermal waters in Yellowstone National Park, Wyoming, USA. II. Formation and decomposition of thiosulfate and polythionate in Cinder Pool. *Journal of Volcanology and Geothermal Research* 97(1-4), pp. 407–423, doi: 10.1016/S0377-0273(99)00173-0.

Yang, Y. and Zhang, D. (**1995**); Concentration effect on the fluorescence spectra of humic substances. *Communications in Soil Science and Plant Analysis* 26(15-16), pp. 2333–2349, doi:10.1080/00103629509369451.

Zepp, R. G., Sheldon, W. M., and Moran, M. A. (**2004**); Dissolved organic fluorophores in southeastern US coastal waters: Correction method for eliminating Rayleigh and Raman scattering peaks in excitation-emission matrices. *Marine Chemistry* 89(1-4), pp. 15–36, doi:10.1016/j.marchem.2004.02.006.

Table 4.1: Hot spring classification, terminology, and chloride/sulfate concentrations

Spring type	Sub-types/other terms	Chloride (μmol/kg)	Sulfate (μmol/kg)
Hydrothermal-only (HO)	(Acid/neutral)-HO	8,500 to 11,000	1,000 to 3,000
	(Acid/neutral)-chloride	$>$ 1,000	$>$ 1,000
	Acid-sulfate-HO	1,000 to 10,000	$>$ 3,000
Hydrothermal-boiling (HB)		$>$ 10,000	$<$ 1,000
Hydrothermal-boiling -gas (HGB)		$>$ 20,000	$>$ 5,000
Meteoric-gas (MG)	(Acid/neutral)-sulfate Vapor-phase dominated	$<$ 100	$>$ 100*
Meteoric-only (MO)	Surface/ground water	$<$ 10	$<$ 100
Alkaline-chloride	Liquid-phase dominated Hot water	6,000 to 9,000	$<$ 1,000

*Compositions vary greatly with MO- mixing, spring volume, and gas discharge.
The HO-, HB-, HGB-, MG-, and MO-type designations come from Nordstrom et al. (2009).
Other terminology comes from White et al. (1971), Brock (1971), and Fournier (1989).

Table 4.2: Regional hot spring geochemistry. Values are averages for samples collected in the 2012 to 2018 field seasons.

Location	pH	Temperature ℃	Conductivity μS/cm	Cl^- μmol/kg	SO_4^{-2} μmol/kg	DOC μM	Total Fluorescence
				Average (std. dev) number of samples			
Amphitheater Springs	**3.72** (1.19) 17	**46.7** (19.1) 17	**964.9** (854.4) 16	**365.6** (529.9) 17	**2763.1** (2379.0) 17	**126.4** (69.6) 17	**18.22** (6.85) 12
Bog Creek							
lower	**6.49** (0.31) 6	**80.9** (9.0) 6	**1336.2** (68.5) 6	**3183.6** (741.8) 6	**2708.1** (623.8) 6	**190.6** (159.7) 6	**16.47** (13.29) 6
middle	**4.10** (1.23) 5	**59.1** (23.8) 5	**807.9** (906.0) 5	**62.5** (70.8) 4	**1706.8** (1154.4) 4	**175.6** (81.6) 5	**16.87** (10.54) 5
upper	**1.89** (0.15) 7	**83.8** (9.0) 7	**4962.7** (949.9) 7	— —	— —	**137.8** (29.0) 5	**21.17** (5.27) 5
Calcite Springs	**5.97** (1.54) 5	**74.6** (15.7) 5	**2021.0** (127.6) 5	**6093.6** (419.5) 5	**5928.2** (1454.3) 5	**288.0** (95.4) 5	**714.88** (140.24) 5
Crater Hills	**2.51** (0.74) 12	**70.2** (17.8) 12	**4787.3** (2145.0) 12	**6487.9** (11043.4) 11	**13697.1** (6967.5) 11	**441.3** (822.5) 12	**43.14** (53.19) 12
Forest Springs	**2.19** (0.38) 22	**56.9** (19.3) 22	**3271.8** (1945.5) 22	**14.4** (18.9) 22	**10683.5** (6858.7) 22	**517.7** (791.9) 22	**72.06** (61.89) 19
Gibbon Geyser Basin							
Geyser Creek	**4.88** (2.01) 17	**80.4** (12.5) 17	**1857.7** (757.5) 17	**7533.6** (5866.1) 17	**2955.8** (2688.8) 17	**122.5** (93.9) 16	**16.00** (10.03) 16
Gibbon Hill	**5.62** (1.8) 13	**72.3** (18) 13	**1472.5** (1226.3) 13	**5116** (5759.6) 13	**2982.6** (6258.4) 13	**194.7** (129.4) 13	**28.03** (24.71) 13
GOPA	**4.83** (1.41) 12	**63.3** (17.1) 12	**1750.2** (997.2) 12	**5621.5** (4402.6) 12	**4027.3** (4338.5) 12	**295.8** (299.2) 12	**46.07** (36.79) 12
Hot Springs Basin	**3.94** (1.22) 19	**73.3** (16.2) 19	**1224.2** (846.6) 19	**14.9** (17.5) 19	**4335.6** (3003.8) 19	**323.4** (290.3) 19	**57.64** (36.46) 19
Imperial and Spray	**3.63** (0.68) 7	**59.9** (15.4) 7	**604.5** (418.7) 6	**37.8** (16.3) 6	**2058.8** (2212.5) 6	**291.7** (399.1) 7	**44.044** (68.62) 7
Lewis Lake							
channel	**6.85** (0.28) 6	**78.7** (7.8) 6	**625.1** (77.9) 6	**1609.4** (373.2) 6	**284.4** (70.3) 6	**94.6** (37.9) 6	**4.64** (1.06) 6
hill	**6.5** (0.28) 5	**79.4** (13) 5	**447.6** (55.6) 5	**17.9** (4.2) 3	**1590.6** (236.3) 3	**86.4** (16.3) 5	**8.98** (1.61) 5
Lower Geyser Basin							
Sentinel Meadow	**8.2** (0.53) 3	**89.6** (5.8) 3	**1517.5** (42.6) 3	**6357.1** (493.2) 3	**155.0** (7.7) 3	**69.7** (16.1) 3	**9.13** (2.34) 3
White Creek	**7.51** (0.83) 9	**74.0** (11.7) 9	**957.7** (564.1) 9	**3647.4** (2683.4) 9	**225.4** (58.5) 9	**78.9** (40.3) 9	**3.02** (1.20) 9
Norris Geyser Basin	**3.51** (1.37) 23	**79.2** (12.6) 23	**1935.9** (642.8) 23	**12219.2** (4413.0) 23	**1518.6** (689.1) 23	**116.7** (88.0) 22	**19.17** (12.20) 22
Rabbit Creek							
north	**5.91** (2.22) 14	**65.3** (14.6) 14	**815.8** (798.7) 14	**3217.1** (3710.5) 14	**443.6** (486.9) 14	**126.6** (83.9) 14	**10.47** (7.26) 13
south	**4.71** (1.0) 28	**60.1** (11.6) 28	**229.9** (147.8) 28	**24.9** (22.0) 28	**574.6** (405.0) 28	**209.6** (104.9) 28	**45.54** (41.48) 28
Sylvan Springs	**3.75** (1.78) 38	**66.4** (20.8) 38	**2276.3** (973.3) 38	**5407.1** (5295.1) 38	**5096.1** (4027.2) 38	**190.8** (184.5) 38	**36.76** (53.41) 38
Turbid Lake	**6.28** (0.39) 3	**52.0** (15.3) 3	**1566.3** (661.8) 3	**4144.9** (3087.7) 3	**1677.1** (849.8) 3	**105.4** (23.0) 3	**13.48** (1.77) 3
Wahb Springs	**5.64** (1.19) 3	**21.2** (11.4) 3	**6272.6** (6901.8) 3	**810.4** (720.2) 3	**3433.9** (5424.4) 3	**149.6** (21.6) 3	**52.83** (19.20) 3
Washburn							
lower	**5.32** (1.11) 8	**83.2** (6.8) 8	**3626.7** (1328.0) 8	**11.8** (5.1) 8	**15924.5** (4457.2) 8	**1967.5** (1446.9) 7	**686.08** (645.51) 7
upper	**4.11** (1.53) 5	**65.8** (19.1) 5	**4174.3** (2605.5) 5	**26.9** (49.7) 5	**17659.4** (3947.8) 5	**470.4** (46.9) 5	**155.62** (17.82) 5

Table 4.3: Surface water chemistry

Location	pH	Temperature ℃	Conductivity μS/cm	Cl^- μmol/kg	SO_4^{-2} μmol/kg	DOC μM	Comments
Unnamed creek	5.28	12.6	50.9	16	58	147	Near Amphitheater Springs region
Yellowstone River	7.37	16.3	198.5	165	122	203	At Calcite Springs region
Wapiti Lake	6.74	17.2	25.9	6	16	244	Off peninsula near 4W2 campsite
Lewis Lake	7.55	15.7	113.6	100	835	177	Southwest of channel to Shoshone Lake
Turbid Lake	3.43	24.6	254.1	67	499	269	East of Bear Creek inlet into lake
Cache Creek	7.51	15.3	67.4	3	28	149	Death Gulch, upstream of sampled Wahb Springs
Avg. (std. dev.)	**6.31** (1.65)	**17.0** (4.1)	**118.4** (90.1)	**59** (65)	**260** (335)	**198** (50)	

Table 4.4: Chemistry of some diluted HO-type springs.

Region Sample code	pH	Temperature ℃	Conductivity μS/cm	Cl^- μmol/kg	$SO_4{}^{2-}$ μmol/kg	DOC μM	Total Fluorescence
Gibbon Hill 170725SK	6.26	53.4	626.9	1461	558	169.5	26.02
Gibbon Hill 170725SJ	5.75	75.6	585.5	1318	334	142.7	17.82
Rabbit Creek 'north' 120718TL	4.43	68.1	342.6	685	638	159	13.85
White Creek 170722SV	6.87	79.5	556.9	1477	289	39.9	1.87
Sylvan Springs 170716SS	6.44	79.1	1188.8	1944	826	85.4	9.85
Lewis Lake 'channel' 180922D	6.63	68.5	619.3	1517	212	50.8	3.72

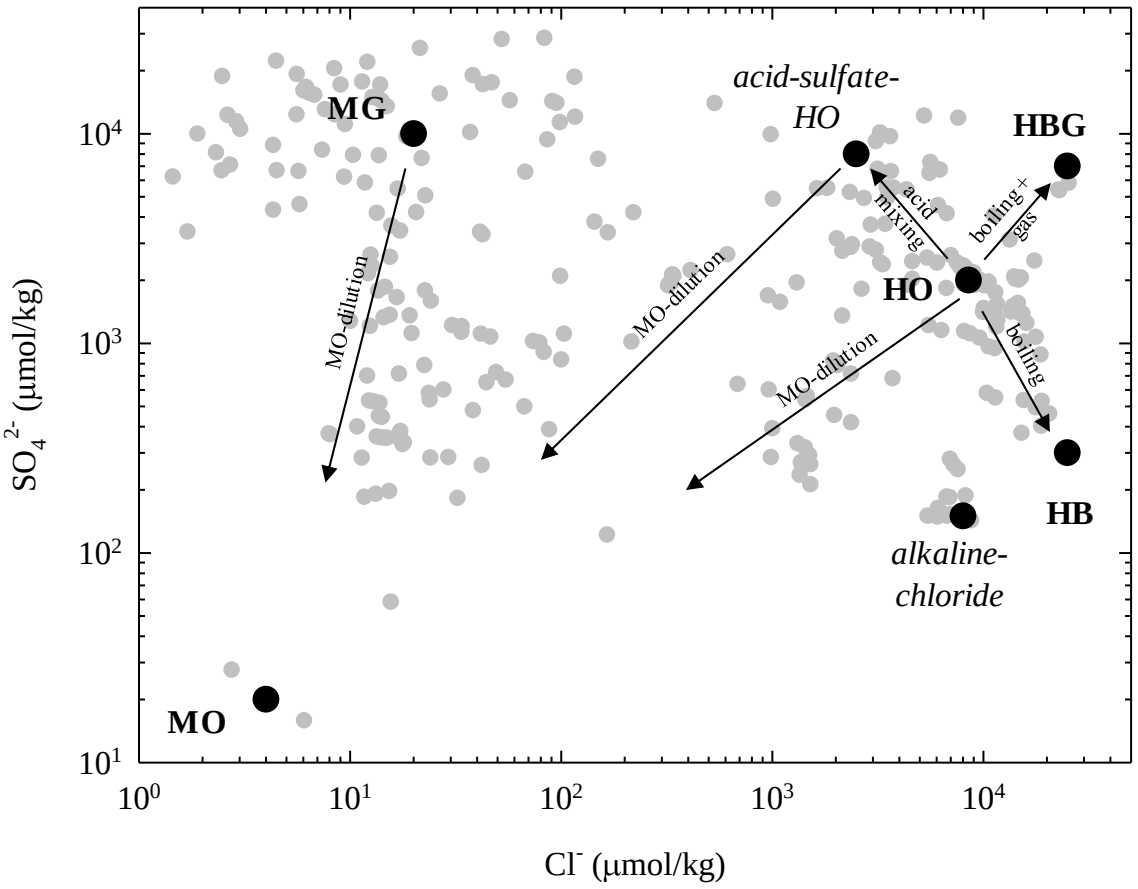

Figure 4.1: Chloride and sulfate concentration data (gray circles) for 281 water samples from YNP. Hot spring types (black circles) as classified by chloride and sulfate compositions (Nordstrom et al., 2009) are those presented in Table 4.1. Mixing and boiling processes are shown by arrows.

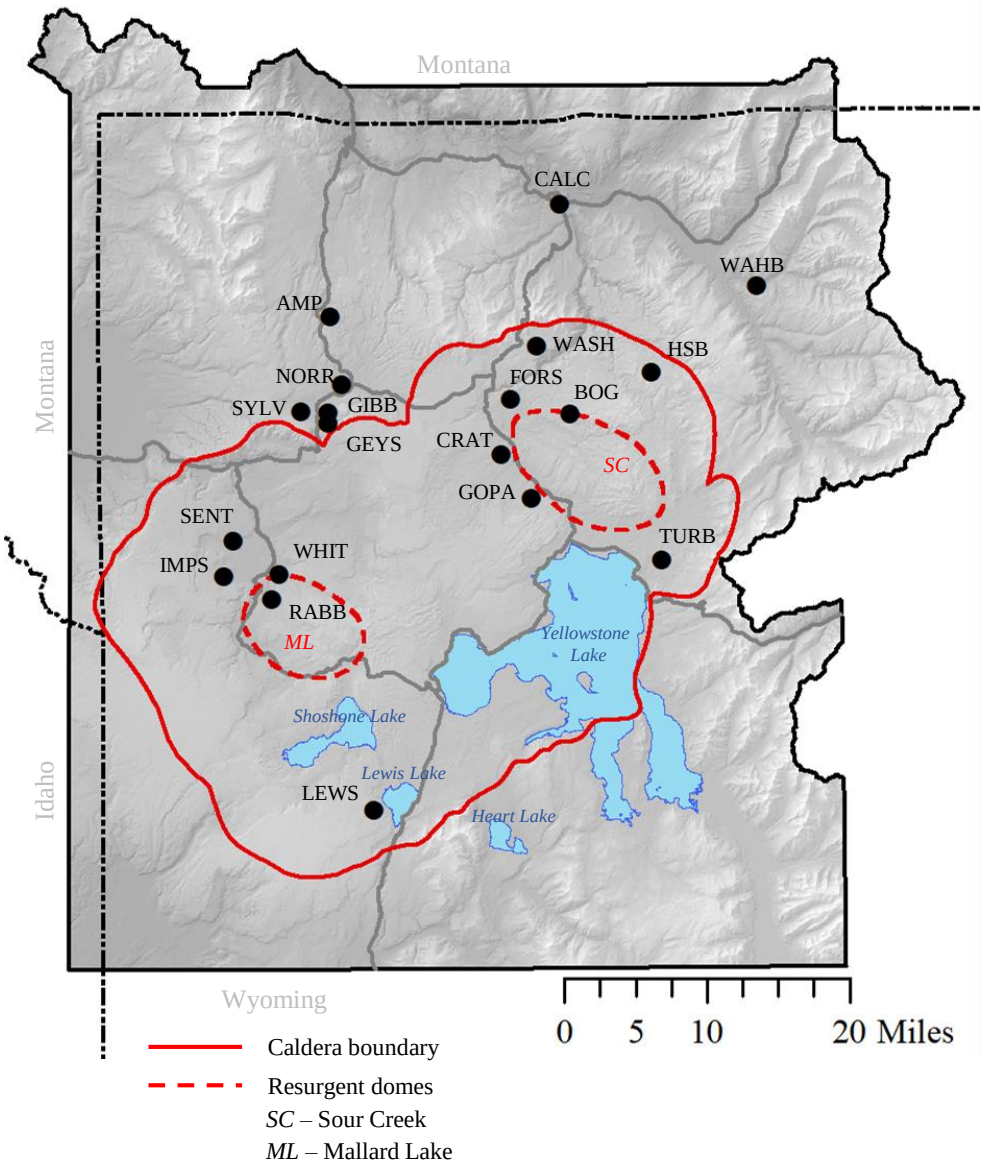

Figure 4.2: Map of Yellowstone National Park. Sampled regions: AMP – Amphitheater Spring, BOG – Bog Creek, CALC – Calcite Springs, CRAT – Crater Hills, FORS – Forest Springs, GEYS – Geyser Creek, GIBB – Gibbon Hill, GOPA – Greater Obsidian Pool Area, HSB – Hot Springs Basin, IMPS – Imperial and Spray Geyser Basins, LEWS – Lewis Lake, NORR – Norris Geyser Basin, RABB – Rabbit Creek, SENT – Sentinel Meadow, SYLV – Sylvan Springs, TURB – Turbid Lake, WAHB – Wahb Springs, WASH – Washburn, WHIT – White Creek. Map was generated using ArcGIS using geographic data from the Wyoming State Geological Survey (Luhr, 2020) and Christiansen (2001).

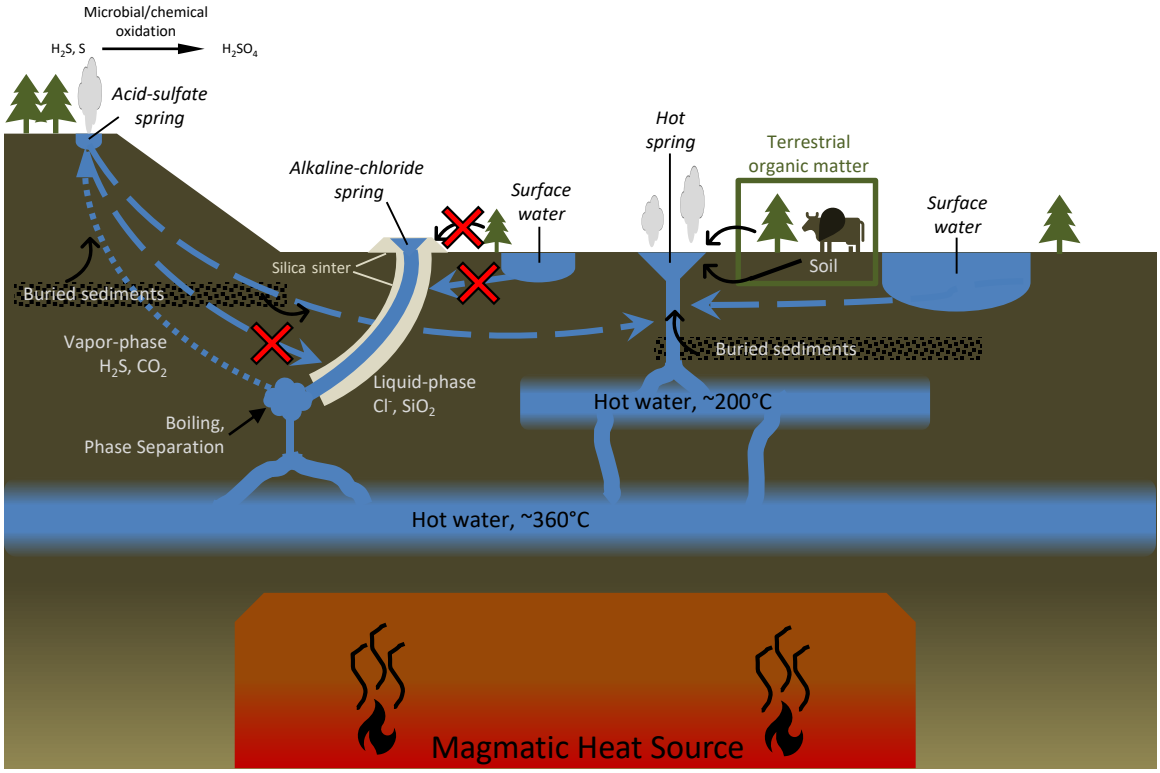

Figure 4.3: Artistic depiction of subsurface hydrology in a hydrothermal system. Illustrations show theoretical fluid mixing between deep, hydrothermal water and cool, surface water as well as alteration processes that change the chemical composition of fluids. The red X symbols indicate where precipitated silica sinter may inhibit mixing.

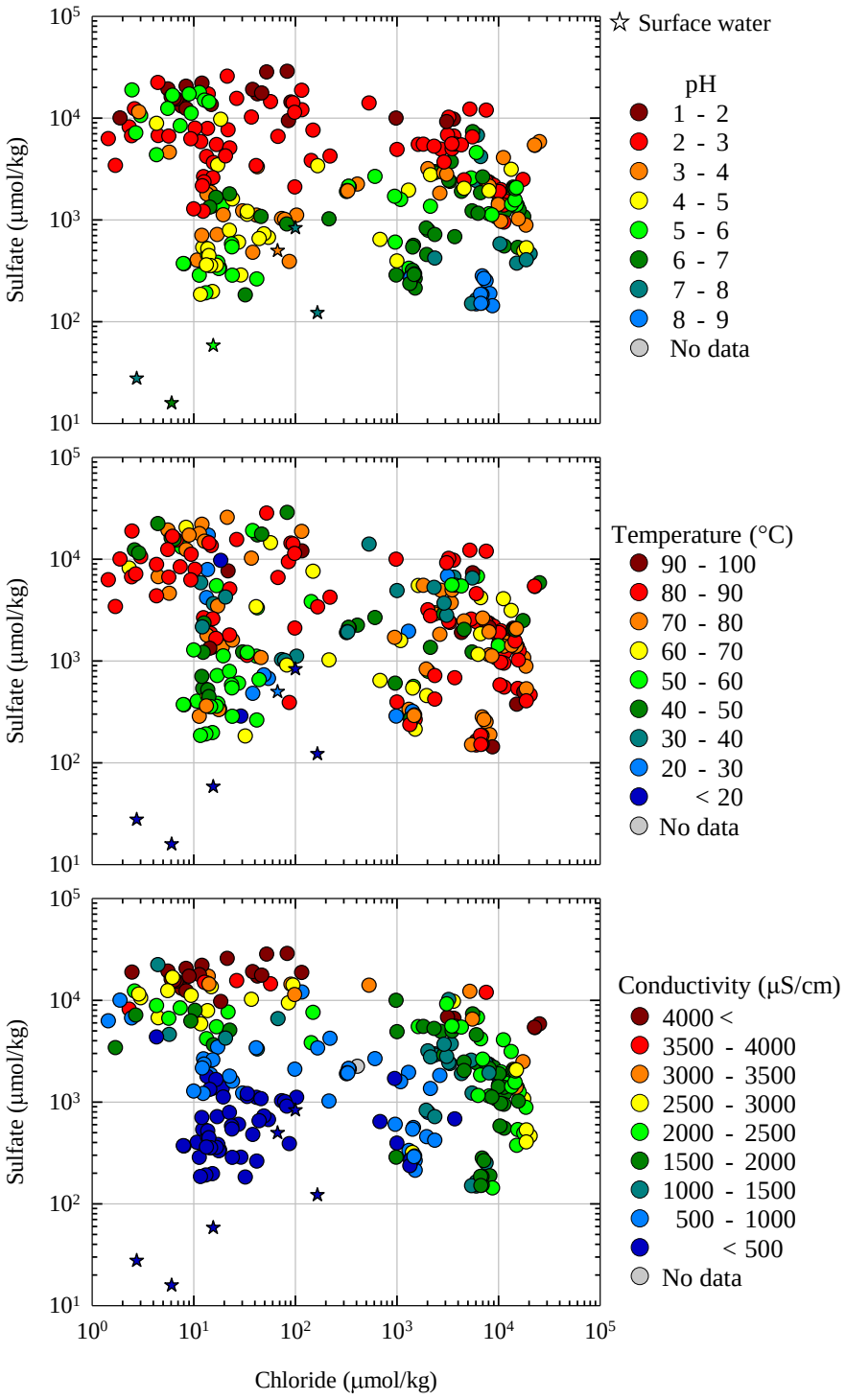

Figure 4.4: Field chemistry data (pH, temperature, and conductivity) data plotted in chloride and sulfate concentration space. Color scales are different for each parameter, but in general warmer colors correspond to higher values of temperature, conductivity, and aH^+

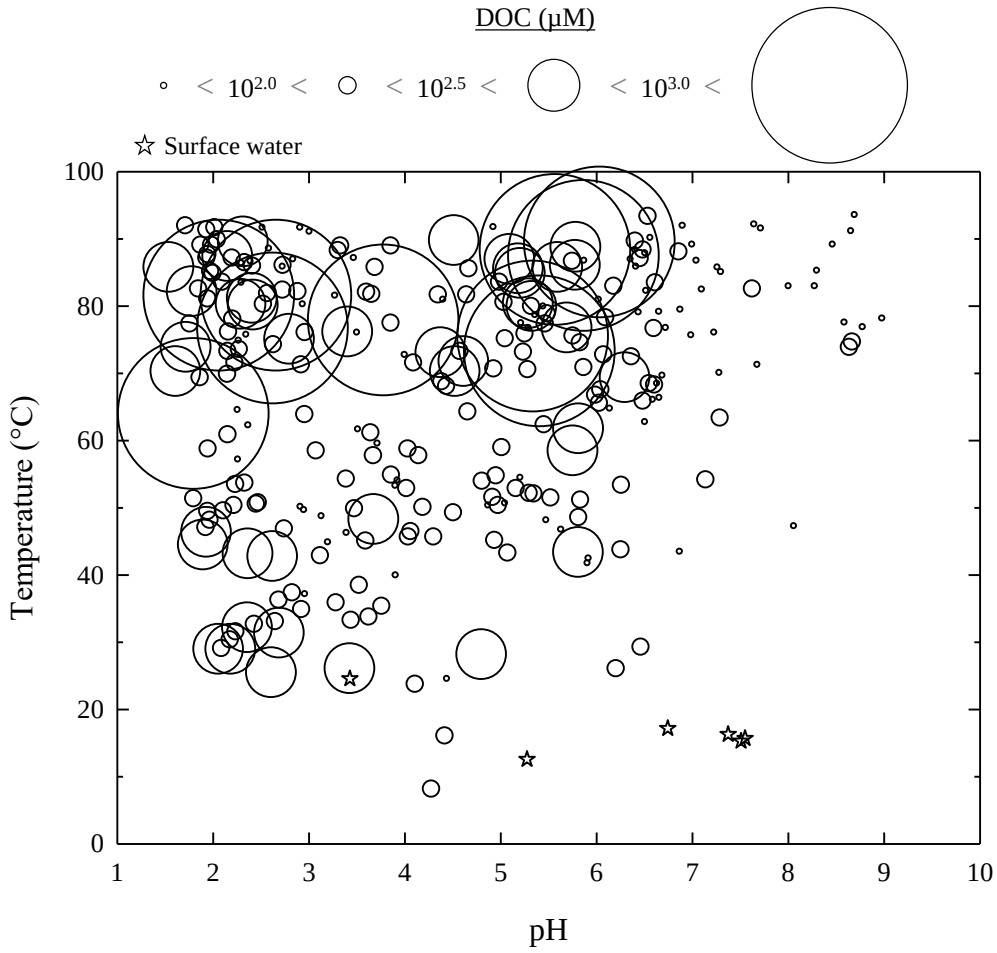

Figure 4.5: Dissolved organic carbon concentrations as a function of hot spring pH and temperature. (circles) Hot springs (n = 288) sampled between 2012 and 2018. (stars) Non-thermal surface water samples (n = 6; i.e. streams, ponds, lakes, etc.). DOC concentrations are represented by symbol size for both hot springs and surface waters.

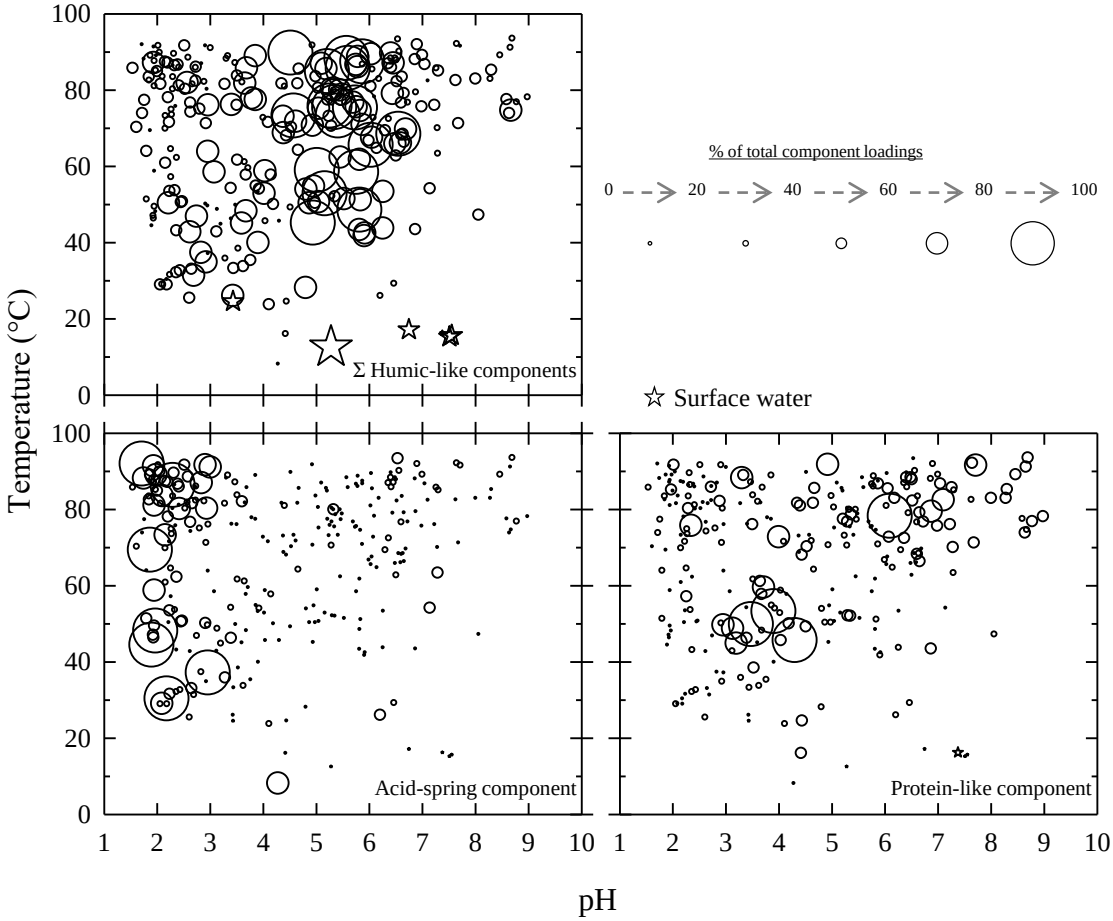

Figure 4.6: PARAFAC component loadings as a function of hot spring pH and temperature. (circles) Hot springs (n = 277) sampled between 2012 and 2018. (stars) Non-thermal surface water samples (n = 6; i.e. streams, ponds, lakes, etc.). PARAFAC components are presented as the relative fraction of total component loadings (symbol size) for both hot springs and surface waters.

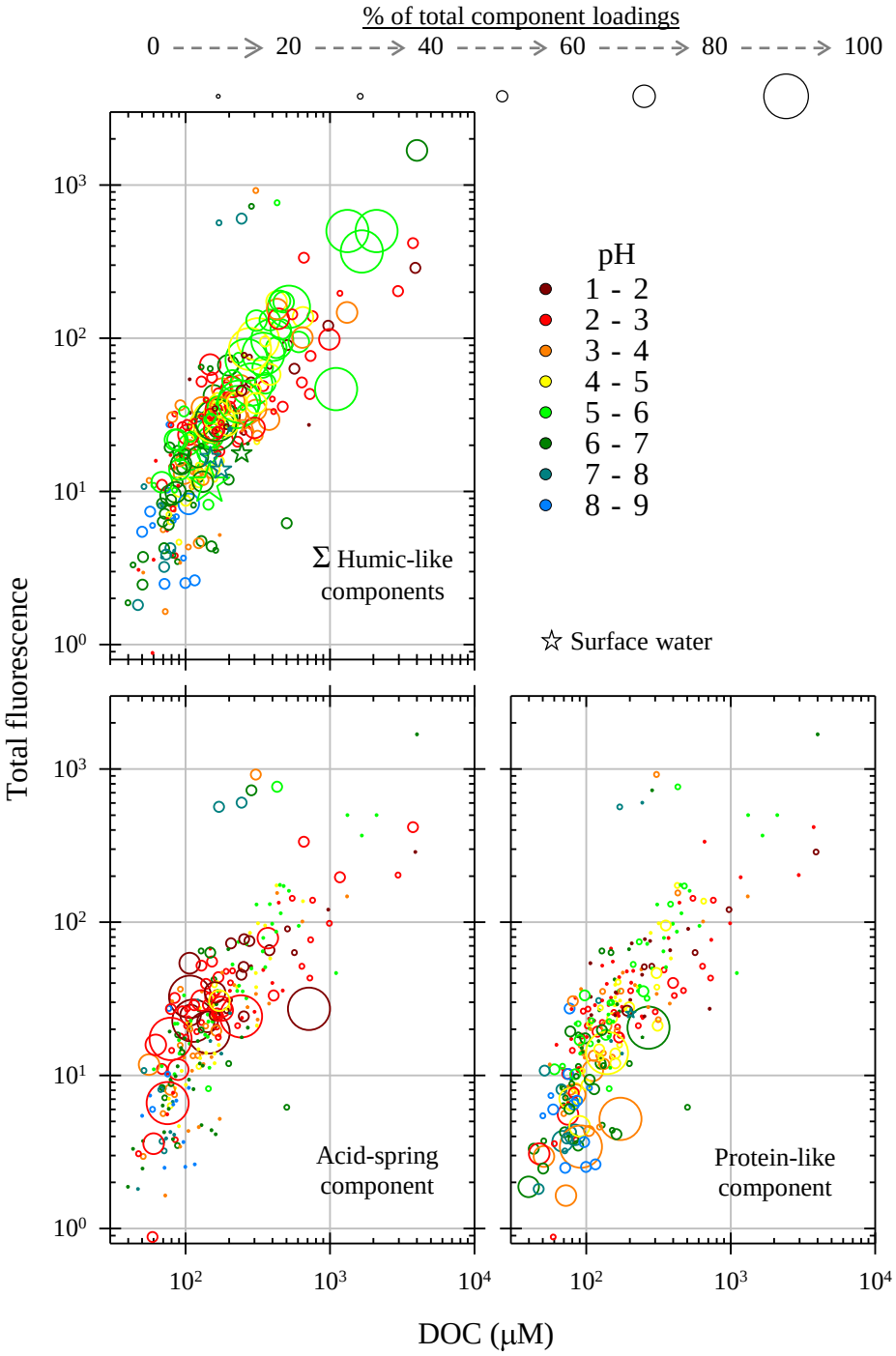

Figure 4.7: PARAFAC component loadings plotted in [DOC] and total fluorescence space. Total fluorescence is quantified as Raman-normalized intensity units. PARAFAC components are presented as the relative fraction of total component loadings (symbol size) for both hot springs and surface waters. The symbol color indicates hot spring pH.

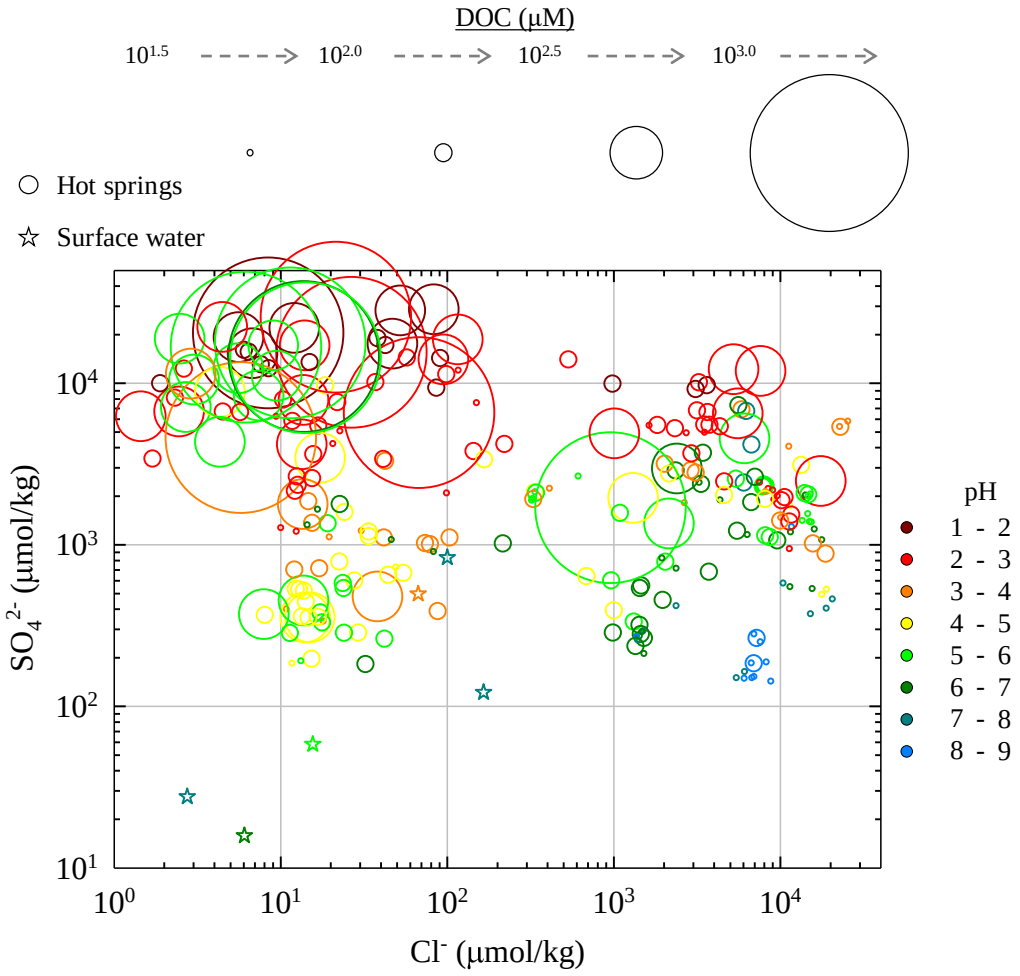

Figure 4.8: Dissolved organic carbon concentrations (circle size) plotted in hot spring chloride and sulfate concentration space. The symbol color indicates hot spring pH.

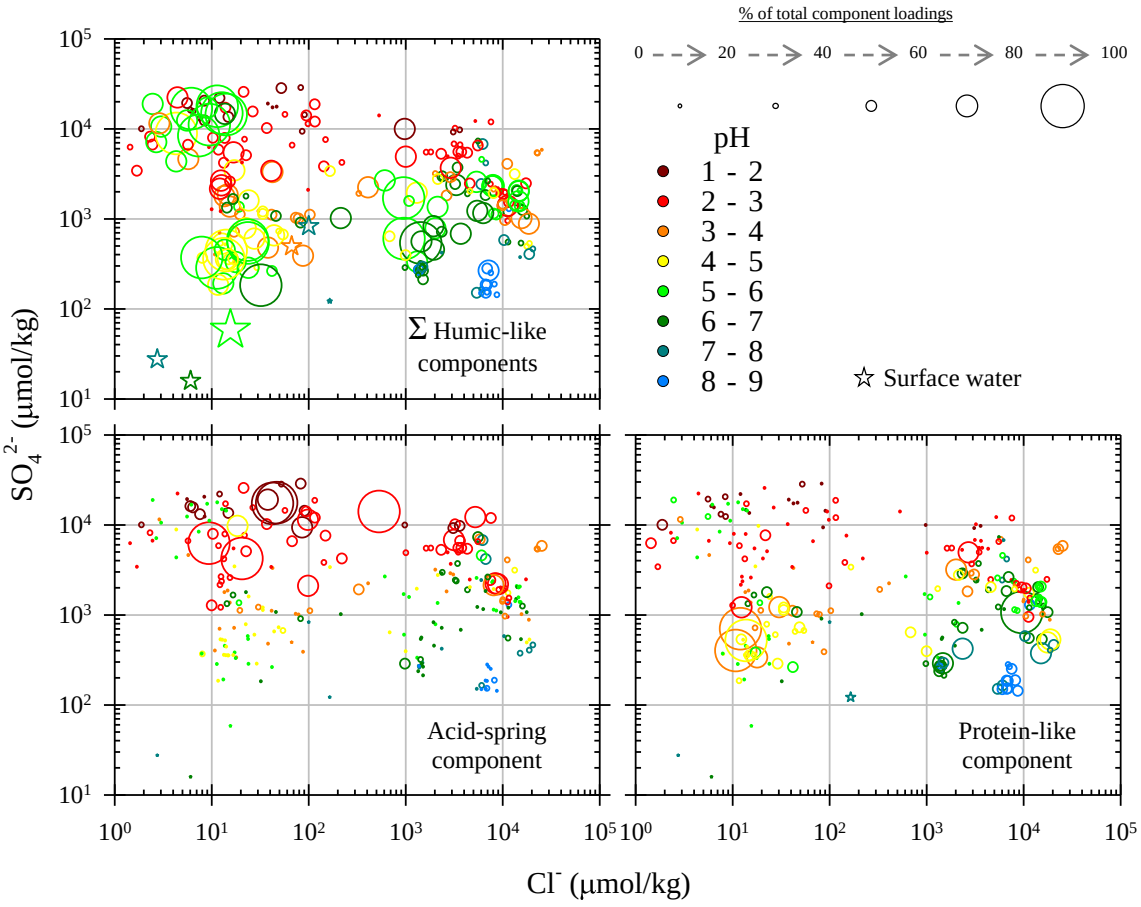

Figure 4.9: PARAFAC component loadings plotted in hot spring chloride and sulfate concentration space. PARAFAC components are presented as the relative fraction of the total component loadings (symbol size). The symbol color indicates hot spring pH.

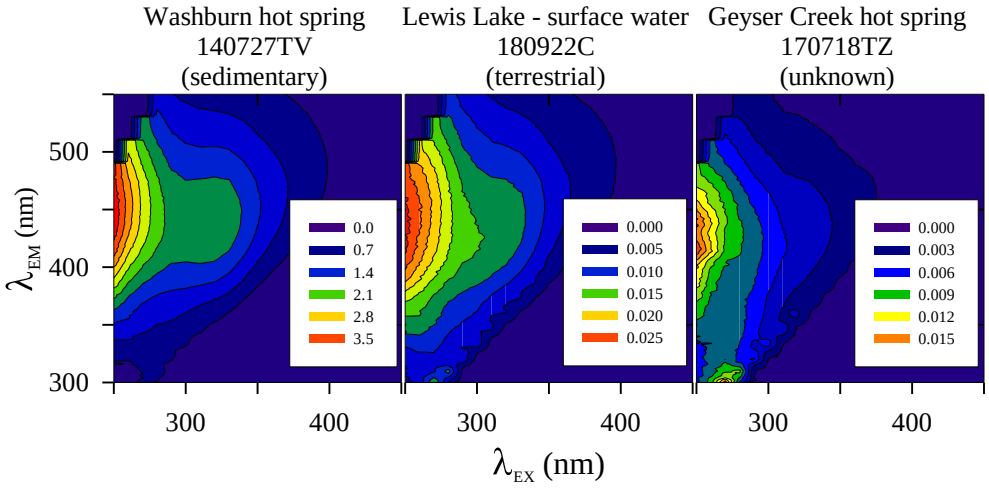

Figure 4.10: Representative examples of "humic-like" fluorescence in three springs from different organic sources. Color scales are fluorescence intensity and are different for each spring

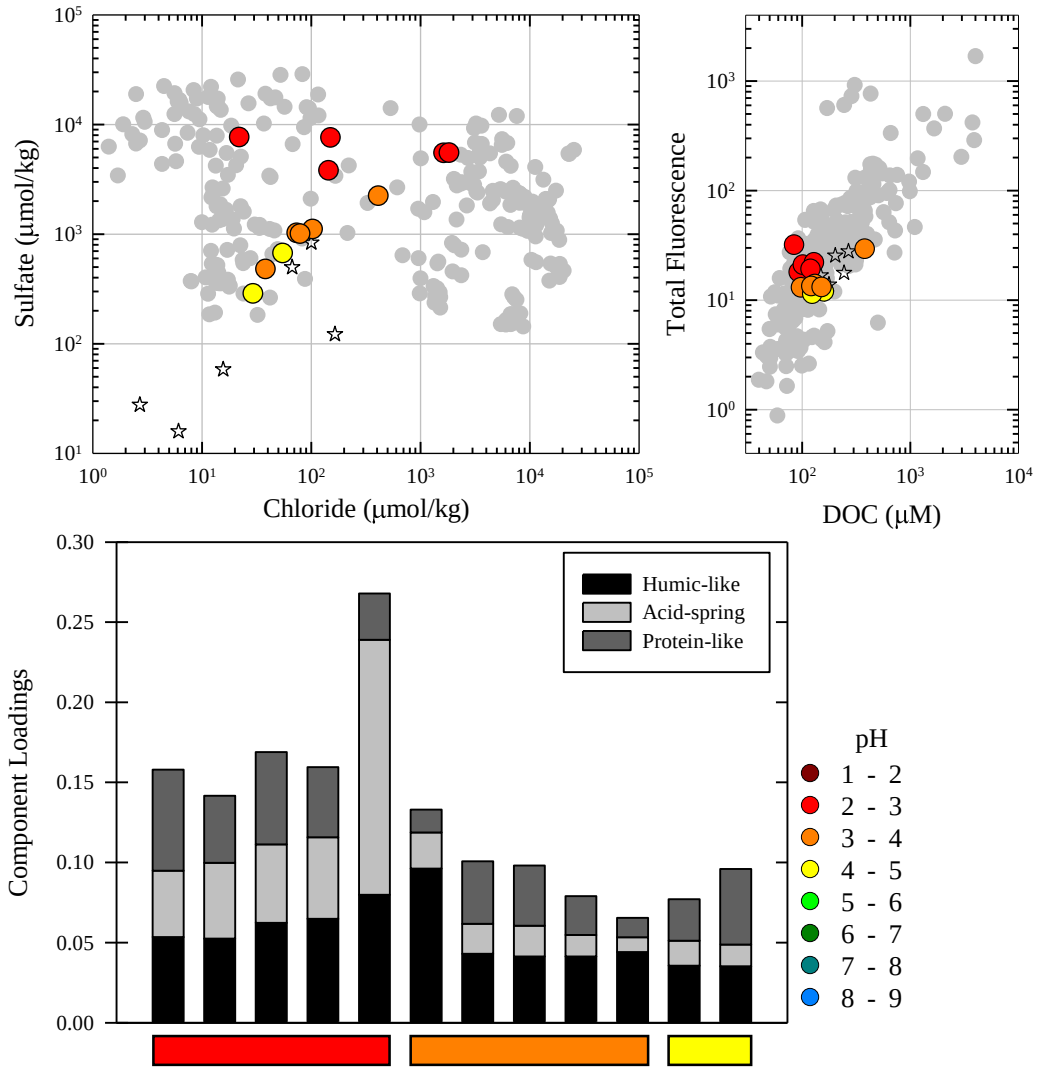

Figure 4.11: Amphitheater Springs hot spring chemistry. (top-left) Chloride and sulfate concentrations. (top-right) DOC concentrations and total fluorescence values. Colored circles represent hot springs from the Amphitheater Springs region. Gray circles represent samples from other regions in Yellowstone. Open stars indicate Yellowstone surface water samples. (bottom) PARAFAC model component loadings for Amphitheater Springs sites. The three humic-like model components were summed and presented as one humic-like component. Columns are arranged left to right from most acidic to most alkaline. The pH color scale applies to all sub-plots.

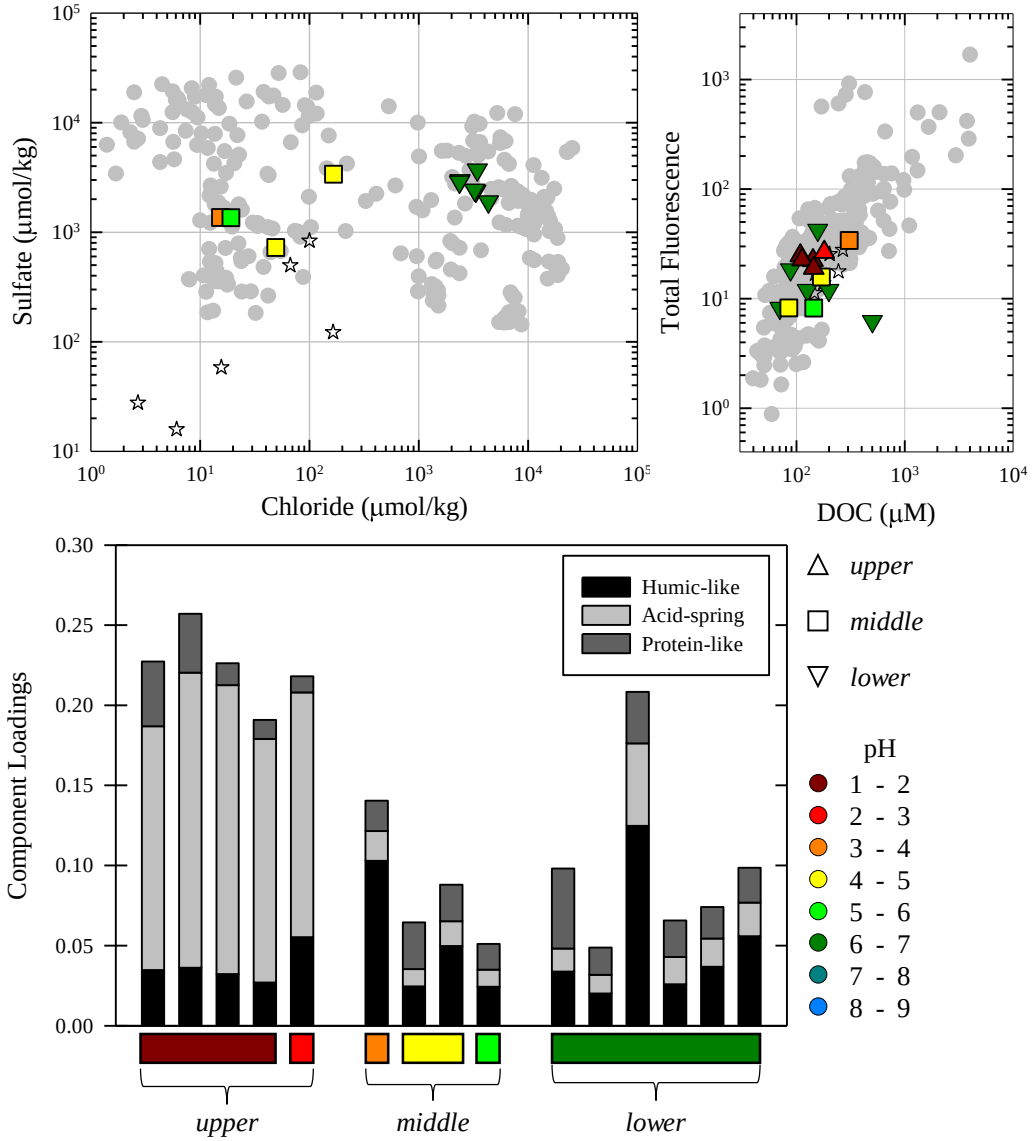

Figure 4.12: Bog Creek hot spring chemistry. (top-left) Chloride and sulfate concentrations. (top-right) DOC concentrations and total fluorescence values. Colored circles represent hot springs from the Bog Creek region. Gray circles represent samples from other regions in Yellowstone. Open stars indicate Yellowstone surface water samples. There are three sub-regions within Bog Creek. 'upper', 'middle' and 'lower', and they are identified by upward triangle, square, and downward triangle symbols, respectively. There is no chloride and sulfate data for upper Bog Creek samples. (bottom) PARAFAC model component loadings for Bog Creek sites. The three humic-like model components were summed and presented as one humic-like component. The sub-regions of Bog Creek are separated into clustered columns. Within each cluster, columns are arranged left to right from most acidic to most alkaline. The pH color scale applies to all sub-plots.

Figure 4.13: Photo of an acidic stream in Bog Creek, flowing over a bed of silica. (Photo credit: J. Nye).

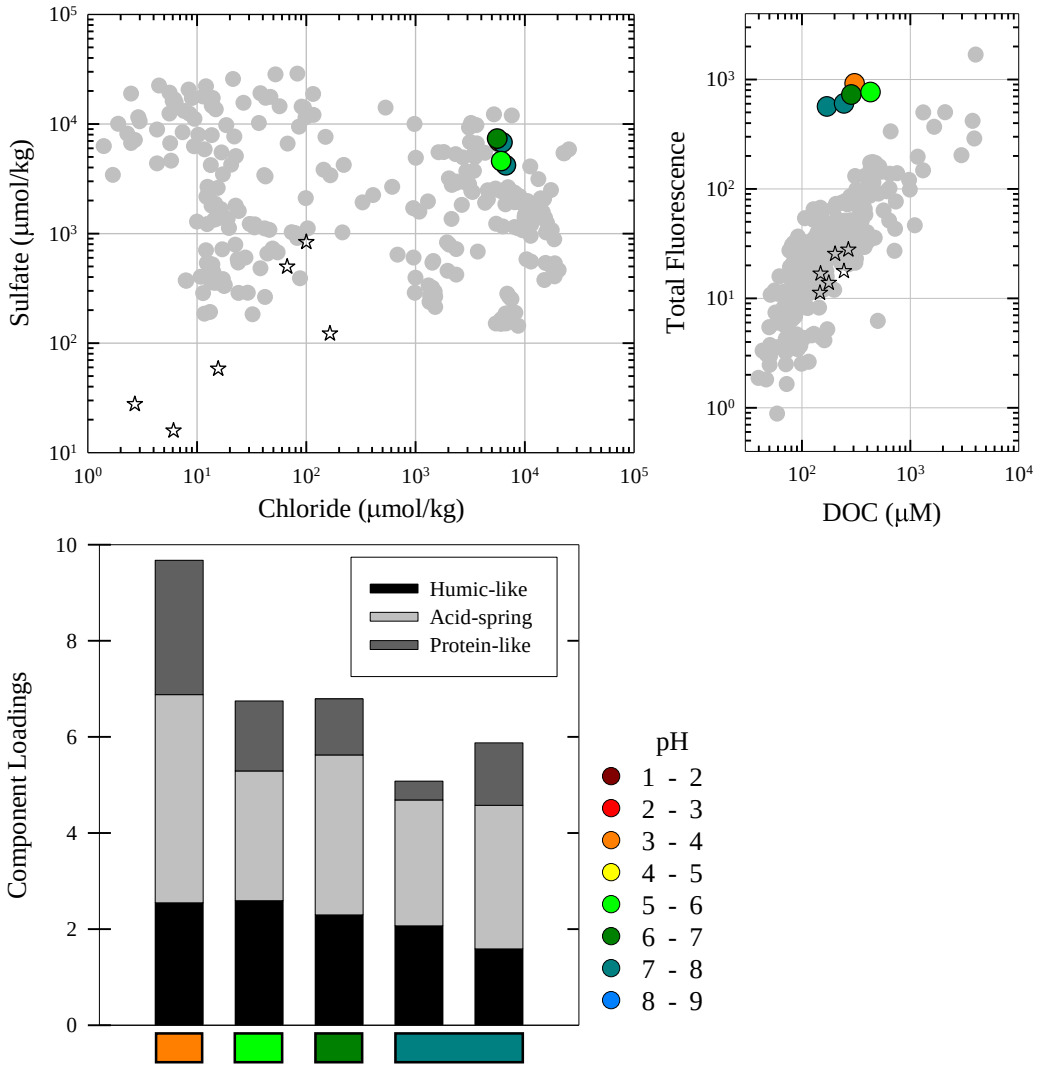

Figure 4.14: Calcite Springs hot spring chemistry. (top-left) Chloride and sulfate concentrations. (top-right) DOC concentrations and total fluorescence values. Colored circles represent hot springs from the Calcite Springs region. Gray circles represent samples from other regions in Yellowstone. Open stars indicate Yellowstone surface water samples. (bottom) PARAFAC model component loadings for Calcite Springs sites. The three humic-like model components were summed and presented as one humic-like component. Columns are arranged left to right from most acidic to most alkaline. The pH color scale applies to all sub-plots.

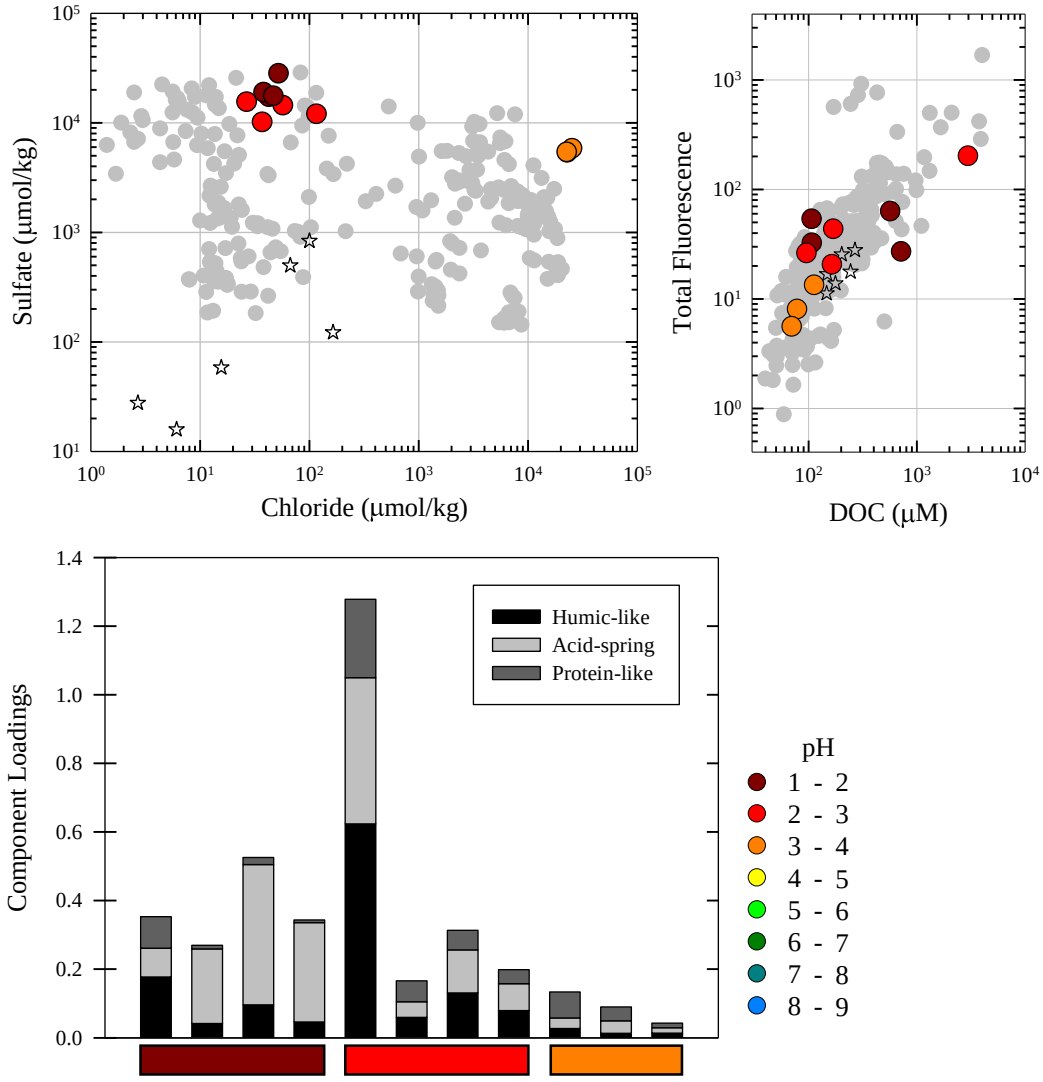

Figure 4.15: Crater Hills hot spring chemistry. (top-left) Chloride and sulfate concentrations. (top-right) DOC concentrations and total fluorescence values. Colored circles represent hot springs from the Crater Hills region. Gray circles represent samples from other regions in Yellowstone. Open stars indicate Yellowstone surface water samples. (bottom) PARAFAC model component loadings for Crater Hills sites. The three humic-like model components were summed and presented as one humic-like component. Columns are arranged left to right from most acidic to most alkaline. The pH color scale applies to all sub-plots.

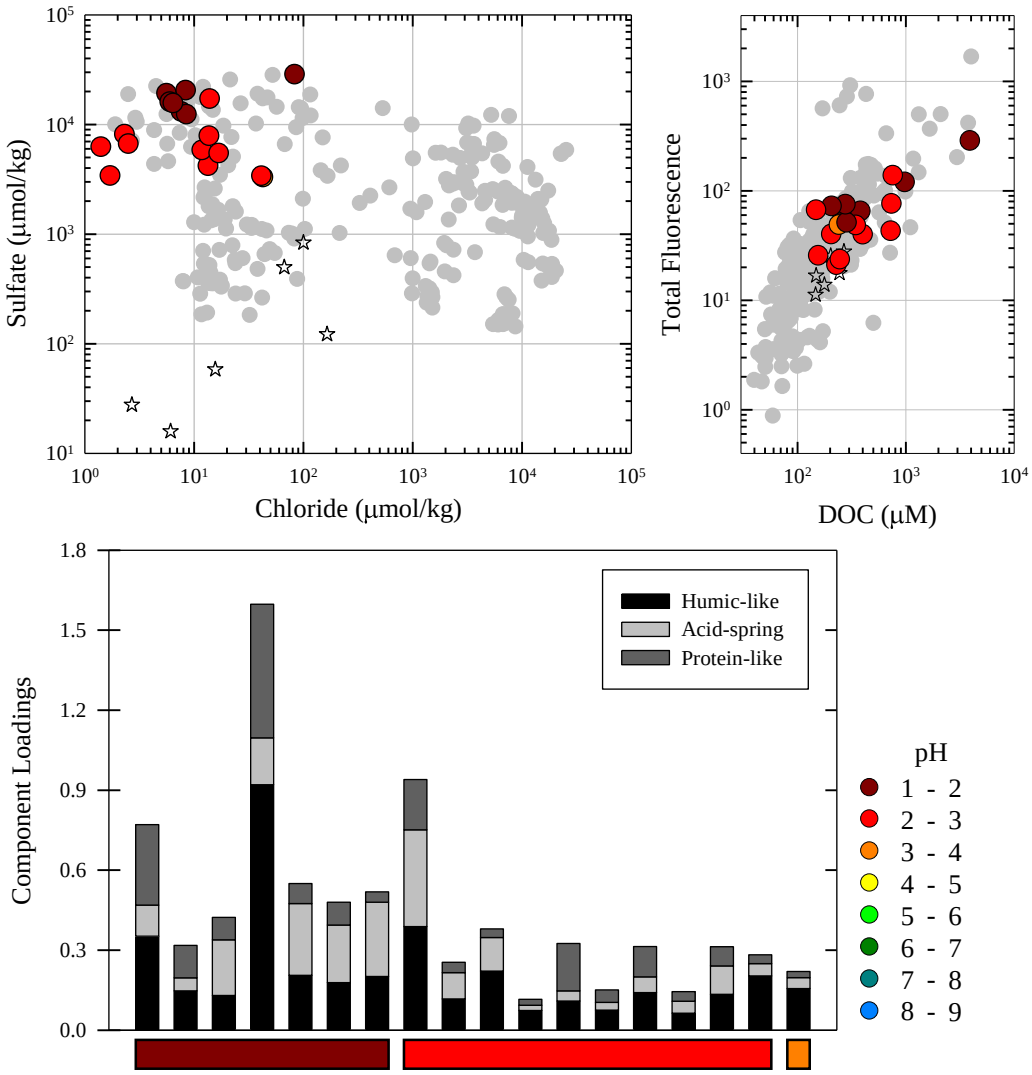

Figure 4.16: Forest Springs hot spring chemistry. (top-left) Chloride and sulfate concentrations. (top-right) DOC concentrations and total fluorescence values. Colored circles represent hot springs from the Forest Springs region. Gray circles represent samples from other regions in Yellowstone. Open stars indicate Yellowstone surface water samples. (bottom) PARAFAC model component compositions loadings for Forest Springs sites. The three humic-like model components were summed and presented as one humic-like component. Columns are arranged left to right from most acidic to most alkaline. The pH color scale applies to all sub-plots.

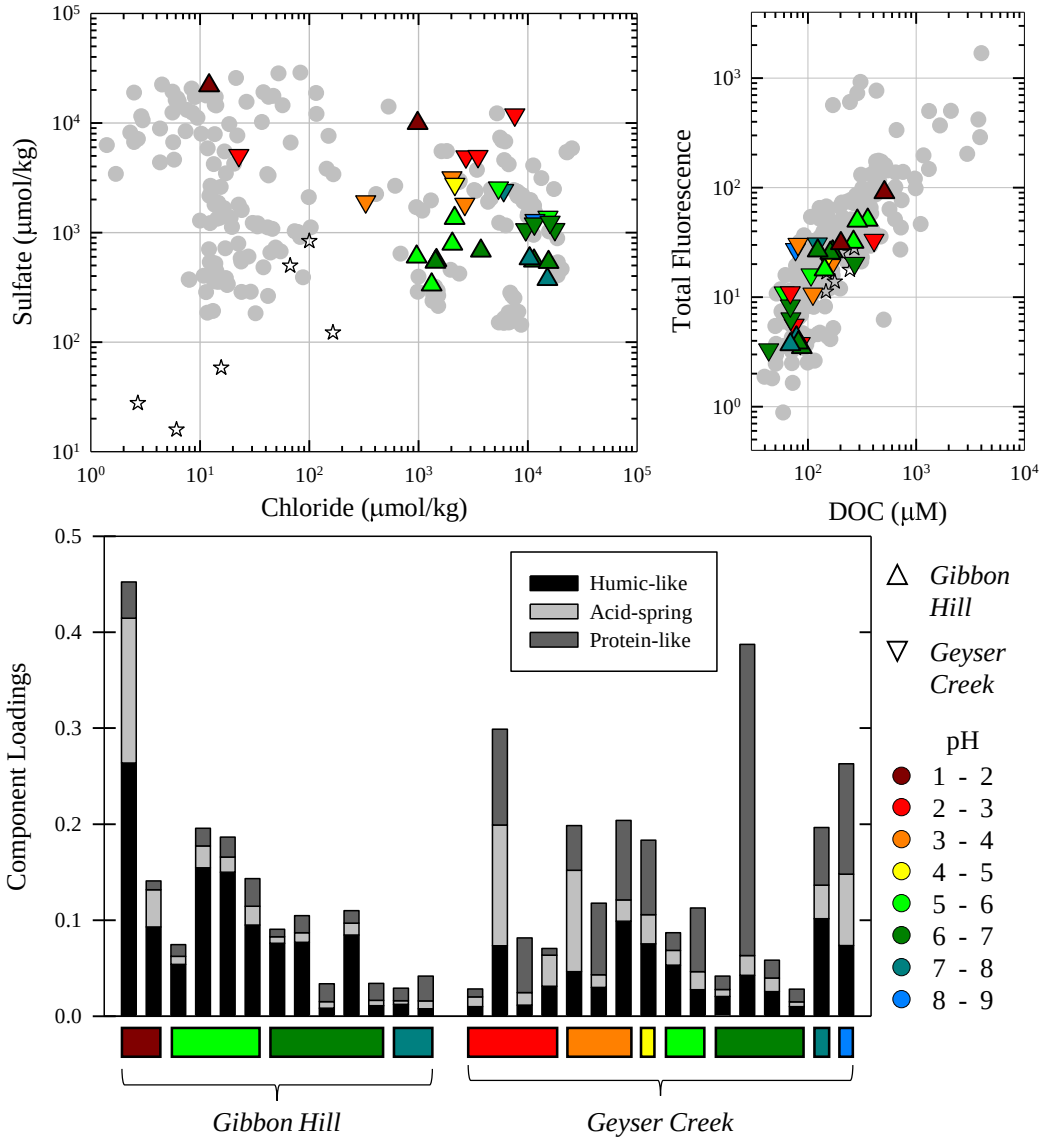

Figure 4.17: Gibbon Geyser Basin hot spring chemistry. (top-left) Chloride and sulfate concentrations. (top-right) DOC concentrations and total fluorescence values. Colored circles represent hot springs from the Gibbon Geyser Basin. Gray circles represent samples from other regions in Yellowstone. Open stars indicate Yellowstone surface water samples. There are two sub-regions within Gibbon Geyser Basin, 'Gibbon Hill' and 'Geyser Creek', identified by upward triangle and downward triangle symbols, respectively. (bottom) PARAFAC model component compositions loadings for Gibbon Geyser Basin sites. The three humic-like model components were summed and presented as one humic-like component. Each sub-region of Gibbon Geyser Basin is separated into clustered columns. Within each cluster, columns are arranged left to right from most acidic to most alkaline. The pH color scale applies to all sub-plots.

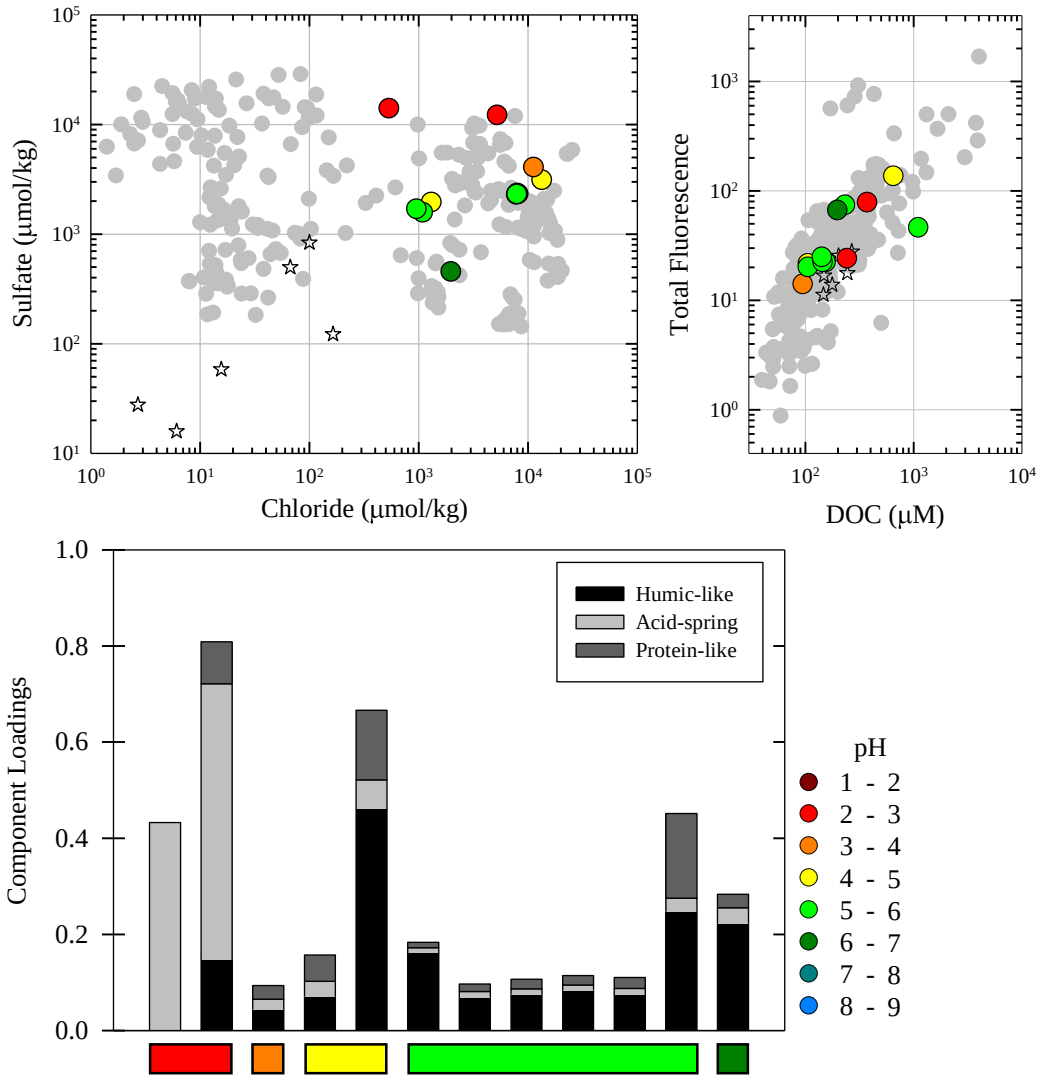

Figure 4.18: Greater Obsidian Pool Area (GOPA) hot spring chemistry. (top-left) Chloride and sulfate concentrations. (top-right) DOC concentrations and total fluorescence values. Colored circles represent hot springs from the GOPA region. Gray circles represent samples from other regions in Yellowstone. Open stars indicate Yellowstone surface water samples. (bottom) PARAFAC model component loadings for Greater Obsidian Pool Area sites. The three humic-like model components were summed and presented as one humic-like component. Columns are arranged left to right from most acidic to most alkaline. The pH color scale applies to all sub-plots.

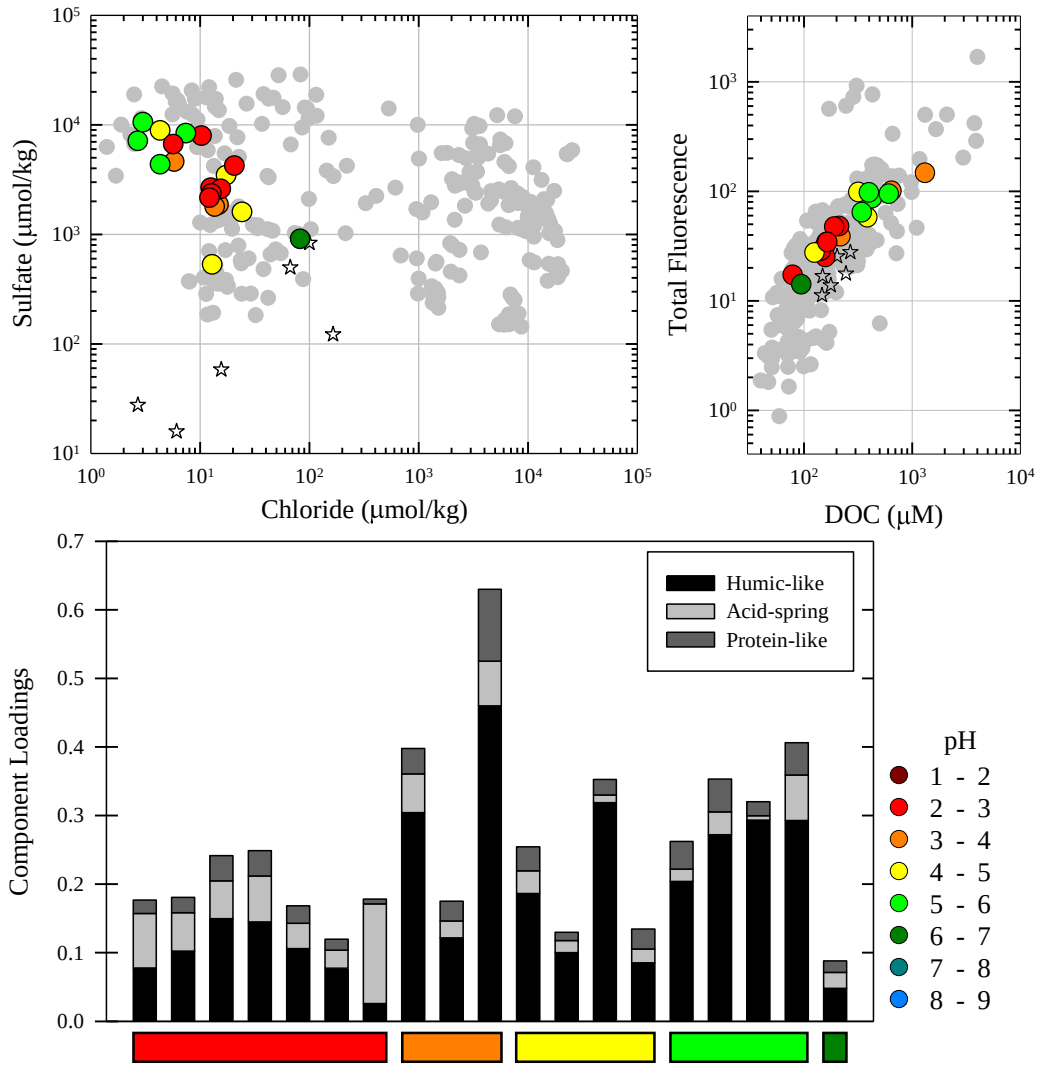

Figure 4.19: Hot Springs Basin hot spring chemistry. (top-left) Chloride and sulfate concentrations. (top-right) DOC concentrations and total fluorescence values. Colored circles represent hot springs from Hot Springs Basin. Gray circles represent samples from other regions in Yellowstone. Open stars indicate Yellowstone surface water samples. (bottom) PARAFAC model component loadings for Hot Springs Basin sites. The three humic-like model components were summed and presented as one humic-like component. Columns are arranged left to right from most acidic to most alkaline. The pH color scale applies to all sub-plots.

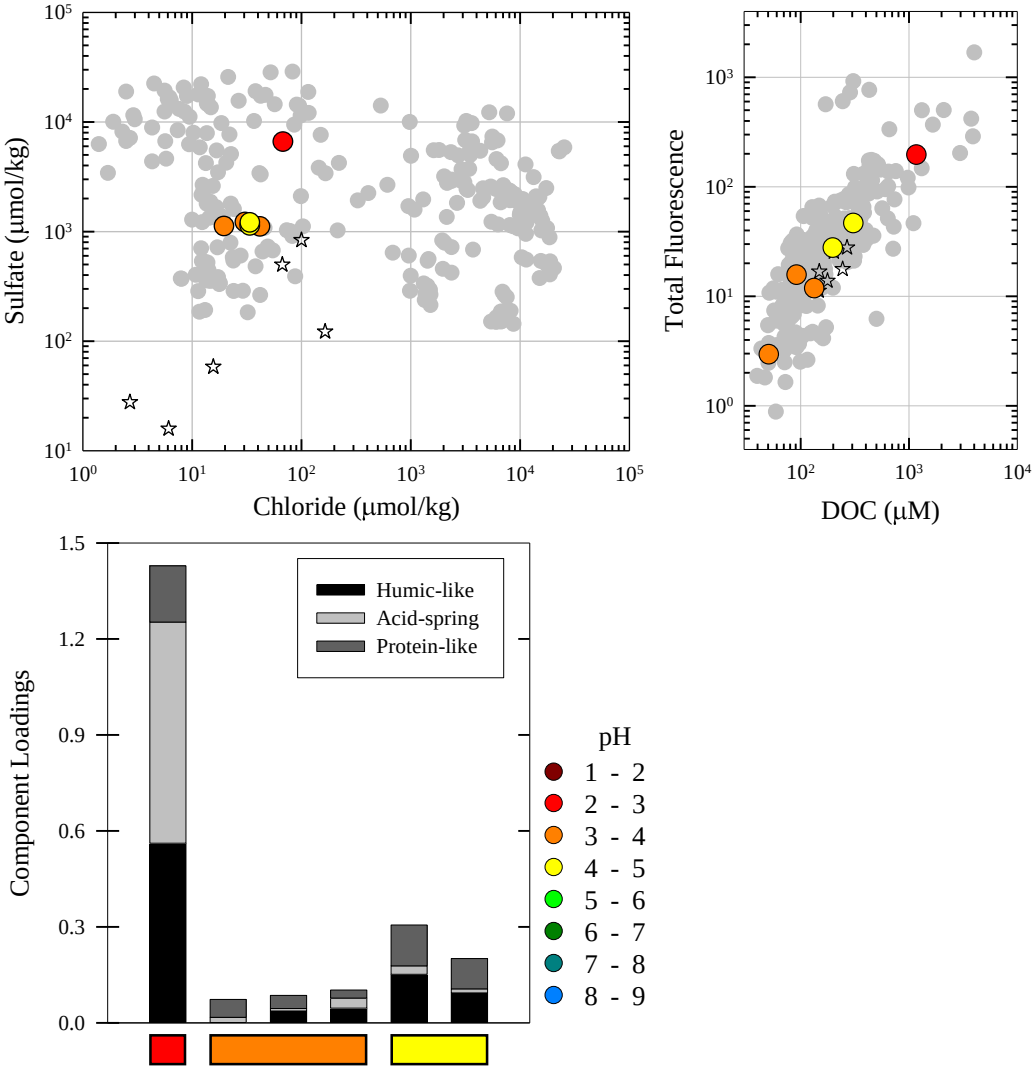

Figure 4.20: Imperial/Spray Geyser Basins hot spring chemistry. (top-left) Chloride and sulfate concentrations. (top-right) DOC concentrations and total fluorescence values. Colored circles represent hot springs from the Imperial/Spray Geyser Basins. Gray circles represent samples from other regions in Yellowstone. Open stars indicate Yellowstone surface water samples. (bottom) PARAFAC model component loadings for Imperial Geyser Basin and Spray Geyser Basin sites. The three humic-like model components were summed and presented as one humic-like component. Columns are arranged left to right from most acidic to most alkaline. The pH color scale applies to all sub-plots.

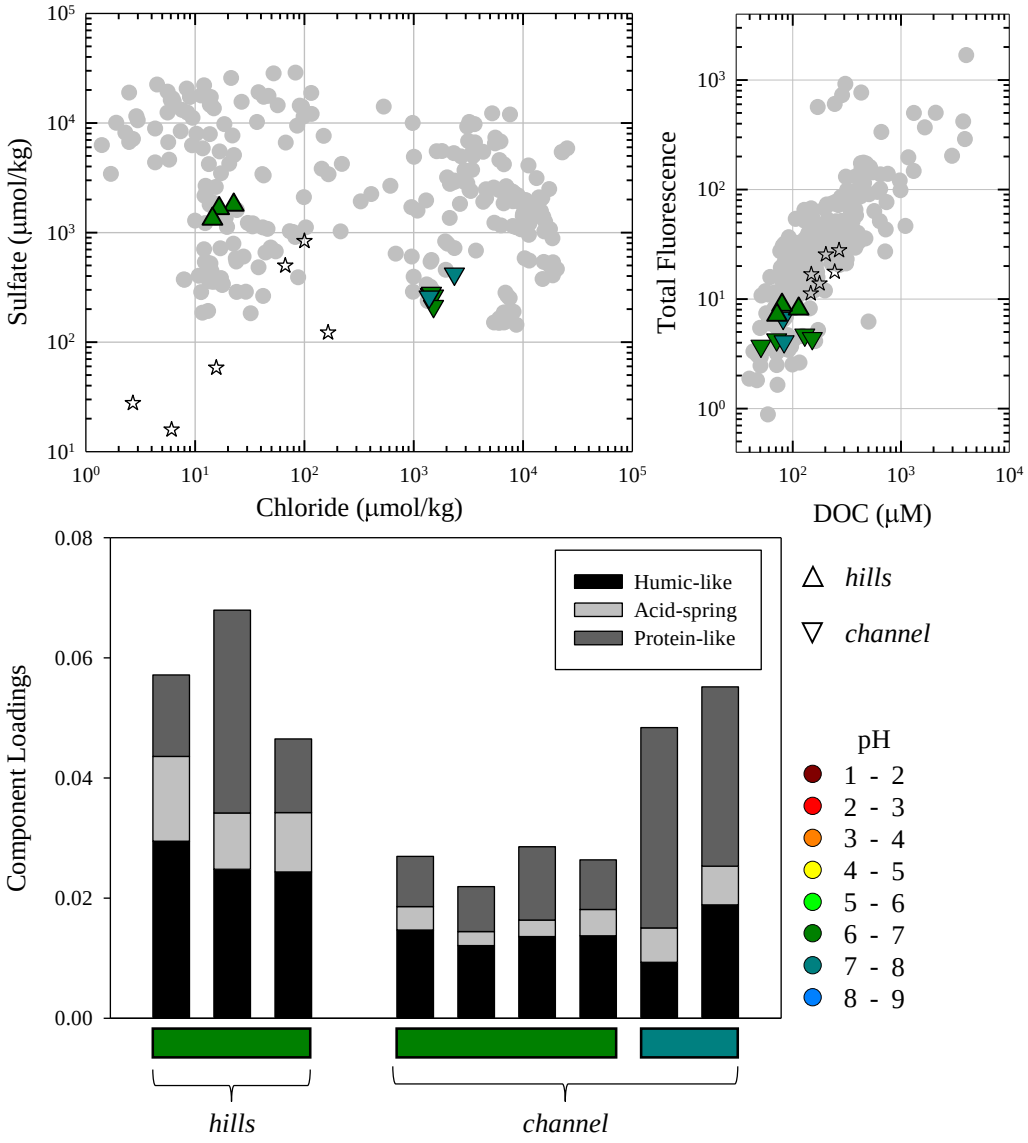

Figure 4.21: Lewis Lake hot spring chemistry. (top-left) Chloride and sulfate concentrations. (top-right) DOC concentrations and total fluorescence values. Colored circles represent hot springs from the Lewis Lake region. Gray circles represent samples from other regions in Yellowstone. Open stars indicate Yellowstone surface water samples. There are two sub-regions within Lewis Lake, 'hills' and 'channel', identified by upward triangle and downward triangle symbols, respectively. (bottom) PARAFAC model component loadings for Lewis Lake sites. The three humic-like model components were summed and presented as one humic-like component. Each sub-region of Lewis Lake is separated into clustered columns. Within each cluster, columns are arranged left to right from most acidic to most alkaline. The pH color scale applies to all sub-plots.

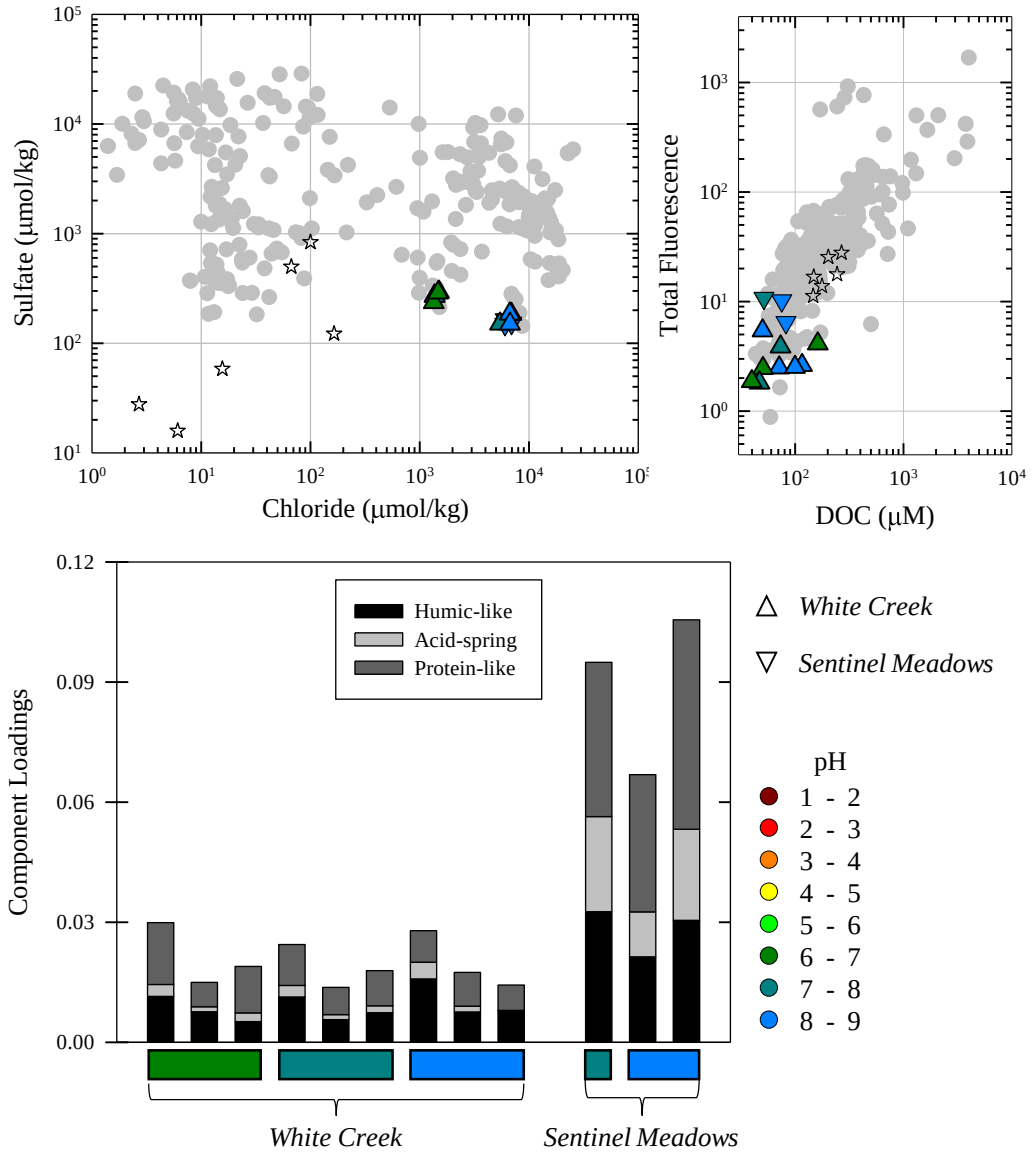

Figure 4.22: Lower Geyser Basins hot spring chemistry. (top-left) Chloride and sulfate concentrations. (top-right) DOC concentrations and total fluorescence values. Colored circles represent hot springs from the Lower Geyser Basin. Gray circles represent samples from other regions in Yellowstone. Open stars indicate Yellowstone surface water samples. There are two sub-regions within the Lower Geyser Basin, 'White Creek' and 'Sentinel Meadow', identified by upward triangle and downward triangle symbols, respectively. (bottom) PARAFAC model component loadings for Lower Geyser Basin sites. The three humic-like model components were summed and presented as one humic-like component. Each sub-region of the Lower Geyser Basin is separated into clustered columns. Within each cluster, columns are arranged left to right from most acidic to most alkaline. The pH color scale applies to all sub-plots.

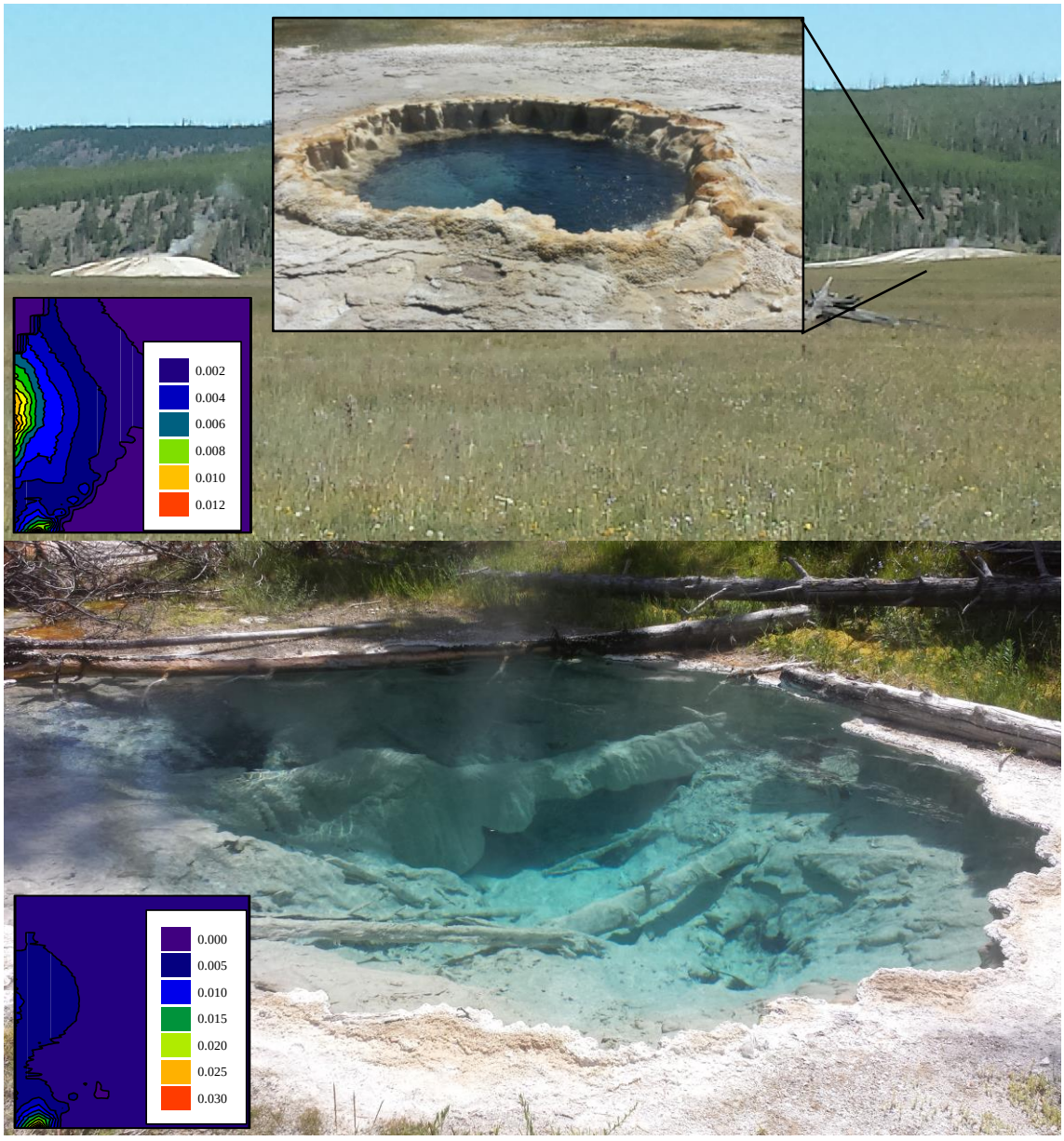

Figure 4.23: Photographs of springs from Lower Geyser Basin spring photos and accompanying EEMs. EEM color scales are fluorescence intensity and are different for each spring. (top) Photo and EEM (sample 160715I) of Flat Cone in Sentinel Meadow. The silica mound stands ∼3 meters above the floor of the meadow. Inset photo shows a closeup of the spring. (bottom) Photo and EEM (sample 160716O) of a spring in White Creek. Evidence of silica deposition is shown by the preserved logs that have fallen into the spring. (Photo credits: J. Nye).

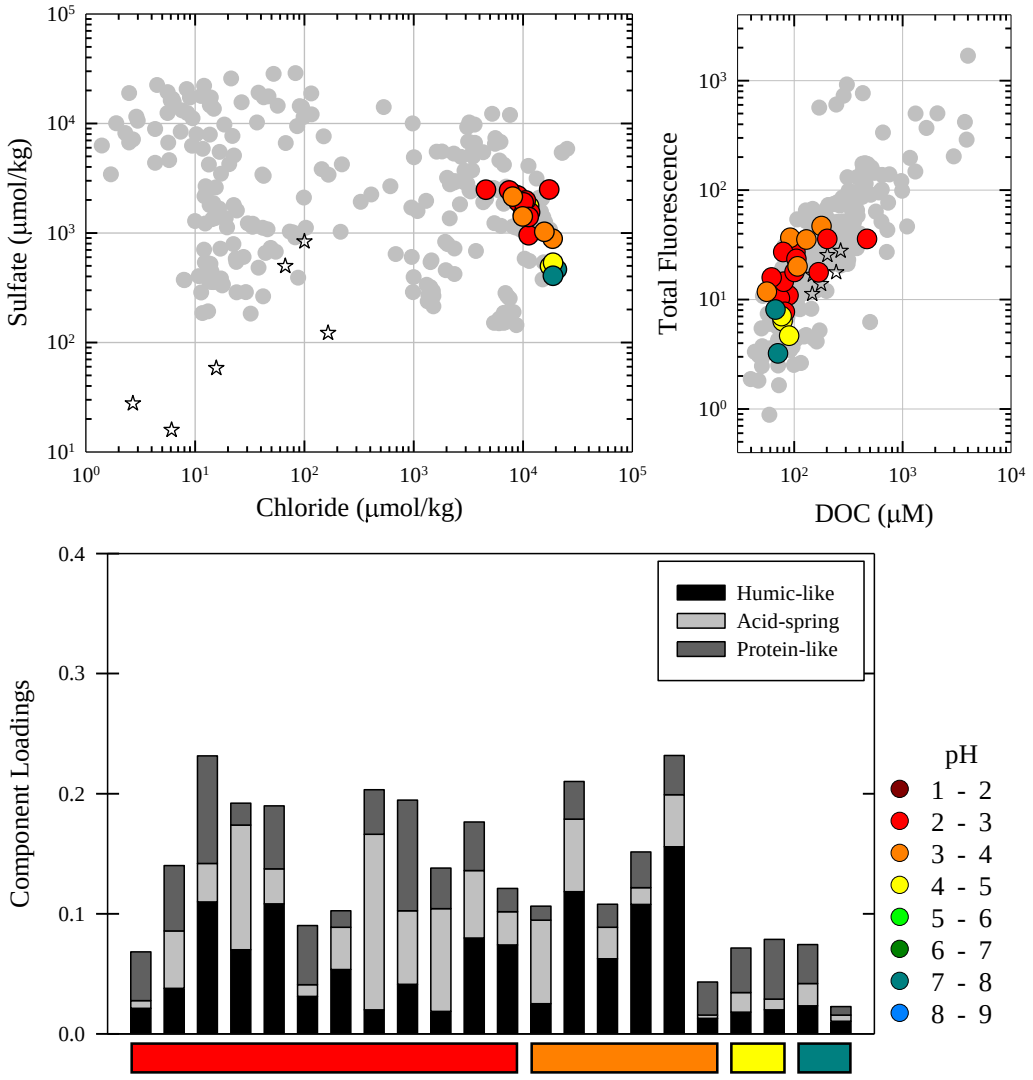

Figure 4.24: Norris Geyser Basin hot spring chemistry. (top-left) Chloride and sulfate concentrations. (top-right) DOC concentrations and total fluorescence values. Colored circles represent hot springs from the Norris Geyser Basin. Gray circles represent samples from other regions in Yellowstone. Open stars indicate Yellowstone surface water samples. (bottom) PARAFAC model component loadings for Norris Geyser Basin sites. The three humic-like model components were summed and presented as one humic-like component. Columns are arranged left to right from most acidic to most alkaline. The pH color scale applies to all sub-plots.

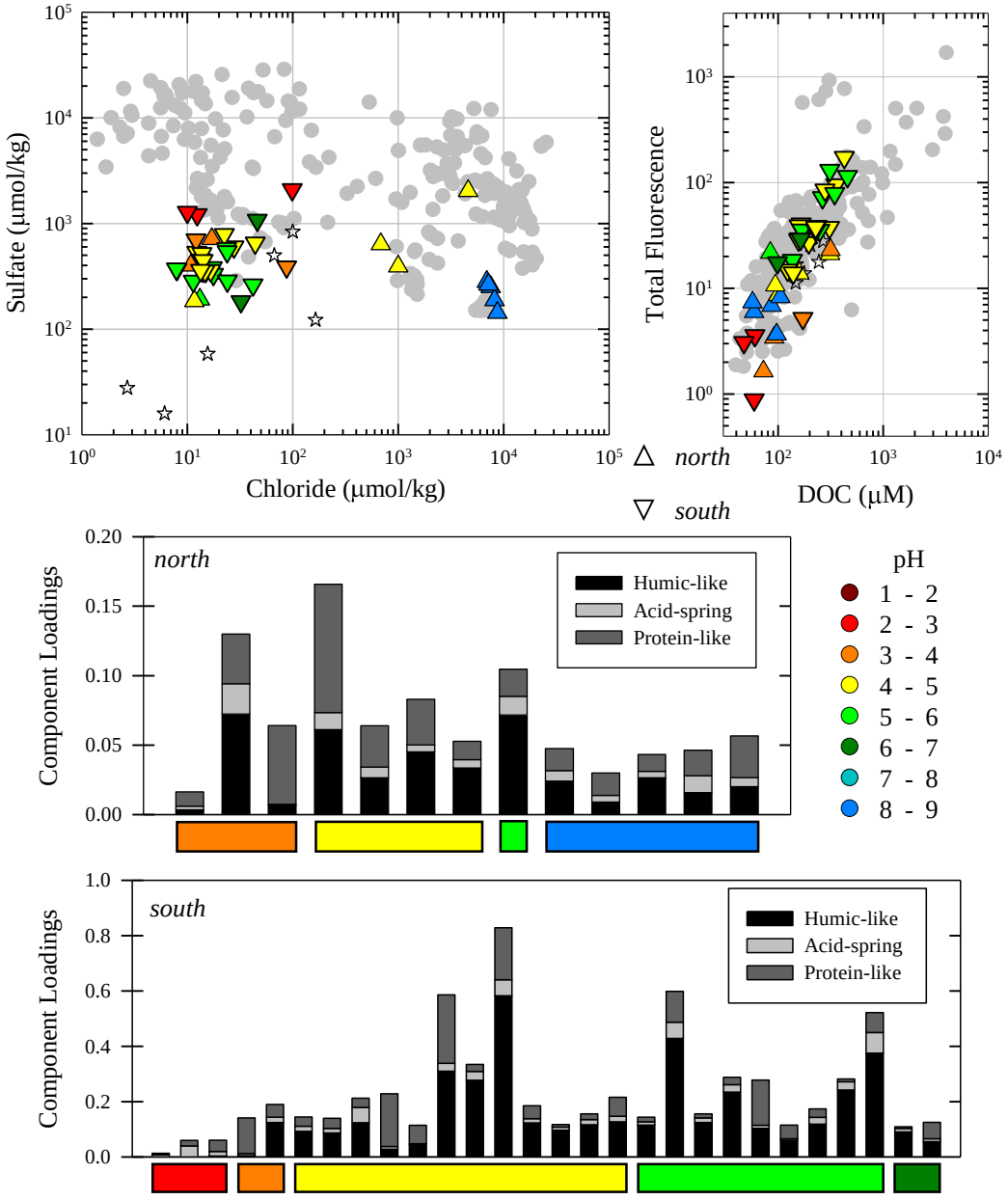

Figure 4.25: Rabbit Creek hot spring data. (top-left) Chloride and sulfate concentrations. (top-right) DOC concentrations and total fluorescence values. Colored circles represent hot springs from the Rabbit Creek region. Gray circles represent samples from other regions in Yellowstone. Open stars indicate Yellowstone surface water samples. There are two sub-regions within Rabbit Creek, 'north' and 'south', identified by upward triangle and downward triangle symbols, respectively. (bottom) PARAFAC model component loadings for Rabbit Creek sites. The three humic-like model components were summed and presented as one humic-like component. Each sub-region of Rabbit Creek is separated into clustered columns. Within each cluster, columns are arranged left to right from most acidic to most alkaline. The pH color scale applies to all sub-plots.

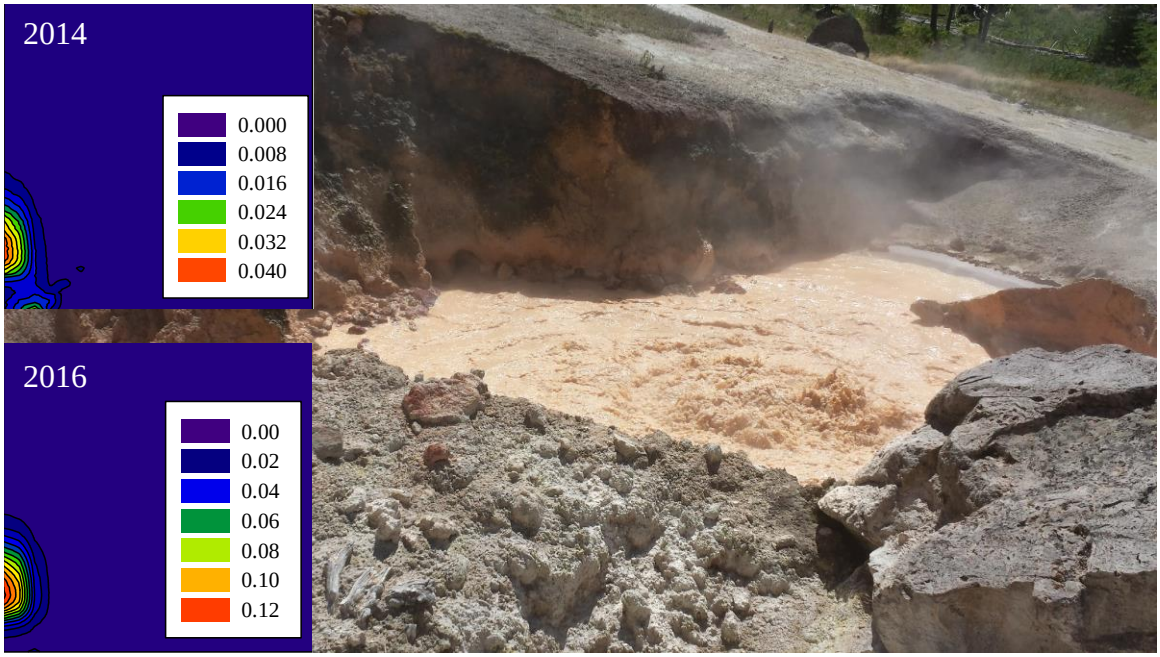

Figure 4.26: Rabbit Creek spring photo and EEM. This large, violently discharging spring first appeared in the Rabbit Creek 'south' area in 2014. EEM color scales are fluorescence intensity and are different for each spring. While the spring has the appearance of a muddy, surface-influenced spring, the EEMs demonstrate the dominance of the acid-spring component and a lack of any humic-like components. The acid-spring component increased in intensity from 2014 (sample code - 140730TK) to 2016 (sample code - 160725M). (Photo credit: J. Nye).

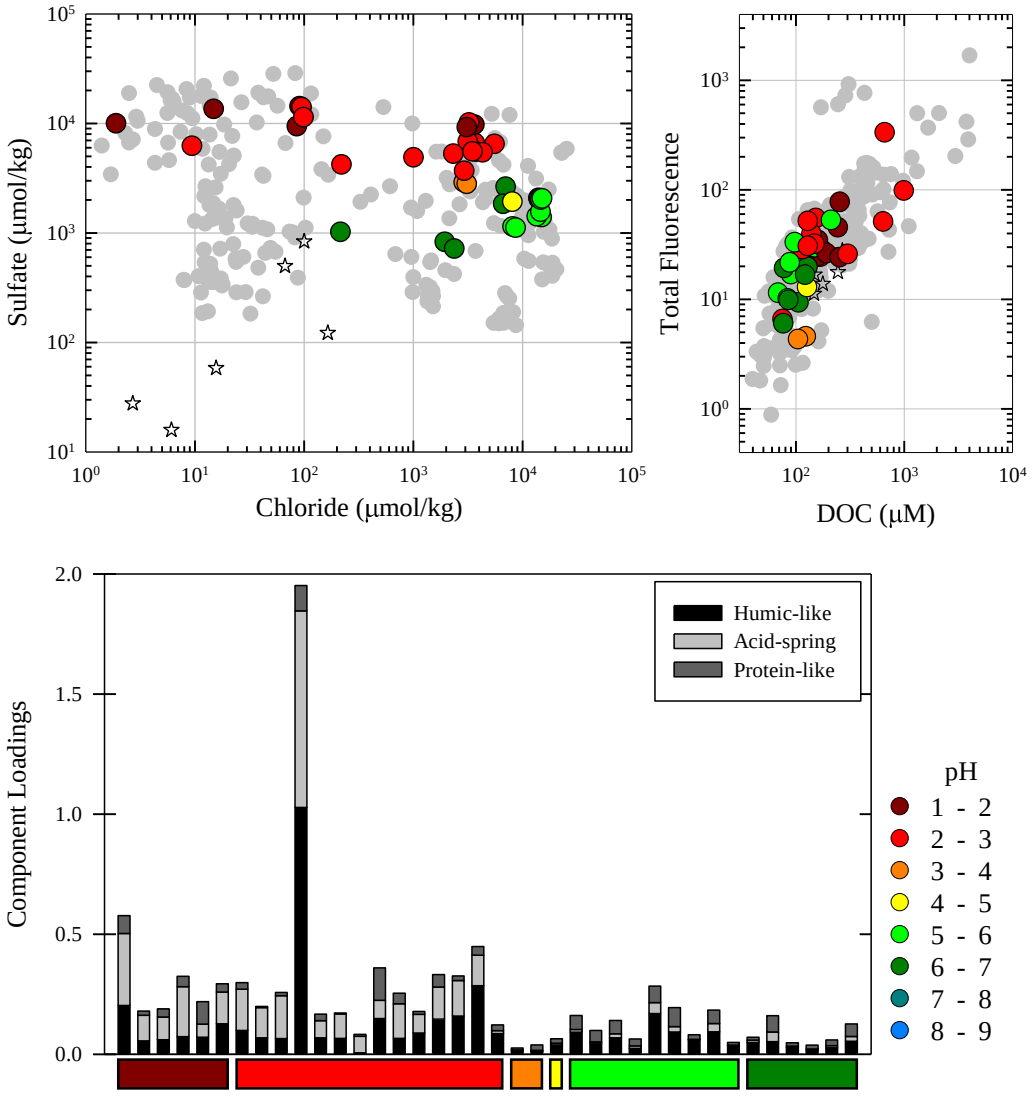

Figure 4.27: Sylvan Springs hot spring chemistry. (top-left) Chloride and sulfate concentrations. (top-right) DOC concentrations and total fluorescence values. Colored circles represent hot springs from the Sylvan Springs region. Gray circles represent samples from other regions in Yellowstone. Open stars indicate Yellowstone surface water samples. (bottom) PARAFAC model component loadings for Sylvan Springs sites. The three humic-like model components were summed and presented as one humic-like component. Columns are arranged left to right from most acidic to most alkaline. The pH color scale applies to all sub-plots.

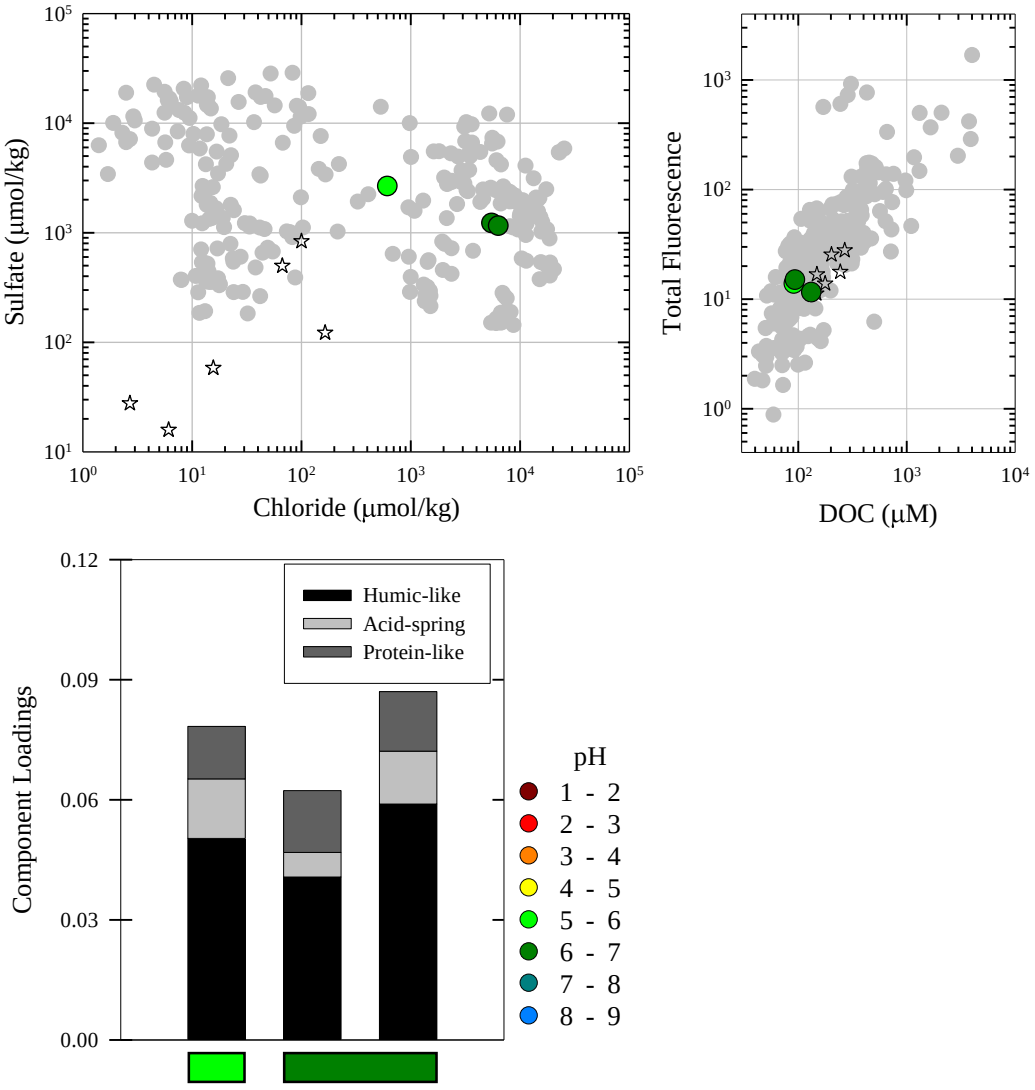

Figure 4.28: Turbid Lake hot spring chemistry. (top-left) Chloride and sulfate concentrations. (top-right) DOC concentrations and total fluorescence values. Colored circles represent hot springs from the Turbid Lake region. Gray circles represent samples from other regions in Yellowstone. Open stars indicate Yellowstone surface water samples. (bottom) PARAFAC model component loadings for Turbid Lake sites. The three humic-like model components were summed and presented as one humic-like component. Columns are arranged left to right from most acidic to most alkaline. The pH color scale applies to all sub-plots.

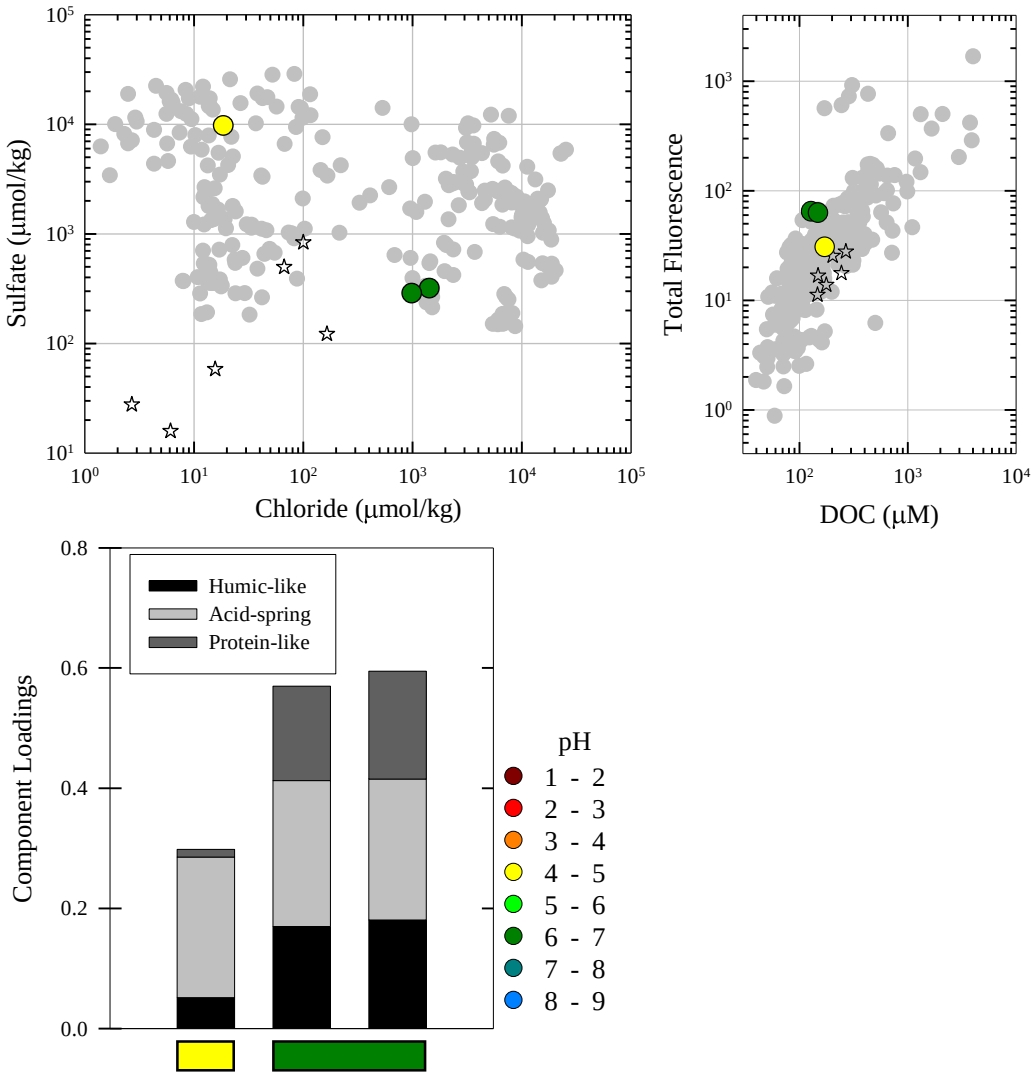

Figure 4.29: Wahb Springs hot spring chemistry. (top-left) Chloride and sulfate concentrations. (top-right) DOC concentrations and total fluorescence values. Colored circles represent hot springs from the Wahb Springs region. Gray circles represent samples from other regions in Yellowstone. Open stars indicate Yellowstone surface water samples. (bottom) PARAFAC model component loadings for Wahb Springs sites. The three humic-like model components were summed and presented as one humic-like component. Columns are arranged left to right from most acidic to most alkaline. The pH color scale applies to all sub-plots.

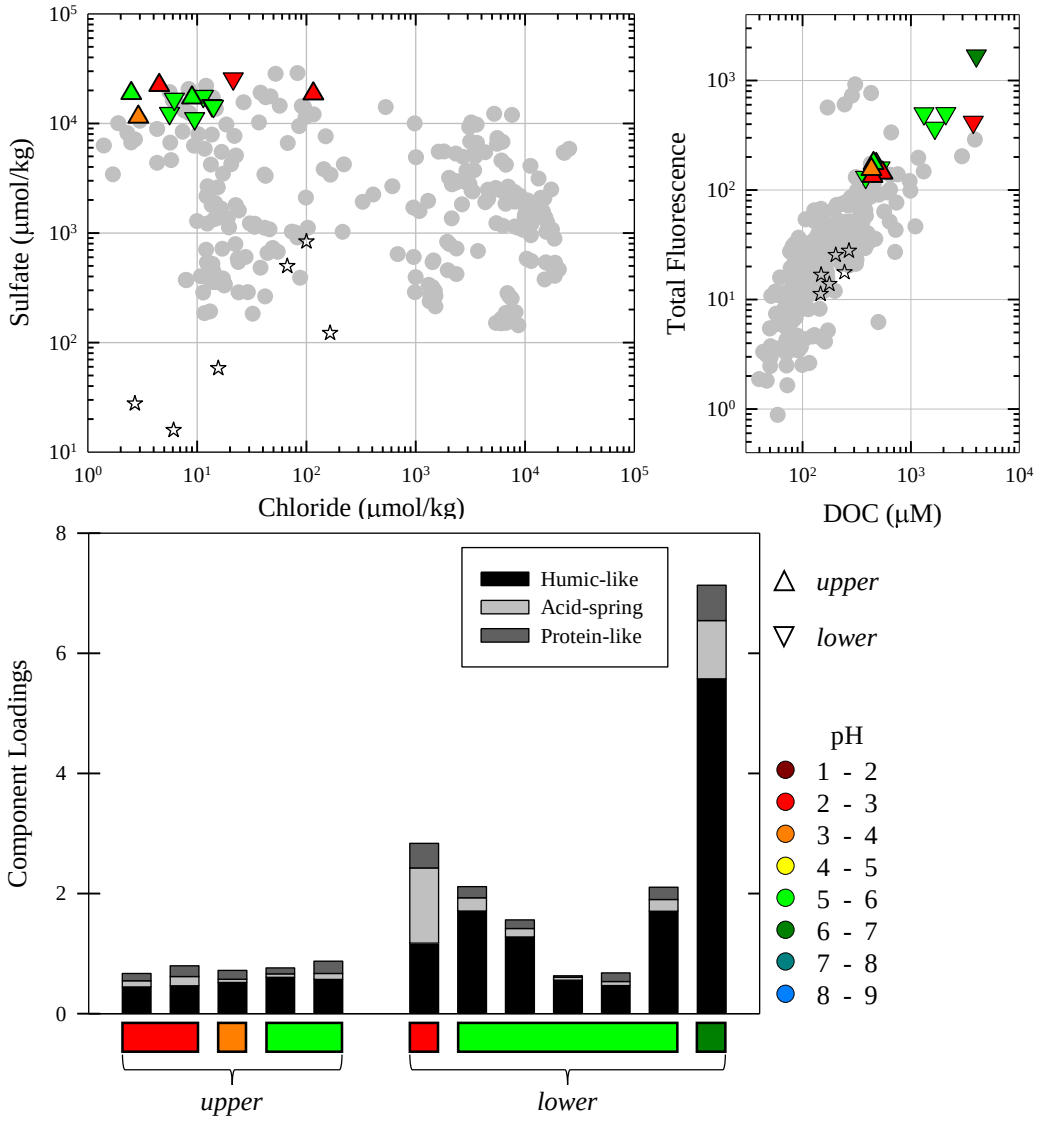

Figure 4.30: Washburn hot spring chemistry. (top-left) Chloride and sulfate concentrations. (top-right) DOC concentrations and total fluorescence values, presented in Raman-normalized intensity units. Colored circles represent hot springs from the Washburn region. Gray circles represent samples from other regions in Yellowstone. Open stars indicate Yellowstone surface water samples. There are two sub-regions within Washburn, 'upper' and 'lower', identified by upward triangle and downward triangle symbols, respectively. (bottom) PARAFAC model component loadings for Washburn sites. The three humic-like model components were summed and presented as one humic-like component. Each sub-region of Washburn is separated into clustered columns. Within each cluster, columns are arranged left to right from most acidic to most alkaline. The pH color scale applies to all sub-plots.

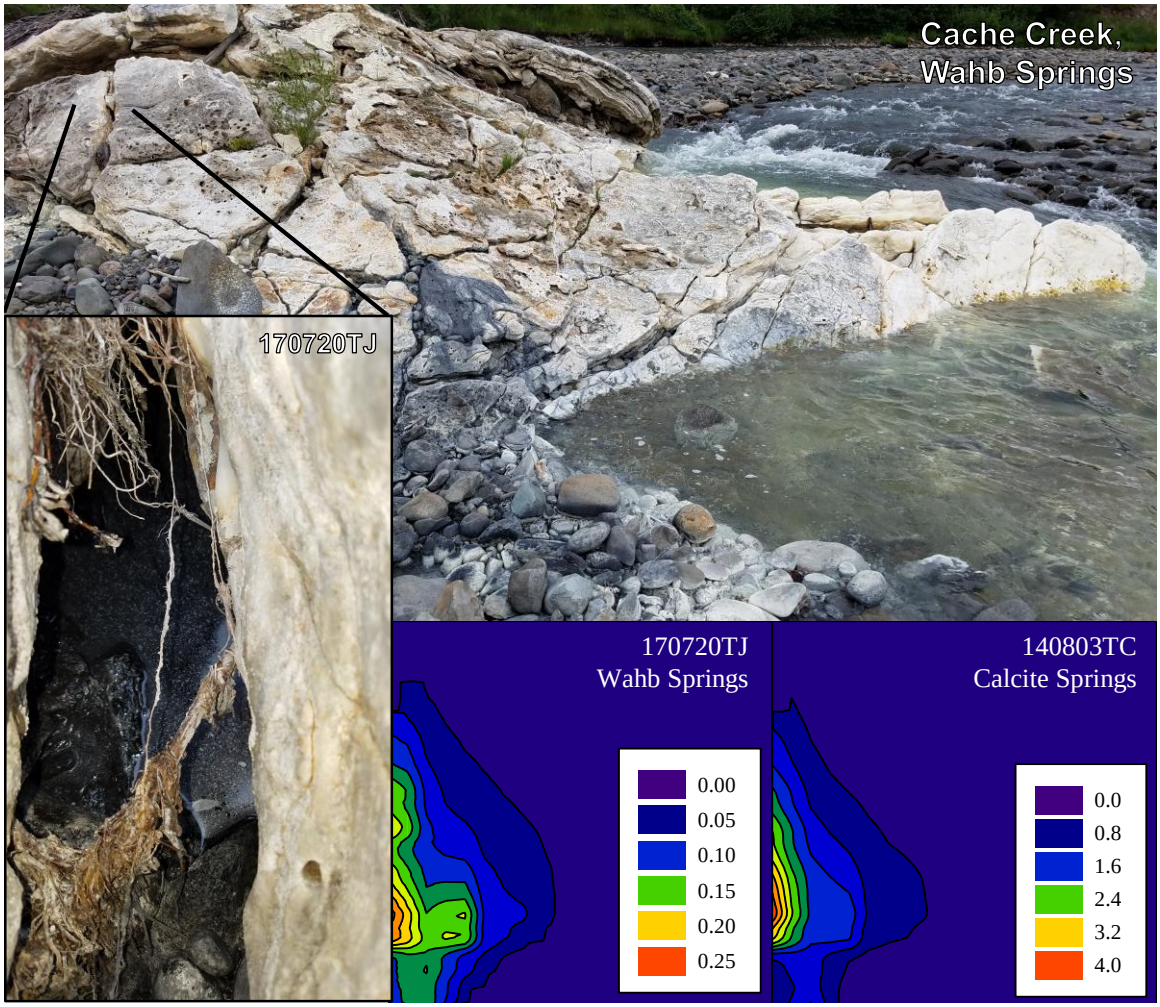

Figure 4.31: EEMs showing PAH fluorescence from Calcite Springs and Wahb Springs and photos from Wahb Springs showing the creek outcropping where two diluted HO-type springs were sampled. The closeup photo shows the oily sheen covering one spring (sample 170720TJ). (Photo credits: J. Nye).

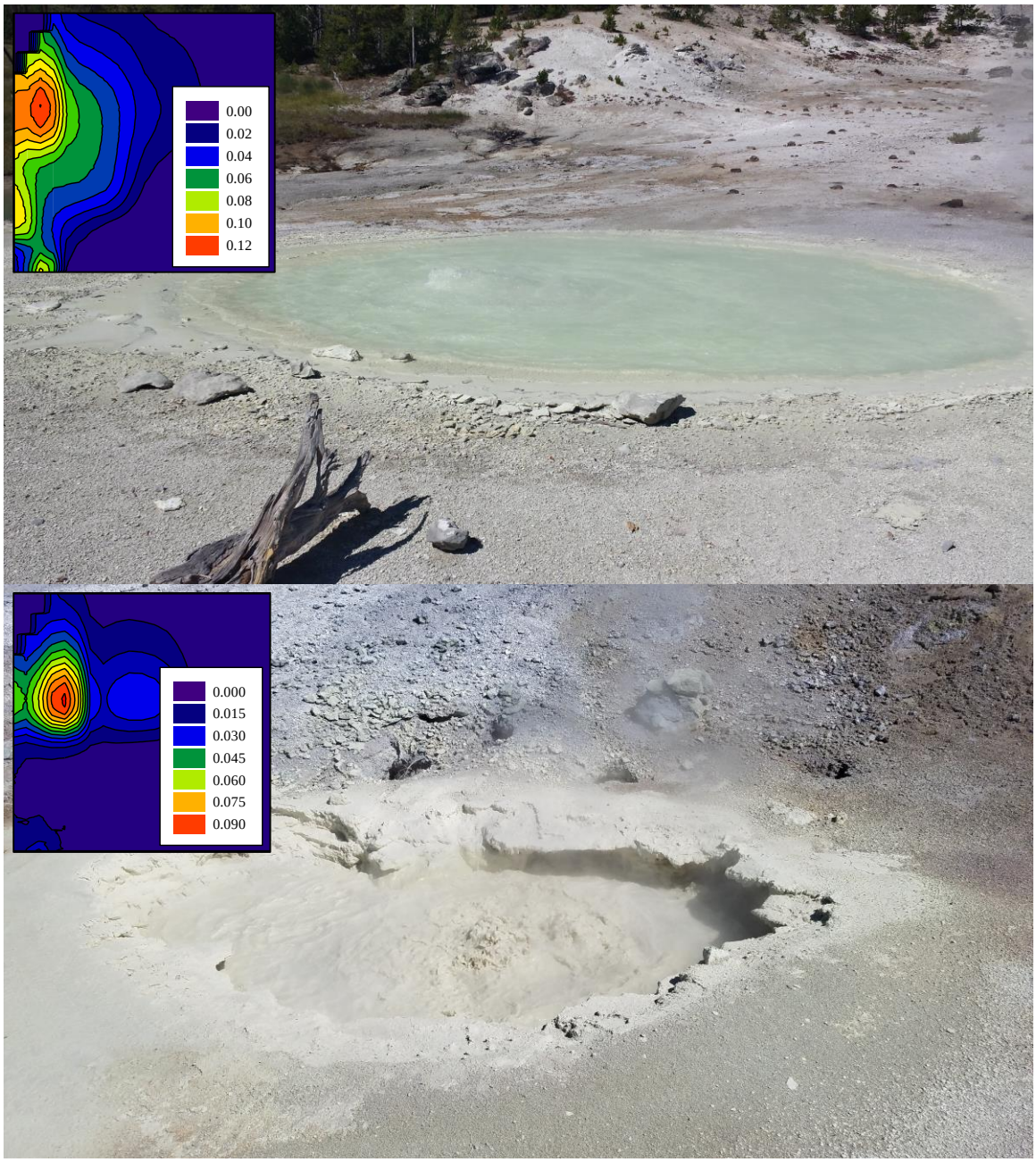

Figure 4.32: Photos and EEMs of springs containing the novel, sulfur-associated fluorescence. EEM color scales are fluorescence intensity and are different for each spring. (top) Photo and EEM (sample 160717U) of Evening Primrose in Sylvan Springs. (bottom) Photo and EEM (sample 170724TA) of an unnamed spring in Crater Hills, just southwest of Sulfur Spring. (Photo credits: J. Nye).

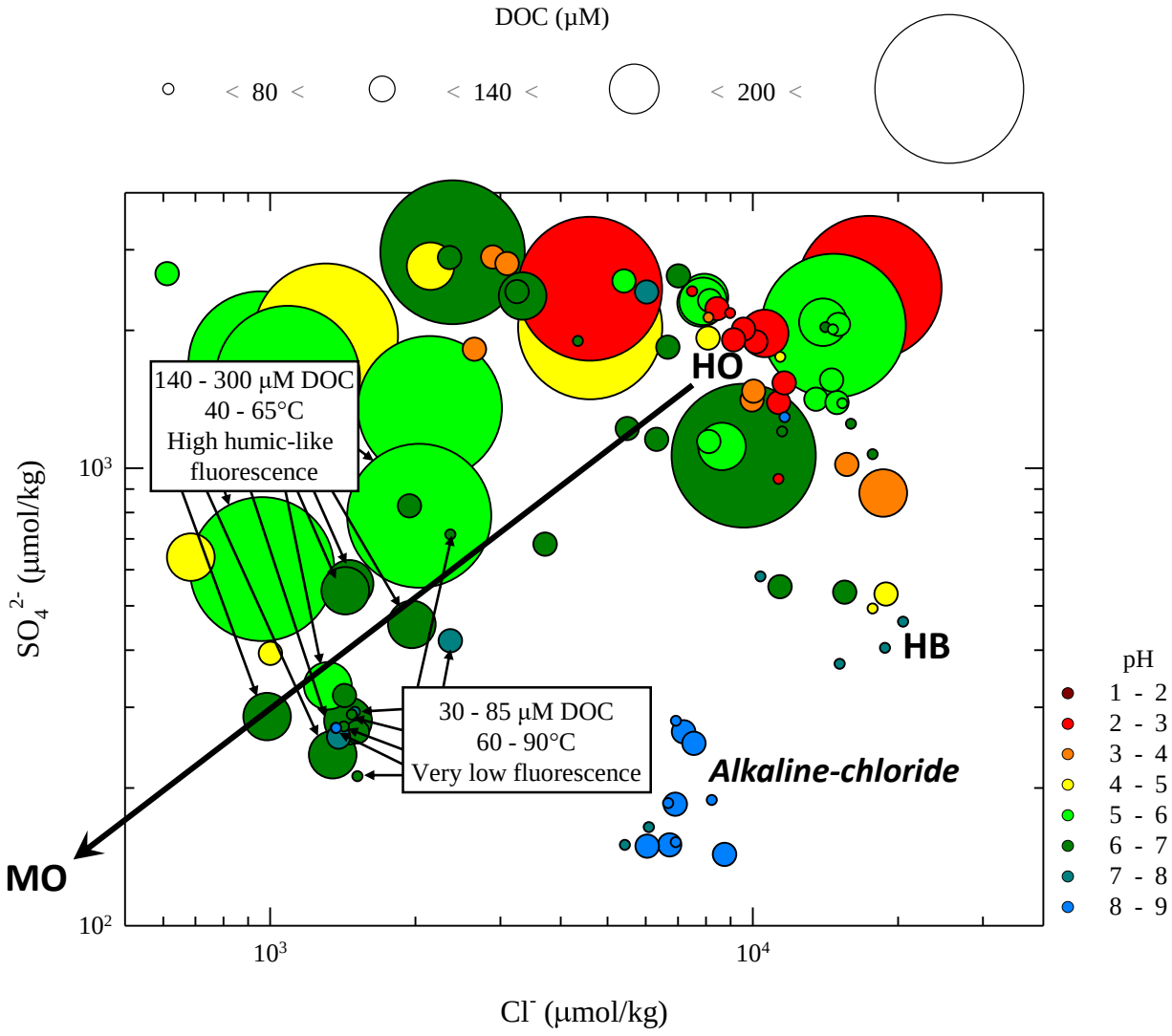

Figure 4.33: Different diluted HO-type springs plotted in a narrower hot spring chloride and sulfate concentration space to focus on the dilution line (thick black line) between end member HO- and MO-type fluids. Arrows (thin black lines) identify springs that have experienced a 5- to 10-fold dilution of chloride and sulfate concentrations. Some diluted HO-type springs demonstrate high DOC (140 to 300 μM) and cooler temperatures (40 to 65℃); this is consistent with expectations for an HO-type fluid diluted by cool, MO-type surface water. Other diluted HO-type springs demonstrate low DOC (30 to 85 μM) and high temperatures (60 to 90℃); this is inconsistent with expectations for an HO-type fluid diluted by cool, MO-type surface water.

Chapter 5

CONCLUSIONS AND FUTURE WORKS

In this dissertation I present the first broad-scale assessment of dissolved organic carbon concentrations (DOC) and characterization of fluorescent dissolved organic matter (FDOM) in Yellowstone National Park hot springs. My research reveals that hot springs are carbon-depleted relative to surface waters, except in the case of inputs from thermally-altered, sedimentary organic matter or in the case of extensive mixing with surface water. Fluorescent DOM serves as a fingerprint indicator of the total DOM pool and there were multiple novel fluorescence signatures in Yellowstone hot springs that have never been documented in surface water systems. Prominent novel features include an exclusively acid-soluble component and a peak associated with the presence of native sulfur in springs. The distribution of DOC and fluorescent DOM within Yellowstone not only revealed distinct trends with hot spring types as defined by traditional inorganic chemical indicators, but also provided new information on mixing between different fluid phases. Previously, it was commonly accepted that acid-sulfate, vapor-phase dominated springs and diluted HO-type springs were highly mixed with and influenced by the surface environment. My data indicates that this is not always true, and reveals a number of vapor-phase dominated hot springs (both acidic and neutral) and diluted hot springs that are hydrothermally "pristine". They are minimally influenced by surface-organic matter despite being significantly diluted or phase-separated from the deep-sourced hydrothermal fluid. The characterization of natural organic matter in aquatic environments is a complex field and hydrothermal DOM is as different from surface water DOM as their respective physicochemical environments are. This dissertation is the first study of the geochemical and geographic

distribution of hydrothermal DOM in a large number of hot springs in Yellowstone. My results demonstrate the utility of fluorescence spectroscopy as a low-cost, minimal preparation, non-destructive analytical technique to evaluate many samples from a diverse array of geochemical environments.

There are far more potential applications of hydrothermal DOM characterization than one person can accomplish during their PhD. There are several paths that I see as potential extensions of my work. The first is to continue molecular characterization and identification of the novel fluorophores I have described in hot spring EEMs. My attempts to identify the acid-spring component fluorophores were hindered by its extremely low abundance in most samples. This does, however, lend credit to just how highly sensitive the fluorescence spectroscopy technique is. I demonstrated that the acid-spring component fluorophores are indicative of an acidic liquid phase that circulates in the subsurface. They are likely the highly condensed, aromatic, recalcitrant products of the thermal alteration of buried sediments. Other fluorescence indicators of thermally altered organic matter include the PAHs from Calcite and Wahb Springs (Figure 4.31) and, potentially, the unusual "humic-like" fluorescence in Washburn, Hot Springs Basin, and Forest Springs, as well as the unknown, double-peaked "humic-like" fluorescence in HO- and HB-type springs (Figure 4.10). In surface waters, indices have been developed that use different parts of the humic-like signal to infer changes in molecular properties, material source, and degree of degradation by various processes. I demonstrated that the surface water indicators are not appropriate for hot springs (Nye et al., 2020); but, similar indices could be developed for hot springs. Such indices could be used to monitor alteration processes such as thermal degradation of surface-derived soil organic matter or buried sediment-derived organic matter. Specific indices could also be applied to monitor the dispersal

and fate of thermally altered organic matter in outflow channels as they interact with surface environments and microbial communities.

The novel fluorescence associated with the presence of native sulfur also has potential applications. Sulfur chemistry in hot springs is complex, but it has been demonstrated that sulfur inclusion into organic compounds occurs readily throughout all hydrothermal environments (Hawkes et al., 2016; Gonsior et al., 2018). This fluorescence signal may come from organo-sulfur compounds. However, the observation that the sulfur-associated peak appears in only very specific springs suggests a more specific source. The springs that have the strongest fluorescence of this type are also known to host sulfur-oxidizing microbes; this may potentially be a biosignature of a specific class of microbes or at least a signature for chemical environments that host such microbes. An excellent field site to target for further exploration would be Sulfur Spring in Crater Hills (Figure 5.1). Over the past five years this spring has changed in appearance from a clear blue to a yellow-green that was accompanied by the appearance of this unique fluorescence signal. This fluorescence was not present before the spring changed color.

A final remark I have is for the assessment of the relationship between hydrothermal DOM and biogeochemical cycles. Currently, research into carbon utilization by microbes in hydrothermal systems is focused mostly on carbon dioxide, small organic acids, hydrocarbons, and other simple compounds. There is very limited research on how complex organic matter is consumed or otherwise utilized by microbes. In addition to serving as an energy source, DOM is known to mobilize and transport nutrients and metals (both essential and toxic) in aquatic systems. In extremely carbon limited springs, the role DOM plays in binding, transporting metals and making them bioavailable has the potential to be critical for the maintenance of microbial communities. Terrestrial, soil-derived organic matter is known to bind and transport metals

in surface waters. I demonstrated that not all dilution of thermal fluids involves the introduction of surface-derived DOM. The source and composition of DOM in such springs may have profound biological implications as they relate to the bioavailability of essential elements.

One roadblock to the application of high-resolution characterization techniques to Yellowstone hot spring DOM is that they often require filtering significant volumes of water in order to obtain sufficient carbon. In some of the lowest carbon springs, arguably the most highly desired targets of such analysis, this could require up to several hundred liters. While we as environmental scientists are driven by the desire to study and understand our natural world, the conservation and preservation of Earth's pristine environments, such as Yellowstone, must always be the top priority. Extensive, invasive sampling, if applied, must be performed in a precise way in order to maximize the potential knowledge gain while minimizing our impact on our natural environment. My research on a large number of Yellowstone hot springs has provided many significant findings, which have a high impact on their own right, that provide a means for making informed decisions about future field work for a wide variety of applications.

REFERENCES

Gonsior, M., Hertkorn, N., Hinman, N., Dvorski, S. E.-M., Harir, M., Cooper, W. J., and Schmitt-Kopplin, P. (**2018**); Yellowstone hot springs are organic chemodiversity hot spots. *Scientific Reports* 8(1), p. 14155, doi:10.1038/s41598-018-32593-x.

Hawkes, J. A., Hansen, C. T., Goldhammer, T., Bach, W., and Dittmar, T. (**2016**); Molecular alteration of marine dissolved organic matter under experimental hydrothermal conditions. *Geochimica et Cosmochimica Acta* 175, pp. 68–85, doi: 10.1016/j.gca.2015.11.025.

Nye, J., Shock, E., and Hartnett, H. (**2020**); A novel PARAFAC model for continental hot springs reveals unique dissolved organic carbon compositions. *Organic Geochemistry* 141(103964), doi:10.1016/j.orggeochem.2019.103964.

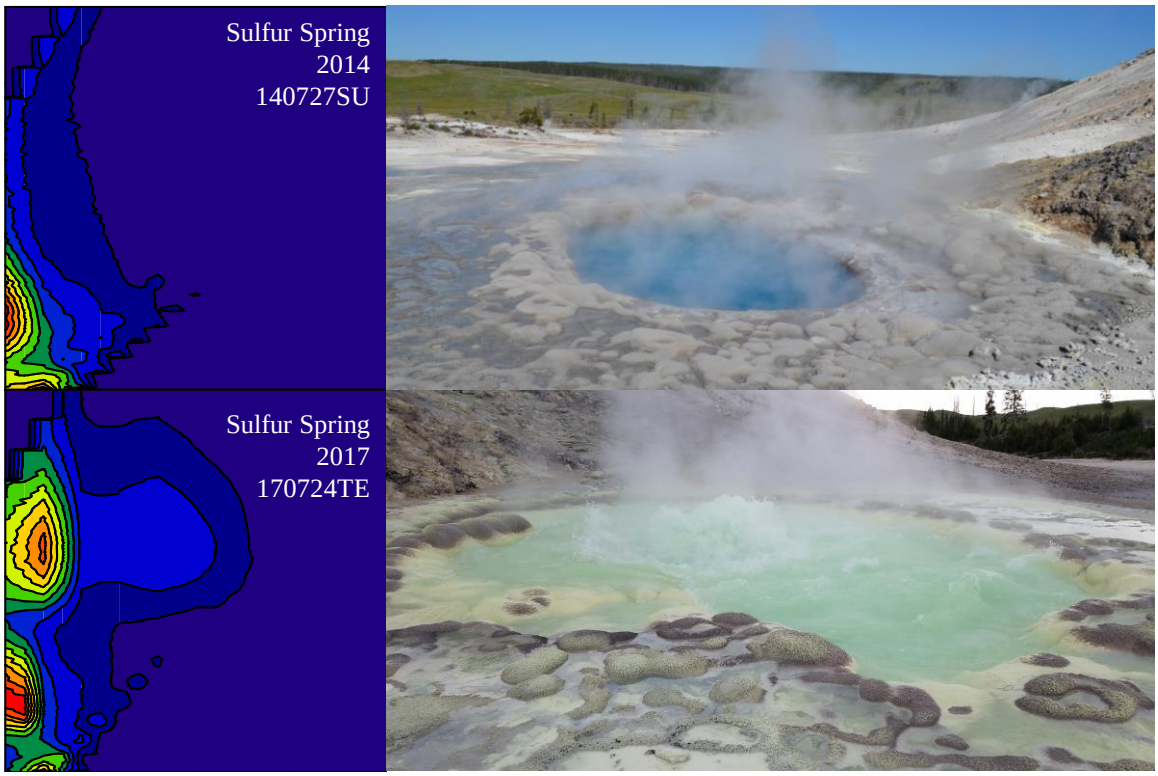

Figure 5.1: Sulfur Spring, Crater Hills in 2014 and 2017. The change in spring color is associated with the appearance of the unknown, sulfur-associated fluorescence signal. Photo credit of Sulfur Spring in 2014 to Randall Debes. Photo credit of Sulfur Spring in 2017 to J. Nye.

Adegboyega, N. F., Sharma, V. K., Siskova, K., Zbořil, R., Sohn, M., Schultz, B. J., and Banerjee, S. (**2013**); Interactions of aqueous Ag with fulvic acids: Mechanisms of silver nanoparticle formation and investigation of stability. *Environmental Science & Technology* 47(2), pp. 757–764, doi:10.1021/es302305f.

Aiken, G. R. (ed.) (**1985**); *Humic Substances in Soil, Sediment, and Water: Geochemistry, Isolation, and Characterization*. Wiley, New York, USA.

Aiken, G. R. (**2014**); Fluorescence and dissolved organic matter: A chemist's perspective. In: Coble, P. G., Lead, J., Baker, A., Reynolds, D. M., and Spencer, R. G. M. (eds.), *Aquatic Organic Matter Fluorescence*, pp. 35–74, Cambridge Environmental Chemistry Series, Cambridge University Press, New York, USA, doi: 10.1017/CBO9781139045452.005.

Alberts, J. J. and Takács, M. (**2004**); Comparison of the natural fluorescence distribution among size fractions of terrestrial fulvic and humic acids and aquatic natural organic matter. *Organic Geochemistry* 35(10), pp. 1141–1149, doi:10.1016/j.orggeochem.2004.06.010.

Albinsson, B., Li, S., Lundquist, K., and Stomberg, R. (**1999**); The origin of lignin fluorescence. *Journal of Molecular Structure* 508(1-3), pp. 19–27, doi:10.1016/S0022-2860(98)00913-2.

Allen, E. T. and Day, A. L. (**1935**); Hot springs of the Yellowstone National Park. Carnegie Institution of Washington Publication 466, Carnegie Institute, Washington D. C., USA.

Arnórsson, S. (**1985**); The use of mixing models and chemical geothermometers for estimating underground temperatures in geothermal systems. *Journal of Volcanology and Geothermal Research* 23(3-4), pp. 299–335, doi:10.1016/0377-0273(85)90039-3.

Arnórsson, S., Stefánsson, A., and Bjarnason, J. O. (**2007**); Fluid-fluid interactions in geothermal systems. *Reviews in Mineralogy and Geochemistry* 65(1), pp. 259–312, doi:10.2138/rmg.2007.65.9.

Bader, R. G., Hood, D. W., and Smith, J. B. (**1960**); Recovery of dissolved organic matter in sea-water and organic sorption by particulate material. *Geochimica et Cosmochimica Acta* 19(4), pp. 236–243, doi:10.1016/0016-7037(60)90031-4.

Baghoth, S., Sharma, S., and Amy, G. (**2011**); Tracking natural organic matter (NOM) in a drinking water treatment plant using fluorescence excitation emission matrices and PARAFAC. *Water Research* 45(2), pp. 797–809, doi:10.1016/j.watres.2010.09.005.

Bailey, S. E., Olin, T. J., Bricka, R., and Adrian, D. (**1999**); A review of potentially low-cost sorbents for heavy metals. *Water Research* 33(11), pp. 2469–2479, doi: 10.1016/S0043-1354(98)00475-8.

Bajpai, P. (**2018**); *Raw material and pulp making*. Third edition, Biermann's Handbook of Pulp and Paper, Elsevier, doi:10.1016/C2017-0-00513-X.

Bandura, A. V. and Lvov, S. N. (**2006**); The ionization constant of water over wide ranges of temperature and density. *Journal of Physical and Chemical Reference Data* 35(1), pp. 15–30, doi:10.1063/1.1928231.

Beggs, K. M. and Summers, R. S. (**2011**); Character and chlorine reactivity of dissolved organic matter from a mountain pine beetle impacted watershed. *Environmental Science & Technology* 45(13), pp. 5717–5724, doi:10.1021/es1042436.

Bergfeld, D., Evans, W. C., Lowenstern, J. B., and Hurwitz, S. (**2012**); Carbon dioxide and hydrogen sulfide degassing and cryptic thermal input to Brimstone Basin, Yellowstone National Park, Wyoming. *Chemical Geology* 330-331, pp. 233–243, doi:10.1016/j.chemgeo.2012.09.001.

Bergfeld, D., Lowenstern, J. B., Hunt, A. G., Shanks, W. C. P., and Evans, W. C. (**2014**); Gas and isotope chemistry of thermal features in Yellowstone National Park, Wyoming. Scientific Investigations Report 2011-5012, United States Geological Survey, doi:10.3133/sir20115012.

Berner, R. A. (**1982**); Burial of organic carbon and pyrite sulfur in the modern ocean; its geochemical and environmental significance. *American Journal of Science* 282(4), pp. 451–473, doi:10.2475/ajs.282.4.451.

Bianco, A., Minella, M., De Laurentiis, E., Maurino, V., Minero, C., and Vione, D. (**2014**); Photochemical generation of photoactive compounds with fulvic-like and humic-like fluorescence in aqueous solution. *Chemosphere* 111, pp. 529–536, doi:10.1016/j.chemosphere.2014.04.035.

Bockisch, C., Lorance, E. D., Hartnett, H. E., Shock, E. L., and Gould, I. R. (**2018**); Kinetics and mechanisms of dehydration of secondary alcohols under hydrothermal conditions. *ACS Earth and Space Chemistry* 2(8), pp. 821–832, doi:10.1021/acsearthspacechem.8b00030.

Boehm, A. B., Yamahara, K. M., Walters, S. P., Layton, B. A., Keymer, D. P., Thompson, R. S., Knee, K. L., and Rosener, M. (**2011**); Dissolved inorganic nitrogen, soluble reactive phosphorous, and microbial pollutant loading from tropical rural watersheds in Hawai'i to the coastal ocean during non-storm conditions. *Estuaries and Coasts* 34(5), pp. 925–936, doi:10.1007/s12237-010-9352-8.

Boerjan, W., Ralph, J., and Baucher, M. (**2003**); Lignin biosynthesis. *Annual Review of Plant Biology* 54(1), pp. 519–546, doi:10.1146/annurev.arplant.54.031902.134938.

Boyd, E. S., Hamilton, T. L., Wang, J., He, L., and Zhang, C. L. (**2013**); The role of tetraether lipid composition in the adaptation of thermophilic archaea to acidity. *Frontiers in Microbiology* 4(62), doi:10.3389/fmicb.2013.00062.

Bradley, D. J. and Pitzer, K. S. (**1979**); Thermodynamics of electrolytes. 12. Dielectric properties of water and Debye-Hückel parameters to 350℃ and 1 kbar. *The Journal of Physical Chemistry* 83(12), pp. 1599–1603, doi:10.1021/j100475a009.

Bridges, J. W. and Williams, R. T. (**1968**); The fluorescence of indoles and aniline derivatives. *Biochemical Journal* 107(2), pp. 225–237, doi:10.1042/bj1070225.

Briucaud, A., Morel, A., and Prieur, L. (**1981**); Absorption by dissolved organic matter of the sea (yellow substance) in the UV and visible domains. *Limnology and Oceanography* 26(1), pp. 43–53, doi:10.4319/lo.1981.26.1.0043.

Bro, R. (**1997**); PARAFAC. Tutorial and applications. *Chemometrics and Intelligent Laboratory Systems* 38(2), pp. 149–171, doi:10.1016/S0169-7439(97)00032-4.

Brock, T. and Mosser, J. (**1975**); Rate of sulfuric acid production in Yellowstone National Park. *Geological Society of America Bulletin* 86(2), pp. 194–198, doi:10.1130/0016-7606(1975)86⟨194:ROSPIY⟩2.0.CO;2.

Brock, T. D. (**1971**); Bimodal distribution of pH values of thermal springs of the world. *Geological Society of America Bulletin* 82(5), p. 1393, doi:10.1130/0016-7606(1971)82[1393:BDOPVO]2.0.CO;2.

Brock, T. D. (**1978**); *Thermophilic Microorganisms and Life at High Temperatures*. Springer, New York, USA, doi:10.1007/978-1-4612-6284-8.

Brock, T. D., Brock, K. M., Belly, R. T., and Weiss, R. L. (**1972**); Sulfolobus: A new genus of sulfur-oxidizing bacteria living at low pH and high temperature. *Archiv für Mikrobiologie* 84(1), pp. 54–68, doi:10.1007/BF00408082.

Browne, B. A., McColl, J. G., and Driscoll, C. T. (**1990**); Aluminum speciation using morin: I. Morin and its complexes with aluminum. *Journal of Environmental Quality* 19(1), pp. 65–72, doi:10.2134/jeq1990.00472425001900010008x.

Bublitz, W. J. and Meng, T. Y. (**1978**); The fluorometric behavior of pulping waste liquors. *Tappi* 61, pp. 27–30.

Buna, M., Aaron, J. J., Prognon, P., and Mahuzier, G. (**1996**); Effects of pH and solvent on the fluorescence properties of biomedically important benzamides. Application to determination in drugs and in human urine. *The Analyst* 121(11), pp. 1551–1556, doi:10.1039/an9962101551.

Carlson, C. A., Ducklow, H. W., and Michaels, A. F. (**1994**); Annual flux of dissolved organic carbon from the euphotic zone in the northwestern Sargasso Sea. *Nature* 371(6496), pp. 405–408, doi:10.1038/371405a0.

Carstea, E. M., Baker, A., Bieroza, M., Reynolds, D. M., and Bridgeman, J. (**2014**); Characterisation of dissolved organic matter fluorescence properties by PARAFAC analysis and thermal quenching. *Water Research* 61, pp. 152–161, doi:10.1016/j.watres.2014.05.013.

Castiglioni, C., Mapelli, C., Negri, F., and Zerbi, G. (**2001**); Origin of the D line in the Raman spectrum of graphite: A study based on Raman frequencies and intensities of polycyclic aromatic hydrocarbon molecules. *The Journal of Chemical Physics* 114(2), p. 963, doi:10.1063/1.1329670.

Castiglioni, C., Tommasini, M., and Zerbi, G. (**2004**); Raman spectroscopy of polyconjugated molecules and materials: confinement effect in one and two dimensions. *Philosophical Transactions of the Royal Society of London. Series A: Mathematical, Physical and Engineering Sciences* 362(1824), pp. 2425–2459, doi:10.1098/rsta.2004.1448.

Catalán, N., Marcé, R., Kothawala, D. N., and Tranvik, L. J. (**2016**); Organic carbon decomposition rates controlled by water retention time across inland waters. *Nature Geoscience* 9(7), pp. 501–504, doi:10.1038/ngeo2720.

Cawley, K. M., Butler, K. D., Aiken, G. R., Larsen, L. G., Huntington, T. G., and McKnight, D. M. (**2012**); Identifying fluorescent pulp mill effluent in the Gulf of Maine and its watershed. *Marine Pollution Bulletin* 64(8), pp. 1678–1687, doi:10.1016/j.marpolbul.2012.05.040.

Chen, M., Maie, N., Parish, K., and Jaffé, R. (**2013**); Spatial and temporal variability of dissolved organic matter quantity and composition in an oligotrophic subtropical coastal wetland. *Biogeochemistry* 115(1-3), pp. 167–183, doi:10.1007/s10533-013-9826-4.

Chen, R. F. (**1967**); Fluorescence quantum yields of tryptophan and tyrosine. *Analytical Letters* 1(1), pp. 35–42, doi:10.1080/00032716708051097.

Chiasson-Gould, S. A., Blais, J. M., and Poulain, A. J. (**2014**); Dissolved organic matter kinetically controls mercury bioavailability to bacteria. *Environmental Science & Technology* 48(6), pp. 3153–3161, doi:10.1021/es4038484.

Chin, Y.-P., Aiken, G. R., and O'Loughlin, E. (**1994**); Molecular weight, polydispersity, and spectroscopic properties of aquatic humic substances. *Environmental Science & Technology* 28(11), pp. 1853–1858, doi:10.1021/es00060a015.

Christiansen, R. L. (**2001**); The quarternary and pliocene Yellowstone plateau volcanic field of Wyoming, Idaho, and Montana. Professional Paper 729-G, United States Geological Survey, doi:10.3133/pp729g.

Clifton, C., Walters, C., and Simoneit, B. (**1990**); Hydrothermal petroleums from Yellowstone National Park, Wyoming, U.S.A. *Applied Geochemistry* 5(1-2), pp. 169–191, doi:10.1016/0883-2927(90)90047-9.

Coble, P. G. (**2007**); Marine optical biogeochemistry: The chemistry of ocean color. *Chemical Reviews* 107(2), pp. 402–418, doi:10.1021/cr050350+.

Coble, P. G., Green, S. A., Blough, N. V., and Gagosian, R. B. (**1990**); Characterization of dissolved organic matter in the Black Sea by fluorescence spectroscopy. *Nature* 348(6300), pp. 432–435, doi:10.1038/348432a0.

Coble, P. G., Del Castillo, C. E., and Avril, B. (**1998**); Distribution and optical properties of CDOM in the Arabian Sea during the 1995 Southwest Monsoon. *Deep Sea Research Part II: Topical Studies in Oceanography* 45(10-11), pp. 2195–2223, doi:10.1016/S0967-0645(98)00068-X.

Cole, J. J., Prairie, Y. T., Caraco, N. F., McDowell, W. H., Tranvik, L. J., Striegl, R. G., Duarte, C. M., Kortelainen, P., Downing, J. A., Middelburg, J. J., and Melack, J. (**2007**); Plumbing the global carbon cycle: Integrating inland waters into the terrestrial carbon budget. *Ecosystems* 10(1), pp. 172–185, doi:10.1007/s10021-006-9013-8.

Cory, R. M. and McKnight, D. M. (**2005**); Fluorescence spectroscopy reveals ubiquitous presence of oxidized and reduced quinones in dissolved organic matter. *Environmental Science & Technology* 39(21), pp. 8142–8149, doi:10.1021/es0506962.

Cox, A., Shock, E. L., and Havig, J. R. (**2011**); The transition to microbial photosynthesis in hot spring ecosystems. *Chemical Geology* 280(3-4), pp. 344–351, doi:10.1016/j.chemgeo.2010.11.022.

Cox, L., Celis, R., Hermosín, M. C., Cornejo, J., Zsolnay, A., and Zeller, K. (**2000**); Effect of organic amendments on herbicide sorption as related to the nature of the dissolved organic matter. *Environmental Science & Technology* 34(21), pp. 4600–4605, doi:10.1021/es0000293.

De Laurentiis, E., Minella, M., Maurino, V., Minero, C., Brigante, M., Mailhot, G., and Vione, D. (**2012**); Photochemical production of organic matter triplet states in water samples from mountain lakes, located below or above the tree line. *Chemosphere* 88(10), pp. 1208–1213, doi:10.1016/j.chemosphere.2012.03.071.

Del Vecchio, R. and Blough, N. V. (**2004**); Spatial and seasonal distribution of chromophoric dissolved organic matter and dissolved organic carbon in the Middle Atlantic Bight. *Marine Chemistry* 89(1-4), pp. 169–187, doi:10.1016/j.marchem.2004.02.027.

Des Marais, D. J., Donchin, J. H., Nehring, N. L., and Truesdell, A. H. (**1981**); Molecular carbon isotopic evidence for the origin of geothermal hydrocarbons. *Nature* 292(5826), pp. 826–828, doi:10.1038/292826a0.

Determann, S., Lobbes, J. M., Reuter, R., and Rullkötter, J. (**1998**); Ultraviolet fluorescence excitation and emission spectroscopy of marine algae and bacteria. *Marine Chemistry* 62(1-2), pp. 137–156, doi:10.1016/S0304-4203(98)00026-7.

Donaldson, L. (**2013**); Softwood and hardwood lignin fluorescence spectra of wood cell walls in different mounting media. *IAWA Journal* 34(1), pp. 3–19, doi:10.1163/22941932-00000002.

Duarte, R. M., Smith, D. S., Val, A. L., and Wood, C. M. (**2016**); Dissolved organic carbon from the upper Rio Negro protects zebrafish (*Danio rerio*) against ionoregulatory disturbances caused by low pH exposure. *Scientific Reports* 6(1), p. 20377, doi:10.1038/srep20377.

Dunning Hotopp, J. C., Auchtung, T. A., Hogan, D. A., and Hausinger, R. P. (**2003**); Intrinsic tryptophan fluorescence as a probe of metal and alpha-ketoglutarate binding to TfdA, a mononuclear non-heme iron dioxygenase. *Journal of Inorganic Biochemistry* 93(1-2), pp. 66–70.

Ehrhardt, M. (**1984**); Marine gelbstoff. In: Hutzinger, O. (ed.), *The Natural Environment and the Biogeochemical Cycles*, pp. 63–77, The Handbook of Environmental Chemistry, volume 1/1C, Springer, Berlin, Germany, doi:10.1007/978-3-540-38829-6_3.

Engineering Toolbox (**2017**); Amines, diamines and cyclic organic nitrogen compounds - pKa values. https://www.engineeringtoolbox.com/amine-diamine-pyridine-cyclic-quinoline-aminobenzene-structure-pka-carboxylic-dissociation-constant-d_1949.html.

Fellman, J. B., Hood, E., and Spencer, R. G. M. (**2010**); Fluorescence spectroscopy opens new windows into dissolved organic matter dynamics in freshwater ecosystems: A review. *Limnology and Oceanography* 55(6), pp. 2452–2462, doi:10.4319/lo.2010.55.6.2452.

Fernández, D. P., Mulev, Y., Goodwin, A. R. H., and Sengers, J. M. H. L. (**1995**); A database for the static dielectric constant of water and steam. *Journal of Physical and Chemical Reference Data* 24(1), pp. 33–70, doi:10.1063/1.555977.

Fondriest Environmental, Inc. (**2013**); pH of Water. Fundamentals of Environmental Measurements. 19 Nov 2013. https://www.fondriest.com/environmental-measurements/parameters/water-quality/ph/.

Fondriest Environmental, Inc. (**2014**); Water Temperature. Fundamentals of Environmental Measurements. 7 Feb 2014. https://www.fondriest.com/environmental-measurements/parameters/water-quality/water-temperature/.

Fournier, R. (**1977**); Chemical geothermometers and mixing models for geothermal systems. *Geothermics* 5(1-4), pp. 41–50, doi:10.1016/0375-6505(77)90007-4.

Fournier, R. O. (**1989**); Geochemistry and dynamics of the Yellowstone National Park hydrothermal system. *Annual Review of Earth and Planetary Sciences* 17(1), pp. 13–53, doi:10.1146/annurev.ea.17.050189.000305.

Frost, R. L., Williams, P. A., and Martens, W. (**2003**); Raman spectroscopy of the minerals boléite, cumengéite, diaboléte and phosgenite - implications for the analysis of cosmetics of antiquity. *Mineralogical Magazine* 67(1), pp. 103–111, doi:10.1180/0026461036710088.

Fu, S. and Li, B. (**2019**); Structure and characteristics of lignin. In: Huang, J., Fu, S., Gan, L., and Zhang, L. (eds.), *Lignin Chemistry and Applications*, pp. 25–50, Natural Polymer Based Novel Materials, Elsevier, doi:10.1016/B978-0-12-813941-7.00002-3.

Gagliardi, L. G., Tascon, M., and Castells, C. B. (**2015**); Effect of temperature on acid-base equilibria in separation techniques. A review. *Analytica Chimica Acta* 889, pp. 35–57, doi:10.1016/j.aca.2015.05.053.

Gardner, W. P., Susong, D. D., Solomon, D. K., and Heasler, H. P. (**2011**); A multitracer approach for characterizing interactions between shallow groundwater and the hydrothermal system in the Norris Geyser Basin area, Yellowstone National Park. *Geochemistry, Geophysics, Geosystems* 12(8), doi:10.1029/2010GC003353.

Giggenbach, W. F. (**1997**); Relative importance of thermodynamic and kinetic processes in governing the chemical and isotopic composition of carbon gases in high heatflow sedimentary basins. *Geochimica et Cosmochimica Acta* 61(17), pp. 3763–3785, doi:10.1016/S0016-7037(97)00171-3.

Gledhill, M. (**2012**); The organic complexation of iron in the marine environment: A review. *Frontiers in Microbiology* 3(69), doi:10.3389/fmicb.2012.00069.

Gomez-Saez, G. V., Niggemann, J., Dittmar, T., Pohlabeln, A. M., Lang, S. Q., Noowong, A., Pichler, T., Wörmer, L., and Bühring, S. I. (**2016**); Molecular evidence for abiotic sulfurization of dissolved organic matter in marine shallow hydrothermal systems. *Geochimica et Cosmochimica Acta* 190, pp. 35–52, doi:10.1016/j.gca.2016.06.027.

Gonsior, M., Hertkorn, N., Hinman, N., Dvorski, S. E.-M., Harir, M., Cooper, W. J., and Schmitt-Kopplin, P. (**2018**); Yellowstone hot springs are organic chemodiversity hot spots. *Scientific Reports* 8(1), p. 14155, doi:10.1038/s41598-018-32593-x.

Gooch, F. A. and Whitfield, J. E. (**1888**); *Analyses of Waters of the Yellowstone National Park*. Bulletin of the United States Geological Survey no. 47, United States Geoglical Survey, doi:10.3133/b47.

Guidry, S. A. and Chafetz, H. S. (**2002**); Factors governing subaqueous siliceous sinter precipitation in hot springs: examples from Yellowstone National Park, USA. *Sedimentology* 49(6), pp. 1253–1267, doi:10.1046/j.1365-3091.2002.00494.x.

Gunter, B. (**1978**); C1-C4 hydrocarbons in hydrothermal gases. *Geochimica et Cosmochimica Acta* 42(1), pp. 137–139, doi:10.1016/0016-7037(78)90223-5.

Hamilton, T. L., Boyd, E. S., and Peters, J. W. (**2011**); Environmental constraints underpin the distribution and phylogenetic diversity of nifH in the Yellowstone geothermal complex. *Microbial Ecology* 61(4), pp. 860–870, doi:10.1007/s00248-011-9824-9.

Hansell, D., Carlson, C., Repeta, D., and Schlitzer, R. (**2009**); Dissolved organic matter in the ocean: A controversy stimulates new insights. *Oceanography* 22(4), pp. 202–211, doi:10.5670/oceanog.2009.109.

Hansell, D. A. and Carlson, C. A. (eds.) (**2014**); *Biogeochemistry of Marine Dissolved Organic Matter*. Second edition, Academic Press, doi:10.1016/C2012-0-02714-7.

Hardison, A., Canuel, E., Anderson, I., and Veuger, B. (**2010**); Fate of macroalgae in benthic systems: carbon and nitrogen cycling within the microbial community. *Marine Ecology Progress Series* 414, pp. 41–55, doi:10.3354/meps08720.

Hawkes, J. A., Rossel, P. E., Stubbins, A., Butterfield, D., Connelly, D. P., Achterberg, E. P., Koschinsky, A., Chavagnac, V., Hansen, C. T., Bach, W., and Dittmar, T. (**2015**); Efficient removal of recalcitrant deep-ocean dissolved organic matter during hydrothermal circulation. *Nature Geoscience* 8, pp. 856–860, doi:10.1038/ngeo2543.

Hawkes, J. A., Hansen, C. T., Goldhammer, T., Bach, W., and Dittmar, T. (**2016**); Molecular alteration of marine dissolved organic matter under experimental hydrothermal conditions. *Geochimica et Cosmochimica Acta* 175, pp. 68–85, doi:10.1016/j.gca.2015.11.025.

Hawkes, J. A., Patriarca, C., Sjöberg, P. J. R., Tranvik, L. J., and Bergquist, J. (**2018**); Extreme isomeric complexity of dissolved organic matter found across aquatic environments: Extreme isomeric complexity of DOM. *Limnology and Oceanography Letters* 3(2), pp. 21–30, doi:10.1002/lol2.10064.

He, J. and Chen, J. P. (**2014**); A comprehensive review on biosorption of heavy metals by algal biomass: Materials, performances, chemistry, and modeling simulation tools. *Bioresource Technology* 160, pp. 67–78, doi:10.1016/j.biortech.2014.01.068.

He, W., Lee, J.-H., and Hur, J. (**2016**); Anthropogenic signature of sediment organic matter probed by UV-Visible and fluorescence spectroscopy and the association with heavy metal enrichment. *Chemosphere* 150, pp. 184–193, doi:10.1016/j.chemosphere.2016.01.116.

Hearn, E., Kennedy, B., and Truesdell, A. (**1990**); Coupled variations in helium isotopes and fluid chemistry: Shoshone Geyser Basin, Yellowstone National Park. *Geochimica et Cosmochimica Acta* 54(11), pp. 3103–3113, doi:10.1016/0016-7037(90)90126-6.

Hedges, J., Keil, R., and Benner, R. (**1997**); What happens to terrestrial organic matter in the ocean? *Organic Geochemistry* 27(5-6), pp. 195–212, doi:10.1016/S0146-6380(97)00066-1.

Hedges, J. I., Bergamaschi, B. A., and Benner, R. (**1993**); Comparative analyses of DOC and DON in natural waters. *Marine Chemistry* 41(1-3), pp. 121–134, doi:10.1016/0304-4203(93)90110-A.

Hem, J. D. (**1985**); Study and interpretation of the chemical characteristics of natural water. Water Supply Paper 2254, United States Geological Survey, doi:10.3133/wsp2254.

Hem, J. D. and Cropper, W. H. (**1959**); Survey of ferrous-ferric chemical equilibria and redox potentials. Water Supply Paper 1459-A, United States Geological Survey, doi:10.3133/wsp1459A.

Hernes, P. J., Bergamaschi, B. A., Eckard, R. S., and Spencer, R. G. M. (**2009**); Fluorescence-based proxies for lignin in freshwater dissolved organic matter. *Journal of Geophysical Research* 114, p. G00F03, doi:10.1029/2009JG000938.

Holloway, J. M., Nordstrom, D. K., Böhlke, J., McCleskey, R. B., and Ball, J. W. (**2011**); Ammonium in thermal waters of Yellowstone National Park: Processes affecting speciation and isotope fractionation. *Geochimica et Cosmochimica Acta* 75(16), pp. 4611–4636, doi:10.1016/j.gca.2011.05.036.

Hou, W., Wang, S., Dong, H., Jiang, H., Briggs, B. R., Peacock, J. P., Huang, Q., Huang, L., Wu, G., Zhi, X., Li, W., Dodsworth, J. A., Hedlund, B. P., Zhang, C., Hartnett, H. E., Dijkstra, P., and Hungate, B. A. (**2013**); A comprehensive census of microbial diversity in hot springs of Tengchong, Yunnan Province China using 16S rRNA gene pyrosequencing. *PLoS ONE* 8(1), p. e53350, doi:10.1371/journal.pone.0053350.

Hudson, N., Baker, A., and Reynolds, D. (**2007**); Fluorescence analysis of dissolved organic matter in natural, waste and polluted waters: A review. *River Research and Applications* 23(6), pp. 631–649, doi:10.1002/rra.1005.

Huguet, A., Vacher, L., Relexans, S., Saubusse, S., Froidefond, J., and Parlanti, E. (**2009**); Properties of fluorescent dissolved organic matter in the Gironde Estuary. *Organic Geochemistry* 40(6), pp. 706–719, doi:10.1016/j.orggeochem.2009.03.002.

Hurwitz, S. and Lowenstern, J. B. (**2014**); Dynamics of the Yellowstone hydrothermal system. *Reviews of Geophysics* 52(3), pp. 375–411, doi:10.1002/2014RG000452.

Hutnik, C. M. L., MacManus, J. P., Banville, D., and Szabo, A. G. (**1991**); Metal induced changes in the fluorescence properties of tyrosine and tryptophan site-specific mutants of oncomodulin. *Biochemistry* 30(30), pp. 7652–7660, doi:10.1021/bi00244a038.

Ishii, S. K. L. and Boyer, T. H. (**2012**); Behavior of reoccurring PARAFAC components in fluorescent dissolved organic matter in natural and engineered systems: A critical review. *Environmental Science & Technology* 46(4), pp. 2006–2017, doi:10.1021/es2043504.

Jiao, N., Herndl, G. J., Hansell, D. A., Benner, R., Kattner, G., Wilhelm, S. W., Kirchman, D. L., Weinbauer, M. G., Luo, T., Chen, F., and Azam, F. (**2010**); Microbial production of recalcitrant dissolved organic matter: Long-term carbon storage in the global ocean. *Nature Reviews Microbiology* 8(8), pp. 593–599, doi:10.1038/nrmicro2386.

Johnson, J. W. and Norton, D. (**1991**); Critical phenomena in hydrothermal systems: State, thermodynamic, electrostatic, and transport properties of H_2O in the critical region. *American Journal of Science* 291(6), pp. 541–648, doi:10.2475/ajs.291.6.541.

Kalbitz, K., Solinger, S., Park, J.-H., Michalzik, B., and Matzner, E. (**2000**); Controls on the dynamics of dissolved organic matter in soils. *Soil Science* 165(4), pp. 277–304, doi:10.1097/00010694-200004000-00001.

Kalle, K. (**1937**); Meereskundliche chemische untersuchungen mit hilfe des Zeiss-Pulfrich photometers. *Annales hydrographiques* 65, pp. 276–282.

Kandasamy, S. and Nagender Nath, B. (**2016**); Perspectives on the terrestrial organic matter transport and burial along the land-deep sea continuum: Caveats in our understanding of biogeochemical processes and future needs. *Frontiers in Marine Science* 3, doi:10.3389/fmars.2016.00259.

Kawka, O. E. and Simoneit, B. R. (**1994**); Hydrothermal pyrolysis of organic matter in Guaymas Basin: I. Comparison of hydrocarbon distributions in subsurface sediments and seabed petroleums. *Organic Geochemistry* 22(6), pp. 947–978, doi:10.1016/0146-6380(94)90031-0.

Kelemen, S. R. and Fang, H. L. (**2001**); Maturity trends in raman spectra from kerogen and coal. *Energy & Fuels* 15(3), pp. 653–658, doi:10.1021/ef0002039.

Kellerman, A. M., Guillemette, F., Podgorski, D. C., Aiken, G. R., Butler, K. D., and Spencer, R. G. M. (**2018**); Unifying concepts linking dissolved organic matter composition to persistence in aquatic ecosystems. *Environmental Science & Technology* 52(5), pp. 2538–2548, doi:10.1021/acs.est.7b05513.

Kennedy, B., Lynch, M., Reynolds, J., and Smith, S. (**1985**); Intensive sampling of noble gases in fluids at Yellowstone: I. Early overview of the data; regional patterns. *Geochimica et Cosmochimica Acta* 49(5), pp. 1251–1261, doi:10.1016/0016-7037(85)90014-6.

Kharaka, Y., Sorey, M., and Thordsen, J. (**2000**); Large-scale hydrothermal fluid discharges in the Norris-Mammoth corridor, Yellowstone National Park, USA. *Journal of Geochemical Exploration* 69-70, pp. 201–205, doi:10.1016/S0375-6742(00)00025-X.

Kharaka, Y., Thordsen, J., and White, L. (**2002**); Isotope and chemical compositions of meteoric and thermal waters and snow from the greater Yellowstone National Park region. Open File Report 02-194, United States Geological Survey, doi:10.3133/ofr02194.

Kirk, T. K. and Obst, J. R. (**1988**); Lignin determination. In: Wood, W. A. and Kellogg, S. T. (eds.), *Biomass Part B: Lignin, Pectin, and Chitin*, *Methods in Enzymology*, volume 161, pp. 87–101, Elsevier, doi:10.1016/0076-6879(88)61014-7.

Kirschke, S., Bousquet, P., Ciais, P., Saunois, M., Canadell, J. G., Dlugokencky, E. J., Bergamaschi, P., Bergmann, D., Blake, D. R., Bruhwiler, L., Cameron-Smith, P., Castaldi, S., Chevallier, F., Feng, L., Fraser, A., Heimann, M., Hodson, E. L., Houweling, S., Josse, B., Fraser, P. J., Krummel, P. B., Lamarque, J.-F., Langenfelds, R. L., Le Quéré, C., Naik, V., O'Doherty, S., Palmer, P. I., Pison, I., Plummer, D., Poulter, B., Prinn, R. G., Rigby, M., Ringeval, B., Santini, M., Schmidt, M., Shindell, D. T., Simpson, I. J., Spahni, R., Steele, L. P., Strode, S. A., Sudo, K., Szopa, S., van der Werf, G. R., Voulgarakis, A., van Weele, M., Weiss, R. F., Williams, J. E., and Zeng, G. (**2013**); Three decades of global methane sources and sinks. *Nature Geoscience* 6(10), pp. 813–823, doi:10.1038/ngeo1955.

Klevenz, V., Sumoondur, A., Ostertag-Henning, C., and Koschinsky, A. (**2010**); Concentrations and distributions of dissolved amino acids in fluids from Mid-Atlantic Ridge hydrothermal vents. *Geochemical Journal* 44(5), pp. 387–397, doi: 10.2343/geochemj.1.0081.

Kompanichenko, V. N., Poturay, V. A., and Karpov, G. A. (**2016**); Organic compounds in thermal water: The Mutnovskii area and the Uzon caldera. *Journal of Volcanology and Seismology* 10(5), pp. 305–319, doi:10.1134/S0742046316050031.

Kowalczuk, P., Durako, M. J., Young, H., Kahn, A. E., Cooper, W. J., and Gonsior, M. (**2009**); Characterization of dissolved organic matter fluorescence in the South Atlantic Bight with use of PARAFAC model: Interannual variability. *Marine Chemistry* 113(3-4), pp. 182–196, doi:10.1016/j.marchem.2009.01.015.

Krauss, M., Jensen, J. O., and Hameka, H. F. (**1994**); Electronic structure of the excited states and phenol fluorescence. *The Journal of Physical Chemistry* 98(40), pp. 9955–9959, doi:10.1021/j100091a004.

Kvenvolden, K. A., Simoneit, B. R. T., and Love, J. D. (**1989**); Chemical and isotopic compositions of natural gas from seeps in Yellowstone and Grand Teton National Parks, Wyoming. In: *Gas Resources of Wyoming, Fourtieth Annual Field Conference Guidebook*, pp. 241–246, Wyoming Geological Association.

Lakowicz, J. R. (ed.) (**2010**); *Principles of fluorescence spectroscopy*. Third edition, Springer, Boston, Massachusetts, USA, doi:10.1007/978-0-387-46312-4.

Lang, S. Q., Butterfield, D. A., Lilley, M. D., Paul Johnson, H., and Hedges, J. I. (**2006**); Dissolved organic carbon in ridge-axis and ridge-flank hydrothermal systems. *Geochimica et Cosmochimica Acta* 70(15), pp. 3830–3842, doi: 10.1016/j.gca.2006.04.031.

LaRowe, D. E. and Van Cappellen, P. (**2011**); Degradation of natural organic matter: A thermodynamic analysis. *Geochimica et Cosmochimica Acta* 75(8), pp. 2030–2042, doi:10.1016/j.gca.2011.01.020.

LaRowe, D. E., Koch, B. P., Robador, A., Witt, M., Ksionzek, K., and Amend, J. P. (**2017**); Identification of organic compounds in ocean basement fluids. *Organic Geochemistry* 113, pp. 124–127, doi:10.1016/j.orggeochem.2017.07.017.

Laurion, I., Ventura, M., Catalan, J., Psenner, R., and Sommaruga, R. (**2000**); Attenuation of ultraviolet radiation in mountain lakes: Factors controlling the among- and within-lake variability. *Limnology and Oceanography* 45(6), pp. 1274–1288, doi: 10.4319/lo.2000.45.6.1274.

Leenheer, J. A. (**1981**); Comprehensive approach to preparative isolation and fractionation of dissolved organic carbon from natural waters and wastewaters. *Environmental Science & Technology* 15(5), pp. 578–587, doi:10.1021/es00087a010.

Leenheer, J. A. (**2009**); Systematic approaches to comprehensive analyses of natural organic matter. *Annals of Environmental Science* 3, pp. 1–130.

Li, X., Cai, W., An, J., Kim, S., Nah, J., Yang, D., Piner, R., Velamakanni, A., Jung, I., Tutuc, E., Banerjee, S. K., Colombo, L., and Ruoff, R. S. (**2009**); Large area synthesis of high quality and uniform graphene films on copper foils. *Science* 324(5932), pp. 1312–1314, doi:10.1126/science.1171245.

Liebscher, A. (**2007**); Experimental studies in model fluid systems. *Reviews in Mineralogy and Geochemistry* 65(1), pp. 15–47, doi:10.2138/rmg.2007.65.2.

Liebscher, A. (**2010**); Aqueous fluids at elevated pressure and temperature: Aqueous fluids at elevated pressure and temperature. *Geofluids* 10(1-2), pp. 3–19, doi:10.1111/j.1468-8123.2010.00293.x.

Lin, H.-T., Cowen, J. P., Olson, E. J., Amend, J. P., and Lilley, M. D. (**2012**); Inorganic chemistry, gas compositions and dissolved organic carbon in fluids from sedimented young basaltic crust on the Juan de Fuca Ridge flanks. *Geochimica et Cosmochimica Acta* 85, pp. 213–227, doi:10.1016/j.gca.2012.02.017.

Lloyd, E. F. (**1959**); The hot springs and hydrothermal eruptions of Waiotapu. *New Zealand Journal of Geology and Geophysics* 2(1), pp. 141–176, doi:10.1080/00288306.1959.10431319.

Longnecker, K., Sievert, S. M., Sylva, S. P., Seewald, J. S., and Kujawinski, E. B. (**2018**); Dissolved organic carbon compounds in deep-sea hydrothermal vent fluids from the East Pacific Rise. *Organic Geochemistry* 125, pp. 41–49, doi:10.1016/j.orggeochem.2018.08.004.

Lorenson, T. D. and Kvenvolden, K. A. (**1993**); A comparison of hydrocarbon gases from natural sources in the Northwestern United States. In: Howell, D. G., Wiese, K., Fanelli, M., Zink, L., and Cole, F. (eds.), *The Future of Energy Gases*, pp. 453–469, Professional Paper 1570, United States Geological Survey, doi:10.3133/pp1570.

Lorenson, T. D., Kvenvolden, K. A., Simoneit, B. R. T., and Leif, R. N. (**1991**); Composition of gas seeps in northwestern Wyoming. Open File Report 91-121, United States Geological Survey, doi:10.3133/ofr91121.

Love, J. D. and Good, J. M. (**1970**); Hydrocarbons in themal areas, northwestern Wyoming. Professional Paper 644-B, United States Geological Survey, doi:10.3133/pp644b.

Lovley, D. R., Coates, J. D., Blunt-Harris, E. L., Phillips, E. J. P., and Woodward, J. C. (**1996**); Humic substances as electron acceptors for microbial respiration. *Nature* 382(6590), pp. 445–448, doi:10.1038/382445a0.

Lowenstern, J. B. and Hurwitz, S. (**2008**); Monitoring a supervolcano in repose: Heat and volatile flux at the Yellowstone caldera. *Elements* 4(1), pp. 35–40, doi:10.2113/gselements.4.1.35.

Lowenstern, J. B., Bergfeld, D., Evans, W. C., and Hurwitz, S. (**2012**); Generation and evolution of hydrothermal fluids at Yellowstone: Insights from the Heart Lake Geyser Basin. *Geochemistry, Geophysics, Geosystems* 13(1), doi:10.1029/2011GC003835.

Luhr, S. (**2020**); GIS Data. Wyoming State Geological Survey, https://www.wsgs.wyo.gov/pubs-maps/gis.

Maie, N., Scully, N. M., Pisani, O., and Jaffé, R. (**2007**); Composition of a protein-like fluorophore of dissolved organic matter in coastal wetland and estuarine ecosystems. *Water Research* 41(3), pp. 563–570, doi:10.1016/j.watres.2006.11.006.

Maie, N., Sekiguchi, S., Watanabe, A., Tsutsuki, K., Yamashita, Y., Melling, L., Cawley, K. M., Shima, E., and Jaffé, R. (**2014**); Dissolved organic matter dynamics in the oligo/meso-haline zone of wetland-influenced coastal rivers. *Journal of Sea Research* 91, pp. 58–69, doi:10.1016/j.seares.2014.02.016.

MATLAB (**2010**); version 7.10.0 R2010a MatLab: The language of technical computing. The Mathworks Inc., Natick, Massachusetts, USA.

Mayer, L. M., Keil, R. G., Macko, S. A., Joye, S. B., Ruttenberg, K. C., and Aller, R. C. (**1998**); Importance of suspended participates in riverine delivery of bioavailable nitrogen to coastal zones. *Global Biogeochemical Cycles* 12(4), pp. 573–579, doi:10.1029/98GB02267.

Mayer, L. M., Schick, L. L., and Loder, T. C. (**1999**); Dissolved protein fluorescence in two Maine estuaries. *Marine Chemistry* 64(3), pp. 171–179, doi:10.1016/S0304-4203(98)00072-3.

McCollom, T., Seewald, J., and Simoneit, B. (**2001**); Reactivity of monocyclic aromatic compounds under hydrothermal conditions. *Geochimica et Cosmochimica Acta* 65(3), pp. 455–468, doi:10.1016/S0016-7037(00)00533-0.

McCollom, T. M. (**2013**); Miller-Urey and beyond: What have we learned about prebiotic organic synthesis reactions in the past 60 years? *Annual Review of Earth and Planetary Sciences* 41(1), pp. 207–229, doi:10.1146/annurev-earth-040610-133457.

McCollom, T. M., Ritter, G., and Simoneit, B. R. T. (**1999**a); Lipid synthesis under hydrothermal conditions by Fischer-Tropsch-type reactions. *Origins of Life and Evolution of the Biosphere* 29(2), pp. 153–166, doi:10.1023/A:1006592502746.

McCollom, T. M., Simoneit, B. R. T., and Shock, E. L. (**1999**b); Hydrous pyrolysis of polycyclic aromatic hydrocarbons and implications for the origin of PAH in hydrothermal petroleum. *Energy & Fuels* 13(2), pp. 401–410, doi:10.1021/ef980089i.

McCollom, T. M., Seewald, J. S., and German, C. R. (**2015**); Investigation of extractable organic compounds in deep-sea hydrothermal vent fluids along the Mid-Atlantic Ridge. *Geochimica et Cosmochimica Acta* 156, pp. 122–144, doi:10.1016/j.gca.2015.02.022.

McKnight, D. M., Boyer, E. W., Westerhoff, P. K., Doran, P. T., Kulbe, T., and Andersen, D. T. (**2001**); Spectrofluorometric characterization of dissolved organic matter for indication of precursor organic material and aromaticity. *Limnology and Oceanography* 46(1), pp. 38–48, doi:10.4319/lo.2001.46.1.0038.

Meng, F., Huang, G., Li, Z., and Li, S. (**2012**); Microbial transformation of structural and functional makeup of human-impacted riverine dissolved organic matter. *Industrial & Engineering Chemistry Research* 51(17), pp. 6212–6218, doi: 10.1021/ie300504d.

Meng, J., Yao, P., Yu, Z., Bianchi, T. S., Zhao, B., Pan, H., and Li, D. (**2014**); Speciation, bioavailability and preservation of phosphorus in surface sediments of the Changjiang Estuary and adjacent East China Sea inner shelf. *Estuarine, Coastal and Shelf Science* 144, pp. 27–38, doi:10.1016/j.ecss.2014.04.015.

Menzel, D. W. and Vaccaro, R. F. (**1964**); The measurement of dissolved organic and particulate carbon in seawater. *Limnology and Oceanography* 9(1), pp. 128–142, doi:10.4319/lo.1964.9.1.0138.

Meybeck, M. (**1993**); Riverine transport of atmospheric carbon: Sources, global typology and budget. *Water, Air, & Soil Pollution* 70(1-4), pp. 443–463, doi: 10.1007/BF01105015.

Meyer-Dombard, D. R., Shock, E. L., and Amend, J. P. (**2005**); Archaeal and bacterial communities in geochemically diverse hot springs of Yellowstone National Park, USA. *Geobiology* 3(3), pp. 211–227, doi:10.1111/j.1472-4669.2005.00052.x.

Meyers, S. R. (**2007**); Production and preservation of organic matter: The significance of iron. *Paleoceanography* 22(4), doi:10.1029/2006PA001332.

Mißbach, H., Schmidt, B. C., Duda, J.-P., Lünsdorf, N. K., Goetz, W., and Thiel, V. (**2018**); Assessing the diversity of lipids formed via Fischer-Tropsch-type reactions. *Organic Geochemistry* 119, pp. 110–121, doi:10.1016/j.orggeochem.2018.02.012.

Miller, H. M., Matter, J. M., Kelemen, P., Ellison, E. T., Conrad, M. E., Fierer, N., Ruchala, T., Tominaga, M., and Templeton, A. S. (**2016**); Modern water/rock reactions in Oman hyperalkaline peridotite aquifers and implications for microbial habitability. *Geochimica et Cosmochimica Acta* 179, pp. 217–241, doi:10.1016/j.gca.2016.01.033.

Müller, M., Handley, K. M., Lloyd, J., Pancost, R. D., and Mills, R. A. (**2010**); Biogeochemical controls on microbial diversity in seafloor sulphidic sediments. *Geobiology* 8(4), pp. 309–326, doi:10.1111/j.1472-4669.2010.00242.x.

Montana State University (**2000**); Evening Primrose Spring details. Yellowstone Research Coordination Network, http://rcn.montana.edu/Features/Detail.aspx?id=1898.

Murozumi, M., Abiko, T., and Nakamura, S. (**1966**); Geochemical investigation of the Noboribetsu Oyunuma explosion crater lake. *Second Series Bulletin of the Volcanological Society of Japan* 11(1), pp. 1–16.

Murphy, K. R., Ruiz, G. M., Dunsmuir, W. T. M., and Waite, T. D. (**2006**); Optimized parameters for fluorescence-based verification of ballast water exchange by ships. *Environmental Science & Technology* 40(7), pp. 2357–2362, doi: 10.1021/es0519381.

Murphy, K. R., Stedmon, C. A., Waite, T. D., and Ruiz, G. M. (**2008**); Distinguishing between terrestrial and autochthonous organic matter sources in marine environments using fluorescence spectroscopy. *Marine Chemistry* 108(1-2), pp. 40–58, doi:10.1016/j.marchem.2007.10.003.

Murphy, K. R., Butler, K. D., Spencer, R. G. M., Stedmon, C. A., Boehme, J. R., and Aiken, G. R. (**2010**); Measurement of dissolved organic matter fluorescence in aquatic environments: An interlaboratory comparison. *Environmental Science & Technology* 44(24), pp. 9405–9412, doi:10.1021/es102362t.

National Park Service (**2019**a); Park Facts - Yellowstone National Park. U.S. National Park Service, https://www.nps.gov/yell/planyourvisit/parkfacts.htm.

National Park Service (**2019**b); Yellowstone's Photo Collection. U.S. National Park Service, https://www.nps.gov/features/yell/slidefile/history/1946_1999/thermalfeatures/Page-1.htm.

Niermann, D. (**2019**); Sylvan Springs group. Volcanic-springs.com, http://volcanic-springs.com/index.php?section=USA&usasection=gibbongeyserbasin&usasubsection=sylvanspringsgroup.

Nordstrom, K. D., McCleskey, B. R., and Ball, J. W. (**2009**); Sulfur geochemistry of hydrothermal waters in Yellowstone National Park: IV Acid-sulfate waters. *Applied Geochemistry* 24(2), pp. 191–207, doi:10.1016/j.apgeochem.2008.11.019.

Notaro, M., Emmett, K., and O'Leary, D. (**2019**); Spatio-temporal variability in remotely sensed vegetation greenness across Yellowstone National Park. *Remote Sensing* 11(7), p. 798, doi:10.3390/rs11070798.

Nye, J., Shock, E., and Hartnett, H. (**2020**); A novel PARAFAC model for continental hot springs reveals unique dissolved organic carbon compositions. *Organic Geochemistry* 141(103964), doi:10.1016/j.orggeochem.2019.103964.

Ohno, T. (**2002**); Fluorescence inner-filtering correction for determining the humification index of dissolved organic matter. *Environmental Science & Technology* 36(4), pp. 742–746, doi:10.1021/es0155276.

Ohno, T., Fernandez, I. J., Hiradate, S., and Sherman, J. F. (**2007**); Effects of soil acidification and forest type on water soluble soil organic matter properties. *Geoderma* 140(1-2), pp. 176–187, doi:10.1016/j.geoderma.2007.04.004.

Ohno, T., Amirbahman, A., and Bro, R. (**2008**); Parallel factor analysis of excitation-emission matrix fluorescence spectra of water soluble soil organic matter as basis for the determination of conditional metal binding parameters. *Environmental Science & Technology* 42(1), pp. 186–192, doi:10.1021/es071855f.

Osburn, C. L., Del Vecchio, R., and Boyd, T. J. (**2014**); Physicochemical effects on dissolved organic natter fluorescence in natural waters. In: Coble, P., Lead, J., Baker, A., Reynolds, D. M., and Spencer, R. G. (eds.), *Aquatic Organic Matter Fluorescence*, pp. 233–277, Cambridge Environmental Chemistry Series, Cambridge University Press, New York, USA, doi:10.1017/CBO9781139045452.012.

Parlanti, E., Wörz, K., Geoffroy, L., and Lamotte, M. (**2000**); Dissolved organic matter fluorescence spectroscopy as a tool to estimate biological activity in a coastal zone submitted to anthropogenic inputs. *Organic Geochemistry* 31(12), pp. 1765–1781, doi:10.1016/S0146-6380(00)00124-8.

Parlanti, E., Morin, B., and Vacher, L. (**2002**); Combined 3D-spectrofluorometry, high performance liquid chromatography and capillary electrophoresis for the characterization of dissolved organic matter in natural waters. *Organic Geochemistry* 33(3), pp. 221–236, doi:10.1016/S0146-6380(01)00154-1.

Pettersen, R. C. (**1984**); The chemical composition of wood. In: Rowell, R. (ed.), *The Chemistry of Solid Wood*, *Advances in Chemistry*, volume 207, pp. 57–126, American Chemical Society, Washington, D. C., USA, doi:10.1021/ba-1984-0207.ch002.

R Core Team (**2018**); version 1.1.453 r-Studio version 3.5.0 R: A language and environment for statistical computing. R Studio for Statistical Computing, Vienna, Austria, https://www.R-project.org/.

Raymond, P. A. and Bauer, J. E. (**2001**); Riverine export of aged terrestrial organic matter to the North Atlantic Ocean. *Nature* 409(6819), pp. 497–500, doi:10.1038/35054034.

Reeburgh, W. S. (**2007**); Oceanic methane biogeochemistry. *Chemical Reviews* 107(2), pp. 486–513, doi:10.1021/cr050362v.

Reeves, E. P., McDermott, J. M., and Seewald, J. S. (**2014**); The origin of methanethiol in midocean ridge hydrothermal fluids. *Proceedings of the National Academy of Sciences* 111(15), pp. 5474–5479, doi:10.1073/pnas.1400643111.

Remko, M., Fitz, D., Broer, R., and Rode, B. M. (**2011**); Effect of metal ions (Ni^{2+}, Cu^{2+} and Zn^{2+}) and water coordination on the structure of L-phenylalanine, L-tyrosine, L-tryptophan and their zwitterionic forms. *Journal of Molecular Modeling* 17(12), pp. 3117–3128, doi:10.1007/s00894-011-1000-0.

Riedel, T., Biester, H., and Dittmar, T. (**2012**); Molecular fractionation of dissolved organic matter with metal salts. *Environmental Science & Technology* 46(8), pp. 4419–4426, doi:10.1021/es203901u.

Robinson, K. J., Gould, I. R., Fecteau, K. M., Hartnett, H. E., Williams, L. B., and Shock, E. L. (**2019**); Deamination reaction mechanisms of protonated amines under hydrothermal conditions. *Geochimica et Cosmochimica Acta* 244, pp. 113–128, doi:10.1016/j.gca.2018.09.020.

Robinson, K. J., Fecteau, K. M., Gould, I. R., Hartnett, H. E., Williams, L. B., and Shock, E. L. (**2020**); Metastable equilibrium of substitution reactions among oxygen- and nitrogen-bearing organic compounds at hydrothermal conditions. *Geochimica et Cosmochimica Acta* 272, pp. 93–104, doi:10.1016/j.gca.2019.12.030.

Rose, A. L. and Waite, T. (**2003**); Kinetics of iron complexation by dissolved natural organic matter in coastal waters. *Marine Chemistry* 84(1-2), pp. 85–103, doi:10.1016/S0304-4203(03)00113-0.

Rossel, P. E., Stubbins, A., Rebling, T., Koschinsky, A., Hawkes, J. A., and Dittmar, T. (**2017**); Thermally altered marine dissolved organic matter in hydrothermal fluids. *Organic Geochemistry* 110, pp. 73–86, doi:10.1016/j.orggeochem.2017.05.003.

Rubin, A. J. (ed.) (**1974**); *Aqueous-Environmental Chemistry of Metals*. Ann Arbor Science Publishers, Ann Arbor, Michigan, USA.

Rudnick, S. M. and Chen, R. F. (**1998**); Laser-induced fluorescence of pyrene and other polycyclic aromatic hydrocarbons (PAH) in seawater. *Talanta* 47(4), pp. 907–919, doi:10.1016/S0039-9140(98)00160-X.

Rye, R. O. and Truesdell, A. H. (**2007**); The question of recharge to the deep thermal reservoir underlying the geysers and hot springs of Yellowstone National Park. Professional Paper 1717-H, United States Geological Survey, doi:10.3133/pp1717H.

Saari, L. A. and Seitz, W. R. (**1983**); Immobilized morin as fluorescence sensor for determination of aluminum(III). *Analytical Chemistry* 55(4), pp. 667–670, doi:10.1021/ac00255a020.

Santos, E. H., Filipe, O. M. S., Duarte, R. M. B. O., Pinto, H., and Duarte, A. C. (**2000**); Fluorescence as a tool for tracing organic contamination from pulp mill effluents in surface waters. *Acta Hydrochimica et Hydrobiologica* 28(7), pp. 364–371.

Seewald, J. S. (**2003**); Organic-inorganic interactions in petroleum-producing sedimentary basins. *Nature* 426(6964), pp. 327–333, doi:10.1038/nature02132.

Senesi, N., Miano, T. M., Provenzano, M. R., and Brunetti, G. (**1991**); Characterization, differentiation, and classification of humic substances by fluorescence spectroscopy. *Soil Science* 152(4), pp. 259–271, doi:10.1097/00010694-199110000-00004.

Shah Walter, S. R., Jaekel, U., Osterholz, H., Fisher, A. T., Huber, J. A., Pearson, A., Dittmar, T., and Girguis, P. R. (**2018**); Microbial decomposition of marine dissolved organic matter in cool oceanic crust. *Nature Geoscience* 11(5), pp. 334–339, doi:10.1038/s41561-018-0109-5.

Shams El-Din, N. G., Mohamedein, L. I., and El-Moselhy, K. M. (**2014**); Seaweeds as bioindicators of heavy metals off a hot spot area on the Egyptian Mediterranean Coast during 2008-2010. *Environmental Monitoring and Assessment* 186(9), pp. 5865–5881, doi:10.1007/s10661-014-3825-3.

Sharp, J., Beauregard, A., Burdige, D., Cauwet, G., Curless, S., Lauck, R., Nagel, K., Ogawa, H., Parker, A., Primm, O., Pujo-Pay, M., Savidge, W., Seitzinger, S., Spyres, G., and Styles, R. (**2004**); A direct instrument comparison for measurement of total dissolved nitrogen in seawater. *Marine Chemistry* 84(3-4), pp. 181–193, doi:10.1016/j.marchem.2003.07.003.

Sharp, J. H. (**1997**); Marine dissolved organic carbon: Are the older values correct? *Marine Chemistry* 56(3-4), pp. 265–277, doi:10.1016/S0304-4203(96)00075-8.

Sharp, J. H., Benner, R., Bennett, L., Carlson, C. A., Dow, R., and Fitzwater, S. E. (**1993**); Re-evaluation of high temperature combustion and chemical oxidation measurements of dissolved organic carbon in seawater. *Limnology and Oceanography* 38(8), pp. 1774–1782, doi:10.4319/lo.1993.38.8.1774.

Shipp, J., Gould, I. R., Herckes, P., Shock, E. L., Williams, L. B., and Hartnett, H. E. (**2013**); Organic functional group transformations in water at elevated temperature and pressure: Reversibility, reactivity, and mechanisms. *Geochimica et Cosmochimica Acta* 104, pp. 194–209, doi:10.1016/j.gca.2012.11.014.

Shock, E., Bockisch, C., Estrada, C., Fecteau, K., Gould, I. R., Hartnett, H., Johnson, K., Robinson, K., Shipp, J., and Williams, L. (**2019**); Earth as organic chemist. In: Orcutt, B. N., Daniel, I., and Dasgupta, R. (eds.), *Deep Carbon: Past and Present*, pp. 415–446, Cambridge University Press, Cambridge, UK, doi:10.1017/97811086 77950.014.

Shock, E. L. and Helgeson, H. C. (**1990**); Calculation of the thermodynamic and transport properties of aqueous species at high pressures and temperatures: Standard partial molal properties of organic species. *Geochimica et Cosmochimica Acta* 54(4), pp. 915–945, doi:10.1016/0016-7037(90)90429-O.

Shock, E. L., Holland, M., Meyer-Dombard, D., Amend, J. P., Osburn, G., and Fischer, T. P. (**2010**); Quantifying inorganic sources of geochemical energy in hydrothermal ecosystems, Yellowstone National Park, USA. *Geochimica et Cosmochimica Acta* 74(14), pp. 4005–4043, doi:10.1016/j.gca.2009.08.036.

Shock, E. L., Canovas, P., Yang, Z., Boyer, G., Johnson, K., Robinson, K., Fecteau, K., Windman, T., and Cox, A. (**2013**); Thermodynamics of organic transformations in hydrothermal fluids. *Reviews in Mineralogy and Geochemistry* 76(1), pp. 311–350, doi:10.2138/rmg.2013.76.9.

SigmaPlot (**2008**); version 11.0, SigmaPlot: Exact graphs and data analysis. Systat Software, San Jose, California, USA, www.systatsoftware.com.

Simoneit, B. R. (**1993**); Aqueous high-temperature and high-pressure organic geochemistry of hydrothermal vent systems. *Geochimica et Cosmochimica Acta* 57, pp. 3231–3243.

Simoneit, B. R. and Fetzer, J. C. (**1996**); High molecular weight polycyclic aromatic hydrocarbons in hydrothermal petroleums from the Gulf of California and Northeast Pacific Ocean. *Organic Geochemistry* 24(10-11), pp. 1065–1077, doi: 10.1016/S0146-6380(96)00081-2.

Simoneit, B. R. T., Summons, R. E., and Jahnke, L. L. (**1998**); Biomarkers as tracers for life on early Earth and Mars. *Origins of Life and Evolution of the Biosphere* 28(4/6), pp. 475–483, doi:10.1023/A:1006508012904.

Singh, B. K., Bardgett, R. D., Smith, P., and Reay, D. S. (**2010**); Microorganisms and climate change: terrestrial feedbacks and mitigation options. *Nature Reviews Microbiology* 8(11), pp. 779–790, doi:10.1038/nrmicro2439.

Smedes, H. W. and Prostka, H. J. (**1972**); Stratigraphic framework of the Absaroka Volcanic Supergroup. Professional Paper 729-C, United States Geological Survey, doi:10.3133/pp729C.

Stedmon, C. A. and Bro, R. (**2008**); Characterizing dissolved organic matter fluorescence with parallel factor analysis, a tutorial: Fluorescence-PARAFAC analysis of DOM. *Limnology and Oceanography: Methods* 6(11), pp. 572–579, doi: 10.4319/lom.2008.6.572.

Stedmon, C. A. and Markager, S. (**2005**); Resolving the variability in dissolved organic matter fluorescence in a temperate estuary and its catchment using PARAFAC analysis. *Limnology and Oceanography* 50(2), pp. 686–697, doi:10.4 319/lo.2005.50.2.0686.

Stedmon, C. A., Markager, S., and Bro, R. (**2003**); Tracing dissolved organic matter in aquatic environments using a new approach to fluorescence spectroscopy. *Marine Chemistry* 82(3-4), pp. 239–254, doi:10.1016/S0304-4203(03)00072-0.

Stedmon, C. A., Thomas, D. N., Granskog, M., Kaartokallio, H., Papadimitriou, S., and Kuosa, H. (**2007**); Characteristics of dissolved organic matter in Baltic coastal sea ice: Allochthonous or autochthonous origins? *Environmental Science & Technology* 41(21), pp. 7273–7279, doi:10.1021/es071210f.

Stubbins, A., Spencer, R. G. M., Chen, H., Hatcher, P. G., Mopper, K., Hernes, P. J., Mwamba, V. L., Mangangu, A. M., Wabakanghanzi, J. N., and Six, J. (**2010**); Illuminated darkness: Molecular signatures of Congo River dissolved organic matter and its photochemical alteration as revealed by ultrahigh precision mass spectrometry. *Limnology and Oceanography* 55(4), pp. 1467–1477, doi: 10.4319/lo.2010.55.4.1467.

Stubbins, A., Lapierre, J.-F., Berggren, M., Prairie, Y. T., Dittmar, T., and del Giorgio, P. A. (**2014**); What's in an EEM? Molecular signatures associated with dissolved organic fluorescence in boreal Canada. *Environmental Science & Technology* 48(18), pp. 10598–10606, doi:10.1021/es502086e.

Taha, H. M., Said, H. A., Abbas, N. H., and Khaleafa, A. F. M. (**2009**); Biosorption and biodegradation of the antifouling compound tributyltin (TBT) by microalgae. *American-Eurasian Journal of Scientific Research* 4(1), pp. 1–6.

Takeno, N. (**2005**); Atlas of Eh pH diagrams. Open File Report 419, Geological Survey of Japan, AIST.

Toner, B. M., Fakra, S. C., Manganini, S. J., Santelli, C. M., Marcus, M. A., Moffett, J. W., Rouxel, O., German, C. R., and Edwards, K. J. (**2009**); Preservation of iron(II) by carbon-rich matrices in a hydrothermal plume. *Nature Geoscience* 2(3), pp. 197–201, doi:10.1038/ngeo433.

Urschel, M. R., Kubo, M. D., Hoehler, T. M., Peters, J. W., and Boyd, E. S. (**2015**); Carbon source preference in chemosynthetic hot spring communities. *Applied and Environmental Microbiology* 81(11), pp. 3834–3847, doi:10.1128/AEM.00511-15.

Ventura, G. T., Simoneit, B. R., Nelson, R. K., and Reddy, C. M. (**2012**); The composition, origin and fate of complex mixtures in the maltene fractions of hydrothermal petroleum assessed by comprehensive two-dimensional gas chromatography. *Organic Geochemistry* 45, pp. 48–65, doi:10.1016/j.orggeochem.2012.01.002.

Wagner, W. and Pruß, A. (**2002**); The IAPWS formulation 1995 for the thermodynamic properties of ordinary water substance for general and scientific use. *Journal of Physical and Chemical Reference Data* 37, pp. 387–535, doi:10.1063/1.1461829.

Wang, H.-B., Zhang, Y.-J., Xiao, X., Jin, D., Zhao, N.-J., Yin, G.-F., Guo, L.-Q., and Liu, W.-Q. (**2010**); Excitation-emission fluorescence characterization study of the three phenolic compounds. *Spectroscopy and Spectral Analysis* 30(5), pp. 1271–1274, doi:10.3964/j.issn.1000-0593(2010)05-1271-04.

Weishaar, J. L., Aiken, G. R., Bergamaschi, B. A., Fram, M. S., Fujii, R., and Mopper, K. (**2003**); Evaluation of specific ultraviolet absorbance as an indicator of the chemical composition and reactivity of dissolved organic carbon. *Environmental Science & Technology* 37(20), pp. 4702–4708, doi:10.1021/es030360x.

Werner, C., Brantley, S. L., and Boomer, K. (**2000**); CO2 emissions related to the Yellowstone volcanic system. *Journal of Geophysical Research: Solid Earth* 105(B5), pp. 10831–10846, doi:10.1029/1999JB900331.

Werner, C., Hurwitz, S., Evans, W. C., Lowenstern, J. B., Bergfeld, D., Heasler, H., Jaworowski, C., and Hunt, A. (**2008**); Volatile emissions and gas geochemistry of Hot Spring Basin, Yellowstone National Park, USA. *Journal of Volcanology and Geothermal Research* 178(4), pp. 751–762, doi:10.1016/j.jvolgeores.2008.09.016.

White, D. E., Muffler, L. J. P., and Truesdell, A. H. (**1971**); Vapor-dominated hydrothermal systems compared with hot-water systems. *Economic Geology* 66(1), pp. 75–97, doi:10.2113/gsecongeo.66.1.75.

White, D. E., Hutchinson, R. A., and Keith, T. E. C. (**1988**); The geology and remarkable thermal activity of Norris Geyser Basin, Yellowstone National Park, Wyoming. Professional Paper 1456, United States Geological Survey, doi:10.3133/pp1456.

Wichard, T. (**2016**); Identification of metallophores and organic ligands in the chemosphere of the marine macroalga ulva (chlorophyta) and at land-sea interfaces. *Frontiers in Marine Science* 3, doi:10.3389/fmars.2016.00131.

Willams, P. M. (**1969**); Determination of dissolved organic carbon in seawater: A comparison of two methods. *Limnology and Oceanography* 14(2), pp. 297–298, doi:10.4319/lo.1969.14.2.0297.

Williams, C. J., Yamashita, Y., Wilson, H. F., Jaffé, R., and Xenopoulos, M. A. (**2010**); Unraveling the role of land use and microbial activity in shaping dissolved organic matter characteristics in stream ecosystems. *Limnology and Oceanography* 55(3), pp. 1159–1171, doi:10.4319/lo.2010.55.3.1159.

Wilson, H. F. and Xenopoulos, M. A. (**2009**); Effects of agricultural land use on the composition of fluvial dissolved organic matter. *Nature Geoscience* 2(1), pp. 37–41, doi:10.1038/ngeo391.

Windman, T., Zolotova, N., Schwandner, F., and Shock, E. L. (**2007**); Formate as an energy source for microbial metabolism in chemosynthetic zones of hydrothermal ecosystems. *Astrobiology* 7(6), pp. 873–890, doi:10.1089/ast.2007.0127.

Wu, J., Zhang, H., He, P.-J., and Shao, L.-M. (**2011**); Insight into the heavy metal binding potential of dissolved organic matter in MSW leachate using EEM quenching combined with PARAFAC analysis. *Water Research* 45(4), pp. 1711–1719, doi:10.1016/j.watres.2010.11.022.

Wu, X., Wu, L., Liu, Y., Zhang, P., Li, Q., Zhou, J., Hess, N. J., Hazen, T. C., Yang, W., and Chakraborty, R. (**2018**); Microbial interactions with dissolved organic matter drive carbon dynamics and community succession. *Frontiers in Microbiology* 9(1234), doi:10.3389/fmicb.2018.01234.

Xie, W., Zhang, C. L., Wang, J., Chen, Y., Zhu, Y., de la Torre, J. R., Dong, H., Hartnett, H. E., Hedlund, B. P., and Klotz, M. G. (**2014**); Distribution of ether lipids and composition of the archaeal community in terrestrial geothermal springs: Impact of environmental variables: Archaeal lipids from terrestrial hot springs. *Environmental Microbiology* 17(5), pp. 1600–1614, doi:10.1111/1462-2920.12595.

Xu, Y., Schoonen, M., Nordstrom, D., Cunningham, K., and Ball, J. (**1998**); Sulfur geochemistry of hydrothermal waters in Yellowstone National Park: I. The origin of thiosulfate in hot spring waters. *Geochimica et Cosmochimica Acta* 62(23-24), pp. 3729–3743, doi:10.1016/S0016-7037(98)00269-5.

Xu, Y., Schoonen, M., Nordstrom, D., Cunningham, K., and Ball, J. (**2000**); Sulfur geochemistry of hydrothermal waters in Yellowstone National Park, Wyoming, USA. II. Formation and decomposition of thiosulfate and polythionate in Cinder Pool. *Journal of Volcanology and Geothermal Research* 97(1-4), pp. 407–423, doi:10.1016/S0377-0273(99)00173-0.

Yamashita, Y. and Jaffé, R. (**2008**); Characterizing the interactions between trace metals and dissolved organic matter using excitation emission matrix and parallel factor analysis. *Environmental Science & Technology* 42(19), pp. 7374–7379, doi:10.1021/es801357h.

Yamashita, Y. and Tanoue, E. (**2003**); Chemical characterization of protein-like fluorophores in DOM in relation to aromatic amino acids. *Marine Chemistry* 82(3-4), pp. 255–271, doi:10.1016/S0304-4203(03)00073-2.

Yamashita, Y., Jaffé, R., Maie, N., and Tanoue, E. (**2008**); Assessing the dynamics of dissolved organic matter (DOM) in coastal environments by excitation emission matrix fluorescence and parallel factor analysis (EEM-PARAFAC). *Limnology and Oceanography* 53(5), pp. 1900–1908, doi:10.4319/lo.2008.53.5.1900.

Yamashita, Y., Panton, A., Mahaffey, C., and Jaffé, R. (**2011**); Assessing the spatial and temporal variability of dissolved organic matter in Liverpool Bay using excitation-emission matrix fluorescence and parallel factor analysis. *Ocean Dynamics* 61(5), pp. 569–579, doi:10.1007/s10236-010-0365-4.

Yamashita, Y., Boyer, J. N., and Jaffé, R. (**2013**); Evaluating the distribution of terrestrial dissolved organic matter in a complex coastal ecosystem using fluorescence spectroscopy. *Continental Shelf Research* 66, pp. 136–144, doi:10.1016/j.csr.2013.06.010.

Yang, Y. and Zhang, D. (**1995**); Concentration effect on the fluorescence spectra of humic substances. *Communications in Soil Science and Plant Analysis* 26(15-16), pp. 2333–2349, doi:10.1080/00103629509369451.

Yang, Z., Gould, I. R., Williams, L. B., Hartnett, H. E., and Shock, E. L. (**2012**); The central role of ketones in reversible and irreversible hydrothermal organic functional group transformations. *Geochimica et Cosmochimica Acta* 98, pp. 48–65, doi:10.1016/j.gca.2012.08.031.

Yasuda, S., Fukushima, K., and Kakehi, A. (**2001**); Formation and chemical structures of acid-soluble lignin I: Sulfuric acid treatment time and acid-soluble lignin content of hardwood. *Journal of Wood Science* 47(1), pp. 69–72, doi:10.1007/BF00776648.

Zepp, R. G., Sheldon, W. M., and Moran, M. A. (**2004**); Dissolved organic fluorophores in southeastern US coastal waters: Correction method for eliminating Rayleigh and Raman scattering peaks in excitation-emission matrices. *Marine Chemistry* 89(1-4), pp. 15–36, doi:10.1016/j.marchem.2004.02.006.

Zheng, H., Xu, C., Yang, L., Chen, J., Chen, C.-T. A., and Wang, B.-J. (**2017**); Diurnal variations of dissolved organic matter in the hydrothermal system of Green Island, Taiwan. *Marine Chemistry* 195, pp. 61–69, doi:10.1016/j.marchem.2017.05.003.

Zsolnay, A., Baigar, E., Jimenez, M., Steinweg, B., and Saccomandi, F. (**1999**); Differentiating with fluorescence spectroscopy the sources of dissolved organic matter in soils subjected to drying. *Chemosphere* 38(1), pp. 45–50, doi:10.1016/S0045-6535(98)00166-0.

APPENDIX A

CHAPTER 2 SUPPLEMENTAL INFORMATION

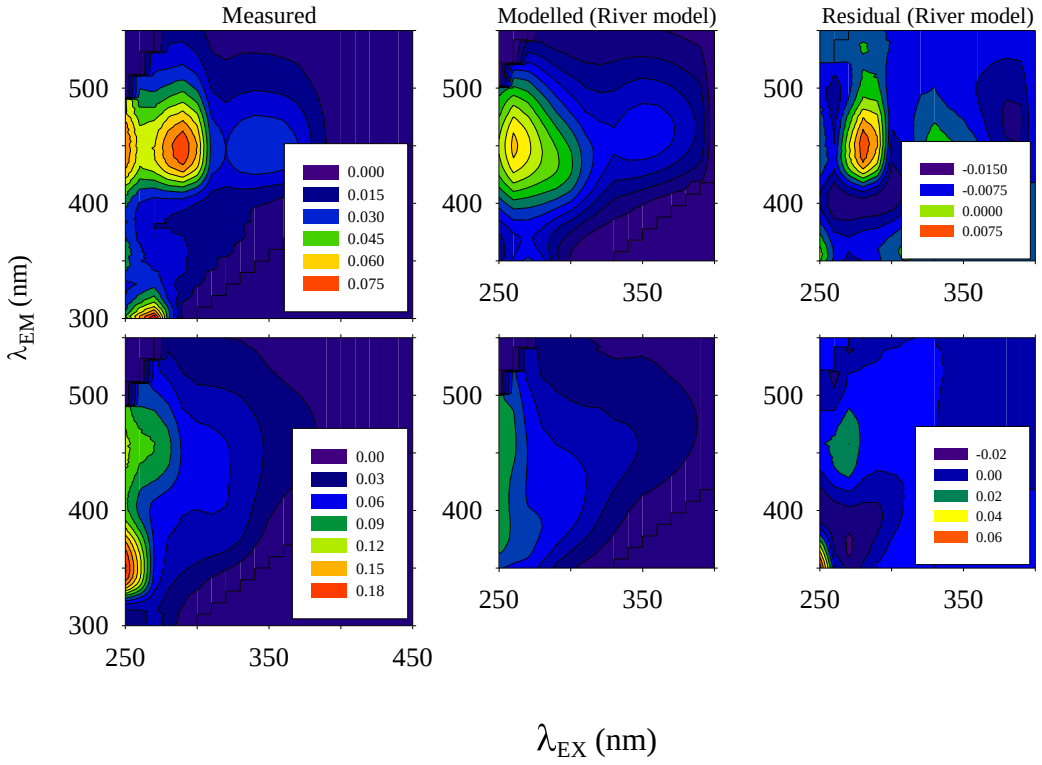

Figure A.1: Residual analysis of several hot spring samples using the standard surface water model (e.g., Cory and McKnight, 2005) reveals an inadequate fit for hot spring fluorescence, especially in the short-wavelength region of the EEM where we observe prominent signals in many acidic springs. Note the Cory and McKnight (2005) model employs a somewhat narrower wavelength range (e.g., λ_{EX} = 250-400, λ_{EM} = 250-550.

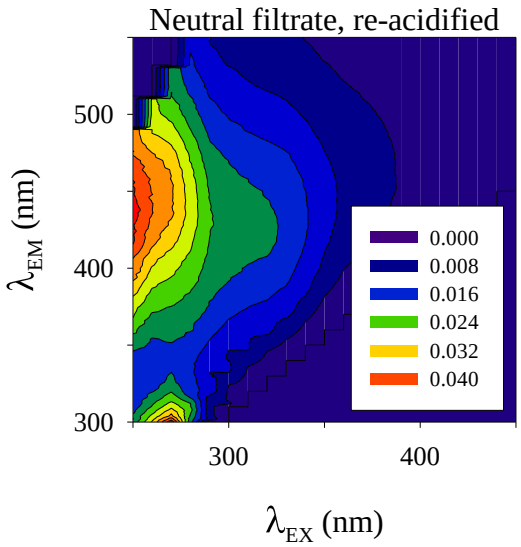

Figure A.2: Neutral filtrate (re-acidified) of the hot spring sample used in acid-spring component solubility experiments (Figure 2.9). Precipitation and removal of the acid-spring component fluorophores reveals the presence of humic-like and protein-like fluorescence when using a narrower intensity scale than used for the filtered, acidified field sample.

Table A.1: Spring geochemistry and fluorescence indices for modelled hot spring samples. Dashes indicate no data was collected.
*Specific (sp.) conductivity is the temperature compensated conductivity value. Field conductivity values were temperature compensated to a standard temperature of 25℃ according to the following reference: Hamilton, T.L., Boyd, E.S., Peters, J.W. (2011), Environmental constraints underpin the distribution and phylogenetic diversity of nifH in the Yellowstone geothermal complex. Microbial Ecology 61, 860–870.
**DOC error was calculated as the standard deviation of three replicate injections

Sample Index	Year	Sample Region	pH	Temp. ℃	Sp. Cond.* μS/cm	DOC mol C/L	DOC error**	Total Fluor.	Fluor. Index	Humification Index	β/α
1	2011	Tengchong	9.36	89.0	1754.4	1.58E-04	2.50E-05	4.86	1.37	0.785	0.936
2	2011	Tengchong	9.35	93.0	1678.0	1.46E-04	1.67E-05	4.72	1.44	0.730	0.982
3	2011	Tengchong	9.25	93.6	1711.6	1.36E-04	1.67E-05	4.53	1.45	0.828	1.114
4	2011	Tengchong	9.39	83.2	1765.2	1.38E-04	1.67E-05	4.45	1.50	1.029	0.940
5	2011	Tengchong	4.79	89.1	176.6	1.61E-04	2.50E-05	10.59	1.43	2.420	0.812
6	2011	Tengchong	8.11	90.0	1630.4	1.42E-04	1.67E-05	4.00	1.44	0.738	0.972
7	2011	Tengchong	8.05	92.3	1509.0	1.60E-04	1.67E-05	4.24	1.44	1.280	0.902
8	2011	Tengchong	8.04	79.8	1312.0	1.65E-04	1.67E-05	10.67	1.36	3.188	0.703
9	2011	Tengchong	8.28	78.2	1322.7	1.38E-04	1.67E-05	8.56	1.35	2.637	0.764
10	2011	Tengchong	7.29	73.8	1417.0	1.21E-04	1.67E-05	3.04	1.58	2.118	0.861
11	2011	Tengchong	7.29	73.8	1417.0	1.23E-04	1.67E-05	2.82	1.54	2.506	0.874
12	2011	Tengchong	6.71	81.6	1022.5	1.35E-04	1.67E-05	2.36	1.46	1.569	0.742
13	2011	Tengchong	7.04	80.7	- - -	2.36E-05	1.38E-07	8.74	1.59	2.137	0.758
14	2011	Tengchong	7.72	75.0	- - -	2.44E-05	4.21E-07	7.55	1.44	1.646	0.666
15	2011	Tengchong	8.10	90.0	- - -	2.97E-05	2.99E-07	9.78	1.42	0.874	0.836
16	2011	Tengchong	8.10	92.0	- - -	1.62E-04	4.58E-06	11.65	1.46	0.680	0.766
17	2011	Tengchong	9.40	93.0	- - -	- - -	- - -	8.50	1.37	0.790	0.839
18	2011	Tengchong	9.40	89.0	- - -	2.31E-05	6.25E-07	8.31	1.40	0.830	0.785
19	2011	Tengchong	9.30	94.0	- - -	2.45E-05	4.86E-07	8.65	1.42	0.704	0.833
20	2011	Tengchong	4.70	92.1	- - -	1.09E-04	3.81E-06	13.10	1.46	3.280	0.721
21	2011	Tengchong	8.27	72.1	- - -	1.36E-04	3.67E-06	11.40	1.43	1.008	0.723
22	2011	Tengchong	7.00	69.0	- - -	1.71E-04	3.12E-06	120.74	1.54	9.459	0.757

Sample Index	Year	Sample Region	pH	Temp. ℃	Sp. Cond.* μS/cm	DOC mol C/L	DOC error**	Total Fluor.	Fluor. Index	Humification Index	β/α
23	2011	Tengchong	9.40	83.5	- - -	1.92E-05	1.31E-06	7.34	1.49	1.101	0.949
24	2011	Tengchong	8.98	84.7	- - -	2.58E-05	2.74E-07	6.01	1.55	1.662	0.840
25	2011	Tengchong	7.01	84.0	- - -	4.41E-04	6.10E-06	7.18	1.60	2.591	0.826
26	2011	Tengchong	6.78	71.9	- - -	1.83E-05	1.05E-06	6.54	1.57	4.293	0.744
27	2011	Tengchong	7.08	63.8	- - -	1.67E-05	3.24E-07	7.62	1.57	3.311	0.776
28	2011	Tengchong	7.28	67.2	- - -	2.37E-05	2.17E-07	6.08	1.57	1.845	0.821
29	2011	Tengchong	7.31	86.0	- - -	1.77E-04	1.31E-07	8.95	1.61	0.972	0.679
30	2013	Tengchong	9.00	90.7	1620.6	1.31E-04	8.34E-08	6.39	1.44	1.299	0.980
31	2013	Tengchong	8.93	88.5	1647.6	1.13E-04	2.21E-07	8.00	1.48	1.618	1.091
32	2013	Tengchong	8.94	84.8	1703.1	1.13E-04	6.48E-07	5.97	1.56	1.260	1.091
33	2013	Tengchong	6.36	74.6	645.1	1.27E-04	1.24E-05	118.44	1.74	7.368	0.859
34	2013	Tengchong	8.39	93.0	1432.2	8.02E-05	5.08E-07	5.83	1.59	1.253	0.790
35	2013	Tengchong	7.83	87.5	1182.2	1.24E-04	1.27E-05	11.27	1.73	1.378	0.762
36	2013	Tengchong	8.20	81.3	1143.0	6.29E-05	9.41E-09	7.24	1.73	2.591	0.852
37	2013	Tengchong	3.72	90.7	164.6	1.20E-04	1.39E-05	15.90	1.52	3.610	0.688
38	2013	Tengchong	5.75	89.8	208.6	1.25E-04	1.42E-05	17.61	1.62	6.414	0.610
39	2013	Tengchong	- - -	- - -	- - -	6.08E-05	9.77E-07	7.02	1.65	1.925	0.928
40	2013	Tengchong	7.72	76.1	1058.4	3.71E-05	3.32E-07	5.95	1.71	1.589	0.943
41	2013	Tengchong	6.38	49.0	1187.2	1.22E-04	1.24E-05	30.22	1.49	7.651	0.640
42	2012	Yellowstone	4.65	64.3	2316.9	1.06E-04	1.87E-06	21.71	1.77	1.708	0.945
43	2012	Yellowstone	2.16	79.3	2785.2	1.74E-04	8.85E-06	22.24	1.84	0.948	0.935
44	2012	Yellowstone	2.15	69.9	3967.3	2.08E-03	3.91E-05	189.59	1.44	0.949	0.608
45	2012	Yellowstone	5.34	52.1	254.1	1.37E-04	8.81E-06	18.35	1.43	2.524	0.678
46	2012	Yellowstone	4.80	54.0	260.6	3.08E-04	9.88E-06	37.64	1.50	3.302	0.741
47	2012	Yellowstone	4.52	70.3	219.8	3.56E-04	1.27E-05	95.13	1.38	2.638	0.619
48	2012	Yellowstone	5.29	52.2	176.4	2.49E-04	8.60E-06	35.34	1.43	1.374	0.721
49	2012	Yellowstone	4.50	49.3	165.7	1.23E-04	9.41E-06	14.81	1.48	1.533	0.674
50	2012	Yellowstone	2.90	91.7	2459.3	8.90E-05	1.20E-05	10.89	1.60	0.292	0.991
51	2012	Yellowstone	2.85	43.9	2839.6	1.64E-04	1.35E-05	23.48	1.47	1.355	0.667
52	2012	Yellowstone	4.40	81.0	2400.9	7.84E-05	1.23E-05	6.32	1.47	0.645	0.806

Sample Index	Year	Sample Region	pH	Temp. ℃	Sp. Cond.* μS/cm	DOC mol C/L	DOC error**	Total Fluor.	Fluor. Index	Humification Index	β/α
53	2012	Yellowstone	2.06	81.6	3710.1	2.97E-03	3.66E-05	202.60	1.52	1.890	0.680
54	2012	Yellowstone	5.78	88.8	2719.7	3.83E-04	2.09E-05	131.03	1.63	3.696	0.777
55	2012	Yellowstone	5.59	85.8	2933.2	5.20E-04	2.36E-05	159.83	1.51	8.861	0.679
56	2012	Yellowstone	5.57	88.4	2866.0	1.66E-03	4.00E-05	367.55	1.53	7.557	0.586
57	2012	Yellowstone	5.40	73.3	4181.1	2.10E-03	1.96E-05	499.71	1.47	6.521	0.612
58	2012	Yellowstone	1.79	51.4	6407.1	2.53E-04	1.17E-05	51.04	1.60	0.806	0.757
59	2012	Yellowstone	1.93	46.4	7633.1	3.82E-04	1.22E-05	65.38	1.50	1.064	0.727
60	2012	Yellowstone	1.71	73.9	5166.8	9.75E-04	9.53E-06	120.48	1.46	1.791	0.680
61	2012	Yellowstone	2.15	60.9	3672.9	2.05E-04	1.30E-05	40.17	1.51	1.494	0.739
62	2012	Yellowstone	2.43	32.7	2636.0	2.29E-04	1.16E-05	21.08	1.46	1.430	0.679
63	2012	Yellowstone	3.07	58.5	1289.2	2.41E-04	1.17E-05	49.04	1.96	4.800	0.631
64	2012	Yellowstone	2.72	85.9	1748.9	7.40E-05	1.00E-05	10.22	1.48	1.234	0.757
65	2012	Yellowstone	2.36	43.2	3173.0	4.71E-04	1.09E-05	35.64	1.49	1.954	0.615
66	2012	Yellowstone	2.26	57.2	1412.4	8.21E-05	1.06E-05	7.67	2.00	1.052	0.629
67	2012	Yellowstone	4.92	91.8	2461.5	7.67E-05	1.11E-05	7.04	1.56	0.813	0.893
68	2012	Yellowstone	2.29	83.5	322.6	8.03E-05	1.09E-05	14.50	1.45	0.752	0.797
69	2012	Yellowstone	4.03	45.7	1531.8	3.12E-04	1.47E-05	21.07	1.51	1.227	0.740
70	2012	Yellowstone	3.90	53.3	180.8	9.20E-05	1.03E-05	3.42	1.63	0.255	0.658
71	2012	Yellowstone	4.43	68.1	342.6	1.59E-04	1.06E-05	13.85	1.51	2.261	0.689
72	2012	Yellowstone	2.34	75.8	1856.6	7.47E-05	1.80E-06	5.55	1.84	0.380	0.578
73	2012	Yellowstone	5.77	86.1	8109.8	4.78E-04	2.79E-05	171.70	1.89	3.879	0.709
74	2012	Yellowstone	2.79	75.1	4545.5	5.48E-04	1.99E-05	143.04	1.73	2.626	0.829
75	2012	Yellowstone	5.69	76.8	4351.7	4.52E-04	1.48E-05	174.94	1.87	5.634	0.692
76	2012	Yellowstone	2.62	42.8	1082.6	4.42E-04	2.65E-05	133.73	1.75	3.594	0.796
77	2012	Yellowstone	3.67	48.3	2781.7	4.32E-04	1.52E-05	154.70	1.86	4.364	0.636
78	2012	Yellowstone	3.30	64.4	454.1	9.36E-05	1.17E-05	3.67	1.65	0.163	0.613
79	2012	Yellowstone	2.23	31.6	4779.2	1.66E-04	1.12E-05	25.31	1.53	1.051	0.656
80	2012	Yellowstone	2.25	64.6	2073.1	9.29E-05	9.08E-07	18.00	1.53	1.140	0.796
81	2012	Yellowstone	2.27	73.6	1938.1	1.02E-04	1.86E-06	21.01	1.57	1.137	0.830
82	2012	Yellowstone	3.90	40.0	1538.5	9.77E-05	1.20E-06	13.03	1.45	3.829	0.692

Sample Index	Year	Sample Region	pH	Temp. ℃	Sp. Cond.* μS/cm	DOC mol C/L	DOC error**	Total Fluor.	Fluor. Index	Humification Index	β/α
83	2012	Yellowstone	5.21	77.5	3468.3	9.02E-05	1.17E-05	16.96	2.63	1.801	0.271
84	2012	Yellowstone	2.23	53.5	3859.9	1.68E-04	1.47E-05	24.47	1.45	1.246	0.685
85	2012	Yellowstone	2.08	29.1	4685.8	1.77E-04	1.36E-05	27.93	1.43	0.865	0.686
86	2012	Yellowstone	1.94	87.7	2972.5	1.59E-04	1.19E-06	24.67	1.58	0.893	0.662
87	2012	Yellowstone	1.85	82.6	3396.8	2.55E-04	1.63E-06	77.30	1.51	0.972	0.777
88	2012	Yellowstone	1.94	81.1	2521.2	1.60E-04	2.36E-06	34.75	1.50	0.542	0.732
89	2012	Yellowstone	5.03	80.6	2556.8	1.46E-04	6.16E-07	29.71	1.95	2.660	0.543
90	2012	Yellowstone	2.40	32.2	3408.2	6.40E-04	1.96E-06	51.36	1.38	1.465	0.673
91	2012	Yellowstone	3.13	48.8	597.6	5.09E-05	1.27E-06	2.95	1.85	0.042	0.573
92	2012	Yellowstone	3.67	57.8	481.3	1.34E-04	8.90E-06	11.85	1.47	1.611	0.634
93	2012	Yellowstone	4.64	81.7	467.7	1.99E-04	1.13E-06	27.70	1.51	1.520	0.673
94	2012	Yellowstone	2.29	80.3	737.9	4.00E-04	5.95E-06	40.04	1.59	1.247	0.646
95	2012	Yellowstone	3.42	26.1	284.1	3.80E-04	9.55E-07	29.41	1.43	4.190	0.560
96	2012	Yellowstone	3.28	35.9	614.1	1.63E-04	7.04E-07	24.94	1.45	1.473	0.648
97	2012	Yellowstone	3.30	88.3	1064.4	1.11E-04	1.67E-06	10.70	1.40	0.685	0.721
98	2012	Yellowstone	2.33	53.7	2214.7	1.29E-04	1.42E-06	22.06	1.49	1.285	0.762
99	2012	Yellowstone	2.01	91.7	2129.4	1.20E-04	2.08E-06	19.23	1.57	1.065	0.810
100	2012	Yellowstone	4.42	16.1	174.1	1.59E-04	2.19E-07	11.97	1.47	1.245	0.683
101	2012	Yellowstone	4.10	23.8	303.3	1.24E-04	1.46E-06	11.43	1.44	1.603	0.681
102	2012	Yellowstone	3.44	33.3	458.0	1.31E-04	1.72E-06	13.97	1.48	1.498	0.726
103	2012	Yellowstone	3.62	33.8	326.1	1.22E-04	2.21E-06	13.43	1.52	1.452	0.733
104	2013	Yellowstone	3.18	92.2	1640.4	7.95E-05	7.38E-07	4.11	1.45	1.023	0.895
105	2013	Yellowstone	3.30	67.3	1645.7	5.05E-05	1.34E-06	6.26	1.52	1.212	0.848
106	2013	Yellowstone	3.17	84.8	1885.2	4.55E-05	2.14E-07	7.33	1.57	1.800	0.837
107	2013	Yellowstone	3.43	66.4	2550.9	4.19E-05	1.20E-06	5.47	1.51	1.331	0.882
108	2013	Yellowstone	3.70	64.6	2607.7	5.87E-05	1.75E-06	7.09	1.38	2.548	0.722
109	2013	Yellowstone	2.79	87.0	1846.0	4.77E-05	6.29E-07	12.06	1.56	0.308	1.119
110	2013	Yellowstone	2.82	80.1	1881.5	5.28E-05	1.66E-06	12.18	1.43	0.821	0.868
111	2013	Yellowstone	2.99	50.0	2166.7	9.63E-05	1.84E-06	9.24	1.45	1.354	0.717
112	2013	Yellowstone	3.03	80.9	1543.9	7.52E-05	1.21E-06	12.22	1.52	1.362	0.874

Sample Index	Year	Sample Region	pH	Temp. ℃	Sp. Cond.* μS/cm	DOC mol C/L	DOC error**	Total Fluor.	Fluor. Index	Humification Index	β/α
113	2013	Yellowstone	2.90	36.6	3251.6	1.12E-04	8.82E-07	14.20	1.38	1.271	0.749
114	2013	Yellowstone	2.78	82.2	1609.1	6.14E-05	1.26E-06	12.41	1.47	0.764	0.857
115	2013	Yellowstone	3.70	87.8	1449.9	7.55E-05	9.94E-07	6.43	1.29	1.428	0.701
116	2013	Yellowstone	2.52	67.4	1570.9	6.20E-05	1.91E-06	3.51	1.68	0.678	0.633
117	2013	Yellowstone	7.86	45.4	2517.0	7.23E-05	8.87E-07	10.63	1.55	2.392	0.773
118	2013	Yellowstone	6.36	62.4	3392.4	1.19E-04	1.14E-06	17.49	1.33	1.657	0.885
119	2013	Yellowstone	8.67	91.0	1778.0	6.27E-05	3.29E-07	4.96	1.28	0.909	0.944
120	2013	Yellowstone	5.44	74.1	4853.7	2.95E-04	2.47E-07	107.27	1.65	3.465	0.826
121	2013	Yellowstone	2.73	89.8	4338.0	2.09E-04	3.74E-07	86.37	1.83	2.707	0.900
122	2013	Yellowstone	5.64	79.6	6711.3	2.75E-04	1.18E-06	121.83	1.81	3.807	0.830
123	2013	Yellowstone	2.43	52.8	1606.7	1.27E-04	1.81E-06	28.57	1.45	1.441	0.731
124	2013	Yellowstone	2.23	27.7	2816.9	2.51E-04	2.10E-06	35.78	1.40	1.182	0.653
125	2013	Yellowstone	5.37	60.1	1921.3	1.09E-04	2.21E-06	19.23	1.38	2.649	0.914
126	2013	Yellowstone	4.64	74.8	735.5	3.24E-04	3.06E-06	33.95	1.27	4.029	0.701
127	2013	Yellowstone	6.19	35.0	1896.7	1.54E-04	3.01E-06	23.95	1.31	3.326	0.841
128	2013	Yellowstone	3.77	39.5	2024.8	2.09E-04	2.05E-06	22.45	1.25	1.665	0.816
129	2013	Yellowstone	5.68	78.9	1799.8	1.55E-04	1.18E-06	30.30	1.35	3.496	0.829
130	2013	Yellowstone	2.14	75.8	2713.3	1.80E-04	2.33E-06	23.36	1.69	1.054	0.918
131	2013	Yellowstone	1.86	88.7	2541.8	5.72E-04	4.59E-06	62.13	1.60	1.276	0.830
132	2013	Yellowstone	2.68	57.9	2913.8	2.57E-04	1.63E-06	61.32	1.69	2.340	0.887
133	2013	Yellowstone	6.24	71.3	3001.0	7.13E-04	1.23E-05	226.48	1.44	6.519	0.701
134	2013	Yellowstone	4.10	85.0	1881.8	1.08E-04	3.40E-08	19.41	1.45	1.775	0.914
135	2013	Yellowstone	2.90	71.0	2344.3	1.24E-04	8.26E-07	11.91	1.46	2.003	0.839
136	2013	Yellowstone	4.10	85.0	2045.9	1.36E-04	2.30E-06	17.62	1.45	1.950	0.742
137	2013	Yellowstone	4.10	85.0	2045.9	1.39E-04	1.54E-06	22.54	1.44	2.297	0.816
138	2013	Yellowstone	6.87	79.5	1588.0	8.24E-05	8.32E-07	3.92	1.96	0.956	0.716
139	2013	Yellowstone	2.16	57.7	4026.6	1.60E-04	9.44E-07	52.18	1.58	1.031	0.828
140	2013	Yellowstone	2.04	46.9	5007.0	2.41E-04	3.29E-07	48.08	1.52	1.005	0.762
141	2013	Yellowstone	2.18	68.2	3417.4	1.58E-04	6.13E-07	44.98	1.55	0.978	0.822
142	2013	Yellowstone	2.09	46.9	4603.6	1.78E-04	5.13E-07	46.13	1.55	0.907	0.799

Sample Index	Year	Sample Region	pH	Temp. ℃	Sp. Cond.* μS/cm	DOC mol C/L	DOC error**	Total Fluor.	Fluor. Index	Humification Index	β/α
143	2013	Yellowstone	2.10	49.6	4497.3	1.88E-04	1.41E-06	39.23	1.55	0.780	0.792
144	2013	Yellowstone	2.53	82.6	464.7	1.70E-04	3.53E-06	17.64	1.39	1.848	0.690
145	2013	Yellowstone	2.32	39.7	3361.7	2.21E-04	7.16E-07	37.86	1.47	0.946	0.747
146	2013	Yellowstone	2.15	82.2	3390.9	1.53E-04	1.63E-07	55.46	1.59	0.419	0.979
147	2013	Yellowstone	5.52	78.6	2533.8	8.92E-05	2.47E-06	14.25	2.26	2.530	0.358
148	2013	Yellowstone	2.60	87.9	1271.9	1.27E-04	1.44E-06	10.22	1.55	0.714	0.857
149	2013	Yellowstone	5.40	78.9	2463.9	9.63E-05	1.03E-06	10.72	2.02	1.073	0.831
150	2013	Yellowstone	2.18	87.1	2435.3	1.51E-04	2.80E-06	24.97	1.58	0.913	0.764
151	2013	Yellowstone	8.18	92.9	1558.5	5.34E-05	1.35E-06	6.33	1.64	0.853	1.209
152	2013	Yellowstone	3.78	86.0	141.4	9.71E-05	5.69E-06	15.59	1.38	3.743	0.692
153	2013	Yellowstone	4.13	54.4	224.4	1.06E-04	5.03E-06	1.90	1.37	0.795	0.786
154	2013	Yellowstone	3.69	63.4	258.8	8.74E-05	2.36E-06	1.87	1.32	0.980	0.722
155	2013	Yellowstone	4.96	51.9	141.0	1.68E-04	6.10E-06	21.96	1.40	4.013	0.755
156	2013	Yellowstone	3.10	81.7	2085.3	1.01E-04	9.05E-07	8.23	1.41	0.565	0.873
157	2013	Yellowstone	3.69	68.9	2129.9	7.74E-05	1.47E-06	10.70	1.53	1.820	0.832
158	2013	Yellowstone	3.56	61.4	2117.5	9.00E-05	2.00E-06	15.15	1.56	1.853	0.839
159	2013	Yellowstone	3.05	89.4	1837.0	8.22E-05	6.66E-07	20.43	1.54	0.556	1.037
160	2013	Yellowstone	2.36	59.5	2388.2	9.04E-05	5.42E-07	19.86	1.60	0.827	0.921
161	2013	Yellowstone	2.38	72.2	2069.4	1.02E-04	3.88E-07	22.72	1.54	0.864	0.950
162	2013	Yellowstone	2.37	52.9	2498.1	1.04E-04	4.59E-07	20.93	1.50	0.938	0.864
163	2013	Yellowstone	2.36	52.2	2529.1	9.86E-05	1.85E-06	19.35	1.48	0.831	0.863
164	2014	Yellowstone	4.61	71.8	140.8	4.27E-04	7.00E-06	173.09	1.30	4.990	0.587
165	2014	Yellowstone	4.21	50.4	152.1	7.16E-05	4.52E-06	5.64	1.42	0.739	0.701
166	2014	Yellowstone	5.81	61.8	146.0	4.57E-04	3.67E-06	114.20	1.33	4.755	0.706
167	2014	Yellowstone	3.47	49.9	185.9	1.72E-04	5.39E-06	5.19	1.49	0.074	0.820
168	2014	Yellowstone	5.04	75.2	159.9	3.11E-04	7.64E-06	130.31	1.37	5.533	0.641
169	2014	Yellowstone	2.83	87.0	1817.0	6.22E-05	2.94E-06	15.82	1.60	0.233	1.144
170	2014	Yellowstone	8.69	93.6	1566.6	7.52E-05	3.33E-06	10.19	1.56	0.939	1.206
171	2014	Yellowstone	4.80	28.2	669.2	6.51E-04	1.15E-05	137.02	1.36	4.340	0.633
172	2014	Yellowstone	5.99	66.8	662.3	2.33E-04	6.83E-06	74.32	1.41	2.715	0.621

Sample Index	Year	Sample Region	pH	Temp. ℃	Sp. Cond.* μS/cm	DOC mol C/L	DOC error**	Total Fluor.	Fluor. Index	Humification Index	β/α
173	2014	Yellowstone	6.48	65.9	698.0	1.98E-04	6.97E-06	66.58	1.38	6.101	0.643
174	2014	Yellowstone	2.42	80.2	3208.2	3.71E-04	1.12E-05	78.65	1.35	0.381	0.814
175	2014	Yellowstone	2.40	81.2	994.4	3.46E-04	8.16E-06	48.68	1.49	1.749	0.702
176	2014	Yellowstone	2.32	86.5	1547.1	1.56E-04	1.89E-06	25.67	1.46	2.156	0.669
177	2014	Yellowstone	1.76	77.4	4165.0	2.85E-04	9.27E-06	51.40	1.50	2.190	0.618
178	2014	Yellowstone	1.92	47.1	4958.4	2.77E-04	1.10E-05	75.33	1.54	1.115	0.736
179	2014	Yellowstone	2.05	29.0	3088.9	7.58E-04	5.77E-06	138.59	1.53	1.371	0.632
180	2014	Yellowstone	1.94	49.5	4503.4	2.07E-04	8.07E-06	72.67	1.56	1.108	0.768
181	2014	Yellowstone	2.92	71.3	2000.5	1.03E-04	3.44E-06	27.08	1.48	1.557	0.899
182	2014	Yellowstone	3.27	81.6	863.0	9.21E-05	5.11E-06	36.51	1.44	2.230	0.801
183	2014	Yellowstone	2.88	82.2	2048.5	1.69E-04	7.40E-06	17.67	1.43	0.605	0.809
184	2014	Yellowstone	2.20	78.1	2696.4	1.69E-04	9.76E-06	43.60	1.74	1.380	0.943
185	2014	Yellowstone	2.51	91.7	697.1	9.55E-05	5.12E-06	26.18	1.88	1.358	0.946
186	2014	Yellowstone	4.03	84.5	1142.5	1.80E-04	5.46E-06	44.71	1.40	2.385	0.709
187	2014	Yellowstone	4.03	85.6	1131.1	2.43E-04	7.14E-06	52.91	1.39	2.290	0.678
188	2014	Yellowstone	4.67	85.6	1001.4	1.51E-04	4.69E-06	23.50	1.44	1.490	0.771
189	2014	Yellowstone	6.09	78.3	1843.2	2.70E-04	6.73E-06	20.45	1.61	0.337	0.958
190	2014	Yellowstone	7.64	92.2	1495.7	5.15E-05	3.26E-06	10.74	1.60	1.044	1.078
191	2014	Yellowstone	8.27	83.0	1490.3	8.23E-05	2.77E-06	6.45	1.82	1.094	1.018
192	2014	Yellowstone	5.24	77.0	157.5	3.27E-04	9.63E-06	135.70	1.39	6.150	0.653
193	2014	Yellowstone	4.97	50.4	139.5	1.66E-04	4.31E-06	40.65	1.42	2.954	0.734
194	2014	Yellowstone	3.68	85.8	120.0	1.74E-04	4.45E-06	35.39	1.45	3.363	0.685
195	2014	Yellowstone	4.49	54.1	205.8	2.48E-04	8.79E-06	26.65	1.46	2.369	0.722
196	2014	Yellowstone	2.93	80.3	672.8	6.01E-05	5.90E-06	3.57	1.36	0.089	0.983
197	2014	Yellowstone	1.89	75.7	934.0	2.20E-04	6.69E-06	24.85	1.39	1.640	0.661
198	2014	Yellowstone	2.65	33.1	1885.5	1.53E-04	5.15E-06	55.25	1.45	1.648	0.687
199	2014	Yellowstone	1.99	84.9	2807.1	2.44E-04	9.78E-06	45.36	1.52	1.287	0.694
200	2014	Yellowstone	3.86	54.9	189.6	8.66E-05	8.79E-06	23.06	1.40	2.195	0.695
201	2014	Yellowstone	5.04	50.7	63.7	3.16E-04	5.24E-06	21.68	1.46	3.539	0.720
202	2014	Yellowstone	2.04	89.9	1218.5	1.39E-04	8.81E-06	39.55	1.54	0.914	0.747

Sample Index	Year	Sample Region	pH	Temp. ℃	Sp. Cond.* μS/cm	DOC mol C/L	DOC error**	Total Fluor.	Fluor. Index	Humification Index	β/α
203	2014	Yellowstone	1.97	85.2	816.7	1.92E-04	6.47E-06	26.38	1.41	1.053	0.793
204	2014	Yellowstone	2.41	86.0	927.0	1.15E-04	5.35E-06	28.69	1.61	0.681	0.890
205	2014	Yellowstone	2.15	87.4	2895.9	6.61E-04	1.58E-05	334.61	1.44	1.945	0.836
206	2014	Yellowstone	5.32	80.0	2481.0	2.11E-04	6.31E-06	52.88	1.68	2.658	0.661
207	2014	Yellowstone	5.36	78.7	2292.7	9.77E-05	6.82E-06	33.19	2.57	1.908	0.342
208	2014	Yellowstone	2.47	50.8	2180.1	1.29E-04	2.27E-06	52.00	1.46	1.447	0.724
209	2014	Yellowstone	2.36	62.3	2499.4	8.42E-05	6.35E-06	31.96	1.51	0.742	0.910
210	2014	Yellowstone	3.85	77.5	2112.7	1.79E-04	7.54E-06	46.73	1.30	3.850	0.563
211	2014	Yellowstone	3.31	44.5	407.2	8.41E-05	5.90E-06	7.48	1.54	0.163	1.376
212	2014	Yellowstone	3.92	54.1	302.5	9.20E-05	6.11E-06	15.72	1.51	1.760	0.752
213	2014	Yellowstone	2.66	81.6	1432.0	1.18E-03	2.50E-05	196.07	1.60	0.967	0.788
214	2014	Yellowstone	4.19	50.1	346.2	3.07E-04	8.40E-06	46.49	1.39	2.024	0.667
215	2014	Yellowstone	4.44	52.2	276.5	6.48E-04	1.11E-05	122.44	1.43	4.285	0.700
216	2014	Yellowstone	4.02	52.9	200.0	1.59E-04	5.69E-06	29.38	1.50	3.218	0.636
217	2014	Yellowstone	4.14	57.8	123.1	1.59E-04	4.67E-06	38.91	1.41	2.386	0.773
218	2014	Yellowstone	4.30	45.7	161.6	1.39E-04	4.16E-06	13.95	1.46	0.341	0.747
219	2014	Yellowstone	2.94	49.7	571.0	4.73E-05	5.45E-06	3.07	1.51	0.110	1.075
220	2014	Yellowstone	4.03	58.8	215.1	1.96E-04	6.11E-06	26.95	1.42	2.829	0.688
221	2014	Yellowstone	5.52	51.5	168.8	1.68E-04	4.62E-06	35.53	1.39	3.809	0.697
222	2014	Yellowstone	4.58	50.5	202.3	2.44E-04	6.75E-06	43.59	1.34	3.640	0.605

APPENDIX B

PUBLICATION CITATION

Chapter 2 titled "A novel PARAFAC model for continental hot springs reveals unique organic carbon compositions" is reprinted in this dissertation with permission from co-authors: Everett Shock and Hilairy Hartnett. The original article was published in 2020 in the journal Organic Geochemistry in volume 141 article 103964. doi: 10.1016/j.orggeochem.2019.103964. A dataset related to this publication can be found at https://data.mendeley.com/datasets/47rp3drbfs/draft?a=28b34e5b-bd72-44a2-a1e8-c4283eb47f70, an open-source online data repository hosted at Mendeley Data (Nye, Shock, and Hartnett, 2019). doi: 10.17632/47rp3drbfs.1.

APPENDIX C

EXPLORATORY ANALYSIS ON ISOLATED PRECIPITATES CONTAINING THE ACID-SPRING COMPONENT FLUOROPHORES

Gas Chromatography: Isolated acid-spring component samples were analyzed by gas-chromatography according to the methods described in Robinson et al. (2019). Briefly, the samples were analyzed on a Bruker-Scion 456 gas chromatograph (GC) equipped with a Supelco Equity-5 fused silica column and a flame ionization detector (FID). Dichloromethane (DCM) was used as a solvent with an internal standard of 0.01M dodecane. Several different extraction methods were employed to retrieve the target acid-spring fluorophores into DCM. Liquid-liquid extraction using three 1 mL aliquots of the DCM-dodecane solution had a poor extraction efficiency (<10%, determined by fluorescence of the remaining aqueous phase). One sample of the isolated acid-spring fluorophores was completely evaporated and dried at 60℃ before attempting to directly dissolve into DCM, this was also ineffective. Finally, a derivatization was attempted to functionalize the acid-spring component residue to encourage solubilization and detection. This derivatization method involves the addition of 2mL acetic anhydride to the isolated, dried residue with n-methyl imidazole as a catalyst in order to replace amine, carboxylic acid, and alcohol functional groups with acetyl groups. Excess acetic anhydride was quenched by the addition of water. The resulting solution was then liquid-liquid extracted with the 0.01M dodecane in DCM solution. An experimental blank was also prepared with deionized water (18.2 MΩ·cm, Barnstead^{tm} Nanopure) to account for contaminants and side products introduced at any point in the isolation and derivatization stages. The blank was acidified to pH 2.5 with HCl, neutralized with NaOH, filtered and then the filter was acid-extracted and that filtrate was treated to the same derivatization reaction as the sample.

Nuclear Magnetic Resonance Spectroscopy: Isolated solutions of the acid-spring component material were analyzed by proton (^{1}H) nuclear magnetic resonance (NMR) spectroscopy using two different methods. There was insufficient sample to perform

^{13}C NMR analysis. Initially the isolated, dried residue was dissolved in deuterated chloroform ($CDCl_3$) containing 1% tetramethylsilane used as an internal standard reference for chemical shift and analyzed in a 500MHz Bruker Avance III Spectrometer equipped with a broadband 5 mm H-X probe. The spectrum was obtained with a 2.67 microsecond, 30°rf pulse, a 2-second recycle delay, and 256 scans. The residue did not all dissolve into the $CDCl_3$ solution and there was particulate matter observed in the NMR tube. A second analysis was performed using DCl in D_2O (pH $<$ 3) as a solvent on an 600MHz Bruker Avance III Spectrometer with a Prodigy probe and a zpgr pulse sequence. The entire residue dissolved in the DCl/D_2O solvent. Both analyses were conducted at room temperature.

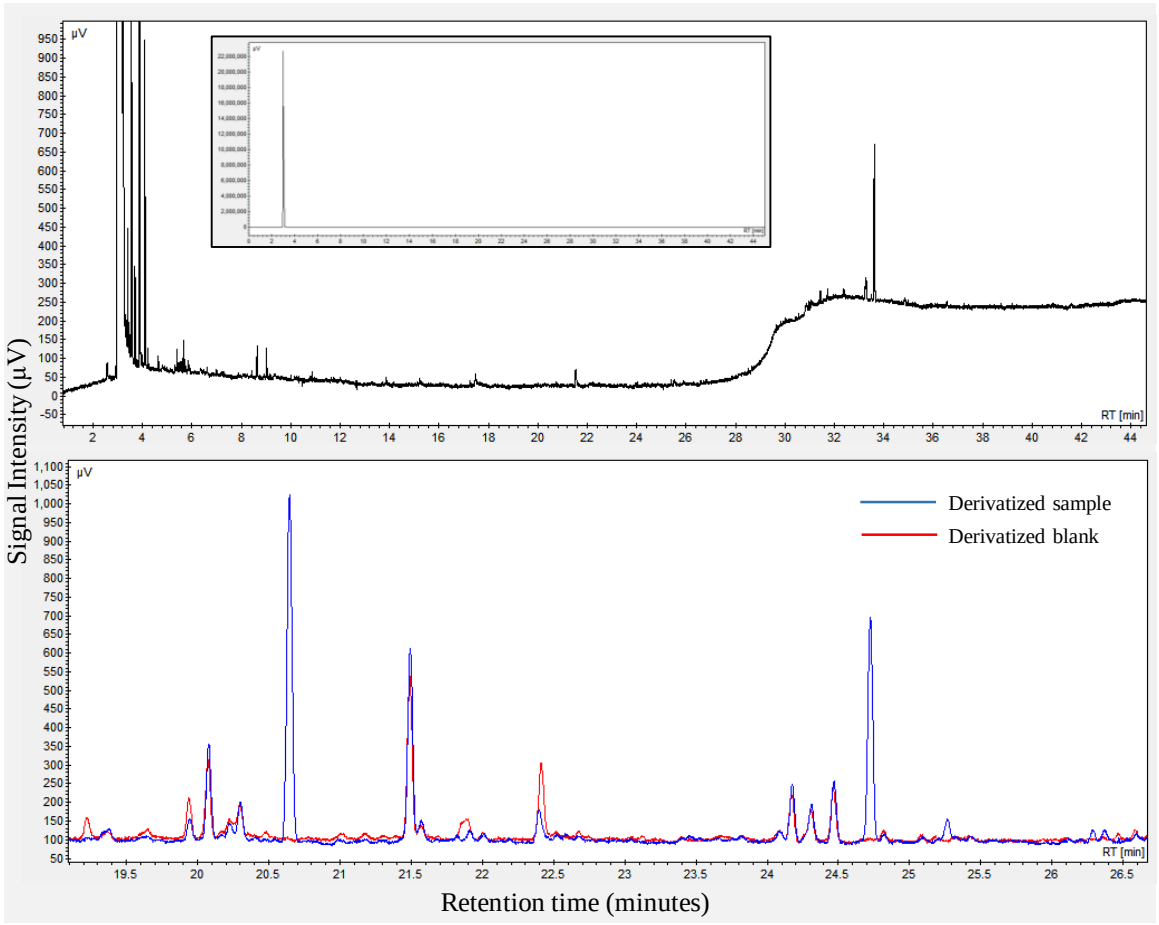

Figure C.1: Gas chromatograms of extracted isolates. (top) Extraction into DCM with a 0.01 M dodecane standard. Inset shows the full scale intensity of the internal standard dodecane peak at 2.95 minutes. The only potential analyte peak showed up at 33.62 minutes; a retention time consistent with 3 and 4 ring compounds by this method. (bottom) Chromatograms of product from attempted derivatization reaction. The only product peaks in the derivatization experiment that are not present in the blank experiment are at 20.65 and 24.75 minutes.

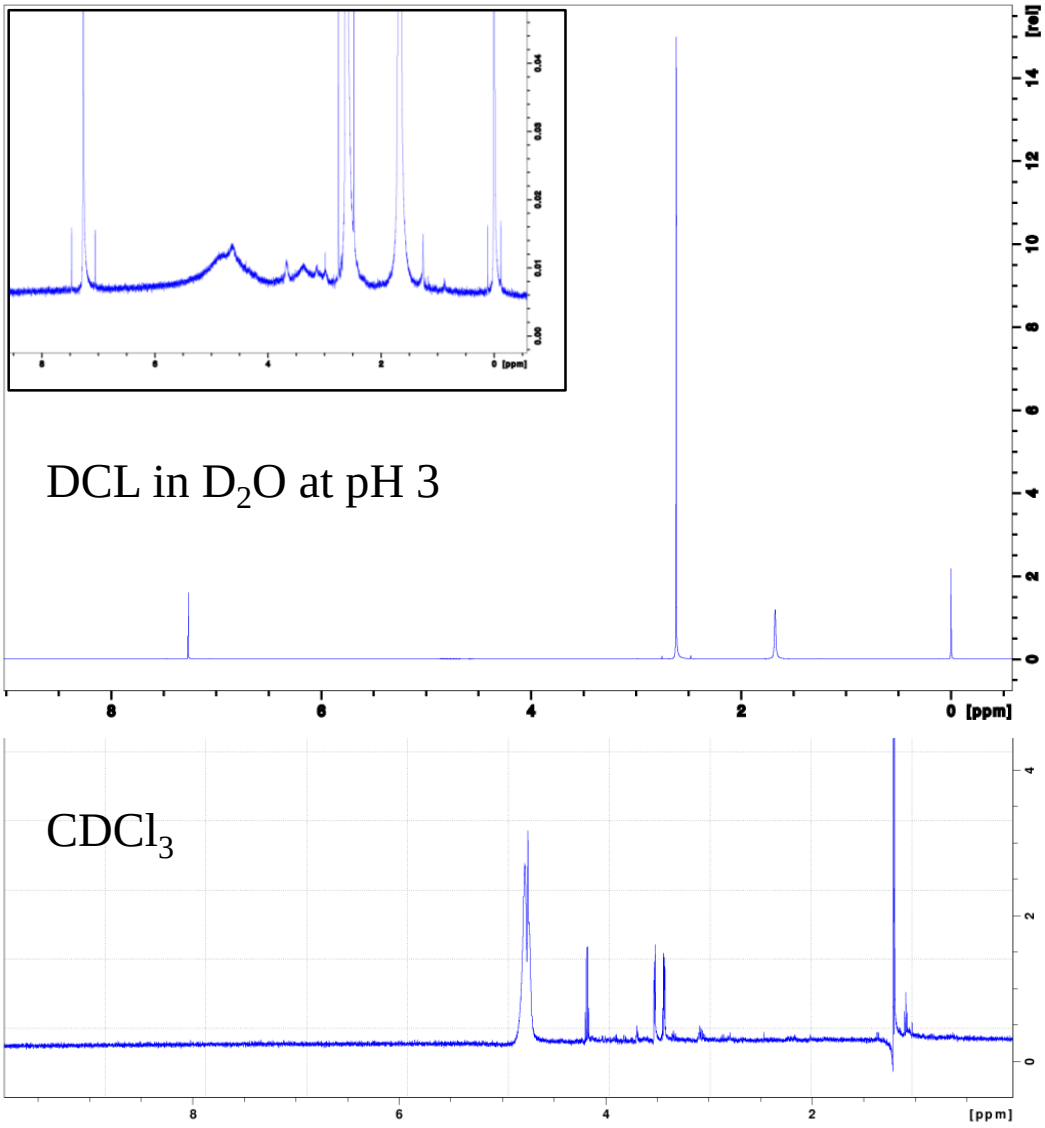

Figure C.2: NMR spectra of extracted isolates. (top) Spectra of the $CDCl_3$ extraction. All major peaks are contaminants - 1.6 ppm is H_2O, 2.6 ppm is dimethylsulfoxide, 7.2 ppm is $CDCl_3$. Low intensity noisy peaks, potentially from target analyte, were observed at 3.4, 3.7, and 4.7 ppm. (bottom) Spectra of the DCl/D_2O extraction. There is a contaminant peak at 4.7 ppm from H_2O. There is a doublet at 1.3 ppm, a doublet of triplets at 3.5 ppm, and a quartet at 4.2 ppm. These peaks were all remarkably clean, unexpected for an environmental extract so they are most likely a contaminant. There is a collection of low intensity peaks around 3.1, 3.3, and 3.7 ppm that are potentially target analyte peaks but they are at such low intensity as to be uninterpretable.

APPENDIX D

WOOD DIGESTION PRODUCTS PH SHIFTING AND FILTRATION EXPERIMENTS

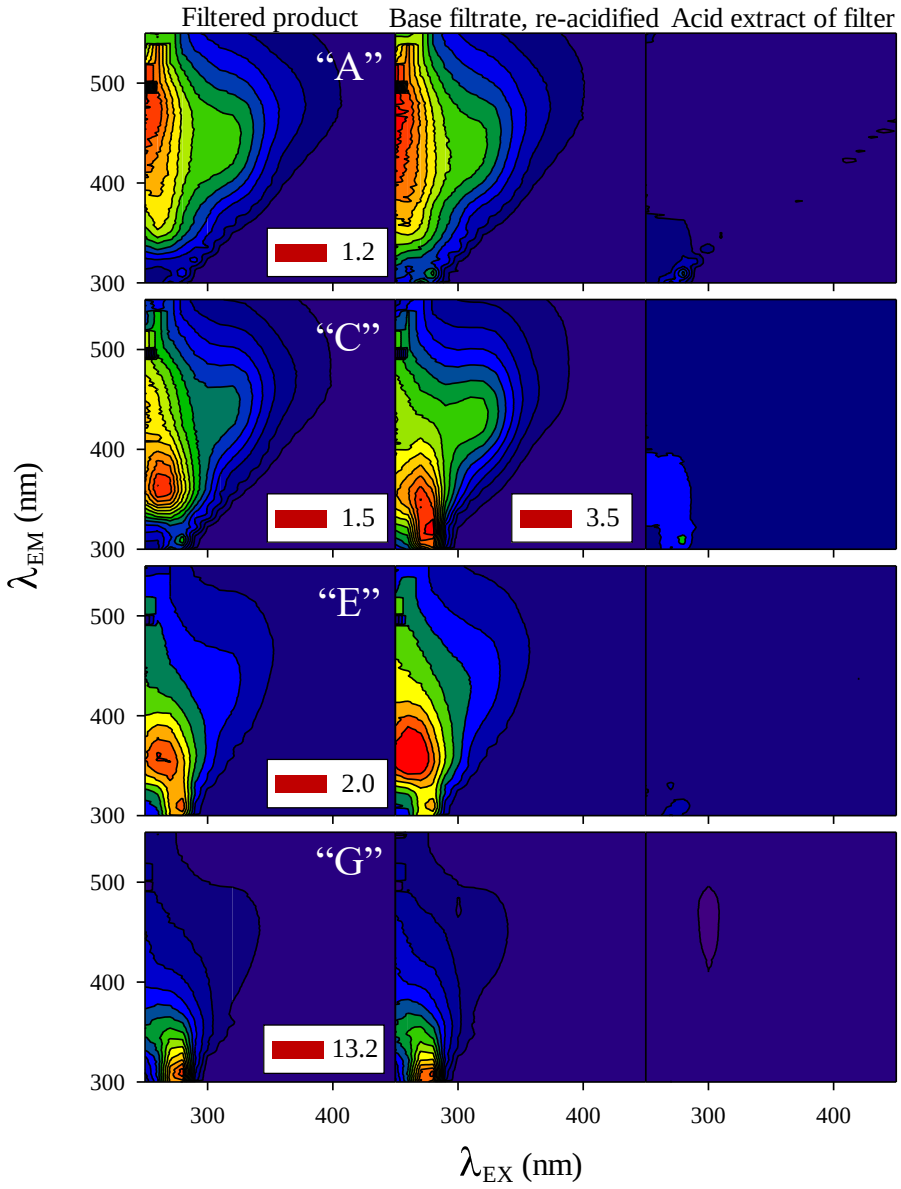

Figure D.1: Isolation experiments on the products of room temperature experiments (A, C, E, and G). (left) Filtered product at end of experiment. (center) Base filtrate of that product, re-acidified to pH = 2. (right) Acid extract of the filter using acidified blank water (pH = 2 with HCl). Each row of EEMs corresponds to the specific experiment A, C, E, or G. Intensity scales for each set of EEMs is normalized to an identical color scale as the "Filtered product" EEM (left). The only exception to this was the base filtrate of experiment "C". This EEM intensity was twice that of the original filtered product and was scaled as such. These EEMs demonstrate that there is no exclusively acid-soluble fluorophores in any wood digestion experiment.

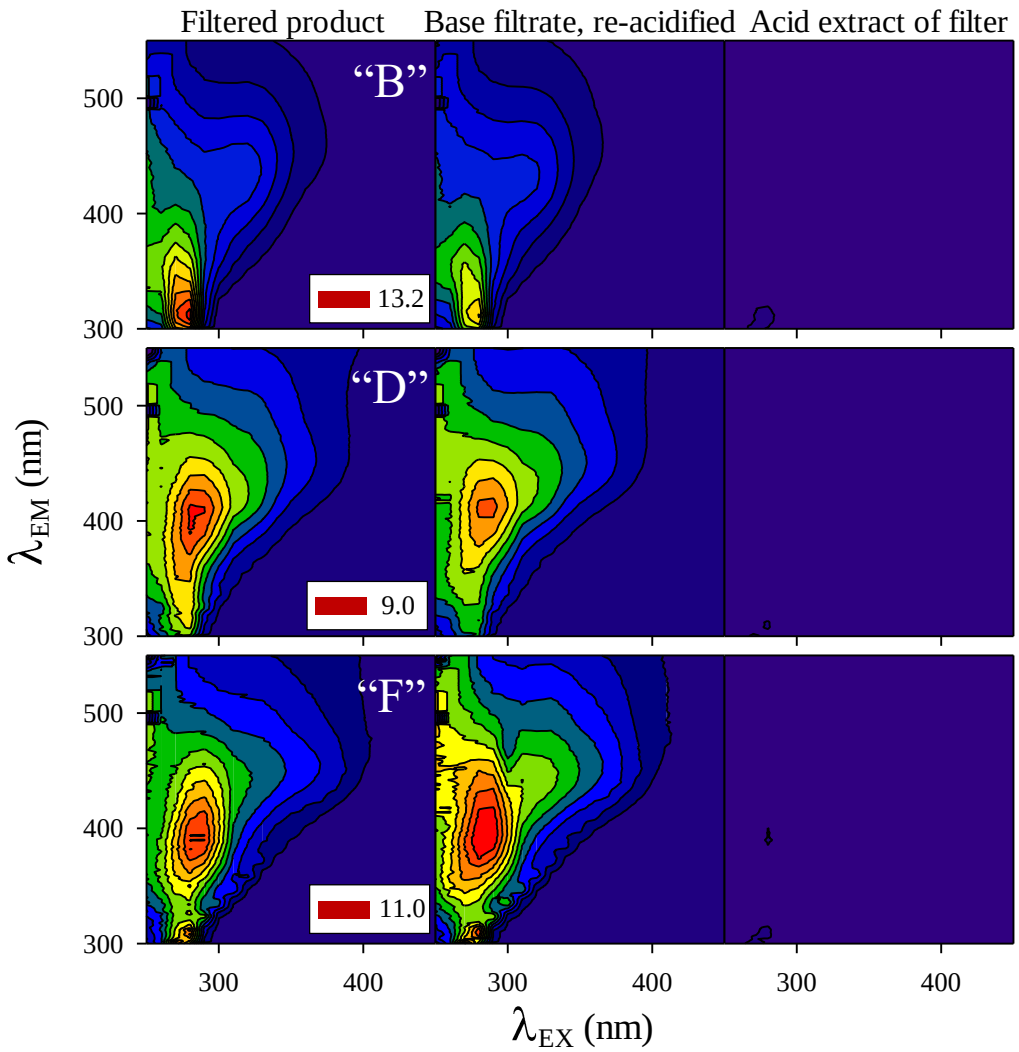

Figure D.2: Isolation experiments on the products of the refluxed experiments (B, D, and F). (left) Filtered product at end of experiment. (center) Base filtrate of that product, re-acidified to pH = 2. (right) Acid extract of the filter using acidified blank water (pH = 2 with HCl). Each row of EEMs corresponds to the specific experiment B, D, or F. Intensity scales for each set of EEMs is normalized to an identical color scale as the "Filtered product" EEM (left). These EEMs demonstrate that there is no exclusively acid-soluble fluorophores in any wood digestion experiment.

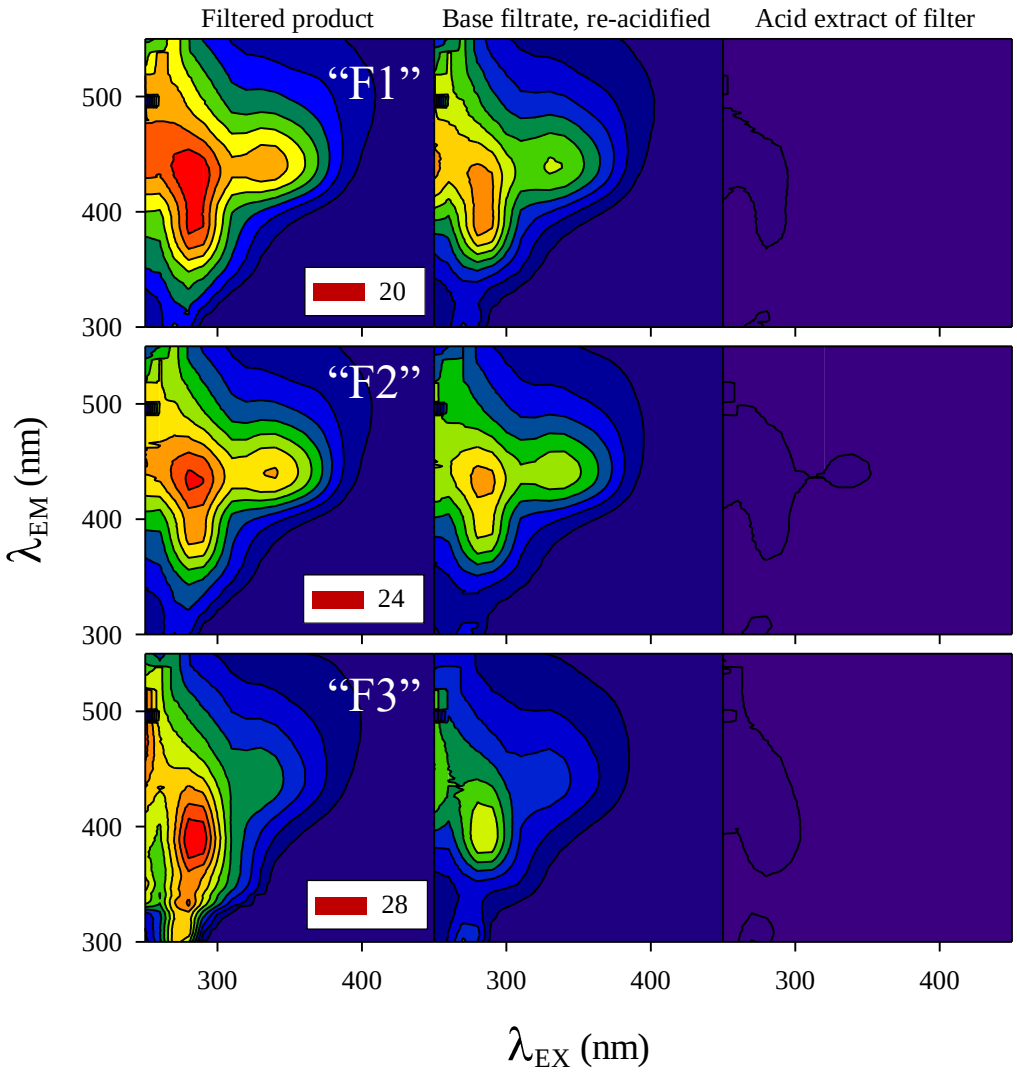

Figure D.3: Isolation experiments on the products of the elevated temperature experiments in fused silica tubes (F1, F2, and F3). (left) Filtered product at end of experiment. (center) Base filtrate of that product, re-acidified to pH = 2. (right) Acid extract of the filter using acidified blank water (pH = 2 with HCl). Each row of EEMs corresponds to the specific experiment F1, F2, or F3. Intensity scales for each set of EEMs is normalized to an identical color scale as the "Filtered product" EEM (left). These EEMs demonstrate that there is no exclusively acid-soluble fluorophores in any wood digestion experiment.

APPENDIX E

GEOCHEMICAL DATA FOR YELLOWSTONE WATER SAMPLES

Table E.1: Hot spring chemistry. AMP – Amphitheater Spring; BOG – Bog Creek; CALC – Calcite Springs; CRAT – Crater Hills; FORS – Forest Springs; GEYS – Geyser Creek; GIBB – Gibbon Hill; GOPA – Greater Obsidian Pool Area; HSB – Hot Springs Basin; IMPS – Imperial and Spray Geyser Basins; LEWS – Lewis Lake; NORR – Norris Geyser Basin; RABB – Rabbit Creek; SENT – Sentinel Meadow; SURF - Surface water; SYLV – Sylvan Springs; TURB – Turbid Lake; WAHB – Wahb Springs; WASH – Washburn; WHIT – White Creek. l - lower; m - middle; u -upper; c - channel; h - hills; n - north; s - south.
*Specific (sp.) conductivity is the temperature compensated conductivity value. Field conductivity values were temperature compensated to a standard temperature of 25°C according to the following reference: Hamilton, T.L., Boyd, E.S., Peters, J.W. (2011), Environmental constraints underpin the distribution and phylogenetic diversity of nifH in the Yellowstone geothermal complex. Microbial Ecology 61, 860–870.
Dashes indicate no data.

Sample Code	Region	pH	Temp. °C	Sp. Cond.* μS/cm	Cl^- μmol/kg	$SO_4{}^{2-}$ μmol/kg	Fe^{+2} μmol/kg	DOC μM	Total Fluorescence
120721SA	AMP	2.25	64.6	2073.1	1627.2	5482.9	45.7	92.9	18.00
120721SB	AMP	2.27	73.6	1938.1	1823.8	5508.8	49.2	101.9	21.01
120721SI	AMP	3.90	40.0	—	410.5	2232.3	1.3	97.7	13.03
120723SR	AMP	4.06	46.5	537.1	336.9	2121.5	0.2	109.7	—
120723SS	AMP	5.07	43.3	528.6	341.0	2095.7	1.8	102.2	—
120723SU	AMP	5.63	46.8	562.7	336.0	2125.3	0.2	67.5	—
120723SW	AMP	5.47	48.2	559.4	321.0	1884.3	3.2	94.8	—
120723SX	AMP	5.20	54.5	544.0	325.8	1931.5	3.4	81.6	—
120724KFQ	AMP	3.42	26.1	284.1	38.2	478.5	—	379.6	29.41
120724TR	AMP	2.33	53.7	2214.7	144.0	3802.8	30.1	129.1	22.06
120724TS	AMP	2.01	91.7	2129.4	21.9	7639.7	12.2	119.6	19.23
120724TT	AMP	4.42	16.1	174.1	29.2	285.9	42.6	159.2	11.97
120724TU	AMP	4.10	23.8	303.3	54.6	669.5	33.3	124.1	11.43
120724TV	AMP	3.44	33.3	458.0	73.6	1023.3	26.7	131.3	13.97
120724TW	AMP	3.62	33.8	326.1	103.2	1108.6	38.0	121.7	13.43
130723TB	AMP	2.38	72.2	2069.4	—	—	65.9	101.8	22.72
130723TW	AMP	7.98	54.6	591.7	—	—	—	123.2	16.51
130723TX	AMP	6.81	49.1	594.5	—	—	0.2	141.8	20.35
130723TY	AMP	2.37	52.9	2498.1	—	—	41.5	104.2	20.93

Sample Code	Region	pH	Temp. ℃	Sp. Cond.* μS/cm	Cl^- μmol/kg	SO_4^{2-} μmol/kg	Fe^{+2} μmol/kg	DOC μM	Total Fluorescence
140803SP	AMP	2.36	62.3	2499.4	149.8	7575.5	51.9	84.2	31.96
170722TO	AMP	3.76	35.4	306.0	78.9	1007.3	57.3	151.5	13.16
180918G	BOG - l	6.45	87.1	1255.6	3336.7	2375.0	—	157.5	42.23
180918H	BOG - l	6.60	76.7	1330.4	3431.0	3709.0	1.8	199.3	11.91
180918I	BOG - l	6.99	89.2	1269.7	3247.8	2427.8	0.2	88.2	18.36
180918J	BOG - l	6.56	90.2	1343.3	4342.7	1895.3	0.4	70.2	8.19
180918K	BOG - l	6.29	69.4	1439.6	2387.8	2960.8	0.7	502.3	6.19
180918L	BOG - l	6.07	72.8	1378.3	2355.5	2881.0	0.2	125.8	11.95
180917A	BOG - m	3.59	45.1	270.7	15.4	1364.3	34.9	307.3	33.95
180917B	BOG - m	4.99	83.6	932.8	166.3	3379.3	0.9	170.0	15.77
180917C	BOG - m	5.28	70.6	247.8	19.1	1357.4	0.5	144.2	8.19
180917D	BOG - m	4.43	24.6	247.0	49.2	726.2	334.8	84.8	8.24
180917F	BOG - m	2.22	71.6	2341.1	—	—	21.5	171.5	18.21
180919M	BOG - u	1.98	89.1	5039.4	—	—	102.1	142.2	22.32
180919N	BOG - u	1.75	88.2	4938.2	—	—	89.5	—	22.49
180919O	BOG - u	1.93	91.4	4905.5	—	—	91.3	108.4	24.68
180919P	BOG - u	1.71	92.0	4871.8	—	—	92.2	113.2	22.70
180919Q	BOG - u	1.86	69.4	6101.7	—	—	97.6	144.5	19.02
180919R	BOG - u	2.15	73.3	3107.8	—	—	—	180.6	26.55
180919S	BOG - u	1.84	83.5	5774.2	—	—	27.8	—	10.44
130720SA	CALC	8.01	93.8	1520.6	—	—	1.1	271.3	510.71
130720SW	CALC	8.21	89.6	1507.0	—	—	5.4	273.8	381.40
130720SY	CALC	4.68	87.2	2428.7	—	—	7.9	234.0	448.42
130720SZ	CALC	2.80	54.3	3068.1	—	—	488.8	185.1	455.18
140731TP	CALC	3.60	82.1	2198.9	5837.5	6879.9	43.7	307.2	918.06
140803TA	CALC	7.28	63.4	2002.3	6704.4	4163.1	0.5	170.6	565.77
140803TB	CALC	7.14	54.2	2063.1	6234.1	6737.2	0.2	244.9	602.30
140803TC	CALC	6.53	93.4	1845.9	5598.1	7306.0	1.1	286.5	724.56
140803TZ	CALC	5.32	80.0	1994.8	6093.9	4554.8	0.2	430.9	763.70
120713SJ	CRAT	2.15	69.9	3967.3	57.2	14410.9	—	164.7	20.67
120713SK	CRAT	3.64	61.2	4808.6	—	—	—	138.0	20.96
120715TU	CRAT	2.06	81.6	3710.1	26.6	15512.2	1104.6	2968.7	202.60

Sample Code	Region	pH	Temp. ℃	Sp. Cond.* μS/cm	Cl^- μmol/kg	SO_4^{2-} μmol/kg	Fe^{+2} μmol/kg	DOC μM	Total Fluorescence
120715TW	CRAT	3.33	89.0	5307.0	22905.8	5366.4	10.0	112.8	13.40
120715TY	CRAT	1.96	48.2	7780.1	42.5	17222.5	366.3	107.4	32.47
130717SI	CRAT	2.14	75.8	2713.3	—	—	241.7	180.3	23.36
130717SJ	CRAT	1.99	66.3	37732.7	—	—	251.6	—	236.75
130717SK	CRAT	3.76	85.3	4243.0	—	—	15.6	137.3	3.56
130717SL	CRAT	1.86	88.7	2541.8	—	—	259.6	572.5	62.13
130717SM	CRAT	3.60	59.9	4181.4	—	—	7.0	92.0	5.49
140727SU	CRAT	3.39	46.3	4284.7	25397.2	5823.5	5.9	78.2	8.05
140727SX	CRAT	1.94	58.8	5310.3	38.1	18994.7	562.2	107.0	53.87
140729SB	CRAT	2.20	78.1	2696.4	37.0	10161.2	275.7	169.4	43.60
140729SG	CRAT	2.51	91.7	697.1	116.4	12018.3	133.2	95.5	26.18
160720H	CRAT	2.06	76.1	3095.9	—	—	266.8	206.8	24.77
160720I	CRAT	2.10	73.1	3470.9	—	—	282.9	106.0	14.66
160720J	CRAT	3.39	87.2	4723.7	—	—	7.9	113.2	5.61
160720K	CRAT	1.69	84.2	5952.4	—	—	107.4	391.4	53.59
170724TA	CRAT	1.54	85.8	8799.6	52.3	28212.1	188.9	567.4	63.16
170724TD	CRAT	1.89	44.5	5964.0	46.9	17550.5	213.1	716.9	27.11
170724TE	CRAT	3.46	87.2	4122.1	22646.5	5395.8	8.8	69.9	5.61
180714SL	CRAT	2.25	81.3	2436.5	—	—	286.5	193.4	34.50
180714SM	CRAT	2.09	87.6	4143.0	—	—	73.4	149.1	32.68
180714SN	CRAT	3.28	78.8	3853.6	—	—	9.7	66.1	5.89
180714SO	CRAT	1.93	64.5	5016.8	—	—	334.8	448.8	52.29
180714SP	CRAT	2.96	46.3	2103.8	—	—	—	2919.6	243.20
120717TA	FORS	1.79	51.4	6407.1	7.6	13074.2	240.3	252.7	51.04
120717TB	FORS	1.93	46.4	7633.1	83.2	28624.4	226.5	381.7	65.38
120717TC	FORS	1.71	73.9	5166.8	5.6	19237.2	23.6	975.4	120.48
120717TD	FORS	2.15	60.9	3672.9	2.3	8137.5	85.9	205.0	40.17
120717TE	FORS	2.60	25.5	2044.6	13.4	4181.9	84.9	726.0	43.09
120717TF	FORS	2.43	32.7	2636.0	11.8	5839.0	—	229.3	21.08
120717TG	FORS	3.07	58.5	1289.2	42.5	3304.4	4.5	241.3	49.04
120723TL	FORS	1.79	64.0	4432.6	8.4	20468.9	49.2	3907.9	287.27
120723TM	FORS	1.78	82.2	6226.7	6.8	15322.2	21.7	394.7	—

Sample Code	Region	pH	Temp. ℃	Sp. Cond.* μS/cm	Cl^- μmol/kg	SO_4^{2-} μmol/kg	Fe^{+2} μmol/kg	DOC μM	Total Fluorescence
120723TN	FORS	2.29	80.3	737.9	1.4	6238.1	19.7	400.2	40.04
120723TO	FORS	2.16	76.2	2994.1	4.5	6684.2	29.5	212.5	—
120723TP	FORS	2.68	36.3	1538.3	15.7	3634.4	43.0	136.8	—
120723TQ	FORS	2.10	49.6	2311.0	2.6	12298.7	166.5	167.6	—
130720TA	FORS	2.16	57.7	4026.6	—	—	282.9	160.3	52.18
130720TU	FORS	2.04	46.9	5007.0	—	—	231.9	241.2	48.08
130720TV	FORS	2.18	68.2	3417.4	—	—	234.6	158.3	44.98
130720TW	FORS	2.09	46.9	4603.6	—	—	209.5	177.6	46.13
130720TX	FORS	2.10	49.6	4497.3	—	—	222.0	188.0	39.23
130720TY	FORS	2.53	82.6	464.7	—	—	12.5	170.5	17.64
130720TZ	FORS	2.32	39.7	3361.7	—	—	175.5	221.4	37.86
140726TM	FORS	2.40	81.2	994.4	2.5	6667.4	14.9	345.7	48.68
140726TN	FORS	2.32	86.5	1547.1	1.7	3409.8	3.2	155.7	25.67
140726TO	FORS	1.76	77.4	4165.0	8.5	12345.4	5.7	284.7	51.40
140726TP	FORS	1.92	47.1	4958.4	6.0	16090.7	320.5	277.3	75.33
140726TQ	FORS	2.05	29.0	3088.9	13.9	17115.6	188.0	758.4	138.59
140726TR	FORS	1.94	49.5	4503.4	6.4	15630.4	187.1	206.5	72.67
170714TH	FORS	2.18	29.0	2513.9	13.7	7870.9	67.1	736.2	76.51
170714TI	FORS	2.95	63.9	949.9	41.3	3398.2	3.0	148.5	67.04
170714TJ	FORS	2.21	50.4	2169.1	16.8	5462.9	101.2	246.4	23.66
120719SS	GEYS	5.87	86.8	2491.1	15335.5	1384.5	—	60.4	10.95
120719SX	GEYS	2.34	75.8	1856.6	2721.0	4927.0	—	74.7	5.55
120719SY	GEYS	6.05	85.5	2239.8	13820.6	1499.0	—	—	10.95
120724SA	GEYS	3.28	35.9	614.1	329.0	1913.1	33.3	163.2	19.52
120724SY	GEYS	3.30	88.3	1064.4	2022.2	3166.2	7.3	111.1	10.70
130712SK	GEYS	7.20	89.4	3522.7	—	—	0.4	55.9	35.15
130712SN	GEYS	6.79	81.8	2682.6	—	—	0.7	47.2	7.18
130713SR	GEYS	3.70	87.8	1449.9	—	—	7.9	75.5	6.43
130713SS	GEYS	2.52	67.4	1570.9	—	—	6.3	62.0	3.51
130713ST	GEYS	5.65	76.3	2670.3	—	—	1.1	110.4	22.39
130713SV	GEYS	6.36	62.4	3392.4	—	—	0.2	119.5	17.49
140724SB	GEYS	8.46	89.2	2508.8	11647.1	1290.9	—	76.8	27.30

Sample Code	Region	pH	Temp. ℃	Sp. Cond.* μS/cm	Cl^- μmol/kg	SO_4^{2-} μmol/kg	Fe^{+2} μmol/kg	DOC μM	Total Fluorescence
140729TB	GEYS	7.62	82.6	1505.6	6033.7	2423.3	—	122.0	30.68
140729TC	GEYS	3.50	76.1	835.8	2651.7	1816.8	12.7	80.9	30.45
140729TY	GEYS	4.67	85.6	1001.4	2150.0	2759.4	9.0	151.0	23.50
140729TZ	GEYS	6.09	78.3	1843.2	9583.7	1062.6	0.5	270.1	20.45
160723A	GEYS	6.97	47.2	2144.0	—	—	—	131.2	14.12
160723U	GEYS	6.03	82.8	1966.6	—	—	—	99.5	6.57
160723V	GEYS	8.37	90.5	3099.6	—	—	—	81.9	9.55
160723X	GEYS	3.91	90.0	1055.7	—	—	5.0	121.3	7.64
160723Y	GEYS	2.42	74.0	1409.1	—	—	2.9	78.6	3.84
160723Z	GEYS	6.31	85.9	2944.1	—	—	—	117.2	9.18
170718TA	GEYS	6.72	76.8	2696.5	17734.1	1071.0	—	43.3	3.31
170718TZ	GEYS	6.02	81.0	1980.7	11506.6	1200.8	1.4	69.5	6.34
170719SE	GEYS	2.26	74.9	1969.5	3502.6	4963.7	5.6	84.9	3.79
170719SF	GEYS	6.35	87.0	2468.8	15992.1	1248.0	0.2	68.8	8.32
170719SG	GEYS	5.75	86.7	1376.5	5411.0	2561.4	2.5	107.0	16.05
170719SH	GEYS	2.39	86.7	1615.9	22.7	5066.1	17.7	68.7	10.99
170719SI	GEYS	2.31	89.6	3512.2	7608.1	11894.6	125.3	408.0	33.16
180713SE	GEYS	6.50	75.6	1774.4	—	—	—	92.1	7.47
180713SF	GEYS	6.04	72.6	274.1	—	—	0.2	115.1	8.20
180713SH	GEYS	8.14	89.5	2502.2	—	—	0.5	102.8	8.62
180713SI	GEYS	1.98	89.9	2611.0	—	—	2685.8	1485.5	121.77
180713SJ	GEYS	6.24	74.9	1060.1	—	—	0.5	95.8	14.01
180722TM	GEYS	5.40	79.4	2226.5	—	—	1.3	96.5	4.96
180722TN	GEYS	6.69	91.0	2616.4	—	—	—	92.1	6.66
180722TO	GEYS	6.42	91.8	2354.5	—	—	—	80.2	6.89
180722TP	GEYS	6.62	92.7	2548.9	—	—	—	114.8	4.83
180722TQ	GEYS	6.32	86.1	1523.9	—	—	16.8	115.6	10.93
180722TR	GEYS	6.65	90.9	1768.8	—	—	—	110.8	4.25
180722TS	GEYS	6.60	92.3	2693.9	—	—	—	63.0	1.82
170719TC	GIBB	6.40	88.4	1895.9	11396.8	550.1	—	88.0	3.48
170719TD	GIBB	5.83	51.2	918.0	2037.1	785.7	3.9	264.1	31.81
170719TE	GIBB	5.81	43.4	906.4	2142.2	1352.3	8.8	356.7	50.72

Sample Code	Region	pH	Temp. ℃	Sp. Cond.* μS/cm	Cl^- μmol/kg	SO_4^{2-} μmol/kg	Fe^{+2} μmol/kg	DOC μM	Total Fluorescence
170719TF	GIBB	7.04	86.8	1800.1	10373.5	579.4	—	78.5	4.26
170719TG	GIBB	6.50	87.9	2435.8	15514.0	534.9	—	81.8	3.83
170719TH	GIBB	5.81	48.6	557.7	962.9	600.8	5.4	286.0	49.72
170719TI	GIBB	7.71	91.6	2204.1	15158.5	373.3	—	68.8	3.70
170725SJ	GIBB	5.75	75.6	585.5	1317.8	333.6	0.4	142.7	17.82
170725SK	GIBB	6.26	53.4	626.9	1460.5	558.5	—	169.5	26.02
170725SL	GIBB	6.03	65.6	610.4	1432.4	538.7	0.4	160.9	25.34
170725SM	GIBB	1.61	70.3	4769.2	12.1	21953.2	121.8	508.3	90.12
170725SN	GIBB	6.40	89.7	174.4	3717.1	680.9	0.4	123.4	26.54
170725SO	GIBB	1.93	87.2	1657.8	982.7	9932.8	—	202.1	31.01
180715TM	GIBB	6.81	80.0	1170.0	—	—	—	108.5	5.46
180715TO	GIBB	6.44	85.4	1130.0	—	—	—	136.3	9.77
180715TP	GIBB	6.84	66.1	1127.9	—	—	—	99.8	3.78
180715TQ	GIBB	6.67	75.2	969.1	—	—	—	179.8	16.15
180715TR	GIBB	6.38	78.9	1155.9	—	—	—	97.0	4.44
120712TA	GOPA	4.65	64.3	2316.9	13352.0	3120.2	2.1	105.7	21.71
130716DC	GOPA	3.79	62.0	2448.3	—	—	—	132.7	13.48
130716SC	GOPA	5.37	60.1	1921.3	—	—	1.3	108.7	19.23
130716SD	GOPA	4.64	74.8	735.5	—	—	19.2	323.6	33.95
130716SF	GOPA	3.77	39.5	2024.8	—	—	43.3	209.5	22.45
130716SG	GOPA	5.68	78.9	1799.8	—	—	5.0	155.0	30.30
140725TH	GOPA	4.80	28.2	669.2	1305.0	1948.5	—	651.3	137.02
140725TK	GOPA	5.99	66.8	662.3	1088.3	1573.8	0.5	233.1	74.32
140726SN	GOPA	6.48	65.9	698.0	1965.9	454.8	—	197.7	66.58
140726SS	GOPA	2.42	80.2	3208.2	5235.2	12186.8	137.2	371.4	78.65
160714B	GOPA	3.99	77.1	1505.4	—	—	29.5	308.8	48.43
160714C	GOPA	4.73	74.4	1519.6	—	—	15.8	304.8	33.42
160714D	GOPA	4.63	81.0	1015.1	—	—	18.6	310.6	42.78
160714E	GOPA	3.61	89.9	274.2	—	—	46.2	227.6	32.26
160724C	GOPA	3.48	67.4	2388.0	—	—	2.7	153.9	15.42
160724D	GOPA	4.30	85.4	398.6	—	—	88.1	361.4	46.18
160724E	GOPA	5.47	61.3	1688.9	—	—	0.5	166.2	19.84

Sample Code	Region	pH	Temp. ℃	Sp. Cond.* μS/cm	Cl^- μmol/kg	SO_4^{2-} μmol/kg	Fe^{+2} μmol/kg	DOC μM	Total Fluorescence
160724G	GOPA	6.21	69.5	654.5	—	—	—	252.0	44.27
160724H	GOPA	3.64	30.7	646.3	—	—	24.7	344.8	4.78
170713TB	GOPA	3.51	61.7	2432.5	11217.4	4069.2	2.7	94.5	14.09
170713TC	GOPA	5.45	62.4	1799.2	8145.3	2321.5	0.5	105.6	20.18
170713TD	GOPA	5.48	78.9	1751.7	7825.0	2292.1	0.2	154.2	22.37
170713TE	GOPA	2.17	30.4	3445.8	533.3	13999.2	171.9	242.7	24.23
170714SI	GOPA	5.34	75.5	451.2	954.7	1692.2	2.0	1106.1	46.42
170714SJ	GOPA	5.86	70.9	1780.5	7946.2	2357.6	—	144.3	22.38
170714SK	GOPA	5.83	74.6	1787.1	7890.0	2311.3	—	142.4	24.93
180719SI	GOPA	3.65	66.8	2282.1	—	—	4.1	129.7	13.55
180719SL	GOPA	5.76	72.6	541.0	—	—	0.5	277.8	76.19
180719SM	GOPA	5.54	71.2	1694.4	—	—	1.4	142.1	30.12
180719SN	GOPA	4.56	35.8	515.6	—	—	4.8	593.6	85.88
170728TA	HSB	4.37	73.1	991.3	17.3	3447.8	0.9	386.4	57.87
170728TB	HSB	3.78	77.9	1302.7	5.8	4599.3	13.4	1313.6	147.02
170729TD	HSB	3.65	81.8	500.9	14.7	1858.9	—	217.8	38.74
170729TE	HSB	5.18	85.6	1995.9	2.7	7109.7	—	425.3	86.52
170729TF	HSB	3.40	76.2	494.1	13.6	1782.3	10.7	645.5	100.86
170729TG	HSB	2.56	81.9	919.6	12.5	2647.6	5.6	211.5	48.04
170729TH	HSB	4.38	68.8	264.4	12.9	528.7	0.5	158.5	32.28
170729TI	HSB	2.72	82.4	840.8	15.5	2584.6	5.4	190.9	47.56
170729TJ	HSB	2.74	46.9	959.0	12.7	2345.8	9.5	162.2	34.44
170729TK	HSB	2.82	37.4	911.1	12.2	2153.4	9.0	158.0	25.09
170730TM	HSB	2.20	87.2	1978.6	10.3	7915.9	—	143.0	28.71
170730TN	HSB	5.09	87.0	2915.2	3.0	10520.8	—	342.8	64.41
170730TO	HSB	4.51	89.8	2373.7	4.3	8830.9	0.9	318.1	98.27
170730TP	HSB	5.20	84.9	2365.8	7.4	8368.1	0.2	399.0	97.40
170730TQ	HSB	2.95	37.2	1011.3	20.6	4221.6	50.5	78.8	17.23
170730TR	HSB	4.92	70.7	523.5	24.2	1593.2	0.2	125.3	27.51
170730TS	HSB	5.29	80.4	217.8	4.3	4335.0	4.1	608.3	94.57
170730TT	HSB	2.52	80.3	2402.7	5.7	6626.3	27.2	164.8	34.39
170730TU	HSB	6.50	62.8	292.1	82.7	907.0	0.5	94.5	14.15

Sample Code	Region	pH	Temp. ℃	Sp. Cond.* μS/cm	Cl^- μmol/kg	SO_4^{2-} μmol/kg	Fe^{+2} μmol/kg	DOC μM	Total Fluorescence
120722TE	IMPS	3.13	48.8	597.6	30.4	1217.6	8.4	50.9	2.95
120722TF	IMPS	3.67	57.8	481.3	41.7	1109.2	0.5	133.5	11.85
120722TG	IMPS	4.64	81.7	467.7	33.7	1130.6	0.2	198.7	27.70
140804TE	IMPS	3.19	44.9	—	—	—	7.9	84.1	7.48
140804TF	IMPS	3.92	54.1	302.5	19.6	1116.9	0.4	92.0	15.72
140804TG	IMPS	2.66	81.6	1432.0	67.7	6574.1	262.3	1175.5	196.07
140804TH	IMPS	4.19	50.1	346.2	33.8	1204.4	7.5	306.9	46.49
180922A	LEWS - c	6.65	79.2	589.7	1421.9	272.1	—	71.2	4.25
180922B	LEWS - c	6.61	83.5	620.3	1516.5	264.5	—	129.2	4.72
180922D	LEWS - c	6.63	68.5	619.3	1516.9	212.2	—	50.8	3.72
180922X	LEWS - c	7.10	82.5	777.7	2363.8	419.5	—	83.4	4.09
180922Y	LEWS - c	6.86	88.1	578.7	1451.1	279.6	—	151.5	4.38
180922Z	LEWS - c	7.28	70.1	565.2	1386.1	258.5	0.2	81.7	6.70
180714TK	LEWS - h	7.78	92.8	793.7	—	—	0.4	147.4	9.66
180714TL	LEWS - h	3.84	84.4	540.2	—	—	—	122.5	8.48
180923E	LEWS - h	6.48	88.4	522.9	22.6	1785.3	0.9	113.6	8.12
180923F	LEWS - h	6.41	85.9	491.0	16.6	1658.8	5.4	79.5	8.82
180923G	LEWS - h	6.90	92.0	410.3	14.4	1327.7	1.4	71.8	7.13
180923H	LEWS - h	6.58	66.1	412.7	—	—	—	78.8	9.38
180923I	LEWS - h	6.14	64.8	400.9	—	—	—	88.3	11.44
120714TO	NORR	2.90	91.7	2459.3	8437.1	2228.5	136.4	89.0	10.89
120714TR	NORR	4.40	81.0	2400.9	11404.0	1748.6	44.0	78.4	6.32
120718SK	NORR	2.72	85.9	1748.9	11307.6	946.3	38.3	74.0	10.22
120718SL	NORR	2.36	43.2	3173.0	17459.0	2476.0	12.5	471.2	35.64
120718SM	NORR	2.26	57.2	1412.4	9572.1	2009.2	31.5	82.1	7.67
120718SP	NORR	4.92	91.8	2461.5	17722.6	493.2	2.3	76.7	7.04
120718SQ	NORR	2.29	83.5	322.6	9132.3	1904.1	60.9	80.3	14.50
130711SC	NORR	3.18	92.2	1640.4	—	—	52.3	50.5	6.26
130711SD	NORR	3.17	84.8	1885.2	—	—	36.2	45.5	7.33
130711SF	NORR	3.43	66.4	1811.3	—	—	26.5	41.9	5.47
130711SG	NORR	3.70	64.6	2607.7	—	—	24.4	58.7	7.09
130712TF	NORR	2.79	87.0	1846.0	—	—	145.0	47.7	12.06

Sample Code	Region	pH	Temp. ℃	Sp. Cond.* μS/cm	Cl^- μmol/kg	SO_4^{2-} μmol/kg	Fe^{+2} μmol/kg	DOC μM	Total Fluorescence
130712TG	NORR	2.82	80.1	1881.5	—	—	51.9	52.8	12.18
130712TH	NORR	7.14	86.7	2744.0	—	—	0.4	53.1	3.85
130712TJ	NORR	3.03	80.9	1543.9	—	—	8.2	75.2	12.22
130712TL	NORR	2.90	36.6	3251.6	—	—	24.5	111.7	14.20
130712TM	NORR	2.78	82.2	1609.1	—	—	—	61.4	12.41
130723SU	NORR	3.10	81.7	2085.3	—	—	—	100.7	8.23
130723SV	NORR	3.69	68.9	—	—	—	—	77.4	10.70
130723SW	NORR	3.56	61.4	2117.5	—	—	—	90.0	15.15
130723SX	NORR	3.05	89.4	1837.0	—	—	—	82.2	20.43
130723SY	NORR	2.95	84.0	2064.7	—	—	—	68.5	21.55
130723SZ	NORR	3.02	81.7	1940.0	—	—	—	91.3	48.46
140725FB	NORR	2.83	87.0	1817.0	8983.6	2179.6	—	62.2	15.82
140727FD	NORR	2.92	71.3	2000.5	11628.9	1534.3	—	102.9	27.08
140727FE	NORR	3.27	81.6	863.0	10046.9	1471.0	—	92.1	36.51
140727FF	NORR	2.88	82.2	2048.5	10590.0	1967.4	—	168.5	17.67
140803FN	NORR	3.50	83.8	1681.5	10590.6	965.1	31.0	—	18.14
140804SR	NORR	7.26	85.8	2761.7	20502.8	461.3	0.7	67.4	8.07
140804SV	NORR	3.85	77.5	2112.7	18660.3	881.4	4.1	179.1	46.73
160719A	NORR	2.89	84.7	2016.4	—	—	22.6	74.2	11.07
160719B	NORR	2.98	77.9	2006.8	—	—	40.8	87.7	23.37
160719C	NORR	2.73	88.8	1835.7	—	—	43.5	87.7	22.08
160719D	NORR	7.12	82.3	2781.9	—	—	—	58.2	3.66
160719E	NORR	2.92	92.5	1543.8	—	—	117.3	133.6	11.72
160719F	NORR	3.54	79.6	1760.0	—	—	29.9	75.7	6.96
160719Z	NORR	4.10	88.5	2092.5	—	—	1.1	109.5	23.24
170715SM	NORR	3.85	89.0	1886.0	15676.2	1016.6	2.9	129.9	35.17
170715SN	NORR	2.58	88.6	1188.4	7490.9	2430.7	39.4	79.3	27.04
170715SO	NORR	2.73	86.1	1941.0	10156.7	1885.7	33.3	100.9	17.79
170715SP	NORR	2.96	76.1	1988.1	11314.0	1390.4	35.8	104.9	23.39
170725TH	NORR	3.39	54.3	1708.7	9965.6	1407.9	36.5	107.5	20.00
170725TI	NORR	4.00	72.8	2561.3	18899.4	530.4	1.6	90.1	4.65
170725TL	NORR	2.63	74.3	1520.1	4600.9	2462.8	22.2	202.9	35.61

Sample Code	Region	pH	Temp. ℃	Sp. Cond.* μS/cm	Cl^- μmol/kg	SO_4^{2-} μmol/kg	Fe^{+2} μmol/kg	DOC μM	Total Fluorescence
170725TM	NORR	3.00	91.1	1703.3	8098.8	2132.4	137.9	56.0	11.75
170725TN	NORR	7.30	85.1	2765.7	18800.9	404.2	—	71.1	3.21
180718SD	NORR	2.96	76.2	1977.8	—	—	27.4	101.8	13.96
180718SE	NORR	3.06	73.6	1959.9	—	—	36.2	130.2	37.14
180718SF	NORR	3.96	91.8	2251.7	—	—	1.6	125.0	38.43
180718SG	NORR	3.84	89.1	2152.1	—	—	9.0	85.2	5.22
180718SH	NORR	3.34	71.5	2007.3	—	—	13.1	103.3	7.80
180721SP	NORR	2.60	87.4	1653.9	—	—	45.3	122.6	21.89
180721SQ	NORR	2.69	83.0	1879.6	—	—	24.0	113.8	10.56
180721SR	NORR	3.63	91.9	2061.6	—	—	9.1	87.7	5.39
180721SS	NORR	4.11	88.0	1991.2	—	—	6.1	72.5	6.44
180721ST	NORR	2.86	45.0	1689.3	—	—	41.7	132.9	14.73
180721SU	NORR	3.09	92.0	1627.8	—	—	87.7	58.9	9.59
180721SV	NORR	6.99	82.6	2513.9	—	—	—	64.0	3.84
180723SB	NORR	6.01	48.6	743.9	—	—	0.2	72.2	12.73
180723SC	NORR	5.30	49.0	213.5	—	—	1.6	139.9	18.49
180723SD	NORR	2.02	84.3	3362.3	—	—	27.0	196.5	20.24
180723SE	NORR	6.21	62.8	1847.4	—	—	—	78.3	3.16
160726S	RABB - h	3.76	93.3	477.6	—	—	17.5	104.5	11.82
160726T	RABB - h	3.78	32.3	163.9	—	—	1.4	101.4	0.82
160726U	RABB - h	4.24	41.6	156.7	—	—	1.1	59.5	0.48
160726V	RABB - h	3.28	50.4	237.7	—	—	3.2	36.9	0.91
160726W	RABB - h	3.09	55.7	291.5	—	—	1.4	100.0	3.82
160726X	RABB - h	2.98	84.3	458.8	—	—	4.5	674.1	51.00
160726Y	RABB - h	4.63	85.0	189.6	—	—	1.6	140.1	10.81
120718TI	RABB - n	4.03	45.7	1531.8	4604.6	2028.3	5.7	312.3	21.07
120718TJ	RABB - n	4.91	51.6	95.0	15.3	197.1	0.5	136.0	—
120718TK	RABB - n	3.90	53.3	180.8	10.8	400.5	1.8	92.0	3.42
120718TL	RABB - n	4.43	68.1	342.6	684.7	638.5	1.1	159.0	13.85
130713TO	RABB - n	8.67	91.0	1778.0	—	—	0.2	62.7	4.96
130713TP	RABB - n	8.79	76.8	1724.5	—	—	—	54.0	3.96
140802SC	RABB - n	8.98	78.2	1468.0	7558.8	250.4	—	86.6	6.83

Sample Code	Region	pH	Temp. ℃	Sp. Cond.* μS/cm	Cl^- μmol/kg	SO_4^{2-} μmol/kg	Fe^{+2} μmol/kg	DOC μM	Total Fluorescence
140802SD	RABB - n	3.86	54.9	189.6	17.1	714.9	19.3	316.1	23.06
140802SE	RABB - n	5.04	50.7	63.7	13.2	190.9	—	84.4	21.68
140805SB	RABB - n	8.77	76.9	1884.2	8226.0	187.9	—	59.1	5.98
140805SE	RABB - n	8.58	77.6	1593.6	6933.9	280.3	—	57.0	7.37
140805SY	RABB - n	4.34	81.7	249.3	1001.0	392.9	4.3	100.7	8.67
170713SC	RABB - n	8.67	74.7	1628.4	7194.5	264.5	—	105.3	8.27
170713SD	RABB - n	3.71	59.6	109.5	18.0	336.4	4.5	72.5	1.64
170713SE	RABB - n	4.86	50.4	62.2	11.7	184.7	14.3	94.2	10.66
170713SF	RABB - n	8.65	91.2	2022.4	8750.3	142.8	0.2	96.9	3.66
120713TH	RABB - s	5.34	52.1	254.1	42.0	261.9	1.8	137.0	18.35
120713TI	RABB - s	4.80	54.0	260.6	27.7	600.7	9.8	308.3	37.64
120713TJ	RABB - s	4.52	70.3	219.8	15.0	354.7	10.9	355.8	95.13
120713TK	RABB - s	5.29	52.2	176.4	17.3	381.0	1.6	249.1	35.34
120713TL	RABB - s	4.50	49.3	165.7	12.3	533.4	10.6	123.0	14.81
130722TK	RABB - s	3.78	86.0	141.4	—	—	1.1	97.1	15.59
130722TL	RABB - s	4.13	54.4	224.4	—	—	3.2	105.8	1.90
130722TM	RABB - s	3.69	63.4	258.8	—	—	3.2	87.4	1.87
130722TP	RABB - s	4.96	51.9	141.0	—	—	2.0	168.2	21.96
140724TB	RABB - s	4.61	71.8	140.8	14.0	355.1	22.6	427.0	173.09
140724TD	RABB - s	5.81	61.8	146.0	13.7	450.9	1.4	457.1	114.20
140724TE	RABB - s	3.47	49.9	185.9	12.1	700.7	4.5	172.4	5.19
140724TF	RABB - s	5.04	75.2	159.9	17.7	330.0	36.5	310.6	130.31
140730TH	RABB - s	4.97	50.4	139.5	16.7	357.5	—	166.2	40.65
140730TI	RABB - s	3.68	85.8	120.0	87.7	388.1	—	174.0	35.39
140730TK	RABB - s	2.93	80.3	672.8	99.0	2093.0	—	60.1	3.57
140730TL	RABB - s	6.98	75.7	372.4	46.2	1074.5	—	98.6	17.43
140805TJ	RABB - s	4.02	52.9	200.0	44.2	651.7	5.4	159.3	29.38
140805TK	RABB - s	4.14	57.8	123.1	8.0	368.0	0.2	158.7	38.91
140805TL	RABB - s	4.30	45.7	161.6	13.8	518.7	5.0	139.1	13.95
140805TM	RABB - s	2.94	49.7	571.0	12.4	1209.1	6.1	47.3	3.07
140805TN	RABB - s	4.03	58.8	215.1	22.5	786.5	0.5	195.9	26.95
140805TO	RABB - s	5.52	51.5	168.8	24.0	284.9	0.5	167.8	35.53

Sample Code	Region	pH	Temp. ℃	Sp. Cond.* μS/cm	Cl^- μmol/kg	SO_4^{2-} μmol/kg	Fe^{+2} μmol/kg	DOC μM	Total Fluorescence
160725J	RABB - s	5.19	51.6	98.3	—	—	11.8	338.1	42.81
160725K	RABB - s	6.12	53.3	161.2	—	—	—	138.6	22.37
160725L	RABB - s	4.63	44.3	146.2	—	—	6.8	101.2	9.78
160725M	RABB - s	2.57	92.8	880.7	—	—	1.6	91.8	8.78
160725N	RABB - s	4.83	77.6	137.8	—	—	24.4	233.4	113.56
160725O	RABB - s	6.72	80.5	408.1	—	—	—	87.3	6.31
160725P	RABB - s	3.55	61.0	324.4	—	—	3.2	83.0	1.43
160725Q	RABB - s	3.67	54.0	288.0	—	—	1.8	56.7	1.36
170723TR	RABB - s	4.93	45.2	151.4	14.1	444.3	4.7	157.0	28.71
170723TS	RABB - s	5.25	75.9	157.1	11.4	284.1	30.6	264.7	72.05
170723TT	RABB - s	5.01	59.0	182.2	23.6	578.9	3.4	228.4	35.54
170723TU	RABB - s	5.16	52.9	187.7	23.9	539.1	3.0	234.8	38.43
170723TV	RABB - s	4.95	54.8	132.5	14.7	353.5	3.0	227.6	37.66
170723TW	RABB - s	6.55	68.5	238.1	32.3	182.4	—	164.0	29.08
170723TX	RABB - s	2.91	50.2	616.4	10.0	1275.2	5.0	59.1	0.88
170723TY	RABB - s	4.57	73.3	134.5	13.4	359.2	18.8	279.6	84.93
170723TZ	RABB - s	5.75	58.5	183.3	7.9	371.2	1.4	345.7	78.77
180718KFE	RABB - s	2.65	91.8	791.1	—	—	—	242.1	10.62
180718KFF	RABB - s	7.29	87.2	215.6	—	—	—	122.4	9.03
180718KFG	RABB - s	6.60	81.3	307.1	—	—	—	879.2	36.54
180718TA	RABB - s	7.23	90.4	319.3	—	—	—	93.7	8.11
180718TB	RABB - s	4.33	64.2	123.0	—	—	14.5	367.4	100.78
180718TC	RABB - s	5.14	52.4	134.6	—	—	1.8	284.1	48.32
180718TD	RABB - s	4.41	83.4	165.3	—	—	—	166.9	31.13
180718TE	RABB - s	4.62	44.7	151.1	—	—	—	90.2	5.28
180718TY	RABB - s	5.47	52.7	169.6	—	—	2.0	329.8	43.85
180718TZ	RABB - s	2.98	49.6	431.0	—	—	5.2	82.6	1.44
130718DE	SENT	8.89	87.5	1546.7	—	—	—	154.0	11.53
130722SO	SENT	7.53	88.7	1594.1	—	—	—	47.4	6.87
130722SQ	SENT	8.18	92.9	1558.5	—	—	0.9	53.4	6.33
140725SH	SENT	8.69	93.6	1566.6	6926.1	152.5	0.2	75.2	10.19
140730SL	SENT	7.64	92.2	1495.7	6095.1	163.7	—	51.5	10.74

Sample Code	Region	pH	Temp. ℃	Sp. Cond.* μS/cm	Cl^- μmol/kg	SO_4^{2-} μmol/kg	Fe^{+2} μmol/kg	DOC μM	Total Fluorescence
140730SM	SENT	8.27	83.0	1490.3	6050.2	148.9	0.2	82.3	6.45
160715G	SENT	3.62	84.4	1181.4	—	—	12.0	2071.1	299.30
160715I	SENT	8.32	66.7	1306.4	—	—	—	104.9	3.92
160715K	SENT	4.40	87.7	377.1	—	—	2.0	4851.2	466.69
180712SD	SENT	7.71	87.8	1518.2	—	—	—	85.9	8.47
170722TP	SURF (AMP)	5.28	12.6	50.9	15.6	58.4	0.4	146.5	11.21
140731TO	SURF (CALC)	7.37	16.3	198.5	165.0	122.2	—	202.9	25.50
160723JN7	SURF (GEYS)	7.88	26.1	775.0	—	—	—	131.0	14.01
180715KFC	SURF (GIBB)	8.06	31.1	533.9	—	—	—	121.5	10.35
160724JN8	SURF (GOPA)	6.92	24.1	637.5	—	—	—	2025.4	306.88
170730TL	SURF (HSB)	6.74	17.2	25.9	6.1	15.9	0.5	244.4	17.71
180922C	SURF (LEWS)	7.55	15.7	113.6	100.1	834.9	—	176.7	13.88
160715JN4	SURF (SENT)	8.03	20.8	121.3	—	—	—	138.3	4.69
160721JN5	SURF (SYLV)	7.72	16.7	263.9	—	—	—	170.1	21.36
170715TO	SURF (TURB)	3.43	24.6	254.1	66.9	498.7	—	268.7	27.86
170720TL	SURF (WAHB)	7.51	15.3	67.4	2.7	27.7	—	148.6	16.80
120721KFL	SYLV	2.23	31.6	4779.2	3650.8	6616.9	—	165.7	25.31
120721TA	SYLV	5.23	73.2	2238.3	8109.5	1142.2	—	108.8	22.68
120721TB	SYLV	5.21	77.5	3468.3	14952.9	1389.5	1.4	90.2	16.96
120721TC	SYLV	3.12	42.9	1631.1	2895.0	2891.1	11.3	123.7	4.58
120721TW	SYLV	2.23	53.5	3859.9	3751.4	5522.0	65.4	168.4	24.47
120721TY	SYLV	2.08	29.1	4685.8	3155.7	6789.4	43.5	176.9	27.93
120722SK	SYLV	1.94	87.7	2972.5	3615.8	9720.8	46.6	159.0	24.67
120722SL	SYLV	1.85	82.6	3396.8	90.8	14291.7	241.7	255.0	77.30
120722SM	SYLV	1.94	81.1	2521.2	85.9	9374.8	137.9	160.0	34.75
120722SP	SYLV	5.03	80.6	2556.8	13992.9	2082.4	0.7	145.7	29.71
120722SQ	SYLV	2.35	32.2	3408.2	5552.4	6487.8	108.3	639.7	51.36
130714TU	SYLV	2.43	52.8	1606.7	—	—	28.8	127.0	28.57
130714TY	SYLV	2.23	27.7	2816.9	—	—	28.6	250.7	35.78
130721SC	SYLV	1.99	76.6	1384.4	—	—	9.3	239.6	19.84
130721SD	SYLV	2.15	82.2	3390.9	—	—	130.7	152.5	71.28
130721SE	SYLV	5.52	78.6	2533.8	—	—	125.3	89.2	14.25

Sample Code	Region	pH	Temp. ℃	Sp. Cond.* μS/cm	Cl^- μmol/kg	SO_4^{2-} μmol/kg	Fe^{+2} μmol/kg	DOC μM	Total Fluorescence
130721SF	SYLV	2.60	87.9	1271.9	—	—	82.4	126.6	10.22
130721SG	SYLV	5.40	78.9	2463.9	—	—	0.7	96.3	10.72
130721SH	SYLV	7.87	45.0	2505.7	—	—	0.2	47.9	49.83
130721SI	SYLV	2.18	87.1	2435.3	—	—	47.5	150.6	24.97
140731ST	SYLV	3.52	38.5	1059.8	3097.9	2796.1	11.5	104.8	4.33
140731SU	SYLV	6.36	72.5	2085.1	7022.7	2628.5	1.4	128.2	19.73
140731SV	SYLV	6.86	43.5	2279.6	14151.4	2029.9	—	77.6	19.30
140731SW	SYLV	5.46	77.4	1503.9	8641.6	1114.2	—	149.9	29.89
140731SX	SYLV	2.65	33.1	1885.5	2330.7	5263.8	41.9	152.9	55.25
140731SY	SYLV	1.99	84.9	2807.1	14.9	13490.1	92.0	244.1	45.36
140802TR	SYLV	2.04	89.9	1218.5	3239.8	10124.3	54.4	139.0	39.55
140802TS	SYLV	1.97	85.2	816.7	1.9	9992.2	9.5	192.1	26.38
140802TT	SYLV	2.41	86.0	927.0	220.2	4207.6	57.7	115.1	28.69
140802TU	SYLV	2.15	87.4	2895.9	94.9	14019.0	633.8	661.2	334.61
140802TV	SYLV	5.32	80.0	2481.0	14715.6	2045.3	1.1	211.4	52.88
140802TW	SYLV	5.36	78.7	2292.7	13532.3	1413.1	—	97.7	33.19
140802TX	SYLV	2.47	50.8	2180.1	4331.4	5412.1	67.7	129.0	52.00
160717T	SYLV	1.96	83.6	3683.2	—	—	139.7	223.9	48.82
160717U	SYLV	5.37	77.4	2558.6	—	—	—	91.0	28.15
160717V	SYLV	5.52	76.0	2846.5	—	—	0.2	172.3	20.19
160717W	SYLV	2.92	34.4	1641.4	—	—	10.7	262.9	6.84
160717X	SYLV	2.14	76.5	2916.3	—	—	53.7	122.3	16.44
160721N	SYLV	6.35	71.6	2061.1	—	—	0.4	172.5	0.77
160721O	SYLV	2.00	84.5	3086.8	—	—	107.1	214.0	23.62
160721P	SYLV	2.42	80.8	874.3	—	—	39.4	116.4	8.84
160721Q	SYLV	6.67	42.4	2193.6	—	—	0.2	77.5	8.18
160721R	SYLV	2.45	49.3	—	—	—	54.6	141.8	31.24
160721S	SYLV	1.82	91.5	84.6	—	—	17.4	308.7	15.62
170716TQ	SYLV	2.69	31.4	1709.2	1007.0	4881.4	31.7	992.2	98.32
170716TR	SYLV	6.60	68.3	2079.3	6673.9	1834.5	—	105.8	9.35
170716TS	SYLV	4.09	71.6	1464.8	8084.7	1923.1	—	126.6	12.95
170716TT	SYLV	2.45	50.6	2206.3	3490.4	5542.2	66.2	148.6	32.05

Sample Code	Region	pH	Temp. ℃	Sp. Cond.* μS/cm	Cl^- μmol/kg	SO_4^{2-} μmol/kg	Fe^{+2} μmol/kg	DOC μM	Total Fluorescence
170716TU	SYLV	1.87	89.1	2147.2	3097.5	9190.1	73.4	253.0	24.22
170720SK	SYLV	5.44	80.0	2461.9	14581.2	1556.5	—	87.9	21.72
170720SL	SYLV	5.90	41.8	2370.5	14670.2	2006.7	—	68.5	11.46
170720SM	SYLV	5.29	76.8	2627.7	15061.1	2058.6	—	83.9	10.16
170720SN	SYLV	2.09	83.6	3029.5	98.7	11346.9	114.6	129.1	30.74
170720SO	SYLV	2.29	86.4	1820.9	9.4	6229.1	68.0	75.2	6.59
170720SP	SYLV	2.92	34.9	1485.0	2924.0	3676.6	46.6	300.8	25.96
180723TU	SYLV	2.17	73.4	2652.4	—	—	76.1	140.9	21.86
180723TV	SYLV	1.98	75.4	3645.4	—	—	4.8	200.3	12.25
180723TW	SYLV	2.13	80.6	2987.7	—	—	7.2	167.1	37.17
180723TX	SYLV	2.34	88.0	1811.5	—	—	36.3	85.5	6.56
180723TY	SYLV	5.46	79.3	2545.5	—	—	1.6	191.6	17.46
180723TZ	SYLV	5.13	45.1	2229.0	—	—	—	95.0	8.22
170716SS	SYLV - s	6.44	79.1	1188.8	1943.8	826.3	—	85.4	9.85
170716SU	SYLV - s	6.04	67.6	615.6	215.4	1017.5	0.5	121.9	16.73
170716SV	SYLV - s	6.51	82.3	1342.0	2364.2	715.5	—	76.5	6.03
170715TL	TURB	6.25	43.8	1453.5	5497.8	1219.5	—	131.9	11.55
170715TM	TURB	5.91	42.5	968.1	611.7	2657.6	—	90.9	13.85
170715TN	TURB	6.68	69.7	2277.2	6325.1	1154.2	—	93.2	15.03
180713TI	TURB	4.91	71.4	295.6	—	—	2.1	344.5	38.87
180713TJ	TURB	5.31	79.7	1536.8	—	—	0.2	511.5	149.89
170720TJ	WAHB	6.46	29.3	2642.7	1426.4	318.3	1.6	128.4	64.72
170720TK	WAHB	6.20	26.1	1943.2	986.3	285.9	0.9	148.6	63.09
170720TM	WAHB	4.27	8.2	14231.9	18.5	9697.5	—	171.7	30.67
120717SC	WASH - l	5.78	88.8	2719.7	5.6	12357.7	0.4	383.2	131.03
120717SD	WASH - l	2.62	76.7	6666.7	21.4	25625.8	1002.7	3764.2	416.51
120717SE	WASH - l	5.59	85.8	2933.2	9.5	11105.2	0.9	520.1	159.83
120717SF	WASH - l	5.57	88.4	2866.0	6.2	16701.5	1.1	1663.6	367.55
120717SG	WASH - l	5.40	73.3	4181.1	11.4	17717.0	0.7	2103.8	499.71
130718SQ	WASH - l	6.24	71.3	3001.0	—	—	4.8	712.9	226.48
130718ST	WASH - l	6.30	86.5	2614.3	—	—	—	695.3	178.90
140727TT	WASH - l	6.03	89.5	2707.4	13.7	14608.6	—	4016.6	1678.52

Sample Code	Region	pH	Temp. ℃	Sp. Cond.* μS/cm	Cl^- μmol/kg	SO_4^{2-} μmol/kg	Fe^{+2} μmol/kg	DOC μM	Total Fluorescence
140727TV	WASH - l	5.73	75.4	3570.7	12.8	14915.9	0.2	—	1736.33
140727TW	WASH - l	5.86	87.5	3368.9	14.1	14364.2	—	1321.2	499.16
180724SF	WASH - l	6.04	86.0	2702.7	—	—	—	532.6	205.33
180724SG	WASH - l	5.83	66.7	2726.3	—	—	0.2	528.6	202.88
180724SH	WASH - l	3.23	82.8	5398.9	—	—	0.2	486.0	145.22
180724SI	WASH - l	5.51	74.0	2399.0	—	—	0.2	445.1	220.64
180724SJ	WASH - l	6.40	76.0	3797.0	—	—	—	488.5	116.30
120719TQ	WASH - u	5.77	86.1	8109.8	2.5	18823.8	0.2	477.9	171.70
120719TR	WASH - u	2.79	75.1	4545.5	115.7	18640.3	455.0	548.5	143.04
120719TS	WASH - u	5.69	76.8	4351.7	9.0	17138.6	3.6	451.8	174.94
120719TT	WASH - u	2.62	42.8	1082.6	4.5	22252.5	179.2	442.4	133.73
120719TU	WASH - u	3.67	48.3	2781.7	2.9	11442.0	39.4	431.5	154.70
130714SA	WASH - u	5.44	74.1	4853.7	—	—	15.2	295.1	107.27
130714SX	WASH - u	2.73	89.8	4338.0	—	—	279.3	208.8	86.37
130714SY	WASH - u	5.64	79.6	6711.3	—	—	—	275.1	121.83
130720DO	WHIT	7.37	86.7	1559.1	—	—	—	63.4	3.21
130720DP	WHIT	8.30	77.0	1574.5	—	—	—	101.2	3.18
130720DQ	WHIT	6.87	79.5	1588.0	—	—	—	82.4	3.92
130720DR	WHIT	8.00	83.9	1523.0	—	—	—	96.5	3.14
160716M	WHIT	8.00	82.5	1060.0	—	—	—	103.2	4.04
160716O	WHIT	7.14	78.3	1325.3	—	—	—	81.8	3.13
160716Q	WHIT	7.62	87.5	1321.3	—	—	0.4	134.6	2.82
160716R	WHIT	7.10	91.0	905.2	—	—	—	64.5	1.42
170718SA	WHIT	8.64	73.9	1635.5	6916.8	184.1	—	115.8	2.62
170718SC	WHIT	7.22	76.1	1360.5	5434.4	150.1	0.4	73.4	3.87
170718SX	WHIT	8.00	83.0	1575.0	6684.4	185.4	0.2	71.5	2.49
170718SZ	WHIT	8.30	85.3	1601.5	6729.5	150.3	0.2	99.7	2.52
170722SR	WHIT	6.65	66.4	500.0	1367.1	270.1	0.5	50.4	2.46
170722SS	WHIT	8.06	47.3	488.9	1371.2	269.8	0.4	50.1	5.43
170722ST	WHIT	6.18	83.0	341.7	1348.2	235.7	0.2	162.0	4.12
170722SU	WHIT	7.67	71.3	559.2	1497.9	293.3	—	46.9	1.81
170722SV	WHIT	6.87	79.5	556.9	1476.9	289.3	—	39.9	1.87

Sample Code	Region	pH	Temp. ℃	Sp. Cond.* μS/cm	Cl^- μmol/kg	$SO_4{}^{2-}$ μmol/kg	Fe^{+2} μmol/kg	DOC μM	Total Fluorescence
180717SA	WHIT	8.08	80.6	1572.4	—	—	—	74.1	2.29
180717SC	WHIT	7.95	84.1	1619.6	—	—	0.2	78.6	2.77
180717SX	WHIT	8.73	72.7	1539.9	—	—	—	59.4	4.27
180717SY	WHIT	7.40	80.5	1594.3	—	—	—	95.0	3.65
180717SZ	WHIT	8.46	83.3	1491.2	—	—	—	124.0	2.79

Table E.2: Hot spring fluorescence indices and PARAFAC model components. AMP – Amphitheater Spring; BOG – Bog Creek; CALC – Calcite Springs; CRAT – Crater Hills; FORS – Forest Springs; GEYS – Geyser Creek; GIBB – Gibbon Hill; GOPA – Greater Obsidian Pool Area; HSB – Hot Springs Basin; IMPS – Imperial and Spray Geyser Basins; LEWS – Lewis Lake; NORR – Norris Geyser Basin; RABB – Rabbit Creek; SENT – Sentinel Meadow; SURF - Surface water; SYLV – Sylvan Springs; TURB – Turbid Lake; WAHB – Wahb Springs; WASH – Washburn; WHIT – White Creek. l - lower; m - middle; u -upper; c - channel; h - hills; n - north; s - south. Refer to Chapter 2 for FI, HIX, and β/α definitions. LC1-5 refer to the five PARAFAC components described in Chapter 2.
Dashes indicate no data.

Sample Code	Region	FI	HIX	β/α	LC1	LC2	LC3	LC4	LC5
120721SA	AMP	1.53	1.14	0.80	0.013585	0.026697	0.012196	0.047330	0.041819
120721SB	AMP	1.57	1.14	0.83	0.014641	0.032250	0.015501	0.048949	0.057549
120721SI	AMP	1.45	3.83	0.69	0.013119	0.021736	0.009268	0.009256	0.012105
120723SR	AMP	—	—	—	—	—	—	—	—
120723SS	AMP	—	—	—	—	—	—	—	—
120723SU	AMP	—	—	—	—	—	—	—	—
120723SW	AMP	—	—	—	—	—	—	—	—
120723SX	AMP	—	—	—	—	—	—	—	—
120724KFQ	AMP	—	—	—	0.032834	0.043041	0.020319	0.022595	0.014189
120724TR	AMP	1.49	1.28	0.76	0.017073	0.032974	0.014851	0.050866	0.043805
120724TS	AMP	1.57	1.06	0.81	0.014577	0.024777	0.014140	0.041362	0.063104
120724TT	AMP	1.47	1.24	0.68	0.009458	0.017809	0.007972	0.013500	0.047164
120724TU	AMP	1.44	1.60	0.68	0.008817	0.018694	0.008062	0.015606	0.025956
120724TV	AMP	1.48	1.50	0.73	0.010562	0.022306	0.010102	0.018757	0.039038
120724TW	AMP	1.52	1.45	0.73	0.010053	0.021720	0.009577	0.019172	0.037542
130723TB	AMP	1.54	0.86	0.95	0.013023	0.030367	0.016412	0.093933	0.016870
130723TW	AMP	1.42	1.49	1.12	0.002115	0.035938	0.017223	0.038645	0.026514
130723TX	AMP	1.36	1.54	1.02	0.007124	0.037878	0.019175	0.039739	0.036152
130723TY	AMP	1.50	0.94	0.86	0.014982	0.027648	0.013267	0.083089	0.017004
140803SP	AMP	1.51	0.74	0.91	0.019034	0.042145	0.018722	0.159106	0.028845
170722TO	AMP	1.44	2.28	0.74	0.010918	0.018639	0.011785	0.013381	0.024268
180918G	BOG - l	1.61	2.82	0.82	0.049789	0.034903	0.040088	0.051440	0.032135
180918H	BOG - l	1.40	1.70	0.88	0.007745	0.017002	0.011973	0.017642	0.019746
180918I	BOG - l	1.37	2.48	0.79	0.015152	0.022410	0.018301	0.020958	0.021771

Sample Code	Region	FI	HIX	β/α	LC1	LC2	LC3	LC4	LC5
180918J	BOG - l	1.52	1.09	1.10	0.001021	0.014806	0.009980	0.017086	0.022807
180918K	BOG - l	1.56	1.39	1.08	0.001023	0.011736	0.007303	0.011732	0.017016
180918L	BOG - l	1.50	1.20	0.77	0.007151	0.014970	0.011684	0.014434	0.049872
180917A	BOG - m	1.31	4.19	0.57	0.041218	0.033823	0.027843	0.018582	0.018953
180917B	BOG - m	1.71	2.10	1.03	0.009988	0.021159	0.018588	0.015506	0.022779
180917C	BOG - m	1.58	1.41	1.00	0.004814	0.010437	0.009066	0.010669	0.016102
180917D	BOG - m	1.55	1.29	0.79	0.005100	0.011819	0.007578	0.010798	0.029164
180917F	BOG - m	1.88	1.75	0.97	0.013546	0.020987	0.020387	0.016405	0.045871
180919M	BOG - u	1.74	0.36	0.98	0.015057	0.006471	0.013156	0.152162	0.040504
180919N	BOG - u	1.71	0.38	1.07	0.015013	0.007462	0.013988	0.151704	0.023165
180919O	BOG - u	1.75	0.32	1.02	0.015334	0.006996	0.013816	0.184209	0.036718
180919P	BOG - u	1.70	0.31	1.02	0.014088	0.005347	0.012794	0.180351	0.013676
180919Q	BOG - u	1.66	0.30	1.03	0.011298	0.005253	0.010350	0.152086	0.011889
180919R	BOG - u	1.53	0.56	0.85	0.017529	0.020642	0.017061	0.152790	0.010030
180919S	BOG - u	1.49	1.99	0.87	0.005174	0.017233	0.011573	0.013853	0.014402
130720SA	CALC	2.08	0.68	2.08	0.000000	0.940448	0.464481	2.918686	1.022433
130720SW	CALC	2.05	0.72	2.14	0.000000	0.695253	0.332116	2.101973	0.869455
130720SY	CALC	2.16	0.80	1.61	0.000000	0.855450	0.432807	2.165078	1.079825
130720SZ	CALC	2.03	1.08	1.50	0.000000	0.948384	0.452388	2.018792	0.753011
140731TP	CALC	2.19	0.70	1.56	0.000000	1.711795	0.832483	4.331920	2.795992
140803TA	CALC	2.12	0.79	1.84	0.000000	1.074154	0.510348	2.990111	1.298056
140803TB	CALC	1.90	1.47	1.45	0.000000	1.437780	0.628035	2.621732	0.391177
140803TC	CALC	1.64	1.09	1.52	0.000000	1.567093	0.728205	3.326098	1.167000
140803TZ	CALC	1.89	1.37	1.38	0.000000	1.813698	0.776713	2.700043	1.454949
120713SJ	CRAT	2.13	1.11	0.74	0.016074	0.027740	0.015638	0.045632	0.060811
120713SK	CRAT	1.26	0.67	0.90	0.017223	0.021367	0.007273	0.050490	0.105174
120715TU	CRAT	1.52	1.89	0.68	0.169770	0.297945	0.155857	0.425977	0.228391
120715TW	CRAT	1.21	0.53	0.77	0.011610	0.009903	0.005487	0.031207	0.075216
120715TY	CRAT	1.60	0.31	0.82	0.021127	0.018739	0.006594	0.289406	0.007826
130717SI	CRAT	1.69	1.05	0.92	0.016590	0.032009	0.016290	0.085832	0.021815
130717SJ	CRAT	1.17	0.89	0.91	0.163780	0.336416	0.089806	0.528020	0.901861
130717SK	CRAT	1.23	0.42	0.90	0.002261	0.003415	0.001320	0.015239	0.019115
130717SL	CRAT	1.60	1.28	0.83	0.064309	0.056529	0.044727	0.172717	0.041303

Sample Code	Region	FI	HIX	β/α	LC1	LC2	LC3	LC4	LC5
130717SM	CRAT	1.28	0.58	0.79	0.004554	0.004545	0.002528	0.018950	0.020431
140727SU	CRAT	1.18	0.36	1.22	0.004386	0.005356	0.003668	0.036009	0.040244
140727SX	CRAT	1.64	0.42	0.89	0.035752	0.040812	0.019562	0.408958	0.020645
140729SB	CRAT	1.74	1.38	0.94	0.031703	0.065806	0.033010	0.125652	0.057222
140729SG	CRAT	1.88	1.36	0.95	0.019083	0.040690	0.019264	0.078702	0.040866
160720H	CRAT	1.62	1.51	0.86	0.020783	0.027814	0.022423	0.063559	0.023000
160720I	CRAT	1.63	1.13	0.87	0.010473	0.015800	0.013639	0.042795	0.020574
160720J	CRAT	2.26	0.98	0.39	0.007540	0.002672	0.003226	0.014902	0.018544
160720K	CRAT	1.72	2.16	0.82	0.057734	0.036713	0.057060	0.085942	0.025875
170724TA	CRAT	1.63	2.08	0.82	0.076927	0.040483	0.059694	0.084122	0.091946
170724TD	CRAT	1.58	0.34	0.80	0.016605	0.012511	0.012568	0.217356	0.010349
170724TE	CRAT	2.39	1.02	0.37	0.008099	0.001983	0.003403	0.015876	0.013279
180714SL	CRAT	1.57	1.70	0.81	0.030005	0.037875	0.032148	0.082371	0.028887
180714SM	CRAT	1.69	1.02	0.86	0.031508	0.022514	0.028203	0.091159	0.074566
180714SN	CRAT	2.29	1.07	0.43	0.007774	0.002142	0.004099	0.018063	0.011442
180714SO	CRAT	1.59	1.83	0.69	0.056082	0.044878	0.046036	0.096231	0.064156
180714SP	CRAT	1.55	0.93	0.72	0.166999	0.234086	0.207693	0.887575	0.314058
120717TA	FORS	1.60	0.81	0.76	0.038379	0.061478	0.029874	0.209098	0.083849
120717TB	FORS	1.50	1.06	0.73	0.055000	0.083035	0.039820	0.216517	0.085642
120717TC	FORS	1.46	1.79	0.68	0.132226	0.126915	0.093381	0.116838	0.301227
120717TD	FORS	1.51	1.49	0.74	0.036355	0.053759	0.026884	0.098822	0.038698
120717TE	FORS	1.49	1.89	0.59	0.047159	0.066597	0.020727	0.106229	0.072248
120717TF	FORS	1.46	1.43	0.68	0.015935	0.032586	0.015018	0.044663	0.035989
120717TG	FORS	1.96	4.80	0.63	0.069455	0.036915	0.049797	0.040805	0.022673
120723TL	FORS	—	—	—	0.307117	0.368932	0.244805	0.175077	0.501438
120723TM	FORS	—	—	—	—	—	—	—	—
120723TN	FORS	1.59	1.25	0.65	0.041303	0.040662	0.027132	0.038316	0.177563
120723TO	FORS	—	—	—	—	—	—	—	—
120723TP	FORS	—	—	—	—	—	—	—	—
120723TQ	FORS	—	—	—	—	—	—	—	—
130720TA	FORS	1.58	1.03	0.83	0.040579	0.066911	0.034784	0.196601	0.016586
130720TU	FORS	1.52	1.00	0.76	0.041447	0.057087	0.028568	0.183681	0.026784
130720TV	FORS	1.55	0.98	0.82	0.034109	0.058603	0.028818	0.174841	0.019831

Sample Code	Region	FI	HIX	β/α	LC1	LC2	LC3	LC4	LC5
130720TW	FORS	1.55	0.91	0.80	0.035265	0.059196	0.027481	0.196145	0.017719
130720TX	FORS	1.55	0.78	0.79	0.029548	0.046504	0.021904	0.186444	0.016669
130720TY	FORS	1.39	1.85	0.69	0.017158	0.020119	0.013387	0.023569	0.035880
130720TZ	FORS	1.47	0.95	0.75	0.032225	0.045239	0.020364	0.151084	0.016282
140726TM	FORS	1.49	1.75	0.70	0.048057	0.055456	0.037194	0.059239	0.113572
140726TN	FORS	1.46	2.16	0.67	0.028034	0.028182	0.018971	0.029209	0.046699
140726TO	FORS	1.50	2.19	0.62	0.067333	0.045593	0.034543	0.048389	0.121887
140726TP	FORS	1.54	1.11	0.74	0.066346	0.096009	0.043559	0.268840	0.074668
140726TQ	FORS	1.53	1.37	0.63	0.141909	0.175147	0.071444	0.362813	0.188782
140726TR	FORS	1.56	1.11	0.77	0.059686	0.096868	0.044392	0.279158	0.038483
170714TH	FORS	1.51	2.56	0.59	0.092115	0.072224	0.057029	0.125984	0.032131
170714TI	FORS	2.06	6.15	0.50	0.121360	0.010312	0.071850	0.045977	0.032878
170714TJ	FORS	1.68	3.36	0.57	0.027967	0.023900	0.021644	0.019399	0.022499
120719SS	GEYS	1.74	0.69	0.85	0.006498	0.013270	0.007827	0.018760	0.066314
120719SX	GEYS	1.84	0.38	0.58	0.002751	0.005476	0.003316	0.012870	0.057152
120719SY	GEYS	1.41	0.82	0.85	0.006256	0.016163	0.007592	0.016239	0.061787
120724SA	GEYS	1.45	1.47	0.65	0.014969	0.027089	0.004328	0.105441	0.046671
120724SY	GEYS	1.40	0.68	0.72	0.004443	0.016467	0.008961	0.013168	0.074714
130712SK	GEYS	1.14	0.75	1.20	0.016958	0.059941	0.014989	0.096455	0.119292
130712SN	GEYS	1.56	1.60	0.94	0.004156	0.013757	0.005545	0.011679	0.016790
130713SR	GEYS	1.29	1.43	0.70	0.002698	0.011469	0.006407	0.010360	0.011708
130713SS	GEYS	1.68	0.68	0.63	0.001656	0.004187	0.003000	0.011480	0.010530
130713ST	GEYS	1.28	1.10	0.89	0.014407	0.034683	0.013917	0.044396	0.056322
130713SV	GEYS	1.33	1.66	0.88	0.011775	0.028287	0.013083	0.024892	0.030212
140724SB	GEYS	1.41	0.77	1.19	0.013281	0.045374	0.014750	0.074574	0.114948
140729TB	GEYS	1.54	1.75	0.78	0.022460	0.052991	0.025978	0.035091	0.060078
140729TC	GEYS	1.40	2.10	0.73	0.029225	0.048330	0.021277	0.022345	0.082730
140729TY	GEYS	1.44	1.49	0.77	0.013908	0.040937	0.020515	0.030337	0.077557
140729TZ	GEYS	1.61	0.34	0.96	0.005475	0.025638	0.011364	0.020525	0.324356
160723A	GEYS	—	—	—	0.013798	0.017698	0.012021	0.010644	0.032479
160723U	GEYS	1.79	1.20	0.80	0.004343	0.008695	0.006151	0.008573	0.027849
160723V	GEYS	1.94	2.18	0.90	0.006135	0.019019	0.008734	0.012470	0.031035
160723X	GEYS	1.44	1.44	0.67	0.004532	0.010787	0.008239	0.010109	0.019940

Sample Code	Region	FI	HIX	β/α	LC1	LC2	LC3	LC4	LC5
160723Y	GEYS	1.84	0.86	0.58	0.002448	0.003547	0.003744	0.009272	0.013733
160723Z	GEYS	2.07	1.54	0.72	0.005443	0.012278	0.010723	0.011490	0.021767
170718TA	GEYS	1.79	1.14	0.76	0.001727	0.005097	0.003165	0.004845	0.013173
170718TZ	GEYS	1.70	2.01	0.77	0.004495	0.009733	0.006305	0.007076	0.014165
170719SE	GEYS	1.89	0.92	0.54	0.002528	0.003604	0.003753	0.010273	0.008226
170719SF	GEYS	1.94	1.46	0.85	0.003841	0.012055	0.009669	0.014047	0.018683
170719SG	GEYS	1.51	3.09	0.67	0.013076	0.022625	0.017434	0.015359	0.018417
170719SH	GEYS	1.55	1.31	0.93	0.006822	0.013473	0.010767	0.032450	0.006991
170719SI	GEYS	1.64	0.57	1.29	0.007900	0.030190	0.035308	0.125669	0.099840
180713SE	GEYS	1.56	1.33	1.05	0.002939	0.009752	0.008268	0.015726	0.019067
180713SF	GEYS	1.45	0.75	0.94	0.002280	0.010586	0.008650	0.015697	0.041105
180713SH	GEYS	1.65	1.68	1.07	0.003362	0.017449	0.008039	0.017318	0.027450
180713SI	GEYS	1.52	0.58	0.88	0.043583	0.097566	0.127726	0.557356	0.188414
180713SJ	GEYS	1.42	2.22	0.83	0.010804	0.022305	0.011822	0.020540	0.021932
180722TM	GEYS	1.44	1.24	0.94	0.001728	0.007163	0.005668	0.009117	0.014212
180722TN	GEYS	1.53	0.83	1.04	0.002206	0.008830	0.007111	0.013542	0.023911
180722TO	GEYS	1.49	1.09	1.22	0.000207	0.012653	0.008456	0.016421	0.016847
180722TP	GEYS	1.50	1.08	0.90	0.003023	0.006118	0.004465	0.008512	0.016991
180722TQ	GEYS	1.62	0.85	0.91	0.007211	0.011589	0.009496	0.028201	0.039547
180722TR	GEYS	1.36	1.50	0.73	0.003526	0.004555	0.003869	0.003298	0.012845
180722TS	GEYS	1.62	0.66	0.97	0.000313	0.002774	0.001812	0.003746	0.010434
170719TC	GIBB	1.68	0.65	0.82	0.002346	0.003335	0.002657	0.006861	0.018409
170719TD	GIBB	1.28	4.01	0.54	0.040337	0.031662	0.022878	0.019561	0.028922
170719TE	GIBB	1.31	6.03	0.54	0.067950	0.048572	0.038005	0.022774	0.018492
170719TF	GIBB	1.68	1.60	0.64	0.003903	0.004491	0.003875	0.003822	0.012965
170719TG	GIBB	1.67	1.12	0.79	0.002706	0.005237	0.002972	0.005539	0.017611
170719TH	GIBB	1.29	7.50	0.49	0.074741	0.041672	0.033514	0.015829	0.020792
170719TI	GIBB	1.32	0.52	0.94	0.002144	0.003214	0.002243	0.008368	0.025692
170725SJ	GIBB	1.30	4.89	0.55	0.023726	0.016688	0.013426	0.008502	0.012224
170725SK	GIBB	1.30	4.96	0.51	0.036793	0.021272	0.018738	0.010020	0.017958
170725SL	GIBB	1.28	8.14	0.49	0.037982	0.020251	0.017571	0.006990	0.007624
170725SM	GIBB	1.50	2.48	0.65	0.105507	0.083575	0.074678	0.150828	0.037720
170725SN	GIBB	1.41	5.25	0.59	0.031502	0.028802	0.024264	0.012432	0.012942

Sample Code	Region	FI	HIX	β/α	LC1	LC2	LC3	LC4	LC5
170725SO	GIBB	1.49	3.08	0.67	0.036233	0.029409	0.027162	0.038948	0.009215
180715TM	GIBB	1.66	0.46	0.82	0.002407	0.004807	0.004584	0.010862	0.042846
180715TO	GIBB	1.35	3.27	0.68	0.010419	0.011370	0.008214	0.007022	0.008615
180715TP	GIBB	1.43	1.03	0.95	0.001387	0.004109	0.004221	0.006632	0.013641
180715TQ	GIBB	1.36	1.65	0.69	0.015481	0.016115	0.013723	0.014565	0.043517
180715TR	GIBB	1.39	1.69	0.95	0.000956	0.016970	0.002397	0.002945	0.013777
120712TA	GOPA	1.77	1.71	0.94	0.013319	0.037842	0.019191	0.031941	0.054587
130716DC	GOPA	1.71	0.92	1.04	0.005096	0.023716	0.012052	0.022997	0.072805
130716SC	GOPA	1.38	2.65	0.91	0.013797	0.033303	0.017098	0.016543	0.023046
130716SD	GOPA	1.27	4.03	0.70	0.030775	0.057215	0.026378	0.013471	0.034697
130716SF	GOPA	1.25	1.67	0.82	0.017944	0.033734	0.016503	0.032886	0.039727
130716SG	GOPA	1.35	3.50	0.83	0.029317	0.044152	0.023459	0.022395	0.023643
140725TH	GOPA	1.36	4.34	0.63	0.147930	0.218290	0.094424	0.060682	0.144806
140725TK	GOPA	1.41	2.72	0.62	0.077554	0.119310	0.050241	0.028477	0.175801
140726SN	GOPA	1.38	6.10	0.64	0.079935	0.098049	0.044117	0.033109	0.028106
140726SS	GOPA	1.35	0.38	0.81	0.035293	0.077945	0.033343	0.574903	0.087092
160714B	GOPA	—	—	—	0.059300	0.053391	0.041959	0.020081	0.020593
160714C	GOPA	1.25	4.04	0.77	0.035619	0.038723	0.029084	0.020114	0.021667
160714D	GOPA	1.31	6.27	0.66	0.051763	0.048618	0.037758	0.017640	0.017092
160714E	GOPA	1.40	3.35	0.67	0.029181	0.043954	0.032252	0.026768	0.024018
160724C	GOPA	1.88	2.04	0.82	0.011274	0.022213	0.016478	0.019818	0.029444
160724D	GOPA	1.46	6.16	0.61	0.050056	0.063159	0.043407	0.019743	0.016590
160724E	GOPA	1.41	3.14	0.85	0.016979	0.028460	0.019975	0.013932	0.019309
160724G	GOPA	1.42	9.06	0.59	0.057604	0.053106	0.037213	0.013242	0.011936
160724H	GOPA	1.37	1.57	0.74	0.003025	0.005266	0.005252	0.005419	0.010669
170713TB	GOPA	2.02	1.61	0.81	0.009948	0.018512	0.014982	0.021482	0.028364
170713TC	GOPA	1.48	3.40	0.77	0.015717	0.029434	0.022618	0.013099	0.015533
170713TD	GOPA	1.48	3.26	0.72	0.018311	0.031370	0.024769	0.011967	0.020058
170713TE	GOPA	1.23	0.03	0.55	0.000000	0.000000	0.000000	0.432647	0.000000
170714SI	GOPA	1.48	8.43	0.55	0.053754	0.063629	0.043504	0.011323	0.011176
170714SJ	GOPA	1.47	3.19	0.73	0.019678	0.030672	0.023602	0.013252	0.022921
170714SK	GOPA	1.53	3.35	0.66	0.020543	0.034418	0.028182	0.011292	0.019919
180719SI	GOPA	1.54	2.36	0.63	0.008415	0.020605	0.016198	0.011859	0.013250

Sample Code	Region	FI	HIX	β/α	LC1	LC2	LC3	LC4	LC5
180719SL	GOPA	1.30	5.92	0.63	0.092527	0.088061	0.064479	0.029541	0.037551
180719SM	GOPA	1.38	2.54	0.83	0.027213	0.039278	0.029146	0.021067	0.041371
180719SN	GOPA	1.36	5.72	0.59	0.100276	0.102646	0.072330	0.033954	0.034832
170728TA	HSB	1.57	4.79	0.61	0.061213	0.064644	0.060596	0.032905	0.035075
170728TB	HSB	1.38	5.44	0.65	0.168117	0.156766	0.135108	0.065020	0.104967
170729TD	HSB	1.60	4.22	0.58	0.046866	0.039791	0.034971	0.024539	0.028857
170729TE	HSB	2.19	5.02	0.55	0.104203	0.070239	0.097520	0.033291	0.048059
170729TF	HSB	1.35	6.01	0.50	0.142372	0.089181	0.072708	0.056399	0.036992
170729TG	HSB	1.45	3.33	0.76	0.046967	0.057287	0.045345	0.055103	0.036925
170729TH	HSB	1.40	6.39	0.60	0.041051	0.032812	0.026228	0.017542	0.012210
170729TI	HSB	1.52	2.75	0.82	0.039318	0.056493	0.049034	0.066902	0.036973
170729TJ	HSB	1.49	3.01	0.70	0.037238	0.038731	0.029879	0.037062	0.025433
170729TK	HSB	1.49	3.32	0.68	0.027307	0.027798	0.022256	0.026407	0.016033
170730TM	HSB	1.54	1.41	0.74	0.028703	0.025234	0.023813	0.079335	0.019817
170730TN	HSB	1.73	6.29	0.56	0.088627	0.058360	0.057096	0.017875	0.040293
170730TO	HSB	1.84	7.74	0.48	0.118383	0.090920	0.109563	0.011123	0.022782
170730TP	HSB	2.38	8.82	0.32	0.159569	0.036893	0.096911	0.006457	0.020282
170730TQ	HSB	1.74	0.32	0.96	0.008440	0.009863	0.007706	0.145232	0.006941
170730TR	HSB	1.70	3.36	0.70	0.026459	0.027340	0.031395	0.020275	0.028956
170730TS	HSB	1.63	4.27	0.57	0.116325	0.089346	0.087174	0.066347	0.046994
170730TT	HSB	1.68	2.41	0.74	0.035008	0.035507	0.031884	0.055857	0.022564
170730TU	HSB	1.68	2.36	1.06	0.004419	0.025797	0.017838	0.023237	0.016690
120722TE	IMPS	1.85	0.04	0.57	0.000122	0.000171	0.000708	0.015924	0.055725
120722TF	IMPS	1.47	1.61	0.63	0.009307	0.017014	0.010371	0.008034	0.041052
120722TG	IMPS	1.51	1.52	0.67	0.012923	0.052066	0.028243	0.012944	0.094418
140804TE	IMPS	1.54	0.16	1.38	0.000000	0.005231	0.004253	0.036415	0.087696
140804TF	IMPS	1.51	1.76	0.75	0.011248	0.020718	0.014111	0.031065	0.025313
140804TG	IMPS	1.60	0.97	0.79	0.093011	0.307535	0.160908	0.691299	0.175843
140804TH	IMPS	1.39	2.02	0.67	0.035093	0.078235	0.038263	0.026388	0.128010
180922A	LEWS - c	1.48	2.17	0.74	0.003509	0.006187	0.003899	0.002736	0.012190
180922B	LEWS - c	1.56	1.53	0.73	0.003352	0.006402	0.004907	0.003904	0.008363
180922D	LEWS - c	1.61	2.11	0.83	0.002603	0.005462	0.004010	0.002340	0.007494
180922X	LEWS - c	1.85	0.53	0.73	0.002446	0.003555	0.003295	0.005719	0.033341

Sample Code	Region	FI	HIX	β/α	LC1	LC2	LC3	LC4	LC5
180922Y	LEWS - c	1.49	2.06	0.77	0.003302	0.006090	0.004336	0.004359	0.008252
180922Z	LEWS - c	1.61	1.20	0.73	0.005476	0.007505	0.005892	0.006427	0.029842
180714TK	LEWS - h	1.59	0.59	1.06	0.001533	0.011602	0.010836	0.019919	0.058406
180714TL	LEWS - h	1.55	0.58	0.90	0.003057	0.009304	0.007948	0.024406	0.042481
180923E	LEWS - h	1.59	1.10	0.86	0.003646	0.012548	0.008589	0.009361	0.033789
180923F	LEWS - h	1.50	1.88	0.88	0.003998	0.015421	0.010032	0.014115	0.013556
180923G	LEWS - h	1.56	1.94	0.90	0.002816	0.013284	0.008251	0.009865	0.012268
180923H	LEWS - h	1.45	3.35	0.85	0.006422	0.015774	0.010146	0.007247	0.009478
180923I	LEWS - h	1.42	2.16	0.78	0.009845	0.015728	0.010649	0.009117	0.020634
120714TO	NORR	1.60	0.29	0.99	0.003901	0.011548	0.003263	0.085470	0.033858
120714TR	NORR	1.47	0.65	0.81	0.001836	0.011581	0.004609	0.016258	0.037202
120718SK	NORR	1.48	1.23	0.76	0.007254	0.015953	0.007841	0.009815	0.049358
120718SL	NORR	1.49	1.95	0.62	0.033244	0.046596	0.029948	0.032050	0.089589
120718SM	NORR	2.00	1.05	0.63	0.006987	0.008587	0.005651	0.006424	0.040511
120718SP	NORR	1.56	0.81	0.89	0.004078	0.010907	0.004865	0.009044	0.049678
120718SQ	NORR	1.45	0.75	0.80	0.009566	0.019735	0.008494	0.047905	0.054420
130711SC	NORR	1.52	1.21	0.85	0.004410	0.009776	0.004546	0.012650	0.016422
130711SD	NORR	1.57	1.80	0.84	0.005160	0.012563	0.005954	0.010611	0.014725
130711SF	NORR	1.51	1.33	0.88	0.003403	0.009046	0.004094	0.011974	0.011552
130711SG	NORR	1.38	2.55	0.72	0.005877	0.012018	0.005480	0.007714	0.009973
130712TF	NORR	1.56	0.31	1.12	0.005224	0.009975	0.004437	0.098889	0.013050
130712TG	NORR	1.43	0.82	0.87	0.008164	0.016436	0.007238	0.052116	0.011590
130712TH	NORR	1.34	1.01	1.08	0.001672	0.006023	0.003151	0.009286	0.012658
130712TJ	NORR	1.52	1.36	0.87	0.007545	0.020939	0.009183	0.033900	0.013273
130712TL	NORR	1.38	1.27	0.75	0.012178	0.019084	0.008876	0.040022	0.011203
130712TM	NORR	1.47	0.76	0.86	0.008066	0.016424	0.007179	0.056199	0.012686
130723SU	NORR	1.41	0.56	0.87	0.005336	0.009174	0.003974	0.043306	0.012642
130723SV	NORR	1.53	1.82	0.83	0.008416	0.017165	0.008171	0.020019	0.010714
130723SW	NORR	1.56	1.85	0.84	0.011042	0.023834	0.012672	0.026604	0.015848
130723SX	NORR	1.54	0.56	1.04	0.010347	0.024433	0.011885	0.114786	0.020869
130723SY	NORR	1.40	1.61	0.88	0.013696	0.036911	0.016659	0.038581	0.027763
130723SZ	NORR	1.30	1.59	0.86	0.031094	0.088945	0.031070	0.093199	0.058168
140725FB	NORR	1.60	0.23	1.14	0.005499	0.010252	0.004205	0.146130	0.037167

Sample Code	Region	FI	HIX	β/α	LC1	LC2	LC3	LC4	LC5
140727FD	NORR	1.48	1.56	0.90	0.016275	0.038583	0.024981	0.056118	0.040439
140727FE	NORR	1.44	2.23	0.80	0.029324	0.060242	0.028737	0.060539	0.031312
140727FF	NORR	1.43	0.61	0.81	0.011530	0.020311	0.009430	0.061142	0.092225
140803FN	NORR	1.51	1.39	0.85	0.011910	0.030165	0.014607	0.031464	0.043307
140804SR	NORR	1.70	1.00	1.10	0.002763	0.013244	0.007242	0.018593	0.032455
140804SV	NORR	1.30	3.85	0.56	0.051047	0.070569	0.034140	0.043327	0.032644
160719A	NORR	1.45	1.34	0.83	0.009231	0.013017	0.009284	0.027068	0.013517
160719B	NORR	1.37	1.90	0.80	0.018257	0.033609	0.020324	0.035589	0.030754
160719C	NORR	1.52	0.86	0.90	0.015274	0.022394	0.018048	0.086347	0.025886
160719D	NORR	1.86	1.44	0.76	0.002574	0.005841	0.003148	0.004114	0.018254
160719E	NORR	1.54	0.39	0.94	0.005433	0.009458	0.007050	0.076950	0.025620
160719F	NORR	1.49	1.77	0.68	0.005884	0.009433	0.006313	0.005718	0.021862
160719Z	NORR	2.42	3.86	0.75	0.038464	0.007491	0.023231	0.011754	0.028459
170715SM	NORR	2.60	4.47	0.67	0.062750	0.010207	0.034770	0.013948	0.029806
170715SN	NORR	1.59	0.96	0.92	0.019607	0.027869	0.022603	0.103714	0.018247
170715SO	NORR	1.54	1.79	0.84	0.014294	0.021963	0.017290	0.035202	0.013807
170715SP	NORR	1.44	2.77	0.72	0.021560	0.030182	0.022306	0.027607	0.019335
170725TH	NORR	1.46	2.47	0.71	0.017780	0.025459	0.019164	0.026289	0.019251
170725TI	NORR	1.50	1.19	0.61	0.003939	0.004978	0.003992	0.002697	0.027528
170725TL	NORR	1.46	3.15	0.60	0.043761	0.034110	0.030385	0.029035	0.052593
170725TM	NORR	1.63	0.53	0.98	0.006340	0.010169	0.008483	0.069709	0.011582
170725TN	NORR	1.69	2.08	0.96	0.001814	0.005424	0.003298	0.005093	0.007020
180718SD	NORR	1.58	2.60	0.82	0.011600	0.019827	0.012963	0.018185	0.016020
180718SE	NORR	1.29	0.74	0.83	0.027976	0.036926	0.025210	0.072490	0.153324
180718SF	NORR	1.85	4.58	0.81	0.061774	0.004349	0.028740	0.012724	0.019218
180718SG	NORR	1.58	1.05	1.04	0.001963	0.007273	0.005326	0.008988	0.023736
180718SH	NORR	1.63	0.77	0.89	0.004579	0.008059	0.006980	0.017324	0.031944
180721SP	NORR	1.64	0.69	0.96	0.013596	0.020970	0.017178	0.096334	0.037775
180721SQ	NORR	1.54	0.75	0.83	0.008045	0.009493	0.007999	0.032911	0.035347
180721SR	NORR	1.74	0.68	0.92	0.002223	0.006593	0.005002	0.011008	0.031173
180721SS	NORR	1.68	0.86	0.84	0.003486	0.008521	0.005556	0.012273	0.034444
180721ST	NORR	1.66	0.50	0.93	0.008151	0.013006	0.010884	0.033570	0.127737
180721SU	NORR	1.57	0.40	1.05	0.003677	0.008648	0.006140	0.064783	0.016126

Sample Code	Region	FI	HIX	β/α	LC1	LC2	LC3	LC4	LC5
180721SV	NORR	1.89	0.68	0.95	0.001557	0.005294	0.003039	0.008311	0.028688
180723SB	NORR	1.52	3.64	0.85	0.008612	0.021230	0.013956	0.012926	0.009542
180723SC	NORR	1.26	5.10	0.56	0.024051	0.018893	0.013552	0.009138	0.009965
180723SD	NORR	1.58	1.35	0.68	0.023798	0.012079	0.015160	0.057622	0.016973
180723SE	NORR	1.54	1.63	0.69	0.002933	0.002986	0.002789	0.002240	0.011549
160726S	RABB - h	1.43	3.47	0.69	0.007297	0.020073	0.014007	0.004829	0.020939
160726T	RABB - h	1.44	0.80	0.36	0.000952	0.000253	0.000383	0.000000	0.010058
160726U	RABB - h	1.51	2.64	0.09	0.000661	0.000061	0.000207	0.000000	0.004074
160726V	RABB - h	1.30	0.28	0.30	0.000712	0.000000	0.000335	0.005610	0.003323
160726W	RABB - h	1.49	0.43	0.75	0.002645	0.002187	0.002015	0.023650	0.004606
160726X	RABB - h	1.34	1.24	0.65	0.037687	0.057596	0.046007	0.129272	0.082217
160726Y	RABB - h	1.83	3.87	0.55	0.012250	0.010148	0.011182	0.003908	0.013517
120718TI	RABB - n	1.51	1.23	0.74	0.014625	0.028221	0.018335	0.012252	0.092416
120718TJ	RABB - n	—	—	—	—	—	—	—	—
120718TK	RABB - n	1.63	0.25	0.66	0.001095	0.003503	0.002162	0.000579	0.056733
120718TL	RABB - n	1.51	2.26	0.69	0.010692	0.022123	0.012304	0.004993	0.032878
130713TO	RABB - n	1.28	0.91	0.94	0.002649	0.005374	0.004458	0.011043	0.014869
130713TP	RABB - n	1.47	1.13	0.79	0.002922	0.005339	0.002819	0.005285	0.014536
140802SC	RABB - n	1.43	1.20	0.76	0.005403	0.009936	0.004791	0.006425	0.030013
140802SD	RABB - n	1.40	2.20	0.70	0.019454	0.035059	0.017863	0.021776	0.035837
140802SE	RABB - n	1.46	3.54	0.72	0.019783	0.034824	0.017051	0.013435	0.019567
140805SB	RABB - n	1.63	0.99	0.80	0.003800	0.007028	0.005034	0.012133	0.018291
140805SE	RABB - n	1.56	2.10	0.66	0.006558	0.012205	0.005302	0.007630	0.015830
140805SY	RABB - n	1.56	1.39	0.83	0.005350	0.013328	0.007768	0.007751	0.029688
170713SC	RABB - n	1.49	2.75	0.60	0.009123	0.010053	0.007276	0.004729	0.012122
170713SD	RABB - n	1.39	0.53	0.95	0.000086	0.001166	0.002192	0.002576	0.010371
170713SE	RABB - n	1.47	3.19	0.69	0.009302	0.013624	0.010542	0.006062	0.013255
170713SF	RABB - n	1.36	0.83	0.65	0.002841	0.003163	0.003031	0.004780	0.016149
120713TH	RABB - s	1.43	2.52	0.68	0.017861	0.028889	0.013147	0.005470	0.049912
120713TI	RABB - s	1.50	3.30	0.74	0.030787	0.058050	0.033843	0.015603	0.046535
120713TJ	RABB - s	1.38	2.64	0.62	0.098579	0.143468	0.067848	0.028567	0.247115
120713TK	RABB - s	1.43	1.37	0.72	0.029308	0.047534	0.026299	0.011363	0.163217
120713TL	RABB - s	1.48	1.53	0.67	0.012735	0.020525	0.011517	0.003184	0.066580

Sample Code	Region	FI	HIX	β/α	LC1	LC2	LC3	LC4	LC5
130722TK	RABB - s	1.38	3.74	0.69	0.010319	0.029467	0.015109	0.010592	0.009803
130722TL	RABB - s	1.37	0.79	0.79	0.000752	0.002637	0.001798	0.001494	0.009912
130722TM	RABB - s	1.32	0.98	0.72	0.001091	0.002373	0.001571	0.002257	0.007629
130722TP	RABB - s	1.40	4.01	0.76	0.019395	0.031484	0.018614	0.012651	0.012514
140724TB	RABB - s	1.30	4.99	0.59	0.205125	0.262945	0.114133	0.057954	0.188066
140724TD	RABB - s	1.33	4.75	0.71	0.115525	0.174931	0.084626	0.074679	0.072072
140724TE	RABB - s	1.49	0.07	0.82	0.000470	0.002657	0.001326	0.007705	0.128992
140724TF	RABB - s	1.37	5.53	0.64	0.146751	0.186283	0.095299	0.058999	0.110713
140730TH	RABB - s	1.42	2.95	0.73	0.039009	0.056431	0.031340	0.020350	0.068779
140730TI	RABB - s	1.45	3.36	0.68	0.027561	0.065931	0.030871	0.019440	0.046158
140730TK	RABB - s	1.36	0.09	0.98	0.000787	0.001138	0.000020	0.037506	0.020135
140730TL	RABB - s	1.66	1.45	0.63	0.011399	0.026916	0.016673	0.010586	0.059561
140805TJ	RABB - s	1.50	3.22	0.64	0.029867	0.039295	0.023226	0.018438	0.033212
140805TK	RABB - s	1.41	2.39	0.77	0.026449	0.061151	0.035924	0.055731	0.033221
140805TL	RABB - s	1.46	0.34	0.75	0.005982	0.013236	0.008694	0.009536	0.191115
140805TM	RABB - s	1.51	0.11	1.07	0.000254	0.001664	0.001018	0.016616	0.040753
140805TN	RABB - s	1.42	2.83	0.69	0.023921	0.040669	0.021705	0.016527	0.036952
140805TO	RABB - s	1.39	3.81	0.70	0.035485	0.056259	0.026454	0.024501	0.030888
160725J	RABB - s	1.33	5.31	0.67	0.046745	0.046272	0.039151	0.015908	0.026684
160725K	RABB - s	1.41	5.66	0.64	0.027335	0.023985	0.018602	0.006919	0.018338
160725L	RABB - s	1.44	3.84	0.66	0.009405	0.011379	0.009931	0.002842	0.013024
160725M	RABB - s	1.38	0.05	1.10	0.000865	0.000000	0.000089	0.124845	0.010882
160725N	RABB - s	1.33	10.61	0.56	0.145609	0.138883	0.097944	0.027771	0.018851
160725O	RABB - s	1.59	1.61	0.67	0.005304	0.006940	0.006202	0.004582	0.020133
160725P	RABB - s	1.53	0.85	0.54	0.001177	0.001014	0.001036	0.003159	0.006423
160725Q	RABB - s	1.47	0.62	0.61	0.000947	0.000983	0.001050	0.001142	0.011011
170723TR	RABB - s	1.51	5.99	0.68	0.026818	0.039133	0.030128	0.011776	0.009476
170723TS	RABB - s	1.39	5.35	0.63	0.080196	0.085106	0.068713	0.027256	0.026615
170723TT	RABB - s	1.45	5.90	0.67	0.037628	0.042825	0.034349	0.012420	0.016120
170723TU	RABB - s	1.45	5.39	0.69	0.038434	0.047853	0.037938	0.016544	0.014653
170723TV	RABB - s	1.36	4.85	0.68	0.038931	0.042035	0.035442	0.018655	0.020634
170723TW	RABB - s	1.31	7.34	0.61	0.037246	0.030059	0.023156	0.012286	0.006314
170723TX	RABB - s	1.42	0.14	0.62	0.000397	0.000121	0.000134	0.007295	0.004985

Sample Code	Region	FI	HIX	β/α	LC1	LC2	LC3	LC4	LC5
170723TY	RABB - s	1.35	7.48	0.60	0.105610	0.098582	0.072586	0.032076	0.025546
170723TZ	RABB - s	1.31	8.53	0.63	0.102978	0.077364	0.061478	0.029574	0.010369
180718KFE	RABB - s	1.64	0.65	0.79	0.005308	0.011214	0.008877	0.051887	0.009116
180718KFF	RABB - s	1.47	1.52	0.66	0.008502	0.010342	0.008029	0.007066	0.022895
180718KFG	RABB - s	1.41	4.23	0.69	0.037692	0.044788	0.034432	0.015149	0.026747
180718TA	RABB - s	1.36	2.59	0.68	0.009044	0.008540	0.006618	0.004754	0.010649
180718TB	RABB - s	1.30	7.13	0.55	0.134604	0.111848	0.079385	0.035855	0.032305
180718TC	RABB - s	1.43	4.11	0.70	0.051165	0.053182	0.044475	0.025526	0.033708
180718TD	RABB - s	1.34	4.05	0.60	0.027235	0.048076	0.032186	0.012946	0.029098
180718TE	RABB - s	1.41	3.46	0.68	0.004308	0.006658	0.005545	0.002413	0.005810
180718TY	RABB - s	1.38	4.78	0.73	0.043506	0.053543	0.041687	0.019533	0.024719
180718TZ	RABB - s	1.73	0.08	0.68	0.000221	0.000089	0.000652	0.006219	0.021528
130718DE	SENT	1.24	0.64	1.05	0.006932	0.014115	0.006549	0.025107	0.058322
130722SO	SENT	1.61	1.13	1.00	0.003289	0.012164	0.005545	0.015284	0.023909
130722SQ	SENT	1.64	0.85	1.21	0.001509	0.010267	0.005651	0.019412	0.025832
140725SH	SENT	1.56	0.94	1.21	0.003438	0.018976	0.008037	0.022757	0.052312
140730SL	SENT	1.60	1.04	1.08	0.005370	0.018966	0.008288	0.023737	0.038552
140730SM	SENT	1.82	1.09	1.02	0.002634	0.013902	0.004778	0.011243	0.034261
160715G	SENT	1.33	5.60	0.55	0.356643	0.326608	0.278806	0.138978	0.192075
160715I	SENT	1.43	2.65	0.83	0.003102	0.006312	0.003551	0.002881	0.010135
160715K	SENT	1.23	3.85	0.57	0.567355	0.433795	0.386996	0.286339	0.430552
180712SD	SENT	1.63	0.53	1.06	0.003396	0.007847	0.007180	0.019181	0.061841
170722TP	SURF (AMP)	1.43	6.04	0.62	0.011911	0.014322	0.009785	0.004460	0.004793
140731TO	SURF (CALC)	1.40	1.35	0.77	0.019169	0.037353	0.019129	0.031343	0.095773
160723JN7	SURF (GEYS)	1.31	4.38	0.56	0.018891	0.012225	0.009860	0.004537	0.017782
180715KFC	SURF (GIBB)	1.28	4.49	0.58	0.013751	0.009293	0.007261	0.004308	0.008741
160724JN8	SURF (GOPA)	1.41	4.64	0.70	0.334756	0.368766	0.273896	0.176800	0.141148
170730TL	SURF (HSB)	1.35	3.52	0.67	0.019114	0.018759	0.015648	0.013597	0.013792
180922C	SURF (LEWS)	1.34	3.40	0.66	0.014914	0.016177	0.012157	0.011230	0.011375
160715JN4	SURF (SENT)	1.28	6.22	0.51	0.018739	0.011974	0.009794	0.003897	0.010090
160721JN5	SURF (SYLV)	1.28	7.80	0.48	0.031165	0.019067	0.014716	0.003535	0.014445
170715TO	SURF (TURB)	1.39	4.29	0.58	0.033602	0.026731	0.023585	0.021505	0.014843
170720TL	SURF (WAHB)	1.33	6.45	0.53	0.022377	0.017420	0.012187	0.004947	0.009507

Sample Code	Region	FI	HIX	β/α	LC1	LC2	LC3	LC4	LC5
120721KFL	SYLV	1.53	1.05	0.66	0.024611	0.028625	0.012442	0.101984	0.004088
120721TA	SYLV	1.76	1.97	0.67	0.024069	0.028019	0.016067	0.017277	0.054981
120721TB	SYLV	2.63	1.80	0.27	0.025361	0.008302	0.012513	0.005092	0.047597
120721TC	SYLV	1.50	2.25	0.66	0.003471	0.006684	0.004094	0.004047	0.007338
120721TW	SYLV	1.45	1.25	0.68	0.023500	0.031533	0.013390	0.071229	0.027220
120721TY	SYLV	1.43	0.86	0.69	0.025402	0.029840	0.013289	0.125488	0.005140
120722SK	SYLV	1.58	0.89	0.66	0.024434	0.022223	0.013730	0.094055	0.033997
120722SL	SYLV	1.51	0.97	0.78	0.065129	0.091484	0.046264	0.299833	0.074695
120722SM	SYLV	1.50	0.54	0.73	0.025382	0.032330	0.015136	0.208559	0.042917
120722SP	SYLV	1.95	2.66	0.54	0.033684	0.031498	0.026033	0.011253	0.058618
120722SQ	SYLV	1.38	1.47	0.67	0.048154	0.062621	0.037870	0.076130	0.134975
130714TU	SYLV	1.45	1.44	0.73	0.027820	0.034849	0.017287	0.078610	0.012730
130714TY	SYLV	1.40	1.18	0.65	0.035252	0.036208	0.020330	0.118835	0.015260
130721SC	SYLV	1.44	1.21	0.91	0.011857	0.022524	0.017954	0.053294	0.033172
130721SD	SYLV	1.59	0.42	0.98	0.047390	0.010507	0.010244	0.281886	0.025927
130721SE	SYLV	2.26	2.53	0.36	0.017998	0.019559	0.007674	0.013607	0.019939
130721SF	SYLV	1.55	0.71	0.86	0.005527	0.010867	0.008265	0.031135	0.036917
130721SG	SYLV	2.02	1.07	0.83	0.006867	0.013787	0.007677	0.028744	0.030800
130721SH	SYLV	1.06	0.49	1.11	0.036408	0.043702	0.018252	0.132259	0.211147
130721SI	SYLV	1.58	0.91	0.76	0.023073	0.023287	0.015387	0.095534	0.020986
140731ST	SYLV	1.54	0.95	0.79	0.002644	0.006384	0.003304	0.004146	0.022719
140731SU	SYLV	1.64	0.95	0.90	0.012097	0.025539	0.014863	0.039614	0.068351
140731SV	SYLV	1.54	1.41	0.80	0.020524	0.021043	0.012739	0.019973	0.052069
140731SW	SYLV	1.55	2.16	0.82	0.027944	0.045281	0.019762	0.034346	0.056546
140731SX	SYLV	1.45	1.65	0.69	0.058746	0.070450	0.029358	0.147988	0.019597
140731SY	SYLV	1.52	1.29	0.69	0.041319	0.053201	0.032508	0.132164	0.034306
140802TR	SYLV	1.54	0.91	0.75	0.035406	0.040939	0.022287	0.172077	0.027106
140802TS	SYLV	1.41	1.05	0.79	0.018037	0.032254	0.020891	0.054184	0.093424
140802TT	SYLV	1.61	0.68	0.89	0.018292	0.030063	0.017465	0.144347	0.043811
140802TU	SYLV	1.44	1.94	0.84	0.291658	0.491539	0.244009	0.818692	0.105475
140802TV	SYLV	1.68	2.66	0.66	0.049268	0.072309	0.047339	0.045896	0.069067
140802TW	SYLV	2.57	1.91	0.34	0.045993	0.020183	0.025906	0.022567	0.079589
140802TX	SYLV	1.46	1.45	0.72	0.050336	0.064744	0.030661	0.133973	0.052163

Sample Code	Region	FI	HIX	β/α	LC1	LC2	LC3	LC4	LC5
160717T	SYLV	1.55	0.98	0.73	0.044760	0.041675	0.036031	0.189952	0.040302
160717U	SYLV	2.85	5.15	0.14	0.051894	0.000000	0.026891	0.000000	0.019420
160717V	SYLV	2.28	2.25	0.45	0.025268	0.008377	0.021816	0.013821	0.038163
160717W	SYLV	1.45	4.11	0.66	0.005980	0.008390	0.007545	0.004031	0.005635
160717X	SYLV	1.47	0.40	0.73	0.010467	0.009584	0.008496	0.118070	0.015975
160721N	SYLV	1.44	0.09	0.00	0.000227	0.000258	0.000117	0.000000	0.020929
160721O	SYLV	1.56	0.79	0.70	0.022719	0.014742	0.016273	0.103695	0.014576
160721P	SYLV	1.54	0.69	0.71	0.007440	0.006223	0.006060	0.037630	0.014156
160721Q	SYLV	1.68	1.69	0.76	0.008875	0.007773	0.006901	0.003907	0.031996
160721R	SYLV	1.48	1.59	0.69	0.034213	0.028614	0.022544	0.077007	0.017560
160721S	SYLV	1.48	1.65	0.62	0.016274	0.012124	0.014174	0.020508	0.030815
170716TQ	SYLV	1.44	3.19	0.61	0.125917	0.085412	0.073885	0.127158	0.036033
170716TR	SYLV	2.17	1.88	0.63	0.009407	0.008406	0.009316	0.008728	0.023431
170716TS	SYLV	1.77	3.01	0.71	0.013459	0.011558	0.013418	0.007345	0.018880
170716TT	SYLV	1.48	1.70	0.69	0.034910	0.029515	0.023798	0.078048	0.011749
170716TU	SYLV	1.63	0.80	0.65	0.023192	0.015331	0.016740	0.106716	0.017971
170720SK	SYLV	2.79	3.56	0.24	0.037784	0.001097	0.020801	0.002166	0.019694
170720SL	SYLV	1.88	5.51	0.61	0.017172	0.008900	0.009934	0.002244	0.011131
170720SM	SYLV	2.32	1.06	0.41	0.013240	0.002658	0.008106	0.010771	0.028782
170720SN	SYLV	1.59	0.63	0.83	0.023190	0.022653	0.019423	0.178441	0.013315
170720SO	SYLV	1.54	0.16	0.81	0.002355	0.001241	0.002283	0.069111	0.007741
170720SP	SYLV	1.45	4.82	0.55	0.029638	0.031155	0.025036	0.012140	0.023959
180723TU	SYLV	1.43	0.56	0.80	0.015034	0.016889	0.013475	0.126074	0.019719
180723TV	SYLV	1.40	1.82	0.66	0.012847	0.010055	0.011003	0.016551	0.018101
180723TW	SYLV	1.52	0.76	0.79	0.031392	0.028087	0.025241	0.181674	0.019486
180723TX	SYLV	1.42	0.13	0.89	0.002189	0.001036	0.001441	0.074405	0.009026
180723TY	SYLV	2.15	1.19	0.48	0.019816	0.006930	0.017244	0.016501	0.060680
180723TZ	SYLV	1.59	2.71	0.81	0.008662	0.008057	0.007619	0.005576	0.014209
170716SS	SYLV - s	1.64	3.09	0.46	0.013206	0.006951	0.009009	0.004557	0.014065
170716SU	SYLV - s	1.22	4.40	0.53	0.022597	0.014409	0.012473	0.009347	0.011849
170716SV	SYLV - s	1.63	1.44	0.62	0.006350	0.005004	0.005438	0.004836	0.016266
170715TL	TURB	1.70	3.91	0.76	0.009789	0.018755	0.012113	0.006169	0.015468
170715TM	TURB	1.66	3.54	0.81	0.012459	0.025319	0.012569	0.014860	0.013092

Sample Code	Region	FI	HIX	β/α	LC1	LC2	LC3	LC4	LC5
170715TN	TURB	1.97	4.71	0.88	0.011073	0.032528	0.015300	0.013222	0.014879
180713TI	TURB	1.35	3.01	0.68	0.039263	0.041804	0.034039	0.035059	0.037286
180713TJ	TURB	1.84	3.42	0.54	0.161134	0.107807	0.178630	0.082603	0.104531
170720TJ	WAHB	2.08	0.91	1.59	0.000000	0.106856	0.073872	0.234315	0.179632
170720TK	WAHB	1.81	0.88	1.40	0.005406	0.096723	0.067717	0.242646	0.157227
170720TM	WAHB	1.68	0.37	0.84	0.016914	0.020278	0.014114	0.233969	0.012827
120717SC	WASH - l	1.63	3.70	0.78	0.091834	0.239745	0.133660	0.068454	0.143339
120717SD	WASH - l	1.49	1.21	0.78	0.308150	0.568560	0.297503	1.248202	0.412329
120717SE	WASH - l	1.51	8.86	0.68	0.164409	0.251881	0.139664	0.048786	0.025254
120717SF	WASH - l	1.53	7.56	0.59	0.409821	0.558937	0.306243	0.141557	0.142612
120717SG	WASH - l	1.47	6.52	0.61	0.535785	0.751145	0.420626	0.219099	0.187756
130718SQ	WASH - l	1.44	6.52	0.70	0.247992	0.330249	0.178970	0.106944	0.074606
130718ST	WASH - l	1.41	1.29	0.86	0.076645	0.239691	0.183085	0.308122	0.453164
140727TT	WASH - l	1.39	6.13	0.60	1.937952	2.367512	1.267473	0.969807	0.587920
140727TV	WASH - l	1.39	7.46	0.59	2.061138	2.445441	1.252253	0.787596	0.406794
140727TW	WASH - l	1.42	6.82	0.69	0.533605	0.767327	0.403432	0.194971	0.206246
180724SF	WASH - l	1.51	6.29	0.72	0.224765	0.248262	0.199490	0.093961	0.083188
180724SG	WASH - l	1.42	6.91	0.67	0.245667	0.228037	0.182960	0.082639	0.070126
180724SH	WASH - l	1.53	2.78	0.73	0.122667	0.173918	0.161429	0.059480	0.307398
180724SI	WASH - l	1.50	7.33	0.72	0.270975	0.230365	0.207889	0.067376	0.110297
180724SJ	WASH - l	1.49	3.30	0.71	0.105195	0.139003	0.123168	0.083823	0.109349
120719TQ	WASH - u	1.89	3.88	0.71	0.178849	0.221610	0.168616	0.098231	0.205944
120719TR	WASH - u	1.73	2.63	0.83	0.120857	0.194950	0.145365	0.155593	0.178487
120719TS	WASH - u	1.87	5.63	0.69	0.160343	0.261338	0.181089	0.057606	0.098292
120719TT	WASH - u	1.75	3.59	0.80	0.121602	0.190103	0.132421	0.100421	0.123664
120719TU	WASH - u	1.86	4.36	0.64	0.146523	0.211686	0.158309	0.055389	0.147365
130714SA	WASH - u	1.65	3.46	0.83	0.078807	0.181462	0.105318	0.091583	0.089874
130714SX	WASH - u	1.83	2.71	0.90	0.074375	0.110117	0.092972	0.110273	0.070704
130714SY	WASH - u	1.81	3.81	0.83	0.111750	0.165912	0.127815	0.104151	0.076984
130720DO	WHIT	1.61	0.88	0.83	0.001893	0.004390	0.002455	0.004823	0.014732
130720DP	WHIT	1.73	0.58	0.73	0.002137	0.003237	0.002090	0.004344	0.021734
130720DQ	WHIT	1.96	0.96	0.72	0.003326	0.003850	0.002746	0.004237	0.022736
130720DR	WHIT	1.73	0.58	0.87	0.001488	0.003688	0.002426	0.006414	0.017810

Sample Code	Region	FI	HIX	β/α	LC1	LC2	LC3	LC4	LC5
160716M	WHIT	1.58	1.26	0.69	0.003446	0.004248	0.003781	0.003668	0.020947
160716O	WHIT	1.90	0.82	0.63	0.002370	0.003238	0.002597	0.001692	0.025653
160716Q	WHIT	1.74	1.97	0.47	0.003021	0.002843	0.002468	0.001335	0.008977
160716R	WHIT	1.33	0.65	0.59	0.000829	0.001840	0.001076	0.001533	0.011995
170718SA	WHIT	1.81	2.70	0.28	0.003572	0.002088	0.002081	0.000202	0.006328
170718SC	WHIT	1.51	1.71	0.71	0.003681	0.004195	0.003448	0.002879	0.010220
170718SX	WHIT	2.04	1.74	0.52	0.002375	0.002681	0.002330	0.001699	0.008781
170718SZ	WHIT	2.16	1.77	0.48	0.002582	0.002649	0.002325	0.001446	0.008446
170722SR	WHIT	1.49	1.93	0.66	0.002152	0.003160	0.002310	0.001235	0.006114
170722SS	WHIT	1.39	2.43	0.67	0.005562	0.005462	0.004806	0.004144	0.007903
170722ST	WHIT	1.18	1.07	0.70	0.003533	0.004657	0.003242	0.003013	0.015416
170722SU	WHIT	1.39	1.20	0.76	0.000885	0.002835	0.001932	0.001226	0.006845
170722SV	WHIT	1.48	0.68	0.85	0.000349	0.002705	0.002108	0.002164	0.011600
180717SA	WHIT	1.63	0.89	0.78	0.001413	0.002651	0.002039	0.002871	0.014645
180717SC	WHIT	1.54	0.58	0.88	0.001076	0.002845	0.002536	0.004311	0.023157
180717SX	WHIT	2.04	0.44	0.57	0.003135	0.002430	0.003163	0.006762	0.033923
180717SY	WHIT	2.06	0.42	0.76	0.001981	0.002784	0.002847	0.006916	0.030121
180717SZ	WHIT	1.34	0.42	0.81	0.001244	0.002711	0.001850	0.002406	0.037649